Assays and ligands for underexplored membrane proteins with potential as future drug targets

Dissertation

zur

Erlangung des Doktorgrades (Dr. rer. nat.)

der

Mathematisch-Naturwissenschaftlichen Fakultät

der

Rheinischen Friedrich-Wilhelms-Universität Bonn

vorgelegt von

Robin Simon Gedschold

aus

Hanau

Bonn 2023

Table of contents

1 ABSTRACT

In this study, pharmacological assays were established and employed to identify and characterize compounds regarding their potential as tool compounds, lead structures, and drug candidates. Three different membrane proteins were investigated: (i) the MAS-related G protein-coupled receptor X4 (MRGPRX4), (ii) GPR18, and (iii) connexin-43. All three are poorly investigated proteins, that have potential as future drug targets. All of them require tool compounds to enable target validation studies.

MRGPRX4 is a primate-specific orphan receptor, about which only little is known. Potent MRGPRX4 ligands have been hypothesized to be suitable for a wide range of therapeutic applications, such as wound healing, cancer, itch, and pain. In order to investigate the proposed indications, a tool-box containing potent agonists and antagonists, as well as assay systems are required. Yet, only few weakly potent agonists and no antagonists are described in literature so far. The reported agonists are not employable as tool compounds due to their lack of potency and selectivity. When the work for this thesis started, our group had already developed novel agonists, antagonists, and the first potential radioligand [^{3}H]PSB-18061, for MRGPRX4.

Based on these studies, a radioligand binding assay, employing the radioligand [^{3}H]PSB-18061, was successfully established and used for investigating binding and kinetic parameters of the radioligand as well as unlabeled MRGPRX4 ligands. Moreover, autoradiography experiments of human tissues were attempted. The new agonists, which are based on a xanthine scaffold, were further optimized to increase their potency by about 100-fold yielding agonists with sub-nanomolar EC_{50} values. Close investigation of their structure-efficacy relationships allowed the development of xanthine derivatives that acted as potent antagonists. Moreover, recently discovered biphenyl and oxyphenbutazone derivatives were examined with regard to their inhibitory activity on MRGPRX4.

GPR18 is an orphan G protein-coupled receptor (GPCR) with controversially discussed pharmacology. Before the start of this thesis, a series of chalcone-based compounds were identified as GPR18 agonists by our group. As these compounds are known to trigger a specific kind of programmed cell death, namely methuosis, this

thesis aimed to investigate whether GPR18 activation leads to methuosis. We reproduced methuosis in different cell lines and studied the compounds effects on cell viability and morphological changes. Although structurally unrelated GPR18 agonists induced the same morphological changes, methuosis could not yet be unambiguously proven to be GPR18-dependent as not all GPR18-expressing cell lines showed the same morphological effect.

Connexin-43 forms gap junctions (GJs) between two adjacent cells and thereby allows the free diffusion of small molecules. Under pathological conditions this physiological process can be disturbed. We developed a screening assay to detect modulators of GJ activity. In the framework of this thesis the new assay was validated.

2 INTRODUCTION

2.1 G PROTEIN-COUPLED RECEPTORS

2.1.1 Function and relevance of G protein-coupled receptors

G protein-coupled receptors (GPCRs), also called 7-transmembrane domain receptors, are the largest class of membrane proteins, with about 800 members identified in the human genome.[1; 2] These receptors translate stimuli from the extracellular space into signals inside the cell. More than half of them are responsible for sensory functions, mainly mediating olfaction, taste and light sensing. The remaining non-sensory GPCRs are activated by a variety of ligands ranging from small molecules to large peptides.[1] All GPCRs share a common architecture with an extracellular N-terminus, an intracellular C-terminus, and seven transmembrane helices in between. GPCRs harbor a binding domain for a ligand, and on the intracellular side binding domains for different effector proteins.[3] After an agonist activates a GPCR at the ligand binding domain, the conformation of the receptor, including the intracellular segment, is changed. Subsequently, different proteins can bind on the intracellular side and elicit signaling cascades. As the name GPCR suggests, 'guanine nucleotide-binding proteins' (G proteins) are key players transducing signals from activated receptors. However, a second family of proteins, the arrestins, can be recruited upon receptor activation.[4] The members of the large family of GPCRs are differentiated by highly specific ligands binding from the outside of the cell and clearly defined signaling cascades inside the cells, resulting in a complex, but fine-tuned pharmacology. This is exploited by drugs interfering with the signaling of GPCRs. Although roughly one third of marketed drugs target GPCRs, only a small fraction of GPCRs are so far exploited for that purpose.[5; 6] This implies, that there is a great potential for future therapeutics interfering with GPCRs, which is still to be discovered.

The most common classification system for the large family of human GPCRs is based on sequence homology, and divides the proteins into four different clusters: Class A (rhodopsin family), Class B (secretin and adhesion family), Class C (glutamate family), and Class F (frizzled family).[2; 7] Class D and E are skipped, because, in an alternative

classification system, which contains also non-human GPCRs, they were assigned to the 'Ste2-like fungal pheromone receptors' and the 'cAMP receptors', respectively, which are not found in vertebrates.[1; 7] The majority of human GPCRs, namely ~700 of the ~800, are assigned to Class A. This family is further divided into the α, β, γ, and δ-branches.[2] The phylogenetic tree, which visualizes the sequence similarity of the GPCRs, is depicted in Figure 1.
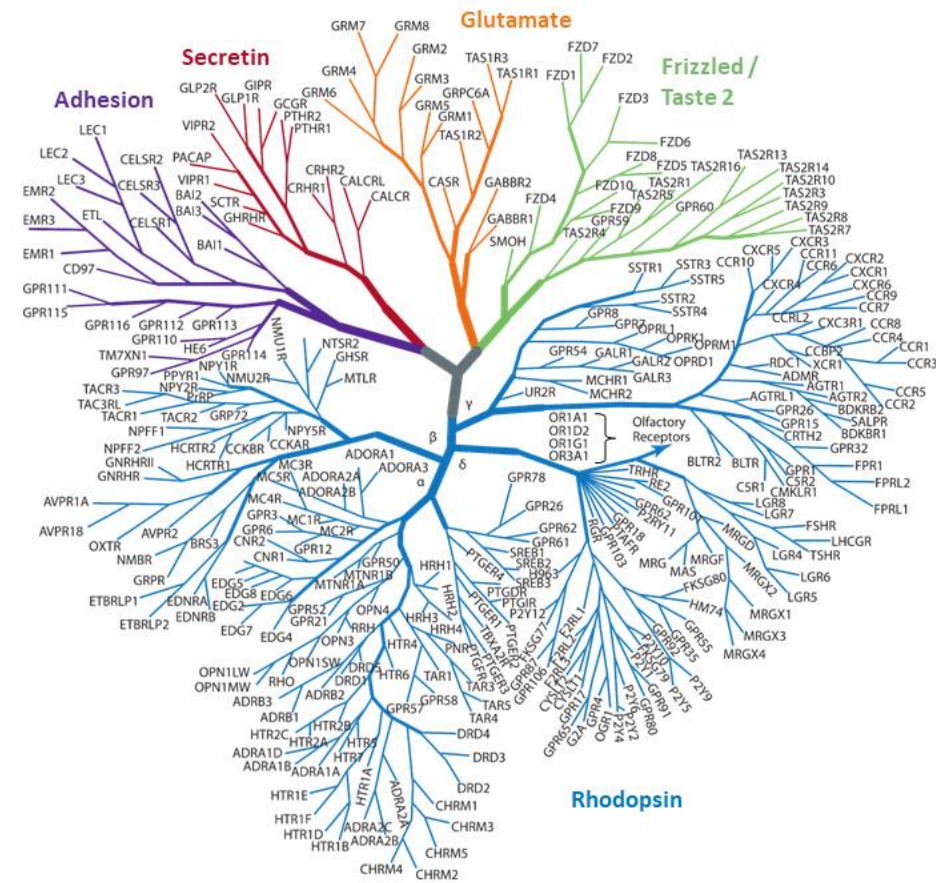
Figure 1: Phylogenetic tree of human GPCRs organized for sequence similarity. Figure was taken from Stevens et al. (2012) and modified.[8]

2.1.2 G protein-coupled receptor signaling

The conformation of a GPCR can shift from an inactive into an active one, leading to the binding of intracellular signaling proteins to the receptor.[3] The active conformation is favored through agonist binding, but GPCRs can exhibit a constitutive activity where the receptor, without the presence of any agonist, spontaneously shifts into an active conformation.[9; 10] The subsequent translation into an intracellular

response mainly depends on Gα proteins. These elicit signaling cascades depending in the Gα protein subtypes that couples. The second protein family recruited by active GPCRs are β-arrestins. After association to the receptor, they mainly induce internalization and consequently arrest GPCR signaling.[4; 11] These canonical pathways are depicted in Figure 2. Although this implies a very clear and straightforward activation and termination of GPCR signaling, the actual biological process is much more complex for several reasons. (i) A GPCR cannot just be described as active or inactive but can adopt a wide spectrum of conformations in between;[12; 13] (ii) some GPCRs can di- or oligomerize to homo- or heteromers which exhibit distinct pharmacological properties;[14; 15] (iii) Gα protein-independent signaling by the Gβγ proteins and β-arrestin has been hypothesized;[4; 15–17] (iv) the binding of the Gα protein subtype is dependent on multiple factors, such as the GPCR, the ligand, and the Gα expression pattern;[17–19] (v) the activation of G proteins and β-arrestins are not necessarily balanced.[15] Regardless of these interactions, the canonical pathways of Gα protein signaling and β-arrestin-dependent desensitization are playing the major and best investigated role in the pharmacology of a GPCR.[17; 20] In the following segment Gα protein and β-arrestin pathways are described in more detail.
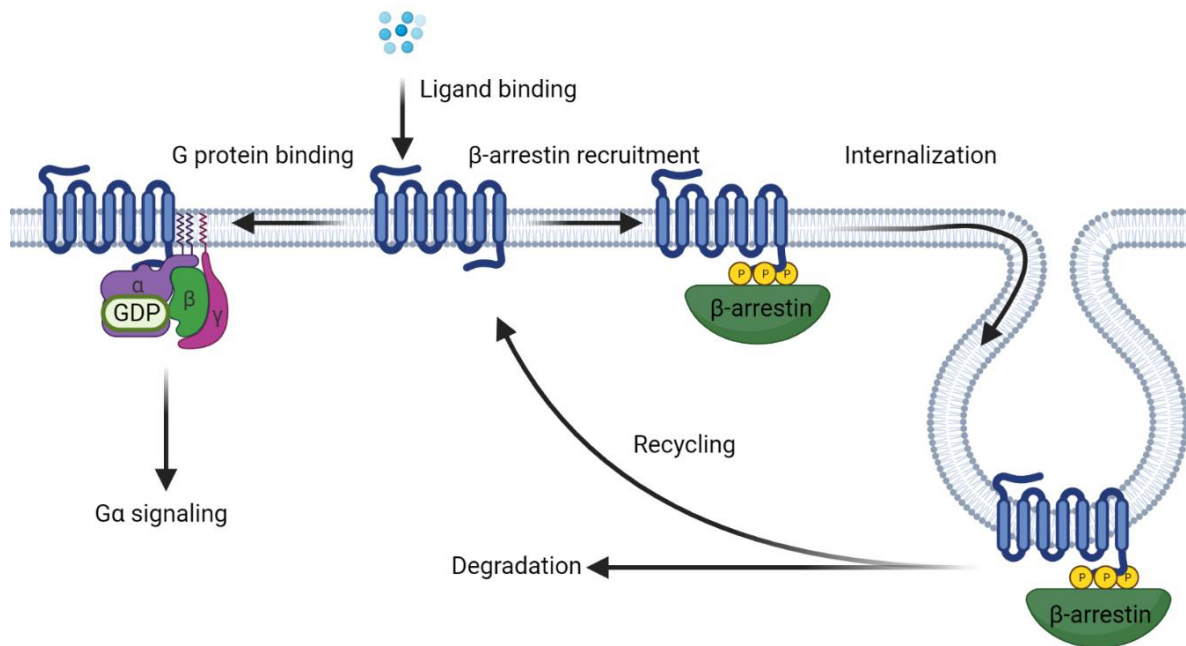
Figure 2: Outline of canonical GPCR pathways. After ligand binding, the GPCR activates two main pathways. To the left: the heterotrimeric G protein is bound and after replacing guanosine diphosphate (GDP) by guanosine trisphosphate (GTP) the Gα is released and elicits a signaling cascade depending on its subtype. To the right: after G protein-coupled receptor kinase(GRK)-dependent phosphorylation of the GPCR, β-arrestin is recruited and the GPCR is internalized. Afterwards, the GPCR traffics back to the membrane (recycling) or is degraded in the lysosome. Created with BioRender.com

G proteins are heterotrimeric proteins, consisting of a α, β, and γ subunit.[20] In the inactive state, the trimer binds guanosine diphosphate (GDP). After interaction with an activated GPCR, the GDP is released and replaced by guanosine triphosphate (GTP), allowing the Gα protein to dissociate from the Gβγ-dimer.[17; 21] The now active and free Gα protein is mainly responsible for further signaling via effector proteins, until its signaling is terminated by hydrolysis of the bound GTP to GDP by the intrinsic GTPase activity of Gα.[21] The 16 different Gα protein subtypes that exist, are grouped into four subfamilies – $G\alpha_s$, $G\alpha_{i/o}$, $G\alpha_{q/11}$, and $G\alpha_{12/13}$.[22] The subfamilies were determined by sequence homology but correspond well with their signaling which is as follows: $G\alpha_s$ proteins activate adenylate cyclase and therefore increase cAMP levels; $G\alpha_{i/o}$ block adenylate cyclase; $G\alpha_{q/11}$ proteins activate phospholipase C-β and subsequently increase intracellular calcium levels; $G\alpha_{12/13}$ interact with small GTPase guanine

exchange factors, and, as a result, modulate the cytoskeletal structure of the cell.[16; 17; 23–25] However, most GPCRs do not selectively couple to one Gα protein subtype, but can activate several subtypes, often from more than one subfamily.[17; 26] Therefore, not only the capability of a GPCR to couple to a specific Gα protein, but the presence of these subtypes in the respective cell modifies the resulting signal. Moreover, it was shown that the ligand that activates the receptor can exhibit a bias for the coupling of specific Gα protein subtypes.[18; 19] Consequently, a complex situation emerges, where the Gα signaling of a receptor cannot be easily predicted, especially in living tissues, but has to be carefully investigated for each ligand – receptor – Gα protein combination.

Arrestins are the second protein class interacting with activated GPCRs. In humans four arrestins were identified. While two types (arrestin-1 and -4) out of the four arrestins are exclusively expressed in the retina, the other two (arrestin-2 and -3, also termed β-arrestin-1 and -2) are ubiquitous expressed in the human body.[11] Prior to the binding of β-arrestin to a GPCR, the activated receptor is required to be phosphorylated by G protein-coupled receptor kinases (GRKs) on the intracellular C-terminal end. Subsequently, this phosphorylated 'tail' is recognized and bound by arrestins.[13; 27] Afterwards, β-arrestin traffics the receptor to clathrin-rich membrane regions inducing internalization of the GPCR, terminating G protein signaling.[11; 13] Additionally to signal arrestment, β-arrestin-dependent signaling has been postulated.[4; 11; 27] However, it is still debated if this signaling is G protein-independent, or whether β-arrestins rather work as scaffolding proteins that modulate the G protein-dependent signaling.[27–31] Some GPCRs were identified that do not couple to G proteins, but only recruit β-arrestin, or not even that. Originally, they were perceived as 'decoy' receptors that only eliminate ligands from extracellular space, but later on, effects on intracellular signaling have been recognized.[32; 33] In summary, the straightforward idea of β-arrestins being solely responsible for terminating signaling is not completely holding up against recent findings. Nonetheless, the exact nature of its involvement in signaling remains elusive.[13; 27–31]

The two discussed pathways, originating from G proteins and β-arrestins, as interconnected as they may be, are not equally activated by all GPCRs. The preference for one or the other is called bias. The bias can root in three different components:

Firstly, the GPCR itself can be biased. As addressed above, some GPCRs even lack G protein coupling and therefore exhibit a strong 'intrinsic' β-arrestin bias.[32; 33] By contrast, mutations of some GPCRs were shown to result in constitutive G protein activity, resulting in a strong G protein bias.[12] Next, the effector proteins influence the different signaling. An overexpression, or a lack of certain effector proteins, as for example G proteins, GRKs or β-arrestins, or downstream kinases, can have the same ultimate effect of one pathway overshadowing the other.[12] Lastly, the ligand activating the GPCR can be biased. The receptor has a variety of active conformations that a ligand can stabilize, each one potentially favoring different pathways.[3; 12; 18; 19] The relevance of biased ligands will be further discussed in the chapter 2.1.3.

2.1.3 Ligands of G protein-coupled receptors

Ligands of GPCRs are generally classified by function into agonists, partial agonists and antagonists.[34] Agonists and partial agonists alter the conformation of a GPCR towards an active state, whereas the partial agonist is significantly less efficacious at transducing an intracellular signal. Antagonists can be either neutral antagonists, only prevent other ligands from binding without manipulating the conformation of the GPCR, or can obtain inverse agonistic properties, which alter the conformation of the receptor towards the inactive state. This, by contrast to neutral antagonists, inhibits the basal activity of a GPCR (Figure 3).[3; 10] Another classification for GPCR ligands is their binding site. A ligand binding to the same location as the endogenous ligand is called orthosteric, while allosteric ligands bind to another region of the GPCR. Therefore, two different orthosteric ligands compete for the limited space, and consequently displace each other. An allosteric ligand, on the other hand, does not directly compete with an orthosteric ligand, but can modulate the GPCRs conformation. With that conformational shift, it can elicit a signal on its own or alter the response produced by an orthosteric agonist, or even prevent binding of the orthosteric lignad.[35]

A.

B.
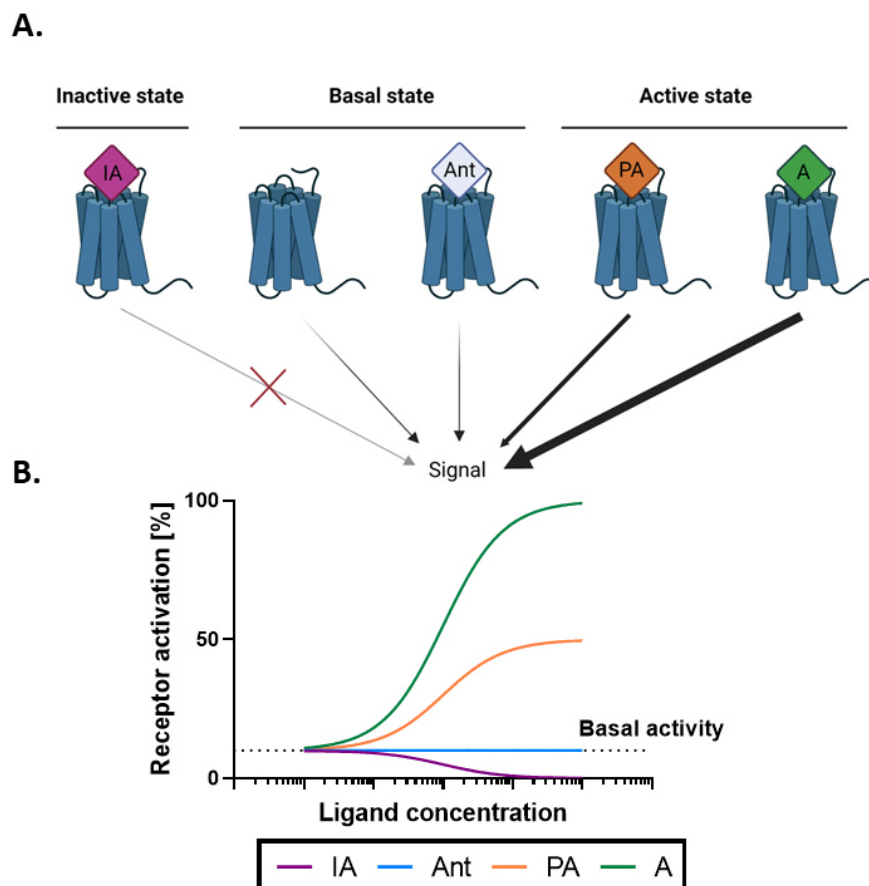
Figure 3: The different ligand types for GPCRs. IA = antagonist with inverse agonistic activity; Ant = neutral antagonist; PA = partial agonist; A = agonist. **A.** The signal transduction of a GPCR with the respective ligands. Created with BioRender.com. **B.** IA and Ant block the signal of an agonist, whereas the IA potentially lowers the signal below the basal state. PA and A elicit a signal after receptor activation, while PA do this to a lower extent. Created with GraphPad Prism.

A ligand's interaction with a GPCR is characterized by three different metrics. Firstly, the affinity, expressed as the K_d value (or dissociation constant, K_i). To determine the K_d value, binding assays are used, as for example, radioligand binding assays or fluorescence resonance energy transfer (FRET) assays. By this means, a clear discrimination between bound and unbound ligand is possible. In addition to binding affinity the function of the ligand has to be determined. The functional potency is expressed as EC_{50} value for agonists (and partial agonists) or as IC_{50} value for antagonists. For their determination, functional assays are used, as for example calcium mobilization or β-arrestin recruitment assays.[36; 37] These assays do not measure a direct interaction of a compound with a GPCR, but instead measures a signaling event. Therefore, the results allow to observe and quantify the functional effect of the ligand, e.g., agonistic, antagonistic, or inverse agonistic behavior. The

third metric, the efficacy, denoted as E_{max}, is derived from functional assays as well. It only applies for agonists because it is defined as the maximal effect that an agonist produces in relation to a control. It can be expressed as percentage compared to a standard agonist, preferably the endogenous agonist. The efficacy allows to discriminate partial agonists from full agonists.

Although all agonists stabilize an active GPCR conformation, they can cause distinct functional effects. This is due to the fact that not just one active conformation of a GPCR exists, but a multitude of conformations, each with its own implications for signaling.[3] One example are partial agonists. They elicit a signal, but to a considerably lower extend than a full agonist, regardless how high the concentration may be. Consequently, a partial agonist can 'antagonize' a full agonist's signal. As the full agonist is displaced, only the considerably lower signal of the partial agonist is transduced. This effect is exploited by different drugs to achieve a so-called ceiling effect. For example, in opioid substitution therapy, the partial opioid receptor agonist buprenorphine can be used. On the one hand, it inhibits the effects of an opiate overdose because it displaces the overdosed opiate without inducing the same full-scale effects. On the other hand, it is used in substitution therapy to reduce withdrawal symptoms by receptor activation, without posing dangerous side effects as the opiate as it cannot be easily overdosed.[38]

Biased agonists favor either G protein coupling or β-arrestin recruitment.[12; 15] This effect, called bias or functional selectivity, is a functional observation and is therefore independent of the affinity of the ligand to the receptor (examples see Figure 4). Winpenny et al. (2016) introduced the mathematical definition of bias, shown in Equation 1, as the difference of the logarithm of the ratio of E_{max} and EC_{50}.[39] The calculated bias is not an absolute value but a relative one and needs to be compared to other compounds tested in the same systems. This is due to two implications: (i) Different assay systems are used for both pathways, but they cannot be expected to deliver the same values even for unbiased ligands. For example, a calcium mobilization assay produces results dependent on receptor expression levels;[37] (ii) the efficacy is normalized to a standard compound, which therefore influences the bias.

Equation 1: Definition of bias according to Winpenny et al. (2016).[39]
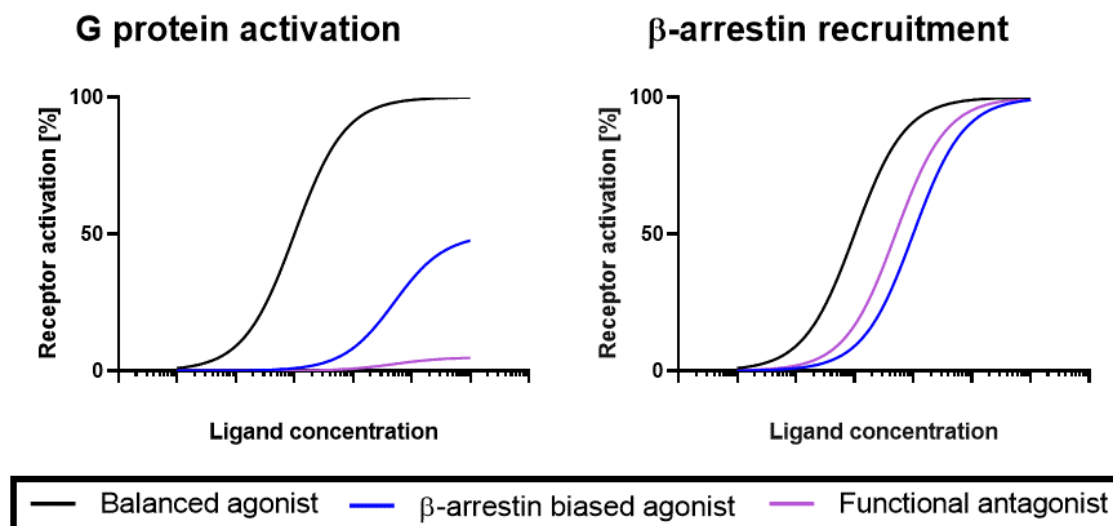
$$Bias = \Delta log \frac{E_{max}}{EC_{50}}$$

Figure 4: Examples of a balanced and two β-arrestin-biased agonists, whereof one constitutes a functional antagonist. The biased agonists favor one pathway regarding potency or efficacy, or both. The functional antagonist is an extreme case of β-arrestin bias, were no, or nearly no G protein activation is detected while the compound still activates β-arrestin recruitment.

The hypothesis that activation of one pathway can have preferable clinical outcomes while activation of the other pathway is responsible for side effects, opened the possibility for the development of biased agonists as drugs.[15; 39] Carvedilol, for example, was described as a β-arrestin biased agonist, showing preferable clinical outcomes compared to other β-blockers for patients with heart failure.[15] TRV130 on the other hand is a newly approved μ-opioid receptor agonist with a strong G protein bias, which was reported to result in reduced opioid side effects.[40; 41] A strong β-arrestin bias, combined with a barely measurable activation of G protein coupling, results in ligands that act as functional antagonists (explanatory curves see Figure 4). Although they are agonists, shifting the GPCRs conformation into an active state, they ultimately fully inhibit the G protein signal. They displace the endogenous agonist, and do not induce relevant G protein activation, but induce receptor deactivation by β-arrestin-dependent internalization. An example for this is fingolimod, a therapeutic to treat multiple sclerosis. Fingolimod binds to sphingosine-1-phosphate receptors and acts as a functional antagonist. It reduces receptor density and blocks the

endogenous agonist, sphingosine-1-phosphate, from inducing proinflammatory effects.[42; 43]

In order to characterize agonists, not only affinity, potency, and efficacy need to be determined, but also potential bias must be evaluated. Thus, at least two functional assay systems, probing G protein coupling and β-arrestin recruitment need to be employed. The understanding how to design a drug with a specific bias, in either direction, is a powerful means to determine the pharmacology of a new drug candidate.

2.2 MAS-RELATED G PROTEIN-COUPLED RECEPTORS

MAS-related G protein-coupled receptors (MRGPRs) belong to the δ-branch of the rhodopsin-like class A of GPCRs; they are named due to their close sequence relation to the gene MAS1 (35% identity).[44; 45] MAS1 was first isolated in 1986 from an epidermoid carcinoma cell line and was named after Massey, the name of the person who donated the tumor from which the gene was isolated.[46; 47] At discovery MAS1 was assumed to be a proto-oncogene, but later on Jackson et al. (1988) proposed an activation of MAS1 by angiotensin II and suggested it to be an angiotensin II receptor.[48] However, subsequent results showed that this effect is attributed to an interaction of MAS1 with the Ang II receptor, rather than the angiotensin II itself.[49] Only in the early 2000s, MAS1 was clearly identified as a GPCR, which is activated by the endogenous ligand angiotensin-(1-7).[46; 50] At about the same time, Dong et al. (2001) discovered around 40 genes, closely related to MAS1, introducing the family of MAS-related genes (Mrg).[50] In parallel, Lembo et al. (2002) identified and named sensory neuron-specific G protein-coupled receptors (SNSR), which, however, were afterwards recognized to be identical to MRGs; to be precise to the MRG subfamily later called MRGPRX.[51] In order to avoid confusion with the gene names, the family of receptors was called MAS-related G protein-coupled receptors (MRGPR) and the nomenclature for the individual receptors was defined.[52; 53] Now, MRGPRs are divided into nine subfamilies, A-H and X. These subtypes are further classified by numbers, as for example the 4 different MRGPRX receptors are called MRGPRX1 - 4. All MRGPRs are only found in tetrapods; more precisely A, B, C, and H are only expressed in rodents, X only in primates, and D-G in different mammalian species, including

rodents and primates.[47; 52] The phylogenetic tree, and therefore the genetic similarity of MRGPRs is shown in Figure 5. Although, the primate-specific MRGPRX subfamily is closely related to the murine-specific MRGPRA proteins, no orthologous receptor pair could be verified yet.[45]

Originally, the mrgpr genes were discovered in small-diameter dorsal root ganglia (DRGs), where all MRGPRs are expressed. Additionally to high expression in DRGs, high MRGPR expression was found in trigeminal ganglia (TGs).[50; 51; 54] DRGs and TGs make up the peripheral somatosensory systems. They consist of clusters of neuronal cell bodies that are found just outside of the spinal cord (DRGs) or at the base of the scull (TGs). The small-diameter DRGs, in which MRGPRs are mainly found, respond to temperature, pruritogens, tissue damage, and chemical as well as mechanical stimuli. Activation often results in pain or elicits the sensation of cold, touch, or itch.[55] Consequently, many reports hold the notion that MRGPRs are important in pain transmission, or in the case of the MRGPRX4, mediate the sensation of itch. Besides these neurons, MRGPRs were found to be expressed in mast cells. MRGPRX2 and to a smaller extent MRGPRX1, but neither MRGPRX3 nor -4 where found to be expressed in human umbilical cord mast cells.[56] Except for MRGPRAs, -Bs and -X1, which are only expressed in DRGs and in part in mast cells, the other MRGPRs were shown to be additionally expressed in a wide variety of tissues.[44; 45]
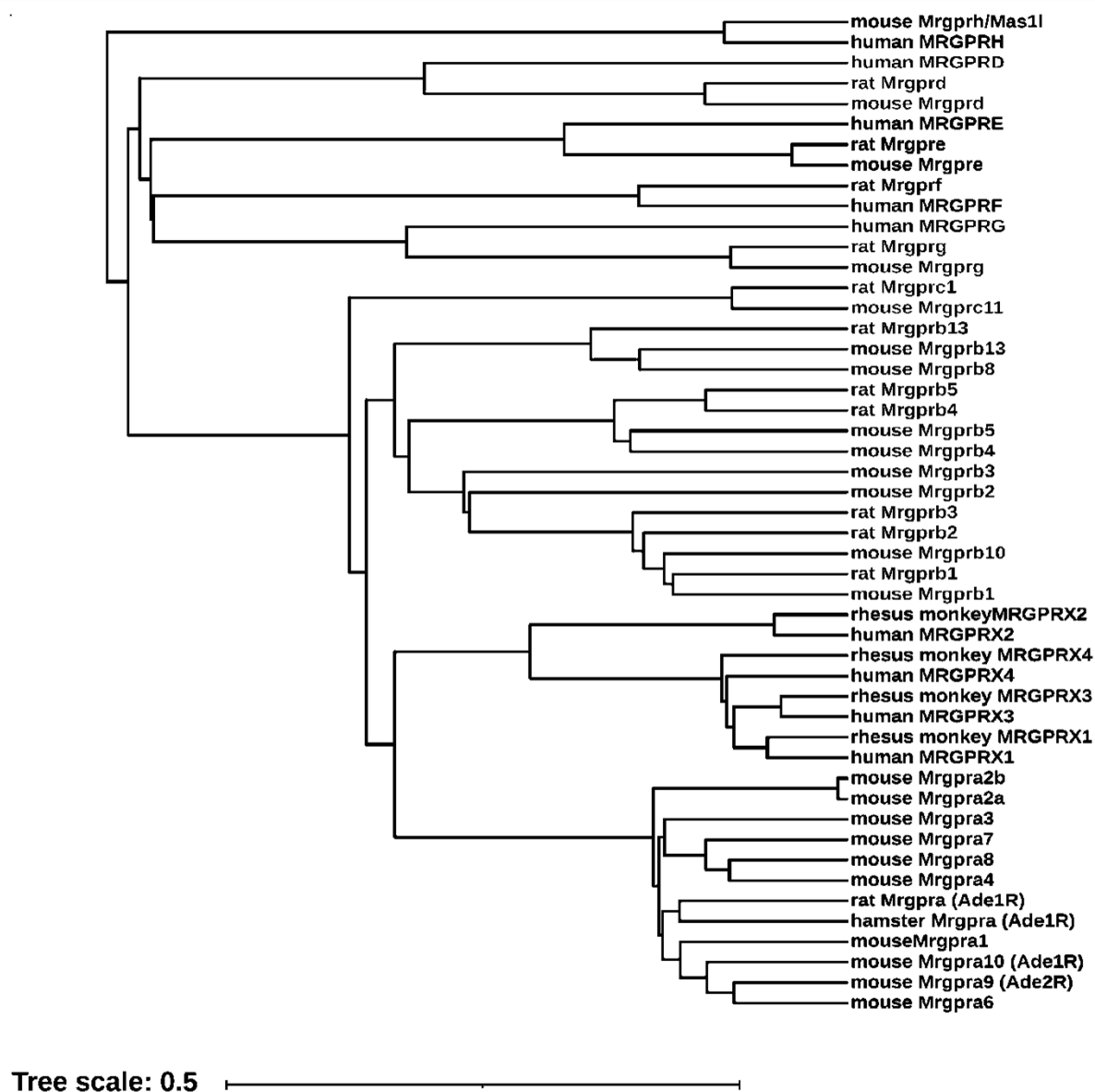
Figure 5: Phylogeny of MRGPRs. Scale bar represents the nucleotide sequence differences (0.5 corresponds to 50% difference in sequence). Figure adapted from Al-Hamwi et al. (2022)[45]

Despite some effort to discover the endogenous ligands has been made, most MRGPRs are still classified as orphan receptors.[52; 53] Although some molecules that activate the receptors have been identified, in most cases, the required concentrations are not reached in vivo.[44] Exceptions are MAS itself, and MRGPRD, for which angiotensin-(1-7) and β-alanine, respectively, have been described as endogenous agonists.[57; 58] For MRGPRX1 there is evidence that the peptide bovine adrenal medulla peptide 8-22

(BAM8-22) may be the endogenous agonist.[53; 59] Nonetheless, the receptor is not yet classified as deorphanized.[44] The lack of identified endogenous ligands was explained by their unusually high constitutive activity. [44; 60–62] The corresponding hypothesis was that an inverse agonist instead of an agonist would a stand as endogenous ligand. Since assays for deorphanization were not designed for that purpose, inverse agonists would have been overlooked.[44] However, high constitutive activity of the MRGPR family is not clearly proven. Uno et al. (2012) investigated MRGPRD and Chen and Ikeda (2004) MRGPRX1, whereby the latter questioned the significance of the observed rather low constitutive activity.[61; 62] Burstein et al. (2006) investigated all four MRGPRX subtypes.[60] The employed assay, established by Weissman et al. (2004), is utilizing a ras/rap chimera that forces $G\alpha_q$-, $G\alpha_i$- and $G\alpha_s$ protein-coupled receptors to activate a pro-proliferative pathway. Thus, receptor activity can be measured by cell-proliferation.[63] For MRGPRX4 the measured constitutive activity was the highest and comparable to the effect produced by the muscarinic receptor M5 with high concentrations of the agonist carbachol (20 µM). However, as the endogenous agonists of all MRGPRXs are still unknown, one cannot discriminate between constitutive activity or agonistic effects by the possibly present ligand. The agonist could be present in the growth medium or secreted by the cells themselves. Moreover, MRGPRX4 is proposed to play a role in proliferation itself, the read-out of the utilized assay.[64; 65] In addition, different agonists have already been discovered for MRGPRX4 (see section 2.2.1). In these assays, an exceptionally high constitutive activity would have resulted in unusual read-outs, such as elevated background signals with small assay windows. However, such effects were not described.

In conclusion, MRGPRs are not well explored, however, they are promising drug targets to treat, among others, pain, itch, and immune system-related disorders. Nonetheless, what is needed beforehand, are closer investigations of the pharmacology, and the availability of different assay systems and potent ligands to probe these receptors and validate them as drug targets.

2.2.1 MRGPRX4

MRGPRX4 is a member of the MRGPRX subfamily which consists of four GPCRs showing 63 – 83% sequence identity.[66] MRGPRX4 was simultaneously discovered by Dong et al. (2001) and Lembo et al. (2002).[50; 51] The latter used the alternative name "sensory neuron-specific G protein-coupled receptor 6" (SNSR6) for MRGPRX4, which is, however, not used anymore. As all MRGPRXs, MRGPRX4 is an orphan receptor and only scarcely investigated.[52; 53] The lack of potent agonists and assay systems to probe MRGPRX4 is impeding its study. MRGPRX4 was shown to couple mainly to $G\alpha_{q/11}$ proteins which allows the usage of calcium mobilization assay to search for agonists or antagonists.[60; 67] Besides calcium assays, β-arrestin recruitment assays are employed.[67; 68] The fact that MRGPRX is exclusively expressed in primates, without a clear mouse orthologue identified, limits the use of rodent animal models.[45; 52] The expression pattern of MRGPRX4 is not well investigated. Initial reports indicated that MRGPRX4 expression is restricted to the small diameter dorsal root ganglia (DRGs) and trigeminal ganglia (TG).[51] However, later on, more tissues were identified to express MRGPRX4, for example, respiratory epithelial cells, CD8^{+} cytotoxic T-cells, different cancers, and skin cells.[45; 65; 69–71] In keratinocytes, the MRGPRX4 expression could be upregulated upon stimulation with the toll-like receptor agonist poly(I:C).[64; 65] The expression levels were, however, mostly shown on the mRNA and not on the protein level, and were generally low. The elevated expression levels in different cancers were heterogenous, since some cases of the same tumor showed no MRGPRX4 expression at all.[70; 72] However, MRGPRX4 was confirmed as one of 15 mutation hot spots in colon cancer, emphasizing its participation in cancer development or tumor progression.[73]

Various natural variants of the receptor are described, but with rather low frequencies. The S83L variant (dbSNP:rs2445179) must be discussed because several sources (NCBI, UniProt; GPCRdb) mistakenly enlists the S83L variant as the wild type. A closer look into these databases, however, reveals that the "variant" 83S occurs in >95%.[74] To avoid further confusion, the term "wild type" will be avoided in this work and replaced by major variant 83S and minor variant 83L. The origin of this mistake is unclear. The original publications from Dong et al. (2001) and Lembo et al. (2002), who first reported on MRGPRX4, detected the more frequent 83S variant.[50; 51] The potencies of agonists were found to greatly differ for the two variants.[75] Despite this,

the exact sequence is rarely stated in publications and interpretation of literature data can therefore be ambiguous.

The physiological role of MRGPRX4 is disputed, as the endogenous ligand is not identified yet. The high expression of MRGPRX4 in the neurons of DRGs infers a role of the receptor in nociception and itch transmission.[44; 60] But some endogenous agonists are proposed in literature and each of them allows a different interpretation for MRGPRX4's physiological role. Therefore, the two proposed pharmacological effects, itching and cell migration, are discussed in the context of the proposed agonists.

Bile acids, bilirubin, and itch

The heterogeneous group of bile acids and bilirubin was shown to activate MRGPRX4 with moderate potencies.[76–79] Bile acids and bilirubin accumulate as a result of liver damage, which results in cholestatic pruritus, that is characterized by itch.[80] Consequently, the discovery that these compounds activate MRGPRX4 is followed by the conclusion that MRGPRX4 activation causes the itching sensation. [76; 77; 79] From many different bile acids that were found to activate MRGPRX4, deoxycholic acid (DCA) and ursodeoxycholic acid (UDCA) are the most potent ones (for structures and potency, see Figure 7). However, bile acids are known to activate another GPCR, the "membrane bile acid receptor" TGR5, which is the main bile acid receptor.[81–83] To exclude that TRG5 activation is the reason for the results, a selective TGR5 agonist was injected into human subjects, but did not induce itch, whereas DCA, activating TRG5 and MRGPRX4, did. [76; 77] Therefore, it was concluded that MRGPRX4, and not the bile acid receptor TGR5, is responsible for the itch reaction induced by bile acids.[76; 77] Additionally, it was tested whether DCA-induced itch is histamine-independent, as cholestatic pruritus is known to be.[80] Expectedly, a pre-treatment with antihistaminic drugs did not alleviate the DCA-induced itch, being in line with observations of cholestatic pruritus.[77] The subsequent question was whether the elevated bile acid plasma levels in patients with cholestatic pruritus are sufficient to activate MRGPRX4. This is an especially critical question, since the most potent bile acids like DCA and UDCA are not elevated in patients suffering from cholestatic pruritus, but only other, less potent bile acids, as for example taurocholic acid (TCA, structure and potency, see Figure 7) shown increased levels.[77; 84; 85] However, a cocktail that was designed to

mimic the bile acid concentration in diseased patients was still able to activate MRGPRX4 in a calcium mobilization assay, whereas a mixture mimicking healthy subjects was not.[77] Therefore, the authors conclude that cholestatic pruritus, at least in part, is due to MRGPRX4 activation by bile acids, and that MRGPRX4 is a promising drug target to treat cholestatic pruritus.[76–78] Despite these compelling results, bile acids cannot be designated as the endogenous ligands of MRGPRX4. Firstly, the potency is low and only reached in pathological conditions. Moreover, the accumulated bile acids are reported to precipitate in skin and activate MRGPRX4.[77] This would not explain the broader expression of MRGPRX4 in tissues that are not reached by bile acids, e.g. in the DRGs, TGs, and tumors. Consequently, MRGPRX4 is not officially deorphanized by this approach, but a link between itch and activation seems evident. As antihistaminic drugs do not help to alleviate the itch in the context of cholestatic pruritus, it is not well treatable.[80] In conclusion, MRGPRX4 antagonists could be a novel approach to treat histamine-independent itch, e.g. in cholestatic pruritus. However, no antagonists are published to date to investigate and validate this possible application.

Host defense peptides and migration

Other proposed ligands are the two host defense peptides (HDPs) AG-30/5C and "antimicrobial peptide derived from insulin-like growth factor-binding protein 5" (AMP-IBP5). They show antimicrobial, immunomodulatory, and pro-wound healing properties.[64; 65] First, AG-30/5C was proposed as a ligand of MRGPRX3 and 4.[65] It stimulates keratinocytes to produce cytokines, e.g. IL-6 and MIP-3α, which, in consequence, migrate and proliferate. The cytokine production was shown to be inhibited by blocking MRGPRX3 and MRGPRX4 expression with the corresponding siRNAs. Moreover, the pro-inflammatory effect of AG-30/5C was shown to be MRGPRX3- and MRGPRX4-dependent, as siRNA for both receptors reduced the anti-inflammatory p-IκB after activation with AG-30/5C.[65] The peptide AMP-IBP5 was proposed as a ligand of all four MRGPRXs.[64] AMP-IBP5 was shown to induce keratinocyte migration and proliferation due to interleukin production; e.g. upregulation of IL-8 and VEGF. The siRNA of all four MRGPRXs reduced AMP-IBP5-dependent cytokine production, and AMP-IBP5-induced migration and proliferation was blocked as well. As a limitation of both studies, the control siRNA strongly

affected the results compared to medium alone. For example, the investigated cytokines were strongly upregulated, and migration and proliferation were induced by control siRNA compared to the effect of medium. For the HDP AG-30/5C, calcium mobilization was shown after activation of MRGPRX4-transfected HEK cells with 10 µM of the peptide, although no β-arrestin recruitment was detected. This was interpreted as a biased agonism by the authors.[68] However, the calcium assay is not specific, whereas the β-arrestin assay systems are typically more specific for a certain receptor. Therefore, the observed effect could very well be due to an activation of another natively expressed receptor since the publication does not state control experiments on native cells. Secondly, the depicted calcium curve for nateglinide (a synthetic activator of MRGPRX4 discussed below) and AG-30/5C are quite different, which is not to be expected for two compounds activating the same receptor. Moreover, only a single concentration of 10 µM of peptide was tested - a high concentration, especially for peptides. Therefore, no compelling proof for a direct interaction of any of the two promiscuous peptides, AG-30/5C and AMP-IBP5, to any MRGPRX subtype was presented. Proliferation and migration are multifactorial cell responses, the investigated upstream mediators are not selective, and indirect interactions were not ruled out. In order to consider the peptides as shared endogenous agonists for MRGPRX receptors further investigation about their direct interaction is needed.

As described, both theories did not hold up to deorphanize MRGPRX4. Therefore, the search for the endogenous agonist is still ongoing. Apart from identifying endogenous ligands, efforts were made to discover exogenous ligands of MRGPRX4. In a screening campaign, nateglinide (structure and potency see Figure 7), an approved drug for the treatment of type 2 diabetes, was found to activate the minor 83L variant of MRGPRX4.[67] Nateglinide exhibits its antidiabetic effects through inhibition of ATP-dependent potassium channels in β-cells of the pancreas. Interestingly, one prominent side-effect of nateglinide is itching, coinciding with the above discussed findings about bile acids.[77] Its potency on MRGPRX4 is rather low, but nateglinide was successfully utilized by Cao et al. (2021) as a scaffold to develop the more potent derivatives ZINC5295 and MS47134 (structures and potencies, see Figure 7).[75] However, the optimization was carried out using the less common 83L variant, and evaluation on 83S showed much lower potency. MS47134 was successfully utilized to

generate a cryogenic electron microscopy (cryo-EM) structure of MRGPRX4-83L, providing structural information on the MRGPRX4, albeit on the minor 83L variant, which, however, may be put to use for further drug design.[75] Surprisingly, it reveals that the polymorphic amino acid 83 does not directly interact with the agonist but is located close to the binding pocket. The authors found the acidic function of the agonists to be vital and observed a high stereoselectivity based on the structure-activity relationships (SARs). The necessity of the acidic function was clearly shown by the protein structure, see Figure 6, which revealed a positively charged binding pocket, with three arginine residues in close proximity. Despite the usefulness of the nateglinide derivatives, the loss of potency at the major 83S variant makes them suboptimal for further drug development.
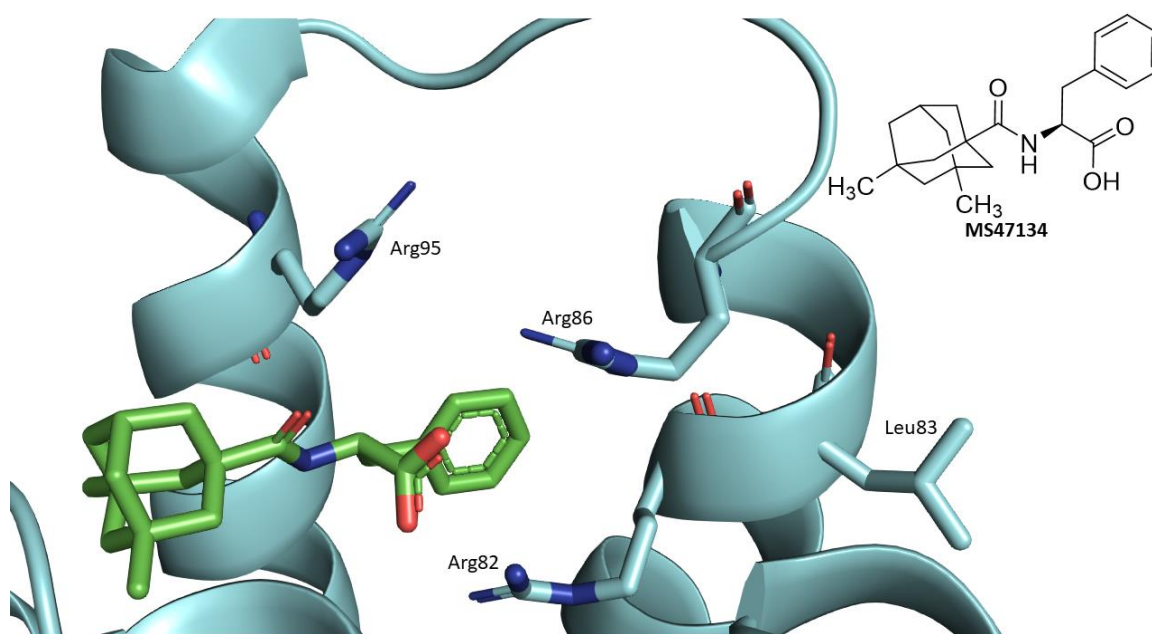

Figure 6: Binding site of MS47134 (green) in MRGPRX4 with the three close arginine residues and the relevant 83L amino acid highlighted. Adapted from Cao et al. (2021).[75] Arg86 was not resolved in the original Cryo-EM structure and was therefore afterwards manually inserted. Picture was made with PyMOL.
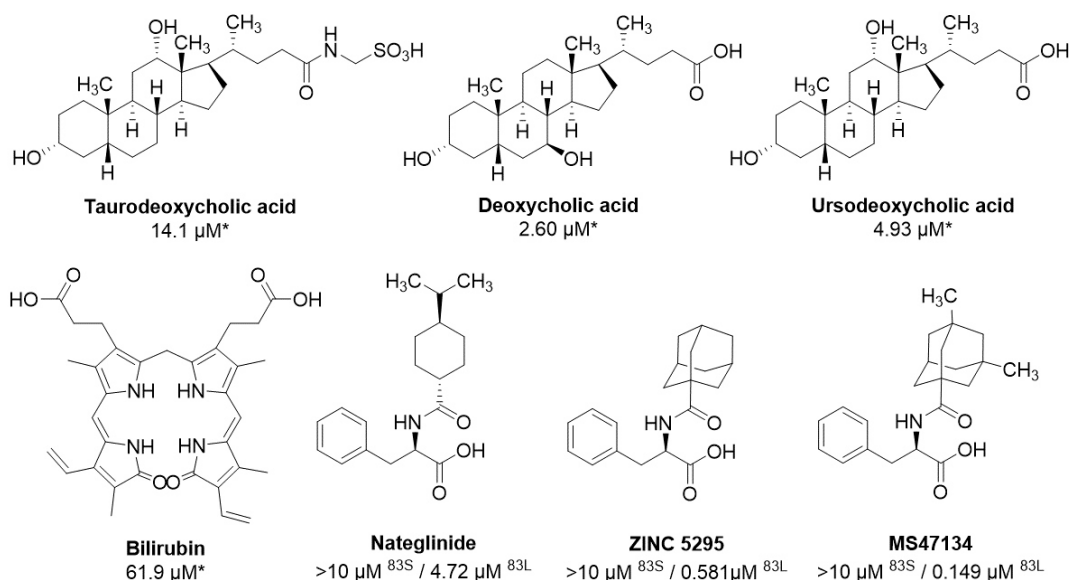
Figure 7: Structures of described MRGPRX4 agonists with EC_{50} determined in calcium assays. Bile acids by Yu et al. (2019)[77] and Meixiong et al. (2019),[76] and bilirubin[79] were described as weak agonists. Nateglinide[67] and its derivatives ZINC 5295 and MS47134 were reported as synthetic activators by Cao et al (2021)[75]. *Variant (83S or 83L) not specified; [83X]Determined at the indicated variant of MRGPRX4.

Additionally to the described agonists, Kozlitina et al. (2019) found high concentrations (>100 µM) of (-)-menthol to decrease agonistic effects of nateglinide on MRGPRX4.[86] Interestingly, this is only true for the β-arrestin pathway, while G protein coupling was not affected. Therefore, the compound is proposed to be an allosteric modulator of MRGPRX4. These experiments were preceded by an exome-wide study, screening for mutations associated with the smoking of menthol cigarettes. Here, a haplotype (= gene containing nucleotide variations that are inherited as one) of MRGPRX4 composed of the two mutations N245S and T43T was identified.[86] It was found to be solely expressed in individuals with African ancestry and it increased the odds of menthol cigarette smoking by 5-to-8 fold. Activation of MRGPRX4 containing these two mutations by nateglinide, measured as β-arrestin recruitment, reached only around 50% of the signal compared to wild type, and both were further inhibited by (-)-menthol. In a Bioluminescence Resonance Energy Transfer (BRET) assay monitoring G protein activation, the haplotype reduced the potency of nateglinide. However, neither haplotype nor the wild type were affected

by (-)-menthol. As described above, MRGPRX4 is suspected to play a role in nociception and pruritus. Therefore, the decreased signaling by (-)-menthol could result in an anesthetic effect that is more pronounced in individuals with the investigated haplotype, as the relative inhibitory effect is higher for an already dampened signaling.[86] However, the used (-)-menthol concentrations are exceptionally high. The proposed anesthetic effects are expected to take place in primary sensory neurons, where these high concentrations will probably not occur. Another target for menthol is the transient receptor potential channel TRPM8, that is suspected to be responsible for the cooling effect of menthol.[87; 88] TRPM8 was shown to be activated by much smaller concentrations, as low as 0.1 µM, and was more clearly linked to effects caused by menthol cigarettes.[89]

An alternative approach to understand the pharmacology of the GPCR would be the usage of animal models. But, as stated above, no mouse ortholog has been identified yet, even though MRGPRA1 had been proposed. The bile acid lithocholic acid (LCA), which was reported to activate MRGPRX4, activates MRGPRA1 as well.[77; 78]. However, LCA was additionally shown to activate MRGPRB2, which is believed to potentially be a mouse ortholog of MRGPRX2. Furthermore, LCA was not able to induce itch in mice, but provoked a low itch response in humans.[78] Whilst LCA is the most potent natural agonist of the bile acid receptor TRG5 with an EC_{50} of 530 nM (cAMP assays),[81] MRGPRX4 is activated only at higher concentrations (9.3 µM, EC_{50} in calcium assays),[77] and MRGPRA1 even requires much higher concentrations of 290.4 µM (EC_{50} calcium assays).[78] Similarly, MRGPRB2 is activated with a potency of 183.3 µM (EC_{50} calcium assay).[78] Therefore, LCA activates a variety of receptors at high concentrations, and receptor activation at such concentrations cannot be taken as a proof for a close connection of the receptors.

In conclusion, some weakly potent ligands for MRGPRX4 have been identified (bile acids, bilirubin, nateglinide and derivatives). Nonetheless, all possess low potency at the major, predominant variant of MRGPRX4. The lack of a more potent agonist largely prevents further studies, as other methods, e.g., siRNA knock-down, are associated with limitations. Thus, the orphan GPCR is to date only scarcely understood, and the linkage to the different illnesses needs further examination to prove a clear involvement of MRGPRX4. The availability of potent tool compounds

would open up the possibility to address the investigation of its expression, signaling pathways, and its pharmacological role, and validate MRGPRX4 as a drug target.

2.3 GPR18

GPR18 is an orphan class A GPCR, first cloned in 1997 by Gantz et al. (1997).[90; 91] GPR18 expression was found in many tissues, with highest in cells of the immune system as leucocytes and lymph nodes. [92–94] The receptor has been linked to the endocannabinoid system, as several cannabinoids were reported to modulate GPR18, however it has only a low sequence homology with the classical cannabinoid receptors (Cannabinoid receptor type 1 (CB_1R) ($\sim13\%$), Cannabinoid receptor type 2 (CB_2R) ($\sim8\%$)) and the cannabinoid-interacting orphan receptor (GPR55 ($\sim21\%$)).[91; 95; 96] The therapeutic potential of GPR18 is widely discussed in literature, the proposed indications ranging from pain, immunomodulation, ocular pressure, to cancers.[91; 94; 97] Quin et al (2011) showed that GPR18 is overexpressed in some cancers and that the inhibition of GPR18 by siRNA enhanced apoptosis and moreover showed that blocking GPR18 activation reduced proliferation. Thus, the receptor is thought to have pro-cancer activity and that antagonists could be employed as a novel therapeutic approach.[94; 97] Additionally, GPR18 was proposed to participate in migration of microglia, endothelial, and tumor cells.[91] However, these observations were made in the absence of a selective agonist.

N-Arachidonoyl-L-serine, an endocannabinoid-like lipid was proposed as the first endogenous GPR18 ligand.[91; 98] It modulates other receptors, e.g. cannabinoid receptors, TRPV-1, and GPR55, however only with low potencies.[99] *N*-Arachidonoyl-L-serine-dependent activation of GPR18 was reported to result in phosphorylated p44/42MAPK.[98] In contrast, *N*-Arachidonoyl-L-serine was later on found to inhibit the effects of other GPR18 agonists, and therefore thought to act as GPR18 antagonist.[91; 95] In 2006 *N*-arachidoylglycine (NAGly) was proposed as an endogenous agonist for GPR18. The compound inhibited cAMP production after forskolin stimulation with an EC_{50} of ~ 20 nM, which was blocked by pertussis toxin. Consequently, GPR18 was assumed to couple to $G\alpha_{i/o}$ proteins.[100] The investigation of multiple signaling pathways after NAGly activation also proposed calcium mobilization with an $EC_{50} \sim 1$

µM, and a phosphorylation of ERK1/2. However, no β-arrestin recruitment was detected.[94] McHugh et al. (2010/2012) reported on an increased migration elicited by NAGly and proposed GPR18 as its target.[96; 101] These results are contradicted by multiple studies showing that no G protein-dependent signaling is induced by NAGly that is dependent on GPR18 expression.[94; 102; 103] Additionally, NAGly was found to modulate GPR55, as well as various ion channels and transporters. Due to selectivity issues, NAGly is prone to false-positive assay results.[91; 94; 104–106] These contradictory reports question NAGly to be a GPR18 agonist, therefore GPR18 is still classified as an orphan GPCR.[91; 94; 107] A number of synthetic, endogenous, and phytogenic cannabinoids were reported as ligands on GPR18. Abnormal Cannabidiol, O-1602, the endocannabinoid anandamide, and Δ9-THC were described as agonists.[94–96; 108; 109] However, again, there are severe selectivity issues with all of these compounds.

3 AIM OF THIS THESIS

This work aimed to implement assay systems, and to introduce and characterize novel ligands for the following understudied pharmacological targets: (i) MRGPRX4, (ii) GPR18, and (iii) connexin-43.

(i) The main focus was set on MRGPRX4, for which our research group identified novel ligand classes, namely xanthine-derived agonists (including the radioligand [^{3}H]PSB-18061), and biphenyl and oxyphenbutazone derivatives. The main aims of this thesis were

- to establish and employ a radioligand binding assay for MRGPRX4
- to investigate the effect of the naturally occurring minor S83L variant of MRGPRX4 on ligand binding
- to illuminate the structure-activity relations (SARs) of various classes of MRGPRX4 ligands
- to optimize these ligands in order to obtain potent and selective agonists and antagonists
- to detect new (endogenous) ligands for MRGPRX4

(ii) The GPR18 project was based on the finding that GPR18 was activated by various chalcone-based compounds. These compounds are known to induce a special form of programmed cell death, namely methuosis, through an unknown molecular mechanism. Our aim was to investigate methuosis, and to study whether GPR18 activation was involved or even responsible for this effect.

(iii) A screening assay for connexin-43 modulators, previously established by our group, was to be optimized and applied to screen for activators and inhibitors.

Thus, this work set out to expand the toolbox of assays and of potent and selective ligands for investigating three poorly studied membrane proteins, MRGPRX4, GPR18, and connexin-43.

4 RESULTS AND DISCUSSION: MRGPRX4

4.1 MANUSCRIPT: RADIOLIGAND BINDING ASSAY

The following manuscript was prepared in the scope of this thesis. The author performed the experiments (excluding synthesis and part of the cell-based assays) and has written the manuscript (excluding synthesis) in close cooperation with Prof. Dr. Christa E. Müller.

Design, synthesis, and characterization of a radioligand for specific labeling of the MAS-related G protein coupled receptor X4 (MRGPRX4)

Robin Gedschold, Daniel Marx, Sophie Clemens, Yvonne Riedel, Ghazl Al-Hamwi, Beatiz Bueschbell, Jörg Hockemeyer, Christa E. Müller

Introduction

The MAS-Related G protein coupled receptor X (MRGPRX) subfamily are primate-specific receptors which have recently emerged as interesting targets for drug development.[45; 50] The MRGPRXs are orphan receptors, without direct rodent orthologues identified.[45] MRGPRX4 is proposed to play a role in cancer growth, migration, itch, and pain transmission.[45; 64; 73; 77] It is found to be primarily Gαq protein coupled and to recruit β-arrestin upon activation. Several natural receptor variants are known. One of which, inhabiting the point mutation S83L, was shown to substantially impact potency of identified MRGPRX4 ligands.[75] [REF pending] In the past, this rare variant was assumed as wild-type, making interpretation of literature data difficult.[45; 75] [REF pending]

The expression of MRGPRX4 was originally assumed to be restricted to small-diameter dorsal root ganglia and trigeminal ganglia.[50; 51; 54] Later on, MRGPRX4 expression was detected in various human tissues including keratinocytes, CD[8+] cytotoxic T cells, and several cancers.[65; 69–71; 73] While in some cancer samples, high expression levels of MRGPRX4 were found, other samples of the same cancer type did not show any expression.[70; 72] MRGPRX4 was identified as one of 15 mutation hot spots in colon cancer, emphasizing its role in cancer development.[73] In keratinocytes, MRGPRX4 expression was upregulated upon stimulation with the toll-like receptor agonist poly(I:C), implying a role in inflammation.[65]

MRGPRX4 is still an orphan G protein coupled receptor (GPCR) since its cognate agonist remains unknown. Nonetheless, several endogenous and synthetic agonists and have been described. Various bile acids were found to activate MRGPRX4 at high concentrations and have been proposed to elicit MRGPRX4-dependent itch.[76; 77; 79] Deoxycholic acid was the most potent bile acid, displaying micromolar potency at MRGPRX4.[76; 77] Nateglinide was identified as a synthetic ligand for the minor MRGPRX4 83L variant. It served as a lead structure to develop the more potent agonist MS47134, which, however, can only weakly activate the main MRGPRX4-83S variant.[74; 75] (-)-Menthol was identified as a modulator of MRGPRX4-83L. It decreased the efficacy of nateglinide to recruit β-arrestin, but did not affect G protein coupling.[86] Recently, we published on a novel class of MRGPRX4 agonists, based on a xanthine
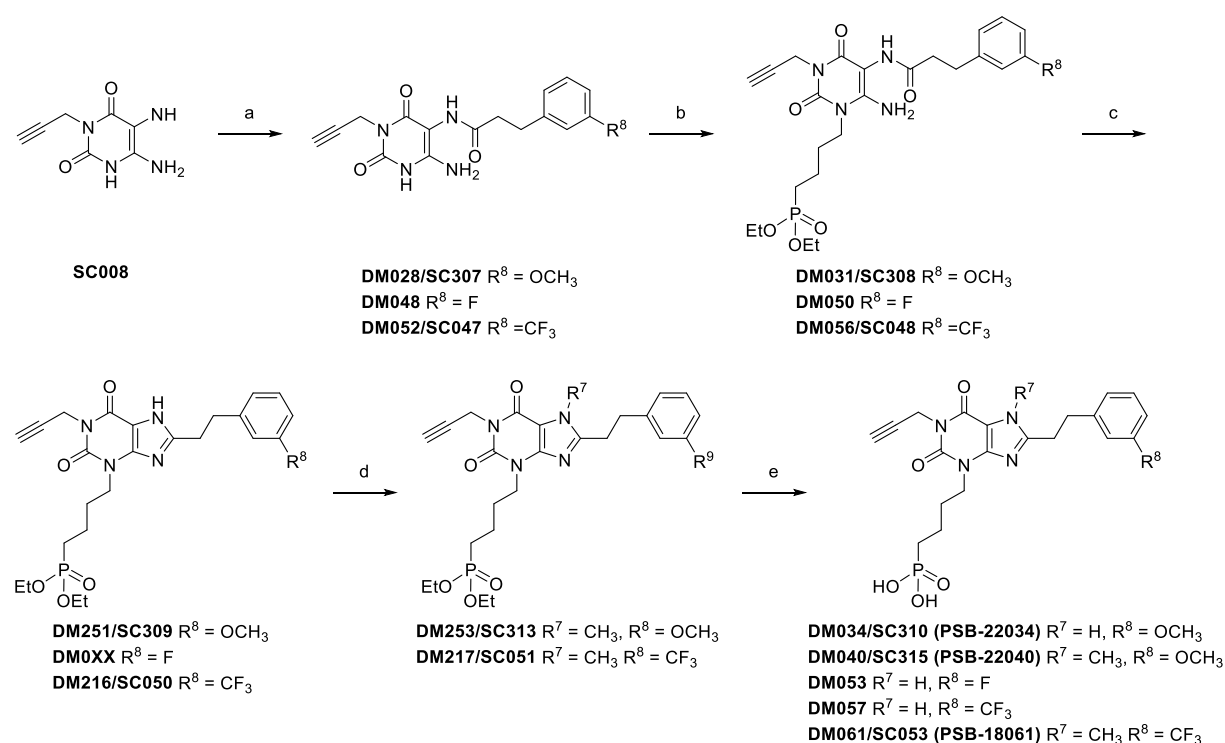
scaffold, which represent the most potent MRGPRX4 agonists at the major receptor variant 83S described to date.[REF pending]

Several functional assays have been developed to characterize MRGPRX4 ligands, including β-arrestin recruitment and calcium mobilization assays.[68; 75–77][REF pending] These assays, measuring downstream signaling events, depend on a variety of parameters, e.g., expression level and signal amplification. To measure direct receptor-ligand interactions binding studies are indispensable. In the present study, we designed, synthesized, and characterized a tritium-labeled radioligand for MRGPRX4 providing a unique tool to study this poorly investigated potential drug target.

Results and discussion

The recently published agonists based on a xanthine scaffold were investigated for their possibility to create a radioligand.[REF pending] The lead compounds PSB-22034 and PSB-22040 were close to, but not ideal, to the needed potency a radioligand should possess. Therefore, we set out to optimize the potency of the xanthine derivatives with minor structural variations. A small number of derivatives with different *meta*-aryl substitutions were synthesized, as this moiety was not studied yet (see Scheme 1 for synthesis and Table 1 for biological data).

Scheme 1. Synthesis of xanthine derivatives differing in their meta-aryl substitution[a]

SC008

DM028/SC307 R^8 = OCH$_3$
DM048 R^8 = F
DM052/SC047 R^8 = CF$_3$

DM031/SC308 R^8 = OCH$_3$
DM050 R^8 = F
DM056/SC048 R^8 = CF$_3$

DM251/SC309 R^8 = OCH$_3$
DM0XX R^8 = F
DM216/SC050 R^8 = CF$_3$

DM253/SC313 R^7 = CH$_3$, R^8 = OCH$_3$
DM217/SC051 R^7 = CH$_3$ R^8 = CF$_3$

DM034/SC310 (PSB-22034) R^7 = H, R^8 = OCH$_3$
DM040/SC315 (PSB-22040) R^7 = CH$_3$, R^8 = OCH$_3$
DM053 R^7 = H, R^8 = F
DM057 R^7 = H, R^8 = CF$_3$
DM061/SC053 (PSB-18061) R^7 = CH$_3$ R^8 = CF$_3$
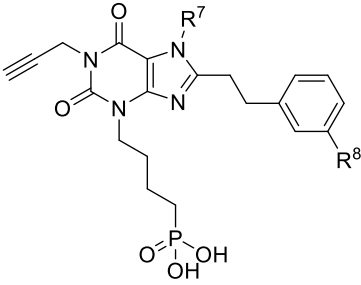
[a]Reagents and conditions: (a) carboxylic acid derivative, COMU, DIPEA, DMF, rt, 10 min (b) diethyl (4-iodobutyl)phosphonate, K$_2$CO$_3$, DMF, 55 °C, 12 h; (c) 2N NaOH, 90 °C, 30 min, 37% HCl; (d) CH$_3$I, K$_2$CO$_3$, DMF, rt, 2 h; (e) TMSBr, CH$_2$Cl$_2$, rt, 16 h, 2N NaOH, 37% HCl. COMU: (1-cyano-2-ethoxy-2-oxoethylidenaminooxy)dimethylamino-morpholino-carbenium-hexafluorophosphate; DIPEA: *N,N*-diisopropylethylamine; DMF: *N,N*-dimethylformamide; TMSBr: trimethylsilyl bromide.

The replacement of the *m*-methoxy by a *m*-fluoro residue led to a reduced potency (PSB-22034 = 11.2 nM vs. DM053 = 63.1 nM). The introduction of *m*-trifluromethyl was superior to the *m*-fluoro residue, however not to the lead with an *m*-methoxy

substitution (DM057 = 38.2 nM). The introduction of a methyl in $N7$, which was not beneficial for a m-methoxy derivative, was an improvement in potency for the m-trifluromethyl derivative by about 10-fold (PSB-18061 = 3.17 nM).

Table 1. Biological data and structures of different xanthine agonists at the main and minor variant of MRGPRX4.

			MRGPRX4-83S (main variant)		MRGPRX4-83L (minor variant)	
			$EC_{50} \pm SEM$ (nM)[a]			
Compd.	R^7	R^8	Ca^{2+} assay[b]	β-Arrestin assay[c]	Ca^{2+} assay[d]	β-Arrestin assay[e]
PSB-22034[REF]	H	OCH_3	**11.2** ± 1.3	**32.0** ± 1.2	**435** ± 78	**5,710** ± 1,230
PSB-22040[REF]	CH_3	OCH_3	**19.2** ± 3.5	**30.0** ± 5.8	**333** ± 7	**6,280** ± 1,380
DM053	H	F	**63.1** ± 18.6	**33.9** ± 5.1	**601** ± 103	**7,940** ± 1450
DM057	H	CF_3	**38.2** ± 10.9	**20.5** ± 2.4	**267** ± 66	**11,900** ± 1800
PSB-18061	CH_3	CF_3	**3.17** ± 0.6	**2.28** ± 0.16	**32.4** ± 5.6	**370** ± 50

aData are means of at least three independent experiments performed in duplicates. bLN229 glioblastoma cells naturally expressing MRGPRX4-83S. cCHO-β-arrestin-MRGPRX4-83S cells. d1321N1 astrocytoma recombinantly expressing the MRGPRX4-83L. eCHO-β-arrestin- MRGPRX4-83L cells.

PSB-18061 was subsequently tested for selectivity on the related MRGPRX1, MRGPRX2, and MRGPRX3 receptor (Figure 8). The same β-arrestin recruitment assays were employed, and no activation or inhibition of the receptors was measured by addition of 10 μM PSB-18061.
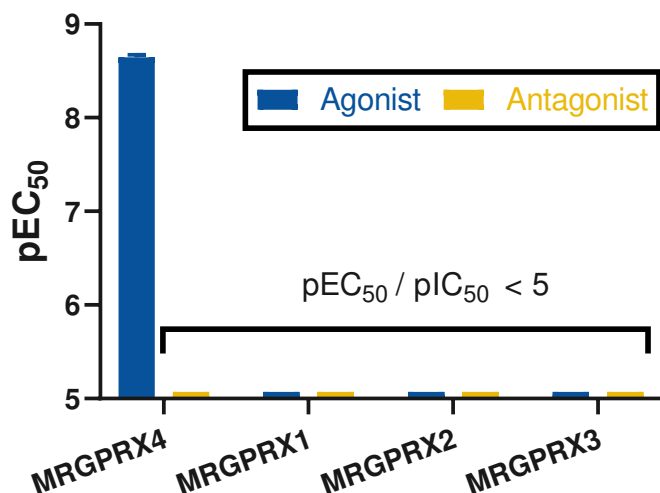
Figure 8. Selectivity study of PSB-18061 on the related MRGPRX receptors in β-arrestin recruitment assays based on β-galactosidase complementation. Results are means ± SEM of three independent experiments performed in duplicates. Antagonist screening tested against 8.5 μM BAM-22P (MRGPRX1), 0.7 μM CST-14 (MRGPRX2), 10 μM TH294 (MRGPRX3).

PSB-18061 showed similarly high potency in calcium mobilization and β-arrestin recruitment assays, combined with selectivity over the other MRGPRX subtypes. After these compelling results, PSB-18061 was selected as a candidate to be synthesized in a tritium-labeled form by the introduction of a tritium-labeled methyl at position *N*7.

Radioligand synthesis

The introduction of a tritium labeled methyl is a frequently used method that could be easily introduced into our synthesis scheme (Scheme 1). The methylation of *N*7 could be performed as final step, minimizing the hazard of synthesis with radiolabeled compounds. By this means we aimed to obtain [^{3}H]PSB-18061 (see Scheme 2).

Scheme 2. Synthesis of [³H]PSB-18061[a]
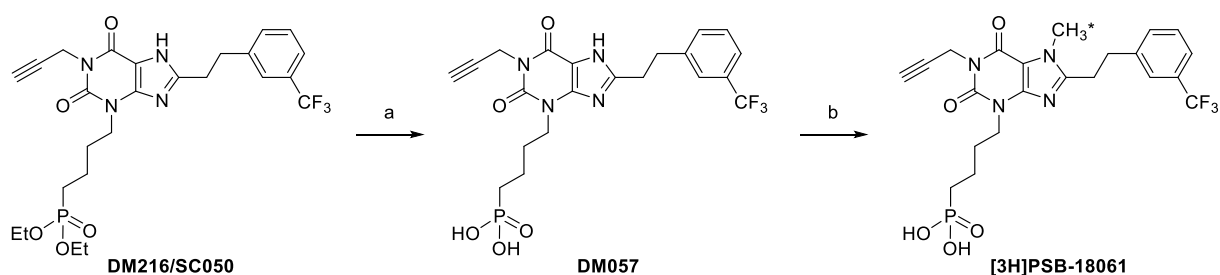
[a]Reagents and conditions: (a) TMSBr, CH₂Cl₂, rt, 16 h, 2N NaOH, 37% HCl; (b) [³H]methyl nosylate, K₂CO₃, DMF. * denotes position of radiolabel.

A radiochemical purity of 98.8% was determined by HPLC assessment detecting UV-absorption at 280 nm and homogenous radiochemical detection. The chemical identity of [³H]PSB-18061 was proven, by co-chromatographs with unlabeled PSB-18061 in the same chromatographic system. The measured mass spectrum is consistent with the proposed structure of [³H]PSB-18061 and the non-labelled reference PSB-18061. The specific activity was determined by mass spectrometry to 2.44 TBq/mmol (66 Ci/mmol). The radiochemical concentration of [³H]PSB-18061 in ethanol comprised 37 MBq/mL (1.0 mCi/mL).

Using this tool compound, we developed a filtration binding assay utilizing a membrane preparation of genetically engineered HEK-293 cells which overexpress the main variant (83S) of MRGPRX4.

Assay development

Initial experiments, performed at room-temperature (RT), indicated a relatively high binding of the radioligand to the glass fiber filters. Thus, we investigated various filter types, differing in thickness and pore size, to optimize the ratio of nonspecific to specific binding. The lowest filter binding was observed for GF/A glass fiber filters (Figure 9A). This is likely due to GF/A being thin filters with relatively big pores, resulting in a low surface area that the radioligand can adhere to. Different supplements added to the rinsing buffer or the use of filter preincubation buffer was tested. The addition of 0.1% bovine serum albumin (BSA) and 0.1 % Tween20, was

optimal (Figure 9B). A pH shift to 8.0 or the addition of EDTA did not reduce filter binding further.
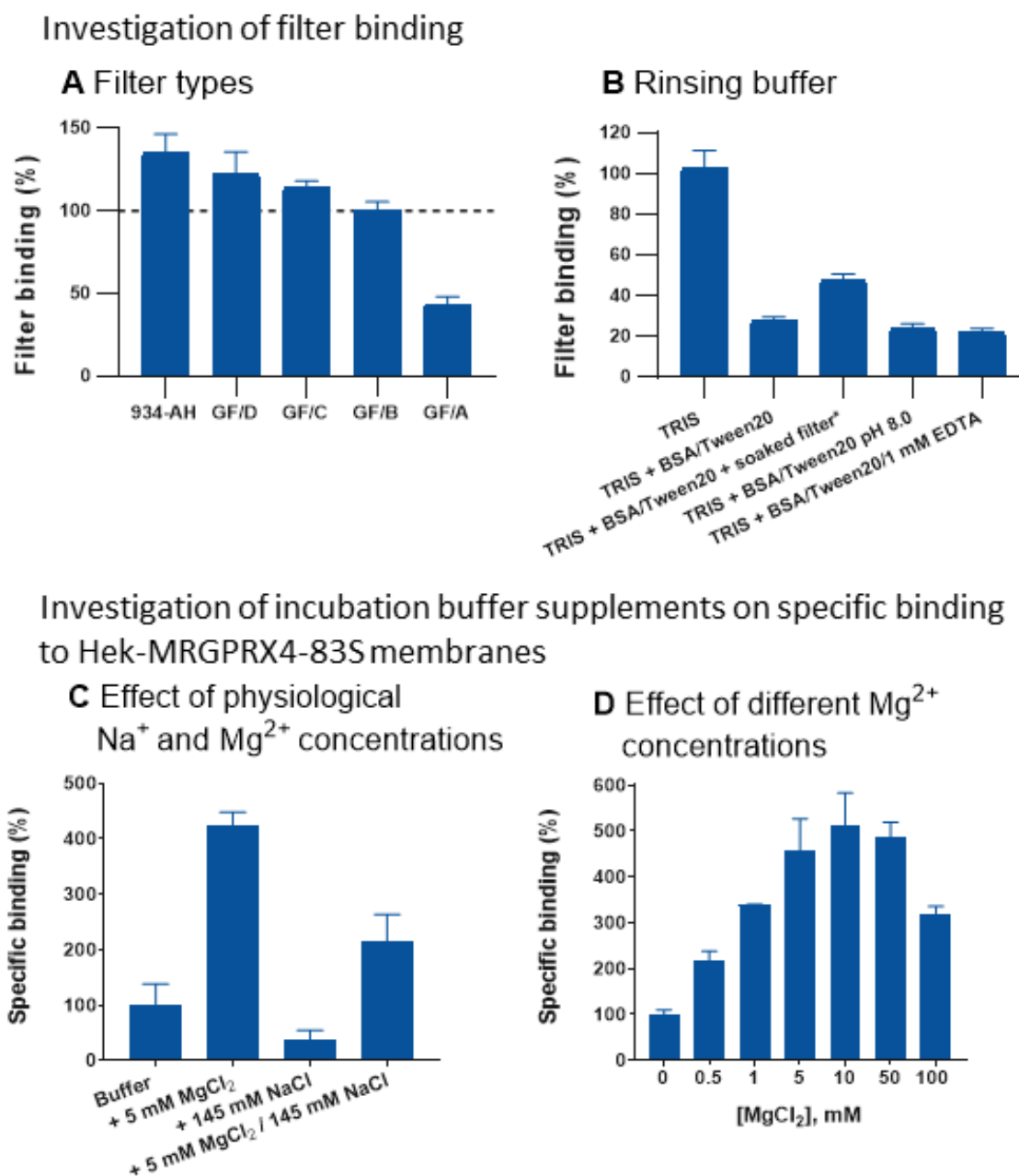
Figure 9. Optimization of ratio of specific to nonspecific binding of 1nM [^{3}H]PSB-18061 performed at RT. **A.** The radioligand was rinsed on respective filters with TRIS (pH 7.4) + 0.1 % BSA / 0.1% Tween20. Results are normalized to GF/B. **B.** The radioligand was rinsed on GF/A filters with the indicated rinsing buffers. *Filter was presoaked in 10 mM EDTA for 30 minutes. Results are normalized to TRIS (pH 7.4) **C/D.** The radioligand was incubated for 1 h with membrane preparation of HEK-MRGPRX4-83S. Optimized conditions to reduce filter binding were used. Results are normalized to buffer (100%).

Using GF/A filters and rinsing buffer supplemented with 0.1% BSA and 0.1% Tween20, the specific binding of HEK-MRGPRX4 membrane was around 25% of total binding. In the next step, the incubation buffer was supplemented with physiological concentrations of NaCl and $MgCl_2$, alone and in combination (Figure 9C). Magnesium (5 mM) was found to increase specific binding by around 4-fold. Sodium chloride (145 mM), on the other hand, decreased specific binding to nearly third. Subsequently, different $MgCl_2$ concentrations and an optimum of specific binding was achieved at 10 mM (Figure 9D). The optimized conditions, using 10 mM $MgCl_2$ in a TRIS incubation buffer, and filtration through GF/A glass fiber filters with TRIS rinsing buffer supplemented with 0.1% BSA and 0.1% Tween20, resulted in a specific binding of around 50% using HEK-MRGPRX4 membrane preparation (50 µg protein). Increasing the protein amount to 100 µg led to a further increase in specific binding of around 67% of total binding, which can be envisaged as suitable for radioligand binding assays.

Different native and genetically engineered cell lines were compared for their specific binding of the radioligand, in order to identify an optimal protein source. Recently, we had identified LN229 glioblastoma cells to natively express MRGPRX4-83S.[Xanthine REF] The specific binding to an LN229 membrane preparation, however, was found to be unsatisfactory (Figure 10). Subsequently, MRGPRX4-83S was cloned into the retroviral expression vector pQCXIP to transfect GP+envAM12 packaging cells. The harvested viruses were used to stably transfect LN229 and HEK-293 with the human MRGPRX4-83S. Moreover MRGPRX4-83S was cloned into the vector pCDNA5 to transiently transfect CHO-suspension (CHO-S) cells. Membrane preparations of the created LN229-MRGPRX4, HEK-MRGPRX4, and CHO-S-MRGPRX4 showed increased specific binding compared to non-transfected cells, with highest levels observed for HEK-MRGPRX4 cells. Membrane preperations of native HEK-293 cells did not show a statistically significant specific binding while binding to membranes of native LN299 glioblastoma cells was small but significant (evaluated by multiple t-test). Now, as the optimal protein source was found, saturation experiments were performed.
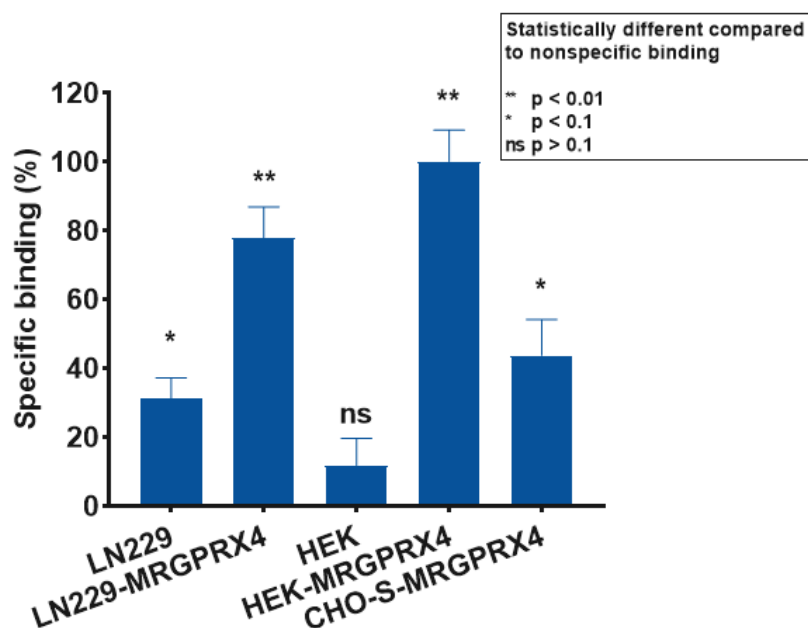
Figure 10: Binding of [^{3}H]PSB-18061 to different cell membrane preparations. The respective membrane preparation (50 µg protein) was incubated with 1 nM of radioligand using the optimized assay settings. Data points are normalized to HEK-MRGPRX4 (100%).

Saturation experiments

Binding of the radiotracer to HEK-MRGPRX4 membrane preparations was found to be saturable (Figure 11). Three independent experiments performed in duplicates revealed a K_d value of 4.69 ± 0.87 nM and a B_{max} value of 267 ± 30 fmol/mg of protein. The nanomolar K_d value is in agreement with the potencies determined in functional assays (EC_{50} = 3.17 nM in calcium mobilization assays).
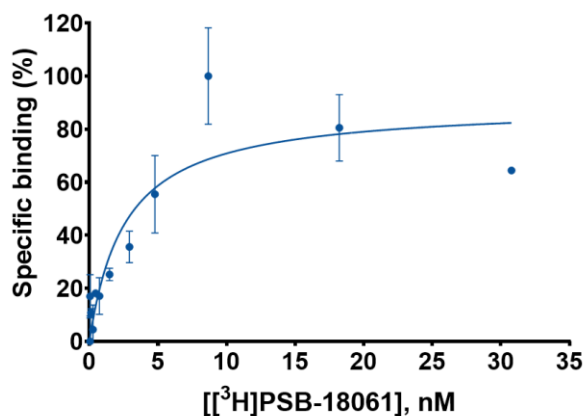
Figure 11: Representative experiment of saturation of [^{3}H]PSB-18061 on HEK-MRGPRX4 membrane preparation. Three experiments were performed in duplicates. Radioligand was added to the membrane preparation (50 µg of protein) in the presence of 1 µM of cold ligand or DMSO, ant the mixture was incubated for 60 min. Then, the mixture was filtered through GF/B filters and washed with 50 mM TRIS buffer supplemented with 0.1% BSA and 0.1% Tween20. The means of three independent experiments resulted in a K_d value of 6.18 ± 1.41 nM, and a B_{max} value of 267 ± 30 fmol/mg of protein.

Kinetic studies

Binding kinetics of the radioligand were determined at room temperature. Association experiments revealed a fast association of the radiotracer ($t_{1/2}$ = 4.34 ± 0.41 min; Figure 12A.). Subsequently performed dissociation experiments showed reversible binding, revealing a residence time (τ) of 16.5 minutes ($t_{1/2}$ = 11.5 ± 0.7 min; Figure 12B.). The residence time is measure for the mean duration, a ligand persists at the binding pocket (calculated as $1/K_{off}$).[110] A K_{on} value of $1.02*10^8$ mol^{-1} min^{-1} and a K_d value of 0.597 nM was calculated from the kinetic parameters.
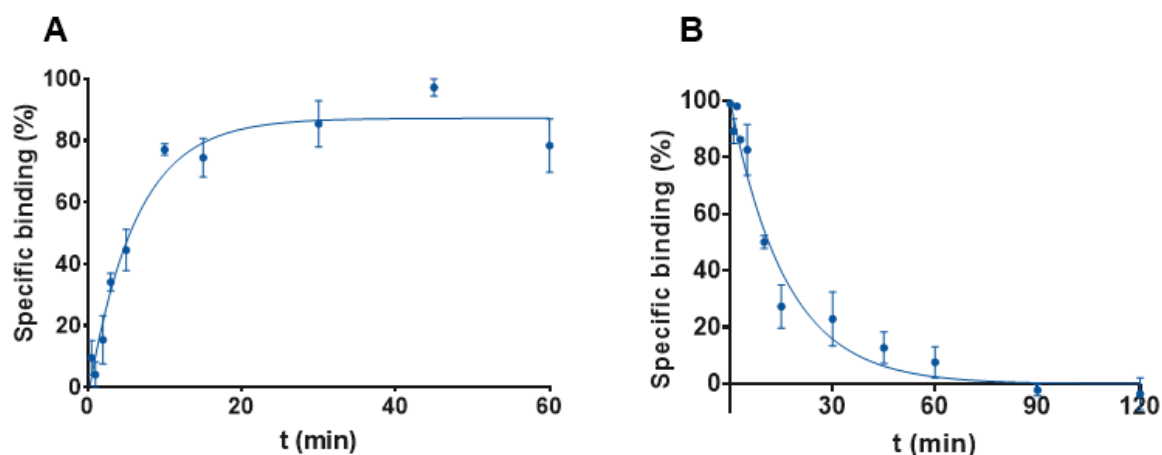
Figure 12. Binding kinetics of [^{3}H]PSB-18061 using HEK-MRGPRX4 membrane preparation. Data points represent three independent experiments performed in duplicates. **A.** Association experiments. Radioligand (1 nM) was incubated with membrane preparation of HEK-MRGPRX4-83S (50 µg of protein). After the respective incubation time, the suspension was filtered through GF/B filters with 50 mM TRIS supplemented with 0.1% BSA and 0.1% Tween20. The calculated values were $t_{1/2}$ = 4.34 ± 0.41 min and K_{obs} = 0.163 ± 0.015. **B.** Dissociation experiments. Radioligand (1 nM) was pre-incubated with membrane preparation of HEK-MRGPRX4-83S (50 µg protein) for 30 minutes. Subsequently it was supplemented with 1 µM cold ligand or DMSO. After the respective incubation time, the mixture was filtered through GF/B filters with 50 mM TRIS supplemented with 0.1% BSA and 0.1% Tween20. The

calculated values are $t_{1/2} = 11.5 \pm 0.7$ min, $K_{off} = 0.0609 \pm 0.0036$ min^{-1}, and $\tau = 16.5 \pm 1.0$ min.

Competition binding experiments

HEK-MRGPRX4 and native LN229 membrane preparations were used for homologous competition studies. HEK-MRGPRX4 membranes revealed a K_d value of 0.761 ± 0.346 nM for the unlabeled ligand PSB-18061 and a B_{max} value of 245 ± 19 fmol/mg of protein (Figure 13A.). The K_d value is in agreement with the kinetic K_d value. At LN229 membranes preperations, a K_d value of 3.62 ± 1.04 of the unlabeled ligand PSB-18061 and a B_{max} value of 79 ± 3 fmol/mg of protein was calculated (Figure 13B.). The low B_{max} is in line with the low specific binding (Figure 10), what is expected for a native cell line without any overexpression.
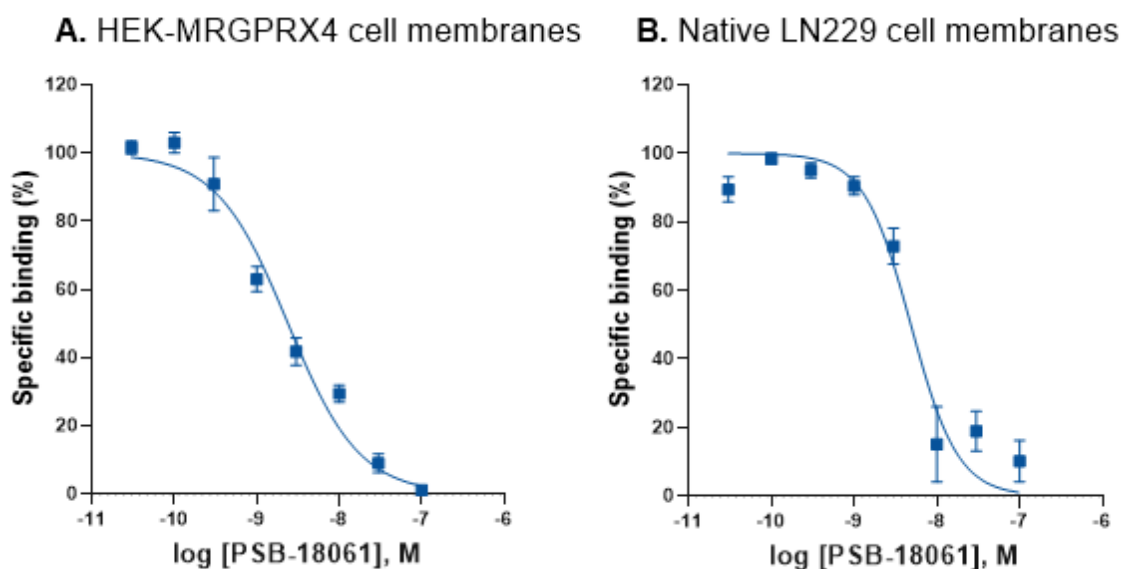
Figure 13: Homologous competition binding experiments. Data point represents three independent experiments performed in duplicates. **A.** HEK-MRGPRX4 membrane preparation (50 μg of protein) was incubated with 1 nM of [^{3}H]PSB-18061 in the presence of 10 mM MgCl$_2$ in TRIS buffer (50 mM, pH 7.4) at RT. After 1 h of incubation, the mixture was filtered through GF/A filters and rinsed with TRIS pH 7.4 containing 0.1% BSA and 0.1% Tween20. A K_d value of 0.761 ± 0.346 nM and B_{max} value 245 ± 19 fmol/mg of protein were determined. **B.** LN229 membrane preparation (30 μg of protein) were incubated with 1 nM [^{3}H]PSB-18061 in the presence of 10 mM MgCl$_2$ in TRIS buffer (50 mM, pH 7.4) at RT. After 1 h of incubation the mixture was filtered through GF/A filters and rinsed with TRIS pH 7.4 containing 0.1% BSA and 0.1% Tween20. A K_d value of 3.62 ± 1.04 nM and B_{max} value of 79 ± 3 fmol/mg of protein were determined.

Next, the radioligand was used for competition binding experiments with various MRGPRX4 ligands (see Figure 14A). All tested ligands displace the radioligand fully. Deoxycholic acid and MS47134 have previously been described as weakly potent agonists of MRGPRX4. [REF pending] Deoxycholic acid showed a K_i value of 1.29 nM and MS47134 a K_i value of 1.09 nM. The MRGPRX4 modulator (-)-menthol inhibited specific binding of the radioligand with a K_i of 151 nM. For the agonists of the xanthine series PSB-22040, PSB-22034, 30h, and 21d K_i values of 0.931, 5.28, 18.5, and 548 nM were determined respectively. The determined binding affinities (pK_i values) and potencies (pEC_{50} values determined in calcium mobilization assays) correlate well (R^2 = 0.84, Figure 14B).
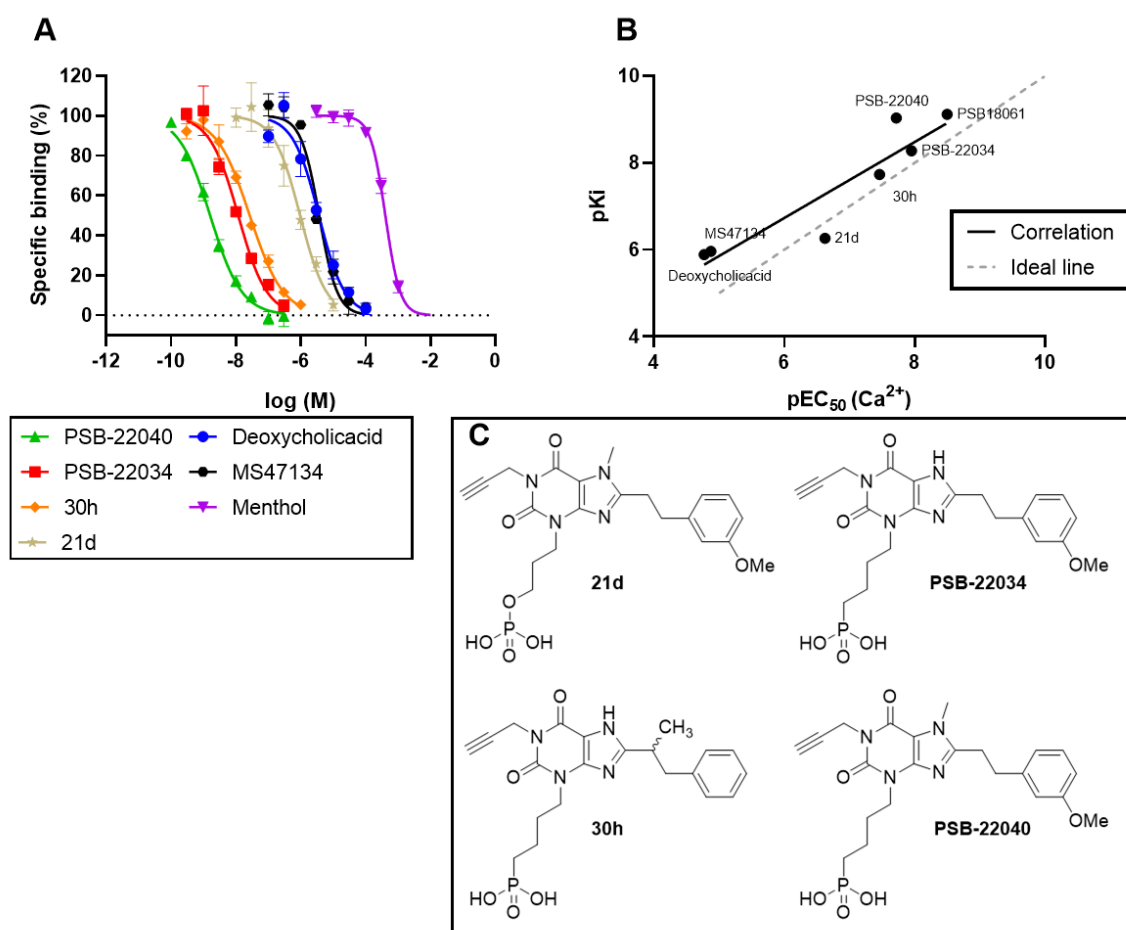
Figure 14: Heterologous competition experiments. **A** Specific binding of 1 nM [³H]PSB-18061 in presence of the respective compounds under optimized assay conditions. Data points represents the mean from at least three experiments performed in duplicates. **B** Correlation of pK_i values (pK_d for PSB-18061) and pEC_{50} values determined in calcium mobilization experiments. **C** Structures of agonists of the xanthine series first published [REF pending].

Conclusion of radioligand studies

The agonist radioligand [^{3}H]PSB-18061 was designed, synthesized, and successfully employed in the first radioligand binding assay for MRGPRX4. The specific binding of the radiotracer was decreased by sodium and enhanced by magnesium. This can be explained by the stabilization of the inactive conformation of class A GPCRs by sodium ions, while divalent cations are known to increase agonist binding.[111; 112] The K_d value of the radioligand is in agreement with the EC_{50} value determined in functional assays of the corresponding unlabeled compound (PSB-18061). The radioligand shows fast association and slower dissociation.

Previous studies suggested MRGPRX4 expression in tumors, which could be confirmed for the glioblastoma cells LN229. The radioligand is well suited tool for further unraveling the badly studied expression pattern of MRGPRX4.

The radioligand was shown to be displaced by previously published agonists, which might indicate binding to the same site. The determined K_i values of the agonists DCA and MS47134 show a low affinity that is well in agreement with their previously determined potencies. The MRGPRX4 modulator (-)-menthol was shown to reduce the specific binding of the radioligand at high concentrations. Kozlitina et al. (2019) showed a signal decrease of nateglinide at the minor MRGPRX4 variant 83L in presence of 300 and 100 μM of (-)-menthol.[86] This is in line with the here presented displacement of the radioligand at 186 μM that was shown for the major MRGPRX4 variant 83S. Albeit these concentrations are exceptionally high, especially as other targets for (-)-menthol are proposed which it modulates with higher potency. E.g. the transient receptor potential channel TRPM8, which is suspected to be responsible for the cooling effect of menthol, is activated by much smaller concentrations down to 0.1 μM of (-)-menthol.[87–89] The determined K_i values of various published MRGPRX4 agonists correlate well with the EC_{50} values obtained by calcium mobilization assays.

We have shown the here introduced radioligand and the established binding assay to be capable to determine binding, and kinetic parameters of the radioligand itself and other MRGPRX4 ligands. This constitutes novel tool for MRGPRX4, a necessity for the better understanding of this scarcely explored orphan GPCR. In future steps it can

help to illuminate the expression of MRGPRX4 in cell lines, and in tissues using autoradiography studies.

Methods

Filtration assay

The total and unspecific binding of the radioligand to protein was determined using a filtration assay. The radioligand (approximately 1 nM, [³H]PSB-18061) was incubated with supplements (10 mM $MgCl_2$ in optimized condition), and excess cold ligand (1 µM, PSB-18061) or DMSO, and the protein source (100 µg protein of HEK-MRGPRX4-83S membrane preparation in optimized condition) in a total volume of 500 µl in TRIS-HCl (pH = 7.4). The protein was added last, and the incubation time was started. After 1.5 h at RT equilibrium is reached and the mixture was filtered through a glass fiber filter (GF/A in optimized condition) using TRIS-HCl supplemented with 0.1% BSA and 0.1% Tween20, with three quick washing steps using approximately 3 ml buffer. The filters were subsequently incubated in scintillation cocktail (LumaSafe®) for 9 h before they were counted in a liquid scintillation counter. The binding was evaluated in counts per minute (CPM) and unspecific binding was subtracted from total binding in order to obtain the specific binding of the radioligand to MRGPRX4-83S.

Saturation experiments

In saturation experiments different concentrations of the radioligand ([³H]PSB-18061) were incubated with 50 µg protein of HEK-MRGPRX4-83S membrane preparation, either with cold ligand (1 µM PSB-18061) or DMSO. After one-hour incubation the samples were filtered through GF/B filters and measured as described above.

Kinetic binding experiments

For association experiments, 50 µg protein of HEK-MRGPRX4-83S membrane preparation was added at several time points to premixed radioligand (approximately 1 nM, [³H]PSB-18061), with DMSO or cold ligand (1 µM, PSB-18061) in TRIS-HCl buffer (pH = 7.4). After the respective incubation time (between 30 seconds and one hour) the mixture was filtered through GF/B filters and measured as

described above. For dissociation experiments the radioligand was pre-incubated with the protein source in TRIS-HCl buffer (pH = 7.4) for 30 minutes. At several time points 1 µM of the cold ligand (PSB-18061) or DMSO was added, and after the respective incubation time (between 30 seconds and two hours) filtered through GF/B and measured as described above.

Competitive binding experiments

The binding affinity of MRGPRX4 ligands was determined in competition binding experiments. Various concentrations of the competitor were mixed with radioligand, supplements, and protein source, filtered, and measured as described above. If applicable the results were normalized to control (DMSO, 100%) and unspecific binding (0%).

4.2 AUTORADIOGRAPHY STUDY

The radioligand [³H]PSB-18061 was employed for autoradiography studies to determine the MRGPRX4 expression in nine different healthy and diseased human tissues (tissues listed in Table 2). Samples from seven different cancerous tissues were collected, each containing healthy probes originating from the same case. Moreover, human brain samples were acquired, originating from two different brain regions from either healthy, or Parkinson or Alzheimer diseased patients. None of the samples showed any significant binding of the radioligand. Exemplary results are presented in Figure 15.

Table 2: Overview of investigated human tissues in the autoradiography studies. Two independent cases (rectal only one) were investigated. Tumor & healthy tissues originate from the same case.

Tissue	Diagnosis
Breast	Tumor & healthy
Colon	Tumor & healthy
Ear nose throat	Tumor & healthy
Kidney	Tumor & healthy
Lung	Tumor & healthy
Rectal	Tumor & healthy
Skin	Tumor & healthy
Medial frontal gyrus	Alzheimer, Parkinson, & healthy
Caudate with putamen	Parkinson & healthy
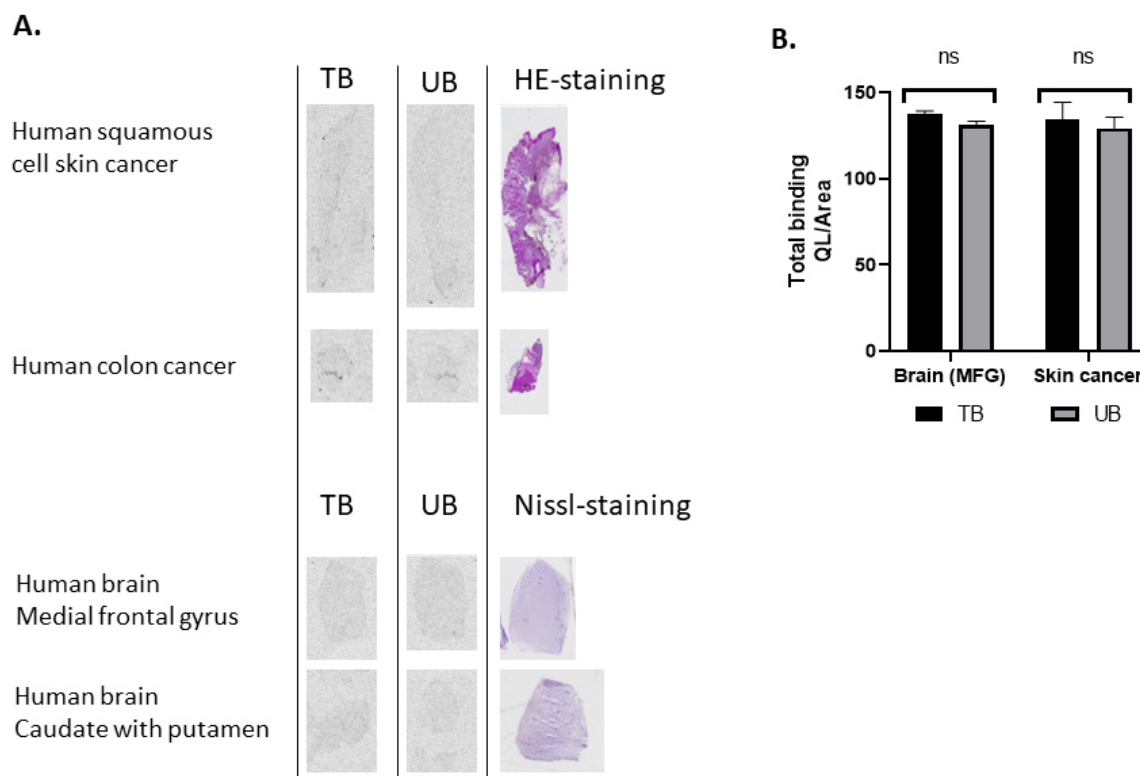
Figure 15: Explanatory autoradiography results. 1.85 nM [^{3}H]PSB-18061 were incubated on tissue slices between 8 and 10 μm thickness for 1 h with or without 10 μM PSB-18061. The experiments were performed in duplicates from two independent cases (except rectal, only one case). **A** Pictures of selected tissues of total binding (TB), unspecific binding (UB) and either Hematoxylin-Eosin(HE)- or Nissl-staining. **B** Evaluation of total binding as grey scale per area (QL/Area) of TB and UB. Multiple t-tests showed no significant differences between specific and unspecific binding. MFG = medial frontal gyrus, skin cancer = human squamous cell skin caner

The performed autoradiography studies of different human samples did not show any binding to any tested tumor or associated healthy tissue, nor in different human brain samples. As previously published results about MRGPRX4 expression are either based on mRNA or were performed in a secondary cell line, e.g., keratinocytes, it is questionable how well it reflects the actual in vitro protein expression. The autoradiography results however illustrate an absence of MRGPRX4 expression in all investigated human tissues. This implies a very restricted expression of MRGPRX4, as it was assumed in original publications where MRGPRX4 was found to be solely expressed in the small diameter dorsal root ganglia (DRGs) and trigeminal ganglia (TG).[51] As MRGPRX4 is primate specific, a specialized role of the receptor can be assumed, which is not needed in non-primate life forms. This would explain the very restricted expression pattern that was shown by these experiments.

4.3 INVESTIGATION OF LITERATURE-KNOWN LIGANDS

Most publications do not specify the amino acid-sequence of the employed receptor, although it is known that the amino acid exchange S83L can greatly influence potency. Therefore, the interpretation of literature is difficult.[75] Consequently, we initially utilized a calcium mobilization assay and a β-arrestin recruitment assay for the major 83S and the minor 83L variant of MRGPRX4 to study reported agonists. Firstly, three different bile acids, and secondly nateglinide and two of its derivatives were investigated. The results, presented in Table 3 are mostly consistent with literature values (for reference see Figure 7).

Table 3: Determined EC_{50} and K_i values of previously published MRGPRX4 agonists. Results are means ± SEM of at least three independent experiments performed in duplicates. DCA = Deoxycholic acid; UDCA = Ursodeoxycholic acid; TDCA = Taurodeoxycholic acid

Name	**Calcium**[a] EC_{50} ± SEM [nM]; efficacy [%]	**β-arrestin**[b] EC_{50} ± SEM [nM]; efficacy [%]	**Radioligand binding**[c] K_i ± SEM (nM)
DCA	**16,900** ± 900; **80** [83S] **11,200** ± 4,100; **62** [83L *]	**1,680** ± 550; **49** [83S] **24,600** ± 8,300; **104** [83L *]	**1,290** ± 200 [83S]
UDCA	**47,500** ± 4,200; **na** [83S] **41,100** ± 651; na [83L]	**3,270** ± 230; **52** [83S] **33,800** ± 14,100; na [83L]	nd
TDCA	**>10,000 (6%)** [83S] **>10,000 (1%)** [83L]	**54,500** ± 20,500; na [83S] **55,700** ± 7,900; na [83L *]	nd
Nateglinide	**>10,000 (0%)** [83S] **198** ± 31; **125** [83L *]	**28,400** ± 10,000; **51** [83S] **4,090** ± 70; **110** [83L *]	nd
ZINC 5295	**>10,000 (1%)** [83S] **126** ± 3; **89** [83L]	**64,100** ± 20,100; **74** [83S] **6,700** ± 4,270; **84** [83L]	nd
MS47134	**13,300** ± 6,100; **79** [83S] **6.56** ± 1.35; **84** [83L]	**3,980** ± 1,980; **75** [83S] **548** ± 60; **70** [83L]	**1,090** ± 60 [83S]

[a]Calcium mobilization assays were performed either using LN229 natively expressing MRGPRX4-83S or 1321N1 astrocytoma cells recombinantly expressing MRGPRX4-83L. Efficacies are normalized to the maximal effect of PSB-18061 (see Figure 20). [b]β-arrestin recruitment assays were performed using CHO-β-arrestin cell lines either expressing MRGPRX4-83S or MRGPRX4-83L. Efficacies are normalized to the maximal effect of PSB-18061 (see Figure 20). [c]Radioligand binding assays performed with 1 nM [³H]PSB-18061 using HEK-MRGPRX4-83S membrane preparation. [83X]= results for the respective MRGPRX4 variant (83S or 83L). *= Data obtained by Yvonne Riedel. na = not applicable, curves did not reach a plateau; nd = not determined. All compounds were tested at multiple concentrations.

In Figure 16 the pEC_{50} values of both variants are plotted against each other. This graph visualizes that the tested bile acids are mostly balanced agonists activating both variants with comparable potency. For nateglinide and its derivatives, the literature-known reduction of activity at the main 83S variant could be reproduced but is more pronounced in the calcium assay.
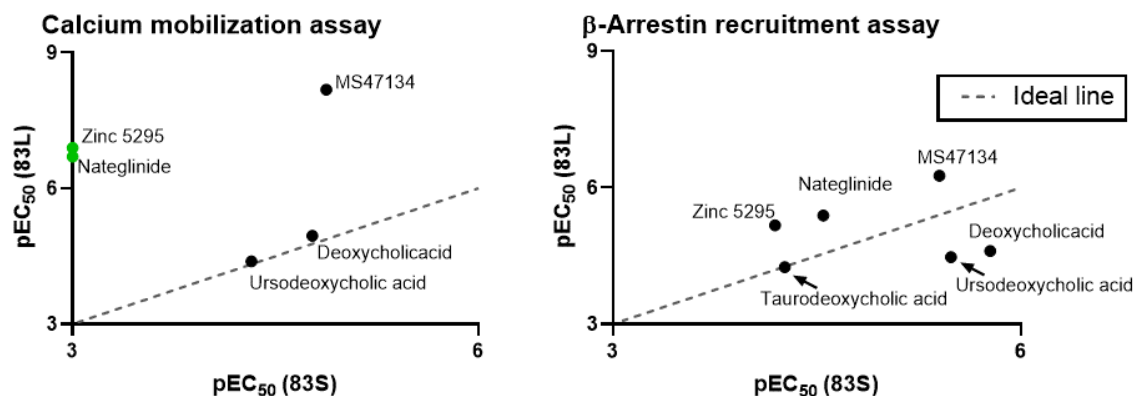
Figure 16: pEC_{50} values of published MRGPRX4 agonists obtained in two different assays on both variants. The ideal line (y=x) represents non-biased potency between the variants. Highlighted in green are compounds that are not active (>10.000 nM) in the calcium assay on the 83S variant.

Concentration dependent activation curves for the nateglinide derivatives ZINC 5295 and MS47134 are presented in Figure 17.
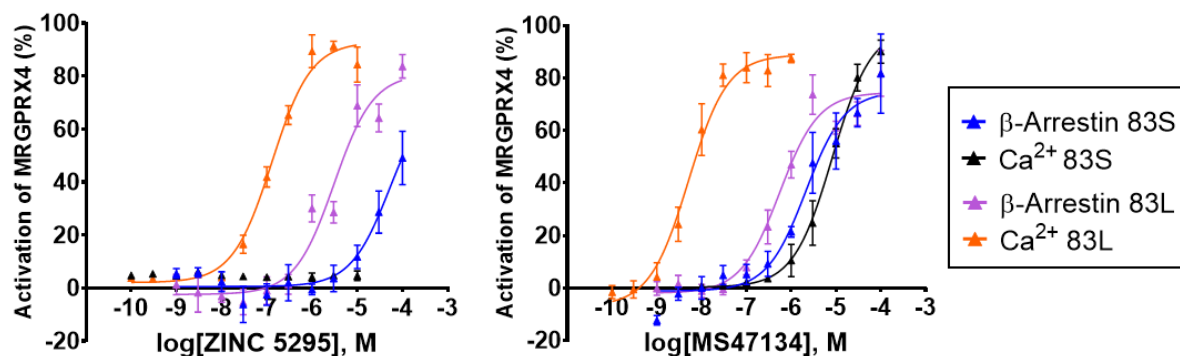
Figure 17: Curves of nateglinide derivatives first published by Cao et al. (2021).[75] Results of β-arrestin recruitment and calcium mobilization assay on the major (83S) and minor variant (83L) are shown. Data points are means ± SEM of at least three independent experiments performed in duplicates normalized to the maximal effect of PSB-18061 (see Figure 18).

4.4 XANTHINE DERIVATIVES

4.4.1 Xanthine derivatives – MRGPRX4 agonists

MRGPRX4 ligands based on the screening-hit MSX-3 were previously optimized resulting in PSB-18061 as the most potent xanthine agonist on the main variant of MRGPRX4 (structures and biological data see Figure 18).

Calcium[a] EC$_{50}$± SEM [nM]	β-arrestin[b] EC$_{50}$± SEM [nM]
460± 13[83S][+] >10,000 [83L][*]	**175± 28**[83S][+] >10,000 [83L][*]

Calcium[a] EC$_{50}$± SEM [nM]	β-arrestin[b] EC$_{50}$± SEM [nM]	Radioligand binding[c] K$_d$± SEM (nM)
1.54± 0.15 [83S] 31.1 ± 1.2 [83L*]	**2.28± 0.16** [83S*] 408± 72 [83L*]	**0.761± 0.346** [83S]
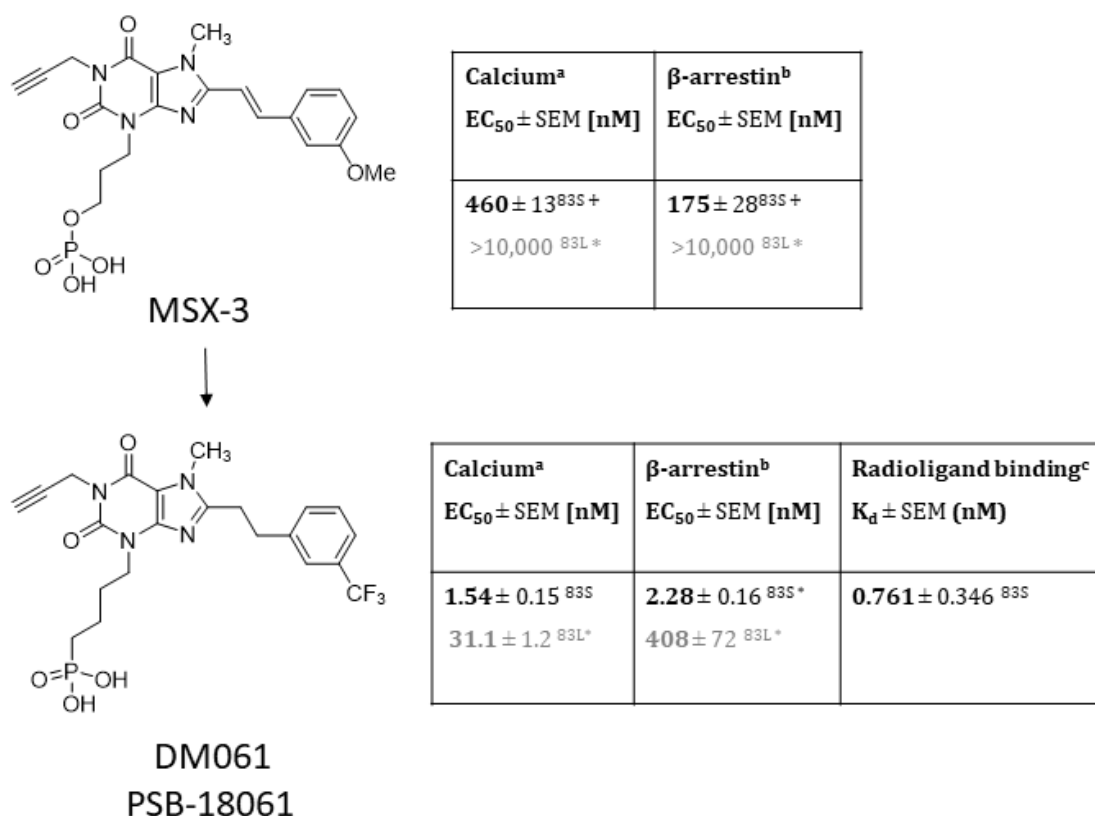
Figure 18: Structure and biological data of screening hit MSX-3 and the optimized PSB-18061. [a]Calcium mobilization assays were performed either using LN229 natively expressing MRGPRX4-83S or 1321N1 astrocytoma cells recombinantly expressing MRGPRX4-83L. [b]β-arrestin recruitment assays were performed using CHO-β-arrestin cell lines either expressing MRGPRX4-83S or MRGPRX4-83L. [c]Radioligand binding assays performed with 1 nM [^{3}H]PSB-18061 using HEK-MRGPRX4-83S membrane preparation. [83X]= results for the respective MRGPRX4 variant (83S or 83L). *= Data obtained by Yvonne Riedel. += Data obtained by Wessam Alnouri. nd = not determined.

This thesis is aimed to further explore the structure-activity relations (SARs) of this class of compounds at MRGPRX4 and to detect compounds with improved potency for MRGPRX4-83S. In Figure 19 the core structure of xanthine derivatives on MRGPRX4 is presented. The respective residues R^3, R^7, and R^8 were the subject of further investigation.
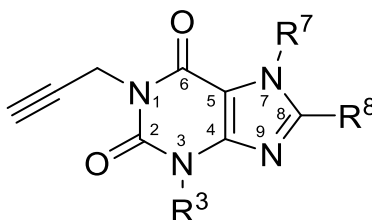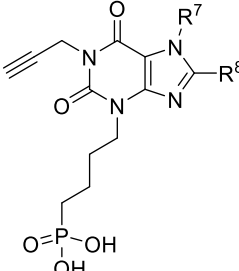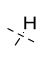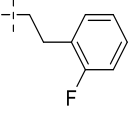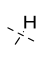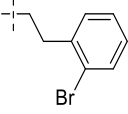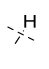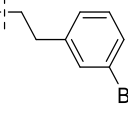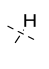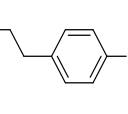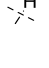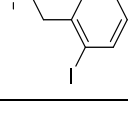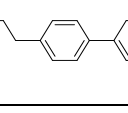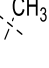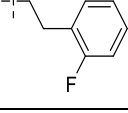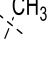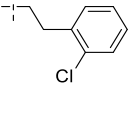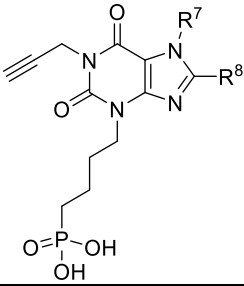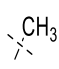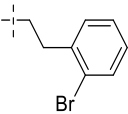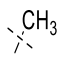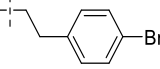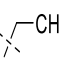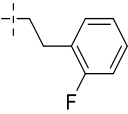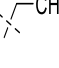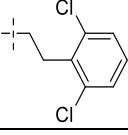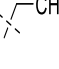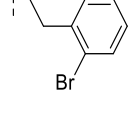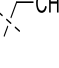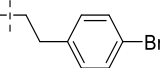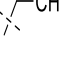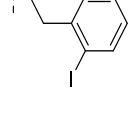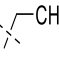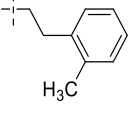

Figure 19: Core structure of the investigated xanthine derivates. For R^3, R^7 and R^8 see Table 4, Table 5, Table 6, Table 7, and Table 8.
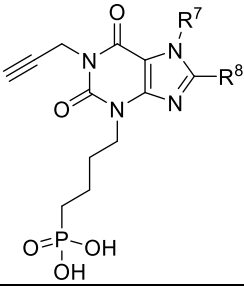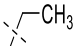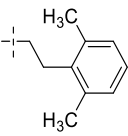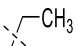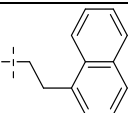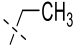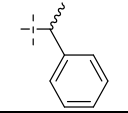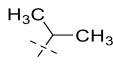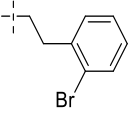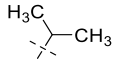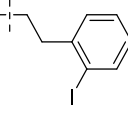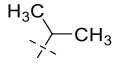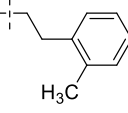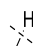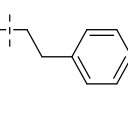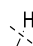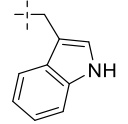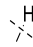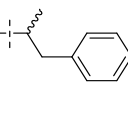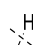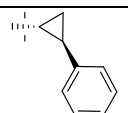
The substitution pattern on the aryl residue and alternatives for the ethyl bridge at C8 were investigated. As previous derivatives were mainly *meta*-substituted, the *ortho-* and *para-* positions were additionally studied (see Table 4). The potency decreased from *ortho-* to *meta-* (**X2** = 0.635 nM vs. **X3** = 4.69 nM). From *meta-* to *para-* the potency did not change (**X4** = 3.68 nM), however, substitutions in *para*-position were found to decrease efficacy in the calcium assay, while the efficacy in β-arrestin assays was retained (e.g., **X4**, **X6**, **X10**, and **X14**). This was exploited for the development of functional antagonists (see chapter 4.4.2). Di-*ortho*-substitution did not result in increased potency (**X17** = 0.543 nM vs. **X16** = 0.441 nM). As their increased molecular weight is expected to be disadvantageous for pharmacokinetic properties, the di-*ortho*-substituted derivatives were not further pursued. Comparison of halides and methyl a group as *ortho*-substituents results in only slight variations in potency, and, moreover, the rank order of potency was dependent on the *N*7 substitution. The *ortho*-substituent is variable but depends on the *N*7-substitution. Omitting any substitution resulted in reduced potency (**X23** = 134 nM). Changing the aryl to a 1-naphthyl residue did not improve potency (**X18** = 0.408 nM). A 3-(1*H*-indole) lead to a loss of potency (**X24** > 10,000 nM). Introduction of a 2-propyl instead of an ethyl group, linking C8 with the aryl moiety, led to an increase in potency (**X25** = 34.5 nM vs. **X23** = 134 nM), and revealed a partial agonistic behavior in the calcium assay. The replacement of the ethyl group to cyclopropane or oxymethyl resulted in a
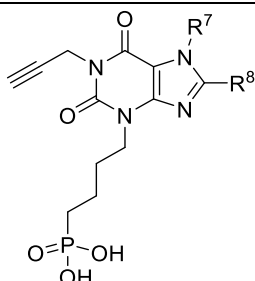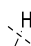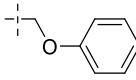
loss of potency (**X26** > 10,000 nM or **X27** > 10,000 nM). Consequently, the ethyl group linking C8 and the aryl moiety showed highest potency while retaining an optimal efficacy.

Table 4: Structures and biological data of xanthine derivatives with different R^8 substitutions at MRGPRX4.

Cmpd.# Internal ID	R^7	R^8	Calcium[a] EC$_{50}$ ± SEM (nM); efficacy (%)	β-Arrestin[b] EC$_{50}$ ± SEM (nM); efficacy (%)	Bias[c]
X1 SC037	H	(2-F-phenethyl)	nd [83S] 1,420 ± 290; (100) [83L]	3.78 ± 0.43; (92) [83S] 8,190 ± 1,810; (98) [83L]	0.8 [83L]
X2 DM366	H	(2-Br-phenethyl)	0.635 ± 0.278; (112) [83S] 22.7 ± 7.2; (114) [83L] *	nd [83S] 243 ± 45; (98) [83L] *	1.1 [83L]
X3 DM115	H	(3-Br-phenethyl)	4.69 ± 1.58; (109) [83S] * 80.8 ± 16.8; (100) [83L] *	3.24 ± 1.16; (110) [83S] * 2,140 ± 850; (103) [83L]*	0.2[βarr] [83S] 1.4 [83L]
X4 SC042	H	(4-Br-phenethyl)	3.68 ± 1.33; (13) [83S] 187 ± 39; (79) [83L]	15.0 ± 3.8; (68) [83S] 2,740 ± 580; (70) [83L]	0.1[βarr] [83S] 1.2 [83L]
X5 SC077	H	(2-I-phenethyl)	0.332 ± 0.104; (99) [83S] 43.1 ± 9.4; (103) [83L]	1.02 ± 0.06; (84) [83S] 381 ± 112; (96) [83L]	0.6[βarr] [83S] 1.1 [83L]
X6 SC256-N7H	H	(biphenyl-ethyl)	34.7 ± 15.3; (13) [83S] nd [83L]	36.7 ± 2.8; (68) [83S] nd [83L]	0.7[βarr] [83S]
X7 SC041	CH$_3$	(2-F-phenethyl)	0.284 ± 0.074; (92) [83S] 39.7 ± 9.6; (62) [83L]	1.48 ± 0.18; (78) [83S] 113 ± 39; (118) [83L]	0.8 [83S] 0.2 [83L]
X8 DM454	CH$_3$	(2-Cl-phenethyl)	0.199 ± 0.049; (114) [83S] 2.23 ± 0.13; (109) [83L] *	1.13 ± 0.43; (73) [83S] 169 ± 60 (114) [83L] *	1.0 [83S] 1.9 [83L]

Cmpd.# Internal ID	R[7]	R[8]	Calcium[a] EC$_{50}$ ± SEM (nM); efficacy (%)	β-Arrestin[b] EC$_{50}$ ± SEM (nM); efficacy (%)	Bias[c]
X9 DM288	CH$_3$	(2-Br-phenethyl)	**0.131 ± 0.04; (116)** 83S 6.35 ± 1.67; (112) 83L *	**0.0575 ± 0.0238; (95)** 83S 93.5 ± 5.4 (132) 83L *	**0.3** βarr 83S 1.1 83L
X10 SC046	CH$_3$	(4-Br-phenethyl)	nd 83S 134 ± 13; (45) 83L	**6.04 ± 0.76; (88)** 83S 2,440 ± 750; (100) 83L	0.9 83L
X11 SC040	CH$_3$	(2-F-phenethyl)	nd 83S 15.5 ± 12.5; (97) 83L	**1.24 ± 0.25; (77)** 83S 262 ± 97; (96) 83L	1.2 83L
X12 SC111	CH$_3$	(2,6-diCl-phenethyl)	**0.363 ± 0.109; (104)** 83S 2.00 ± 0.94; (97) 83L	**0.146 ± 0.033; (110)** 83S 9.02 ± 1.49; (95) 83L	**0.4** βarr 83S 0.7 83L
X13 DM355	CH$_3$	(2-Br-phenethyl)	**0.196 ± 0.054; (127)** 83S 4.26 ± 0.56; (115)83L *	**0.208 ± 0.056; (105)** 83S 25.9 ± 8.9; (144) 83L *	**0.1** 83S 0.7 83L
X14 SC049	CH$_3$	(4-Br-phenethyl)	nd 83S 306 ± 111; (41) 83L	**4.85 ± 2.11; (102)** 83S 521 ± 142; (84) 83L	0.1 βarr 83L
X15 SC078	CH$_3$	(2-I-phenethyl)	**0.983 ± 0.162; (103)** 83S 0.389 ± 0.092; (103) 83L	**0.0937 ± 0.0523; (89)** 83S 87.4 ± 24.2; (94) 83L	**1.0** βarr 83S 2.4 83L
X16 SC181	CH$_3$	(2-CH$_3$-phenethyl)	**0.441 ± 0.157; (111)** 83S nd 83L **Radioligand binding[d] K$_i$ ± SEM (nM): 0.0459 ± 0.0138** 83S	**0.0424 ± 0.0150; (97)** 83S nd 83L	**1.0** βarr 83S
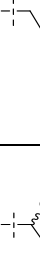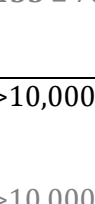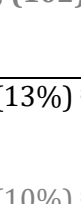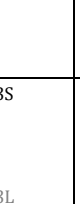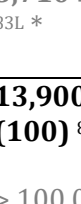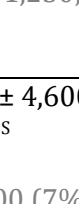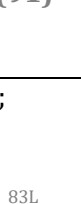
Cmpd.# Internal ID	R[7]	R[8]	Calcium[a] $EC_{50} \pm$ SEM (nM); efficacy (%)	β-Arrestin[b] $EC_{50} \pm$ SEM (nM); efficacy (%)	Bias[c]
X17 SC183			**0.543** ± 0.186; **(113)** 83S nd 83L	**0.0487** ± 0.0201; **(113)** 83S nd 83L	**1.1** βarr 83S
X18 SC294			**0.408** ± 0.141; **(112)** 83S nd 83L	**0.127** ± 0.042; **(77)** 83S nd 83L	**0.3** βarr 83S
X19 SC322			**25** ± 10.2; **(68)** 83S nd 83L	nd 83S nd 83L	
X20 SC095			**0.79** ± 0.262; **(109)** 83S **0.684** ± 0.073; **(108)** 83L	**0.0759** ± 0.0184; **(91)** 83S **13.6** ± 6.1; **(116)** 83L	**0.9** βarr 83S **1.3** 83L
X21 SC124			**1.12** ± 0.1; **(112)** 83S **1.16** ± 0.26; **(118)** 83L	**1.69** ± 0.058; **(96)** 83S **6.85** ± 7.18; **(97)** 83L	**0.3** 83S **0.9** 83L
X22 SC161			**0.984** ± 0.054; **(154)** 83S nd 83L	**0.0705** ± 0.0198; **(102)** 83S nd 83L	**1.0** βarr 83S
X23 Yazh708			**134** ± 17; **(92)** 83S * **3,250** ± 610; **(110)** 83L *	**399** ± 115; **(84)** 83S * > 10,000 (19) 83L *	**0.5** 83S
X24 SC295			>10,000 (1%) 83S nd 83L	**1,210** ± 620; **(40)** 83S nd 83L	
X25 SC297			**34.5** ± 10.7; **(54)** 83S **6,170** ± 980; **(111)** 83L	**27.7** ± 2.7; **(90)** 83S **3,940** ± 840; **(85)** 83L	**0.3** βarr 83S **0.1** βarr 83L
X26 SC300			>10,000 (0%) 83S >10,000 (2%) 83L	> 100,000 (15%) 83S > 100,000 (7%) 83L	
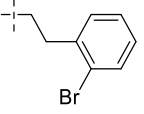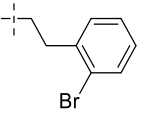
Cmpd.# Internal ID	R[7]	R[8]	Calcium[a] EC$_{50}$ ± SEM (nM); efficacy (%)	β-Arrestin[b] EC$_{50}$ ± SEM (nM); efficacy (%)	Bias[c]
X27 SC268			>10,000 (1%) [83S] >10,000 (10%) [83L]	**1,850** ± 910; **(54)** [83S] >10,000 (1%) [83L]	

[a]Calcium mobilization assays were performed either using LN229 natively expressing MRGPRX4-83S or 1321N1 astrocytoma cells recombinantly expressing MRGPRX4-83L. Efficacies are normalized to the maximal effect of PSB-18061 (see Figure 20). [b]β-Arrestin recruitment assays were performed using CHO-β-Arrestin cell lines either expressing MRGPRX4-83S or MRGPRX4-83L. Efficacies are normalized to the maximal effect of PSB-18061 (see Figure 20). [c]Bias calculated using Equation 1. Calculated as bias towards calcium assays. Values indicated with "βarr" indicate a bias towards the β-Arrestin assay. [D]Radioligand binding assays performed with 1 nM [3H]PSB-18061 using HEK-MRGPRX4-83S membrane preperation. [83X]= results for the respective MRGPRX4 variant (83S or 83L). *= Data obtained by Yvonne Riedel. nd = not determined. All compounds were tested at multiple concentrations.

Next, the R[3] substitution was studied (see Table 5). Exchanging the phosphonate to a carboxylic acid moiety was accompanied by a complete loss of potency (**X32** >10,000 or **X30** >10,000). Similar, a mono-ethyl ester of the phosphonate, compared to the free phosphonate showed a loss of potency (**X29** >10,000 vs. **X24** = 34.5 nM). Comparing homologous compounds with different carbon chain lengths at R[3] (C4 (**X13** = 0.196 nM) > C5 (**X36** = 0.264 nM) > C6 (**X37** = 11.0 nM), reveals a C4 linker to be optimal. In conclusion, the phosphonate function is playing a vital role for MRGPRX4 agonists activity. Any replacement resulted in reduced potency. Consequently, later xanthine derivatives were designed with a phosphonate connected by a C4 carbon chain to *N*3 of the xanthine core structure.

Table 5: Structures and biological data of xanthine agonists with different *N*3 substitutions and different *C*8-aryl connections at MRGPRX4.
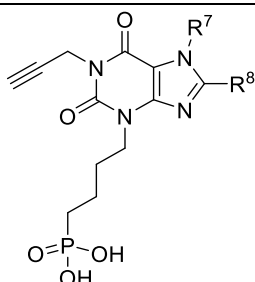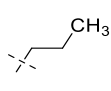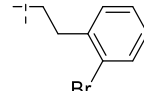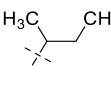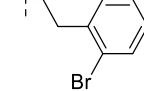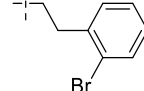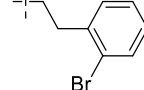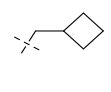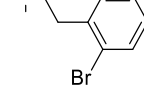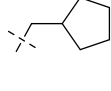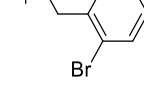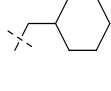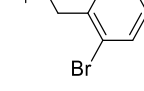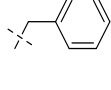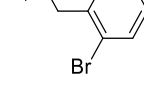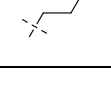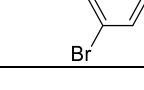
Cmpd.# Internal Id	R3	R7	R8	Calcium[a] EC$_{50}$ ± SEM (nM); efficacy (%)	β-Arrestin[b] EC$_{50}$ ± SEM (nM); efficacy (%)	Bias[c]
X28 DM034 (SC310)	A	H		**11.2** ± 1.3; **(99)** [83S] * **435** ± 78; **(102)** [83L] *	**32.0** ± 1.2; **(110)** [83S] * **5,710** ± 1,230; **(91)** [83L] *	**0.4** [83S] **1.2** [83L]
X29 SC297_ Monoester	B	H		>10,000 (13%) [83S] >10,000 (10%) [83L]	**13,900** ± 4,600; **(100)** [83S] > 100,000 (7%) [83L]	
X30 SC289	C	H		>10,000 (0%) [83S] nd [83L]	**6,720** ± 2,030; **(34)** [83S] nd [83L]	
X31 SC025	D	H		**2.16** ± 0.26; **(52)** [83S] **604** ± 275; **(61)** [83L]	**2.52** ± 0.23; **(70)** [83S] **1,890** ± 280; **(93)** [83L]	**0.1** [βarr 83S] **0.3** [83L]
X32 SC243	E	H		> 100,000 (41%) [83S] nd [83L]	>100,000 (0%) [83S] nd [83L]	
X33 SC088	F	H		**142** ± 28; **(75)** [83S] **57.8** ± 18.9; **(94)** [83L]	**4.72** ± 1.03; **(80)** [83S] **857** ± 220; **(98)** [83L]	**1.5** [βarr 83S] **1.2** [83L]
X34 SC033	D	CH$_3$		nd [83S] **15.5** ± 1; **(113)** [83L]	**0.708** ± 0.122; **(91)** [83S] **1,070** ± 350; **(94)** [83L]	**1.9** [83L]
X35 SC079	F	CH$_3$		**7.9** ± 1.75; **(91)** [83S] **57.8** ± 18.9; **(102)** [83L]	**1.92** ± 0.67; **(77)** [83S] **576** ± 83; **(91)** [83L]	**0.5** [βarr 83S] **1.1** [83L]

Cmpd.# Internal Id	R^3	R^7	R^8	Calcium[a] $EC_{50} \pm$ SEM (nM); efficacy (%)	β-Arrestin[b] $EC_{50} \pm$ SEM (nM); efficacy (%)	Bias[c]
X36 SC030	D	CH_2CH_3	[structure: ethyl-(2-bromophenyl)]	**0.264 ± 0.136; (123)** [83S] **20.1 ± 4.1; (103)** [83L]	**0.226 ± 0.039; (87)** [83S] **534 ± 170; (96)** [83L]	**0.1** [83S] **1.5** [83L]
X37 SC080	F	CH_2CH_3	[structure: ethyl-(2-bromophenyl)]	**11.2 ± 0.0; (89)** [83S] **766 ± 357; (97)** [83L]	**11 ± 0.4; (90)** [83S] **474 ± 152; (98)** [83L]	**0.0** [83S] **0.2** [83L]

[a]Calcium mobilization assays were performed either using LN229 natively expressing MRGPRX4-83S or 1321N1 astrocytoma cells recombinantly expressing MRGPRX4-83L. Efficacies are normalized to the maximal effect of PSB-18061 (see Figure 20). [b]β-Arrestin recruitment assays were performed using CHO-β-Arrestin cell lines either expressing MRGPRX4-83S or MRGPRX4-83L. Efficacies are normalized to the maximal effect of PSB-18061 (see Figure 20). [c]Bias calculated using Equation 1. Calculated as bias towards calcium assays. Values indicated with "[βarr]" indicate a bias towards the β-Arrestin assay. [83X]= results for the respective MRGPRX4 variant (83S or 83L). *= Data obtained by Yvonne Riedel. nd = not determined. All compounds were tested at multiple concentrations.

Finally, different R^7 substituents were investigated. All tested modifications are well tolerated by the receptor (Table 6). Small lipophilic moieties are preferred, as for example methyl is superior to 1-cyclohexylmethyl (**X9** = 0.131 nM vs. **X44** = 0.787 nM). However, polar moieties, such as hydroxyl, amino, or carboxylic acid residues attached via an ethyl, are still tolerated with comparable potency (**X47** = 0.321 nM; **X48** = 1.48 nM; **X49** = 3.05 nM). The bulky 1-(naphthalen-1-ylmethyl) led to a less potent compound than a lipophilic substitution on position R^7 but is still well tolerated (**X50** = 22.7 nM vs. **X4** = 3.68 nM). A 1-(5-phenylpentyl) residue at *N*7 is still tolerated (**X51** = 17.9 nM), indicating that there is still plenty of space in that position, possibly pointing outside the receptor into the extracellular space.

Table 6: Structures and biological data at MRGPRX4 for xanthine agonists with different R^7 substitutions.

Cmpd.# Internal Id	R^7	R^8	Calcium[a] EC$_{50}$ ± SEM (nM); efficacy (%)	β-Arrestin[b] EC$_{50}$ ± SEM (nM); efficacy (%)	Bias[c]
X38 DM358			**0.355 ± 0.046; (117)** [83S] 17.8 ± 6.2; (119) [83L] *	**0.299 ± 0.072; (99)** [83S] 208 ± 49, (176) [83L] *	**0.0** [83S] 0.9 [83L]
X39 SC206			**0.491 ± 0.192; (119)** [83S] nd[83L]	**0.0751 ± 0.0229; (103)** [83S] nd [83L]	**0.8** [βarr] [83S]
X40 SC266			**0.45 ± 0.042; (121)** [83S] nd [83L]	**0.477 ± 0.084; (104)** [83S] 38.3 ± 19.3; (103) [83L]	**0.1** [83S]
X41 DM357			**0.278 ± 0.068; (111)** [83S] 2.02 ± 0.62; (109) [83L] *	**0.553 ± 0.33; (104)** [83S] 89.8 ± 20.9; (163) [83L] *	**0.3** [83S] 1.5 [83L]
X42 SC068			**0.32 ± 0.087; (97)** [83S] 12.7 ± 46; (101) [83L]	**0.298 ± 0.05; (93)** [83S] 85.1 ± 27.9; (99) [83L]	**0.0** [83S] 0.8 [83L]
X43 SC067			**0.588 ± 0.104; (89)** [83S] 89.2 ± 25.5; (84) [83L]	**1.17 ± 0.54; (70)** [83S] 169 ± 23; (87) [83L]	**0.4** [83S] 0.3 [83L]
X44 SC054			**0.787 ± 0.164; (112)** [83S] 25.2 ± 3; (109) [83L]	**4.28 ± 1.83; (84)** [83S] 1,250 ± 410; (95) [83L]	**0.9** [83S] 1.8 [83L]
X45 DM364			**5.72 ± 2.42; (101)** [83S] 5.03 ± 1.59; (103) [83L] *	nd [83S] 59.9 ± 12.8; (176) [83L] *	0.8 [83L]
X46 SC069			**0.095 ± 0.0427; (111)** [83S] 2.28 ± 0.75; (118) [83L]	**0.301 ± 0.021; (84)** [83S] 24.3 ± 3.2; (91) [83L]	**0.6** [83S] 1.1 [83L]

Cmpd.# Internal Id	R[7]	R[8]	Calcium[a] EC$_{50}$ ± SEM (nM); efficacy (%)	β-Arrestin[b] EC$_{50}$ ± SEM (nM); efficacy (%)	Bias[c]
X47 DM365	(2-hydroxyethyl, OH)	(2-bromophenethyl, Br)	**0.321** ± 0.104; **(96)** 83S; 1.86 ± 0.45; (103) 83L *	**0.988** ± 0.471; **(89)** 83S; 32.9 ± 7.5; (124) 83L *	**0.5** 83S; 1.2 83L
X48 SC086	(aminoethyl, NH$_2$)	(2-bromophenethyl, Br)	**1.48** ± 0.4; **(107)** 83S; 79.8 ± 36.7; (102) 83L	**0.932** ± 0.177; **(99)** 83S; 566 ± 106; (93) 83L	**0.2** βarr 83S; 0.9 83L
X49 SC272	(carboxymethyl, OH, O)	(2-bromophenethyl, Br)	**3.05** ± 0.54; **(80)** 83S; nd 83L	**3.1** ± 0.21; **(63)** 83S; nd 83L	**0.1** 83S
X50 SC237	(naphthylmethyl)	(4-bromophenethyl, Br)	**22.7** ± 10.3; **(83)** 83S; nd 83L	**0.542** ± 0.174; **(101)** 83S; nd 83L	**1.7** βarr 83S
X51 SC332	(phenylpentyl)	(2-bromophenethyl, Br)	**17.9** ± 1.2; **(103)** 83S; nd 83L	nd 83S; nd 83L	

[a]Calcium mobilization assays were performed either using LN229 natively expressing MRGPRX4-83S or 1321N1 astrocytoma cells recombinantly expressing MRGPRX4-83L. Efficacies are normalized to the maximal effect of PSB-18061 (see Figure 20). [b]β-Arrestin recruitment assays were performed using CHO-β-Arrestin cell lines either expressing MRGPRX4-83S or MRGPRX4-83L. Efficacies are normalized to the maximal effect of PSB-18061 (see Figure 20). [c]Bias calculated using Equation 1. Calculated as bias towards calcium assays. Values indicated with "βarr" indicate a bias towards the β-Arrestin assay. [83X]= results for the respective MRGPRX4 variant (83S or 83L). *= Data obtained by Yvonne Riedel. nd = not determined. All compounds were tested at multiple concentrations.

In conclusion, we were able to increase the potency of the lead structure PSB-18061 by about 100-fold. Most potent derivative tested in the calcium assay is **X46** (0.095 nM) and in the β-arrestin assay is **X16** (0.0424 nM). **X16** was subsequently tested in the radioligand binding assay, showing a K$_i$ value of 0.0459 ± 0.0138 nM, correlating

well the EC_{50} value determined in the β-arrestin assay. The obtained concentration dependent activation curves are depicted in Figure 20.
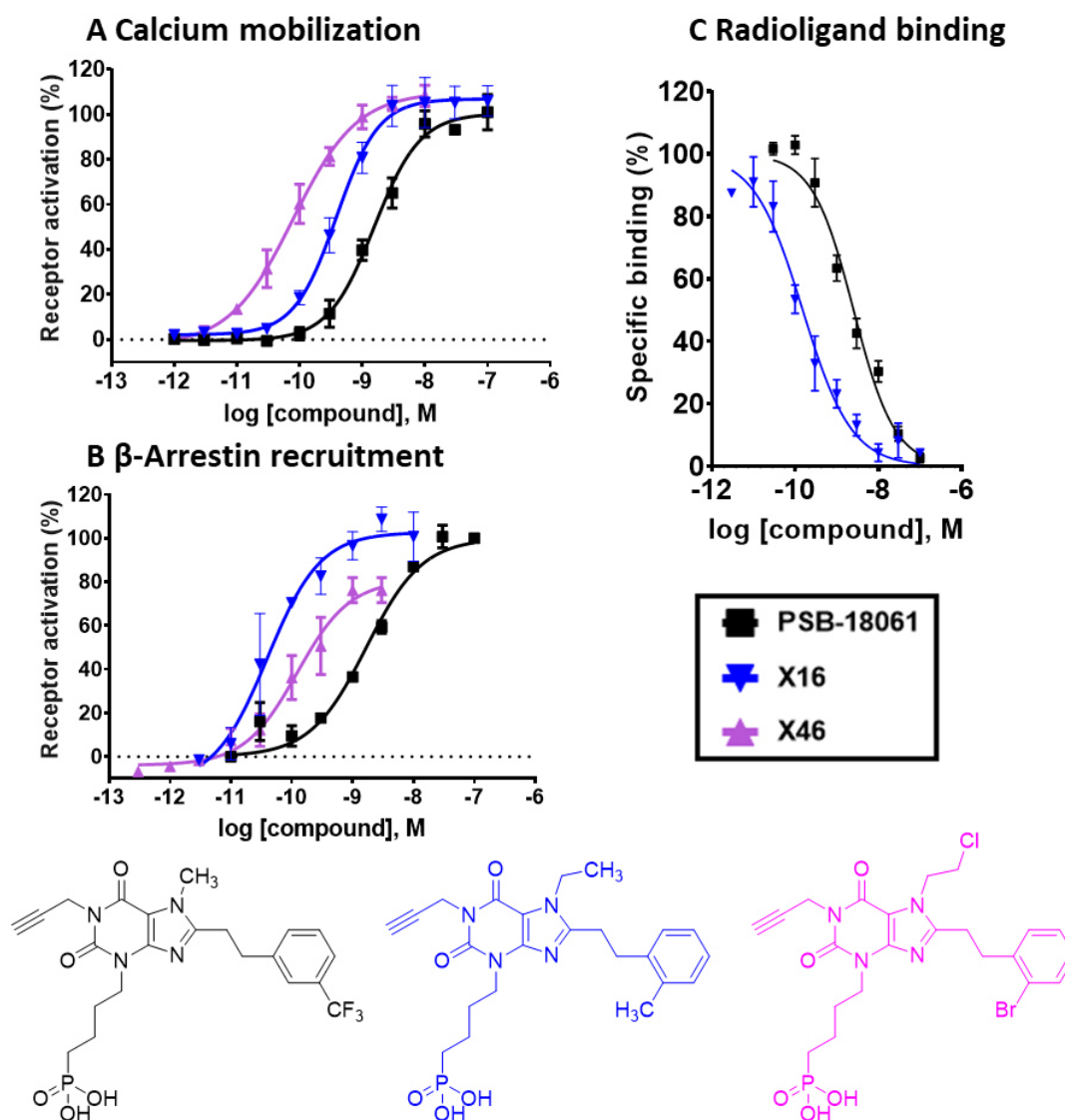
Figure 20: Biological data of the two most potent xanthine agonists and the lead PSB-18061 on MRGPRX4-83S. Data points are means ± SEM of at least three independent experiments performed in duplicates. Efficacies of functional assays are normalized to maximal effect of PSB-18061. **A** Calcium mobilization assays were performed using LN229 glioblastoma cells. **B** β-Arrestin recruitment assays were performed using a CHO-β-Arrestin cell line expressing MRGPRX4-83S. **C.** Radioligand binding assays were performed using 1 nM [³H]PSB-18061 on membrane preparation of Hek-MRGPRX4-83S.

Although the compounds were designed as ligands for the main variant 83S of MRGPRX4, the potency on the minor variant 83L increased as well (see Figure 21).

The implications of the SAR for MRGPRX4-83L deviates only little from the implications drawn from the 83S variant. The linear regression, shown in Figure 21, is nearly parallel to the ideal line, and therefore the potencies on both variants correlate well. The shift towards the x-axis for both assays illustrates the generally increased potency for the main 83S variant over 83L. The xanthine derivatives were, in mean, 40-fold more potent at the 83S variant as determined in calcium mobilization assays, and over 400-fold more potent at the 83S variant as determined in β-arrestin assays. However, single compounds are particularly close to the ideal line, and therefore, relatively favor the 83L variant. Common structural characteristics of these derivatives are an isopropyl moiety at *N*7, found in **X21** or **X20**, and an *ortho*-iodine substituted aryl as in **X21** or **X15**.
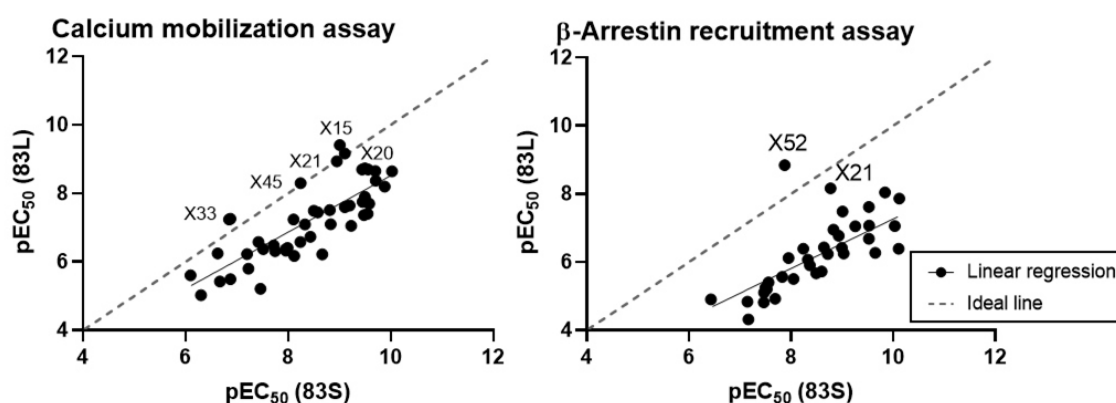
Figure 21: Effect of the amino acid exchange S83L on agonist potencies. pEC_{50} values of xanthine derivatives on both variants are plotted against each other in the respective assays. The ideal line (y=x) represents no effect of the amino acid exchange. Compounds that are potent and particularly close to the ideal line are indicated. Correlation coefficient (R^2) are 0.622 and 0.693 for calcium mobilization and β-arrestin recruitment assays respectively.

4.4.1.1 Biased compounds

GPCR agonists may be biased, either towards G protein activation or towards β-arrestin recruitment (see chapter 2.1.3). A bias factor for the MRGPRX4 agonists is calculated, using Equation 1. In this equation, not only the potency, but the efficacy is considered as well. The logarithm of the ratio of E_{max} to EC_{50} is calculated. Subtraction of the result for β-arrestin recruitment assays, from the result determined from

calcium mobilization assays, is resulting in the bias factor towards G protein coupling; hence positive values show a bias towards G protein-coupling, whereas negative values represent a bias towards β-arrestin recruitment. A bias factor of 0 indicates a balanced agonist. A positive value of 1 corresponds to a compound favoring G protein-coupling 10-fold over β-arrestin recruitment, while a positive value of 2 corresponds to a 100-fold preference, and so on. Negative values are alike but indicate compounds biased towards β-arrestin recruitment.

In Figure 22, the G protein bias for the xanthine agonists on both variants is plotted. For both variants, only marginal differences in the bias factors are observed, revealing that the compounds are mostly balanced agonists. The highest deviations are approximately a factor of 1 from the mean, indicating a 10-fold preference for the respective pathway, only. The generally increased bias factor at the 83L variant is likely not due to a bias, but due to an overestimation of potencies in calcium mobilization assays at this variant.

At the 83S variant, **X7** and **X8** show the highest bias towards G protein coupling. They differ from the other derivatives by a fluorine, or a chlorine, as *ortho*-aryl substituents. However, a closer look at xanthine derivatives with distinct aryl substitutions indicates that this bias shift for a specific aryl substituent is dependent on the *N*7 substitution, e.g., *ortho*-iodo derivative **X15** (*N*7-ethyl) shows a bias towards β-arrestin, but the homologous *ortho*-iodo derivative **X21** (*N*7-isopropyl) is a balanced agonist. However, the *o*-methyl derivatives **X16**(*N*7-ethyl) and **X22** (*N*7-isopropyl) both show a strong β-arrestin bias. Another remarkable β-arrestin-biased derivative is **X33**. It contains an extended *C*6 chain in position *N*3. However, the related **X37** with a *C*6 chain but an ethyl substitution at *N*7 instead of the free *N*7-H (as in **X33**), is a balanced agonist. Taking a look at the 83L variant, **X15** and **X34** are both G protein-biased agonists. **X15** is the above-mentioned *ortho*-iodo derivative with an *N*7-ethyl substitution, that is, by contrast, β-arrestin-biased at the 83S variant. **X34**, however, contains an extended *C*5-chain at *N*3. β-Arrestin-biased compounds are **X25** and **X14**. The former one has a modified *C*8-aryl chain, and the latter one has a *para*-bromo-substituted aryl residue. Both modifications resulted in a considerably lower efficacy in the G protein-dependent calcium assay. The clearest bias, that is consistent for a

single modification, is the bias towards β-arrestin recruitment found in derivatives with a *p*- substitution on the aryl residue, e.g., **X4**, **X6**, **X10**, and **X14**.
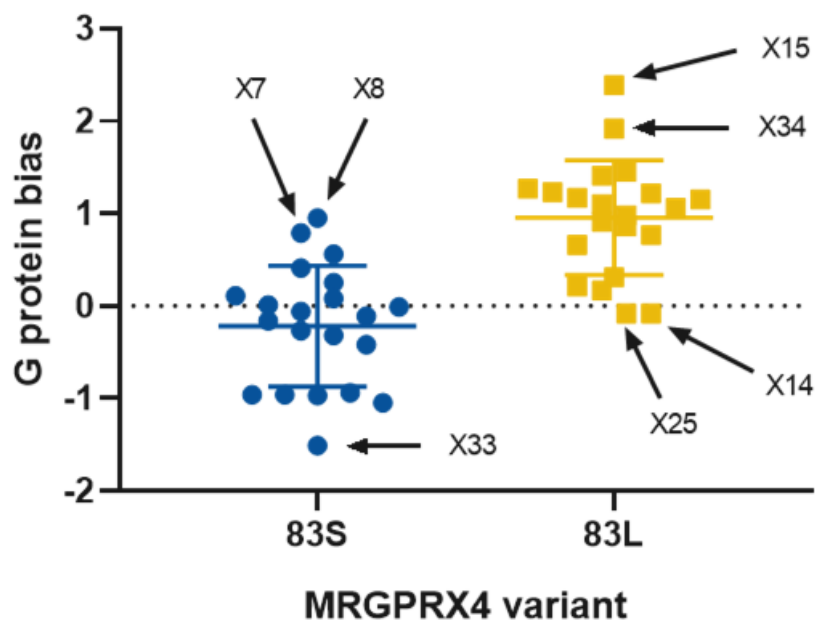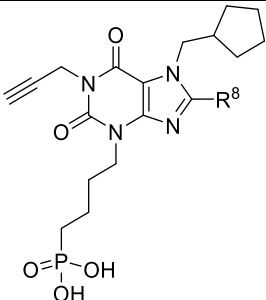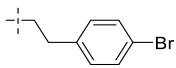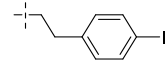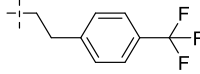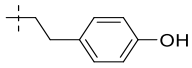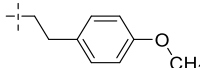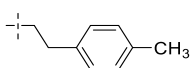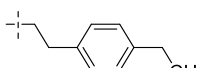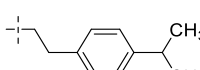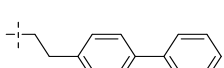
Figure 22: The calcium bias of xanthine agonists on MRGPRX4, calculated using Equation 1 for both variants.

4.4.2 Xanthine derivatives – Functional antagonists

As the *p*-bromine derivatives **X4**, **X10**, and **X14** reduced the efficacy in the calcium assays, while retaining high efficacy in the β-arrestin assays, *p*-substituted derivatives were further optimized to develop functional antagonists. The 1-cyclopentylmethyl moiety at *N*7 of **X43** led to a relatively high bias towards β-arrestin assays at the 83L variant and was therefore combined with *p*-bromine yielding **X52**. This compound showed a further reduced efficacy in the calcium assay of below 10%, while the efficacy in the β-arrestin assay remained (see Table 8 for structure and biological data, and Figure 23A.&B. for agonist curves).

Table 7: Biological data of compounds acting as functional antagonists.

Cmpd.# Internal Id	R[8]	Calcium [a] EC$_{50}$ ± SEM (nM); efficacy (%)	Calcium[a] IC$_{50}$ ± SEM (nM)	β-Arrestin[b] EC$_{50}$ ± SEM (nM); efficacy (%)
X52 SC117		**5.81** ± 1.58; **(8)** [83S] **267** ± 153; **(9)** [83L]	**5.23** ± 2.20 [83S] **0.381** ± 0.088 (IC$_{50}$1) **949** ± 308 (IC$_{50}$2)[83L]	**13.4** ± 2.8; **(79)** [83S] **1.44** ± 0.32; **(92)** [83L]
X53 SC240		**143** ± 66; **(23)** [83S] nd [83L]	**16.1** ± 8.4 [83S] nd [83L]	**0.773** ± 0.106; **(76)** [83S] nd [83L]
X54 SC239		**23.7** ± 7.7; **(8)** [83S] nd [83L]	**13.0** ± 1.4 [83S] nd [83L]	**18.3** ± 6.1; **(77)** [83S] nd [83L]
X55 SC296		**> 10,000** (0%) [83S] nd [83L]	**485** ± 108 [83S] nd [83L]	**420** ± 210; **(42)** [83S] nd [83L]
X56 SC236		**51.4** ± 28.5; **(57)** [83S] nd [83L]	nd [83S] nd [83L]	**3.67** ± 1.21; **(96)** [83S] nd [83L]
X57 SC270		**9.37** ± 4.65; **(24)** [83S] nd [83L]	nd [83S] nd [83L]	**7.98** ± 3.58; **(90)** [83S] nd [83L]
X58 SC258		**17.3** ± 4.5; **(30)** [83S] nd [83L]	nd [83S] nd [83L]	**12.5** ± 1.3; **(92)** [83S] nd [83L]
X59 SC257		**> 10,000 (2%)** [83S] nd [83L]	**10.4** ± 2.4 [83S] nd [83L]	**10.7** ± 7.1; **(53)** [83S] nd [83L]
X60 SC256		**> 10,000 (2%)** [83S] nd [83L]	**0.122** ± 0.033 [83S] nd [83L]	**2.12** ± 0.85; **(43)** [83S] nd [83L]
		Radioligand binding[d] K$_i$ ± SEM (nM): 0.551 ± 0.056[83S]		

[a]Calcium mobilization assays were performed either using LN229 natively expressing MRGPRX4-83S or 1321N1 astrocytoma cells recombinantly expressing MRGPRX4-83L. Efficacies are normalized to the maximal effect of PSB-18061 (see Figure 20). For antagonist assays the cells were preincubated for 30 min with the antagonist and subsequently activated with an EC_{80} of PSB-18061. [b]β-Arrestin recruitment assays were performed using CHO-β-Arrestin cell lines either expressing MRGPRX4-83S or MRGPRX4-83L. Efficacies are normalized to the maximal effect of PSB-18061 (see Figure 20). [c]Radioligand binding assays performed with 1 nM [³H]PSB-18061 using HEK-MRGPRX4-83S membrane preperation. [83X]= results for the respective MRGPRX4 variant (83S or 83L). nd = not determined. All compounds were tested at multiple concentrations.

X52 was tested in calcium assays at both variants as an antagonist (antagonist curves see Figure 23C.&D.) in order to evaluate whether this compound does act as functional antagonist. For this purpose, the compound was 30 minutes pre-incubated in the calcium assay, after which the calcium mobilization by PSB-18061 stimulation was measured. The hereby determined IC_{50} values of 5.23 ± 2.20 nM at the 83S is close to the EC_{50} value measured at the calcium assay. Receptor activation by the full agonist PSB-18061 is completely inhibited by **X52**. This is probably due to the internalization taking place after β-arrestin recruitment. Thus, **X52** acts as a functional antagonist. At the minor variant 83L **X52** produced a biphasic inhibition curve. This could be explained by the two different effects taking place: (i) desensitization by β-arrestin recruitment, and (ii) the displacement of the full agonist. To confirm that the observed inhibition is due to MRGPRX4 blockade, and not to an assay interference, **X52** was additionally tested versus carbachol (data not shown). Carbachol induces calcium mobilization, independent of MRGPRX4, by activation of endogenous muscarinic acetylcholine receptors. No inhibition of the carbachol signal was measured, hence assay interactions, such as quenching of the signal or cell death, can be excluded.

Figure 23: Biological data of **X52** at MRGPRX4. Data points are means ± SEM of at least three independent experiments performed in duplicates. **A. X52** tested as agonist in calcium mobilization assays, using native LN229 glioblastoma cells. Results are normalized to maximal effect of PSB-18061 **B. X52** tested as agonist in β-arrestin recruitment assay using CHO-β-arrestin cells expressing MRGPRX4-83S. Results are normalized to the maximal effect of PSB-18061. **C.** and **D. X52** tested as antagonist at the major 83S and the minor 83L variant of MRGPRX4 using native LN229 glioblastoma cells or 1321N1 astrocytoma cells expressing MRGPRX4-83L.

Based on these encouraging results for **X52**, we investigated further derivatives with a 1-cyclopropylmethyl substitution at *N*7, and different substituents in *para*-position of the phenyl ring (see Table 7 for structures and biological data). In order to improve the compounds' properties as functional antagonists, we tried to increase their MRGPRX4 affinity while reducing the efficacy in G protein dependent calcium mobilization to a minimum.

The *para*-substitutions proposedly cause a clash with the active MRGPRX4 conformation that is capable of recruiting G proteins. This was accomplished by sterically demanding (-trifluoromethyl (**X54**), -isopropyl (**X59**), and -phenyl (**X60**)) and by electron-rich (-bromo (**X52**), -trifluoromethyl (**X54**), -hydroxyl (**X55**), and -phenyl (**X60**)) *para*-substitutions. These substitutions lead to a low efficacy in the

calcium assay or even further reduced it to a non-measurable level. The small lipophilic -methyl (**X57**) or -ethyl (**X58**) substitutions led to a regain of efficacy in the calcium assay. The inhibitory potency could be improved by the lipophilic -phenyl (**X60**), while it was reduced for derivatives that are capable of forming (halide-)hydrogen bonds as the -iodo (**X53**), -trifluoromethyl (**X54**), -hydroxyl (**X55**), and the -methoxy (**X56**) derivatives. Inferring that the optimal *para*-substitutions for the purpose of functional antagonists are sterically demanding and lipophilic moieties. Comparing **X60** to its homologous **X6**, which instead of the cyclopentylmethyl possesses a hydrogen at *N*7, shows an increased efficacy in the calcium assay and a reduction of potency in the β-arrestin assay. This emphasizes the superiority of the lipophilic and sterically demanding cyclopentylmethyl at *N*7 over an unsubstituted *N*7 position.

Being the most potent functional antagonist tested so far, **X60** was subsequently investigated in radioligand binding assays. It displayed a K_i value comparable to its IC_{50} value measured in calcium assays ($K_i = 0.551$ nM; for concentration dependent curves see Figure 24). Additionally, the compound was tested against carbachol, as described for **X52**, without finding any inhibition (data not shown). A screening in the TruPath assay (results and discussion in chapter 0) showed that the coupling to the different Gα subtypes was largely diminished with partial activation only seen for $G\alpha_{15}$ protein.
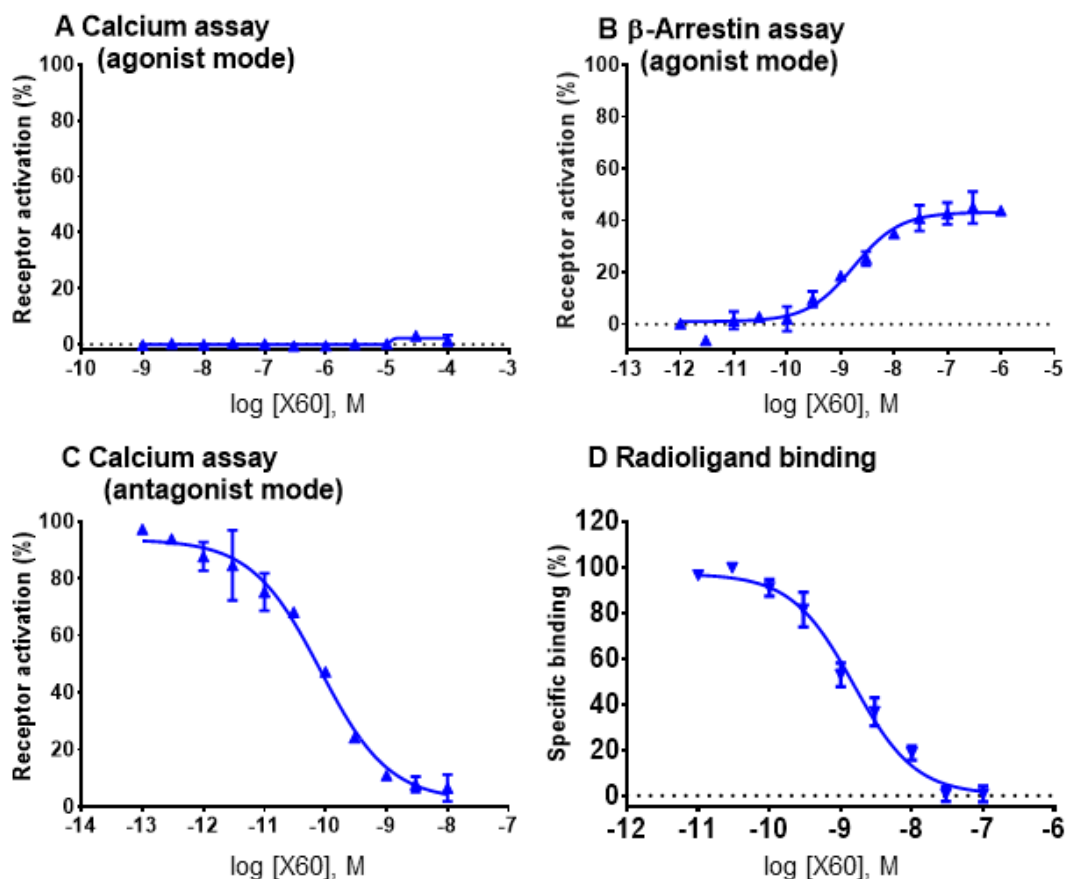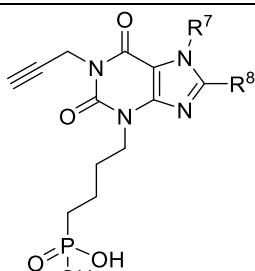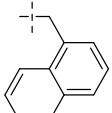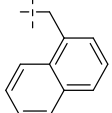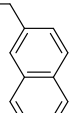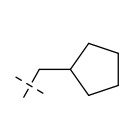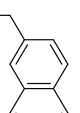
Figure 24: Biological data of **X60** at MRGPRX4-83S. Data points are means ± SEM of at least three independent experiments performed in duplicates. **A X60** tested as agonist in calcium mobilization assays, using native LN229 glioblastoma cells. Results are normalized to maximal effect of PSB-18061 **B X60** tested as agonist in β-arrestin recruitment assay using CHO-β-arrestin cells expressing MRGPRX4-83S. Results are normalized to the maximal effect of PSB-18061. **C X60** tested as antagonist in calcium assays using native LN229 glioblastoma cells. **D X60** tested in radioligand binding assay against 1 nM [³H]PSB-18061.

4.4.3 Xanthine derivatives – Antagonists

Four xanthine derivatives were identified as antagonists at MRGPRX4 (see Table 8). In contrast to functional antagonists, these compounds block the signal of the standard agonist, not only in calcium mobilization assays, but also in β-arrestin assays. However, the compounds did not show 'clean' antagonist curves in the β-arrestin assays, but a small signal increase at higher concentrations. The β-arrestin curves and this effect will be discussed in chapter 4.7.

Table 8: Structures and biological data of antagonistic xanthine derivatives at MRGPRX4-83S.

Cmpd.# Internal Id	R^7	R^8	Calcium[a] $IC_{50} \pm$ SEM (nM)	β-Arrestin[b] $IC_{50} \pm$ SEM (nM)	Radioligand binding[c] $K_i \pm$ SEM (nM)
X61 SC287	H		**1,360** ± 530	nd	nd
X62 SC109	CH_2CH_3		**31.7** ± 19.1 [83S]	**68.2** ± 7.0 [§ 83S]	**39.7** ± 8.4 [83S]
X63 SC280	CH_2CH_3		**41.5** ± 14.6 [83S]	**4.31** ± 1.77 [§ 83S]	**62.8** ± 5.1 [83S]
X64 SC325			**294** ± 90	nd	nd

[a]Calcium mobilization assays were performed using LN229 natively expressing MRGPRX4-83S. Efficacies are normalized to the maximal effect of PSB-18061 (see Figure 20). The cells were preincubated for 30 min with the antagonist and subsequently activated with an EC_{80} of PSB-18061. [b]β-Arrestin recruitment assays were performed using CHO-β-Arrestin cell lines expressing MRGPRX4-83S. Efficacies are normalized to the maximal effect of PSB-18061 (see Figure 20). [c]Radioligand binding assays performed with 1 nM [³H]PSB-18061 using HEK-MRGPRX4-83S membrane preperation. [83S]= results for MRGPRX4-83S. nd = not determined. [§]= Inhibition is incomplete as discussed in chapter 4.7. All compounds were tested at multiple concentrations, and all derivatives did not show activation in the calcium assay up to 10,000 nM.

The MRGPRX4 antagonistic xanthines have the commonality of a naphthalen-2-yl-methyl residue as R^8-substituent. In contrast, the naphthalen-2-yl-ethyl of **X18**, switched the functional effect back to a full agonist. Another closely related structure is **X24** containing a (1*H*-indol-3-yl)methyl residue for R^8, which acted as a full agonist

in the β-arrestin assays, and as a partial agonist in the calcium assays. In position *N*7, a small lipophilic ethyl group is preferred over *N*7-H (**X62** = 31.7 nM vs. **X61** = 1,360 nM). Introduction of a bulky lipophilic 1-cyclopentylmethyl residue in position 7 was also not superior to ethyl (**X64** = 294 nM vs. **X63** 41.5 nM). The two potent inhibitors, **X62** and **X63**, were evaluated in the radioligand binding assay. They showed K_i values that were comparable to the IC_{50} values determined in calcium assays (for curves see Figure 25A. and B.). In order to further confirm that the observed inhibition in the calcium assay was mediated by blockage of MRGPRX4, **X62** was additionally tested against carbachol. Carbachol induces a calcium signal independently of MRGPRX4, which was, however, not blocked by **X62** (data not shown).
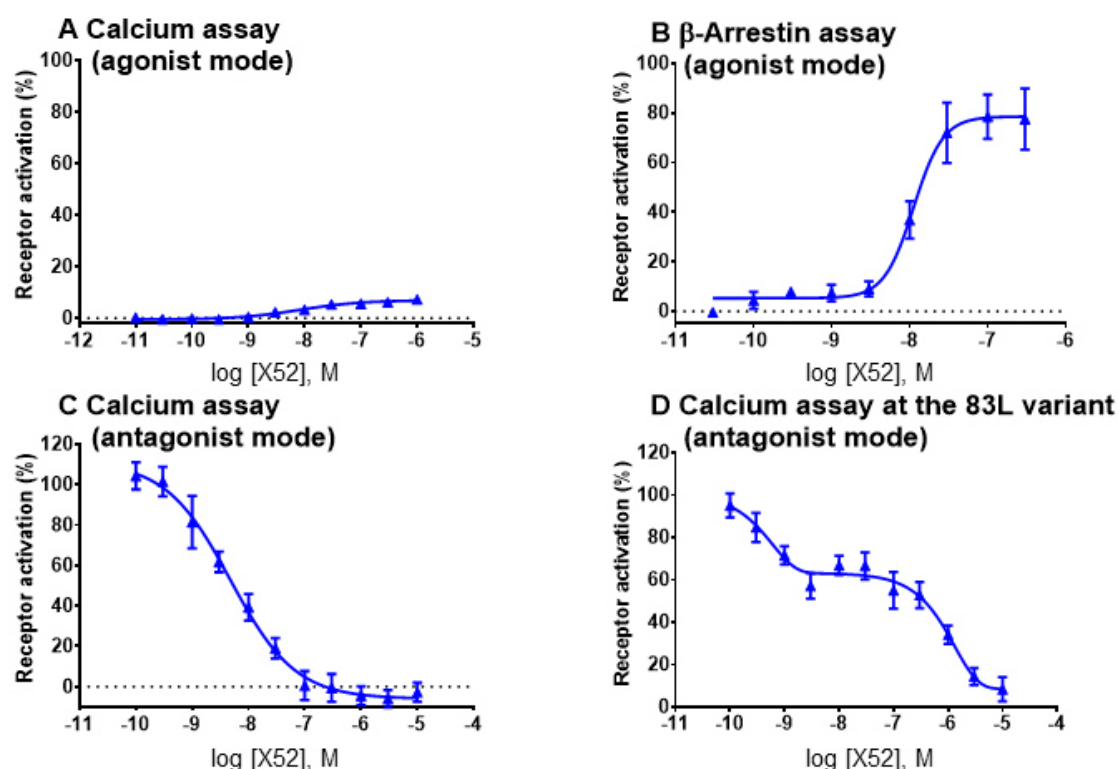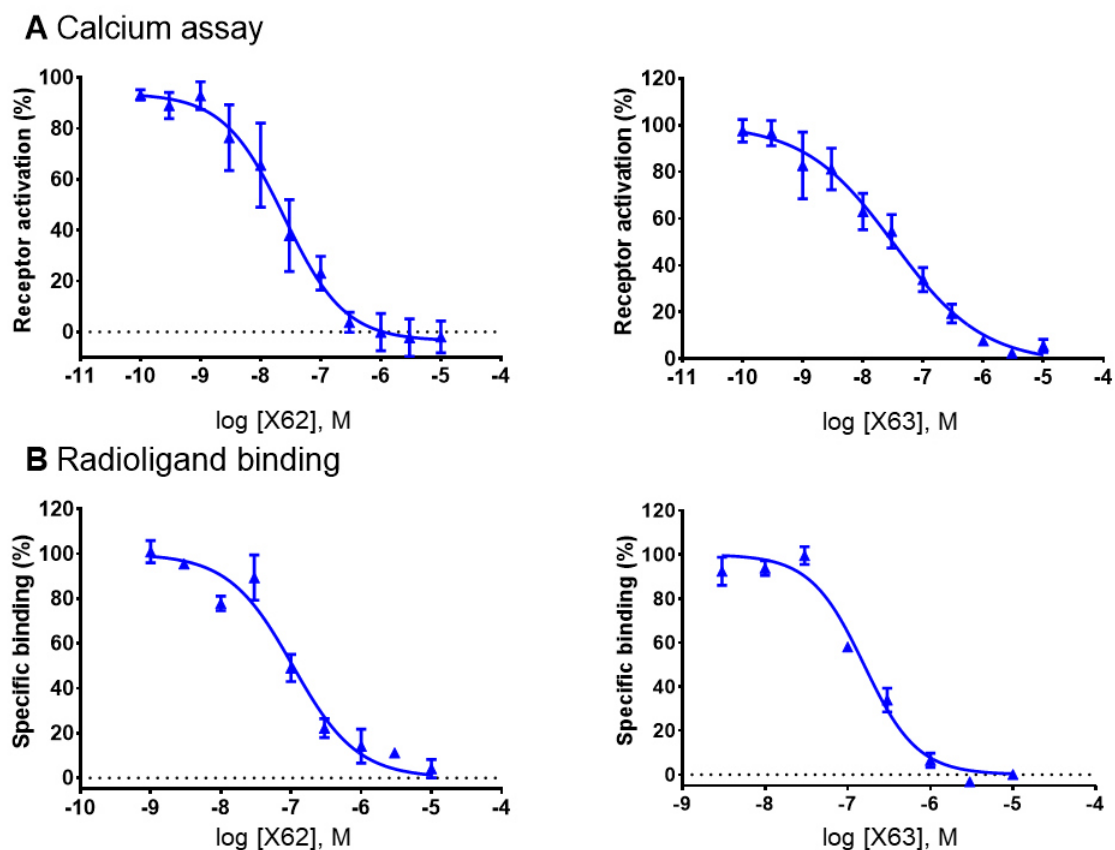

Figure 25: Biological data of **X62** and **X63** at MRGPRX4-83S. Data points are means ± SEM of at least three independent experiments performed in duplicates. **A** Compounds tested as antagonists in calcium mobilization assays, using native LN229 glioblastoma cells. Results are normalized to maximal effect of PSB-18061 **B** Compounds tested in radioligand binding assays against 1 nM [³H]PSB-18061.

4.4.4 Binding kinetics

The different xanthine ligands that interact with MRGPRX4 have very similar structures, despite distinct pharmacological effects. In order to investigate, how this is reflected in their binding kinetics, we evaluated one selected compound of each ligand class: (i) the agonist **X16**, (ii) the functional antagonist **X60**, and (iii) the antagonist **X63**. The compounds were incubated with membrane preparation of HEK-MRGPRX4-83S membrane preparation for 60 minutes until an equilibrium was reached. Afterwards the radioligand [³H]PSB-18061 was added and harvested after the respective time points. By this means the kinetic parameters of the compounds can be calculated. A lowered dissociation half-life compared to the radioligand [³H]PSB-18061 was found for the three compounds (Figure 26). Moreover, the compounds were found to have very similar dissociation half-lives of around 5 minutes.

Cmpd	Dissociation half-life (min)[a]
[³H]PSB-18061	11.5 ± 0.7

Cmpd	Dissociation half-life (min)
X16	6.45 ± 0.99
X60	6.16 ± 0.27
X63	5.43 ± 0.99
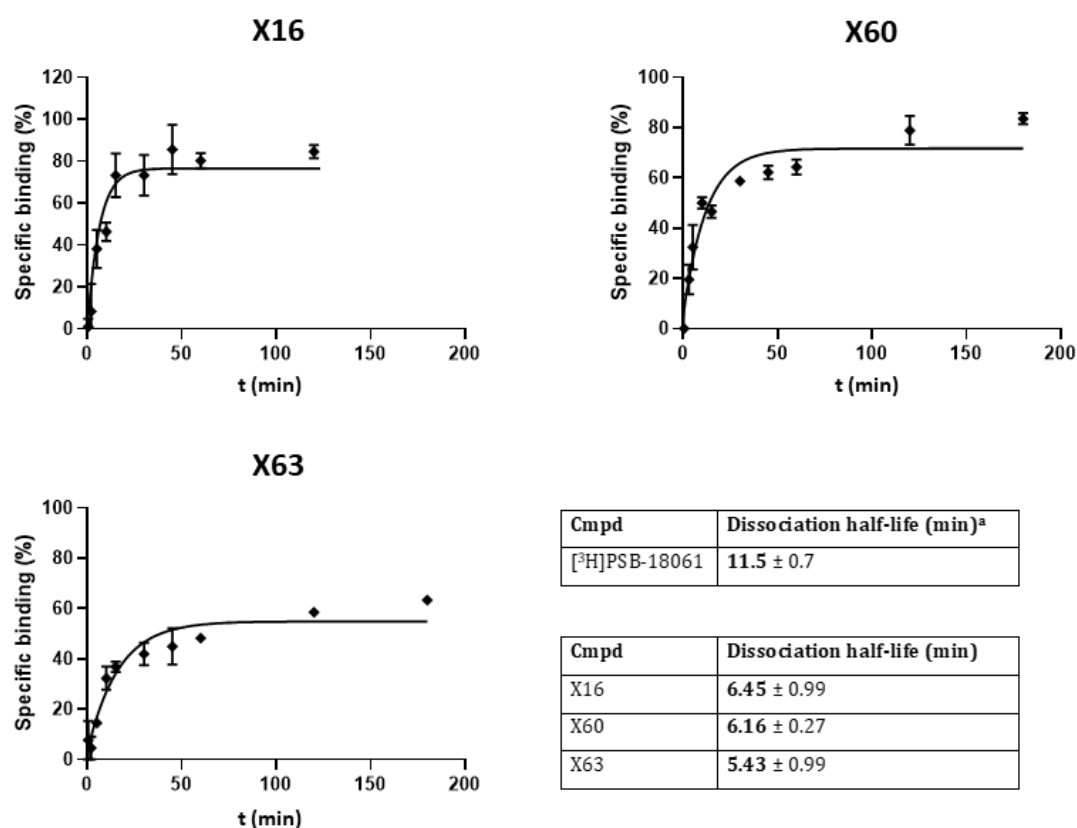
Figure 26: Kinetic parameters of different xanthine derivatives at room-temperature. Data points are means ± SEM of at least three independent experiments performed in duplicates. The half-lifes are means ± SEM calculated with GraphPad Prism 8. The compounds were added in following concentrations: 0.15 nM of **X16**, 1.5 nM of **X60**,

or 150 nM **X63**, to 1 nM [^{3}H]PSB-18061 and membrane preparation of HEK-MRGPRX4-83S membrane preparation for the respective time period. Results are normalized to total and non-specific binding of the radioligand. [a]Determined in chapter 4.1 by dissociation experiments.

4.4.5 Cytotoxicity, Metabolic stability, and membrane permeation of xanthine derivatives

To evaluated drug-like properties of selected compounds, we determined the cytotoxicity, metabolic stability, and membrane penetration of different xanthine derivatives. The agonist PSB-18061, the functional antagonist **X60**, and the antagonist **X62** were tested in a 3-(4,5-dimethylthiazol-2-yl)-2,5-diphenyltetrazolium bromide (MTT) assay. MTT is metabolized in the mitochondria of living cells to formazan, which can be easily quantified by measurement of light absorption. The test compounds were added at the start of the assay to LN229 glioblastoma cells and incubated for three days. No change in viability was recorded - even at high concentrations up to 100 μM (Figure 27A.). This does not only show that the compounds were not cytotoxic, but, as LN229 express MRGPRX4, that receptor activation or inhibition does not lead to changes in cell viability. For metabolic stability determination, we selected **X16**, **X48**, **X60**, and **X63**. Results of the metabolic stability studies are shown in Figure 27B. After one hour of incubation with human liver microsomes, more than 80% of all derivatives remained intact. Thus, the half-lives for all derivatives are >60 min. Moreover, **X48** was incubated for 60 minutes in either the basolateral or apical compartment of a CaCo2 (<u>ca</u>ncer <u>coli</u>) culture. These cells mimic the physiological barrier in the intestine that drugs need to pass to be orally available. After incubation, no compound could be detected in the respective opposite compartment, implying that **X48** is not able to pass cell membranes (results not shown). This is likely due to the phosphonate that is positively charged at physiological pH.
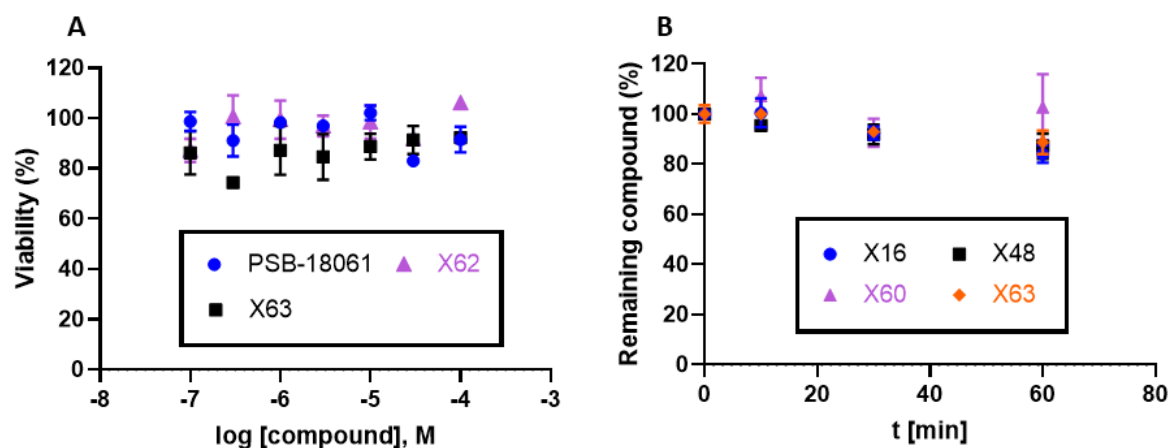
Figure 27: **A** Cytotoxicity of different xanthine derivatives, measured in MTT assays on LN229 glioblastoma cells. Compounds were incubated for 3 days. **B** Metabolic stability of selected xanthine derivatives over 60 minutes incubation with human liver microsomes. Data of metabolic stability obtained by contract research company Pharmacelsus, Saarbrücken.

4.5 BIPHENYL DERIVATIVES

Based on the antagonist screening-hit SDZ-220-040, a commercially available N-methyl-D-aspartate (NMDA) receptor antagonist, MRGPRX4 antagonists were previously developed containing a biphenyl core structure. The antagonist DM473A/**B2** is an optimized MRGPRX4 antagonist by our group (structures see Figure 28). Starting from this point, we aimed to explore the pharmacological effects and SARs of further related biphenyl derivatives.

Screening hit
SDZ-220-040
IC_{50} = **6,360 nM+**

Optimized MRGPRX4 antagonist
DM473A
IC_{50} = **1.77 nM**
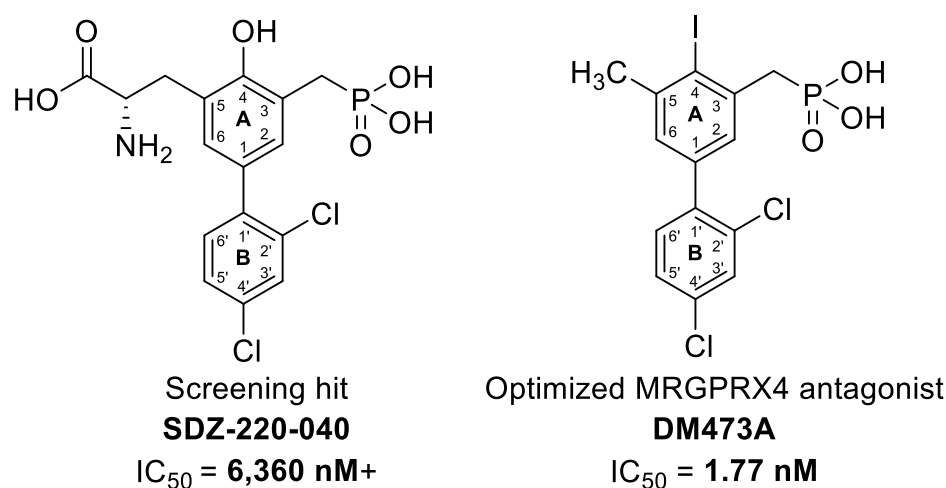
Figure 28: Structure of the screening hit SDZ-220-040 and optimized MRGPRX4 antagonist DM473A/B2. += Data obtained by Wessam Alnouri

The radioligand binding experiments showed that **B2** fully displaces the radioligand, and that the determined K_i value is comparable to the IC_{50} determined in calcium assays (Figure 29C). A dissociation half-life of 6.08 minutes was determined for **B2** at room-temperature. In β-arrestin recruitment assays, the compound showed an antagonistic effect up to a concentration of 30 μM, and an activating effect at higher concentrations. Similar effects were found for most of the here discussed antagonists, partially in the calcium assays as well (discussion of this effect see chapter 4.7).
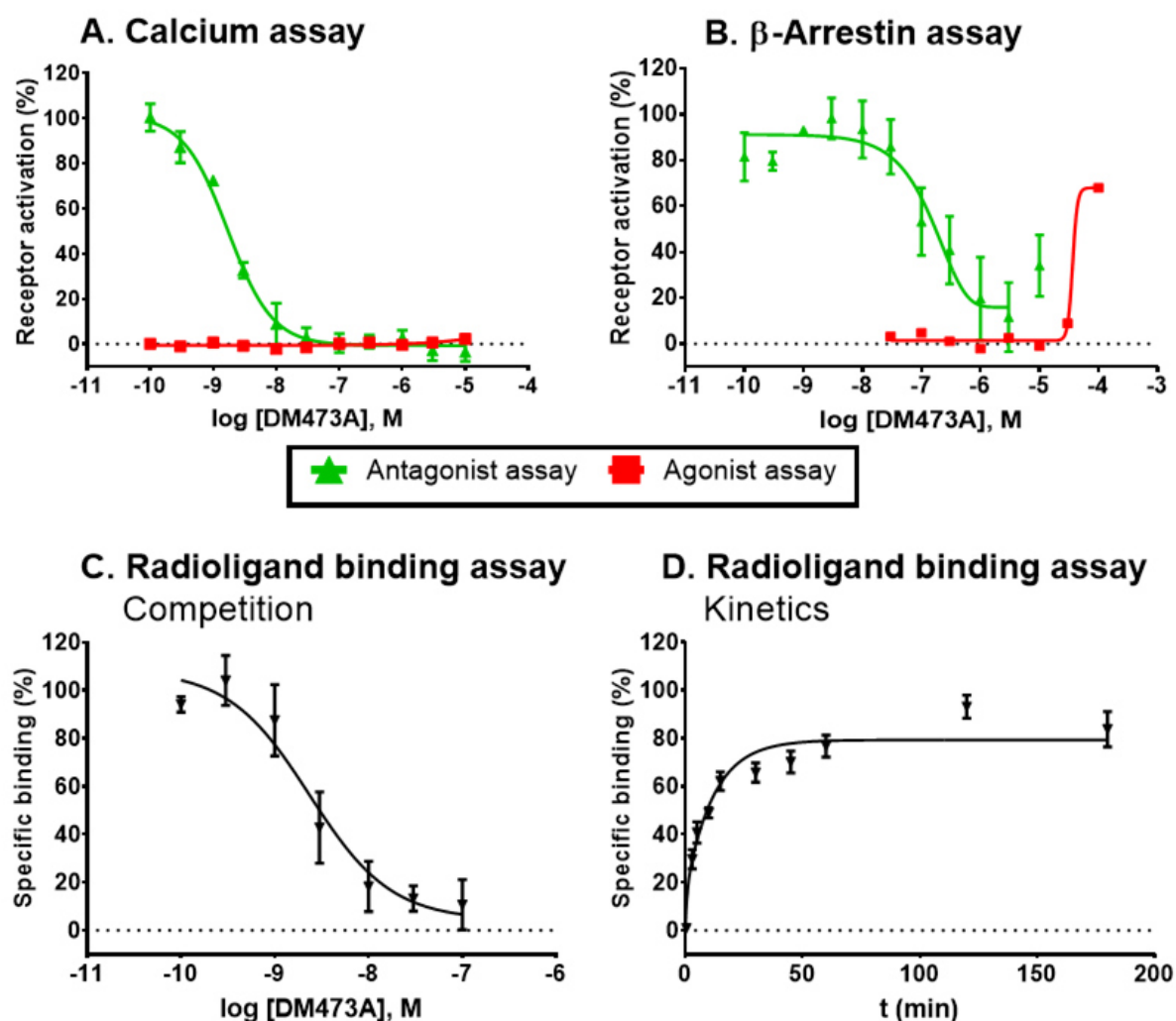
Figure 29: Assay results of **B2**. **A** Calcium assay using native LN229 **B** β-arrestin assay using CHO-β-arrestin-MRGPRX4-83S **C** Competitive radioligand binding assay at HEK-MRGPRX4-83S membrane preparation. **D** Kinetic radioligand binding assay. A half-life of 6.08 ± 1.08 min is calculated. **B2** (4.5 nM) was incubated with 1 nM [^{3}H]PSB-18061 and membrane preparation of HEK-MRGPRX4-83S (50 µg of protein) for the respective time period.
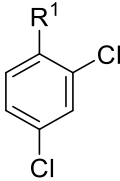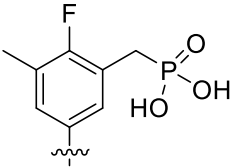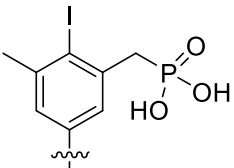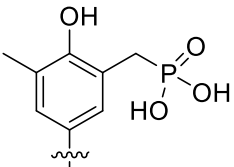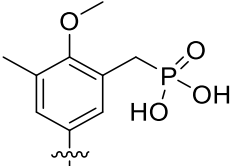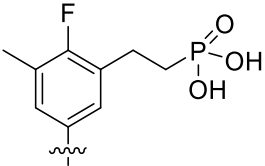
Biphenyl derivatives with modifications of ring A were investigated (see Table 9, used annotations see Figure 28). The exchange of the iodine in position 4 for a fluorine (**B2** = 1.77 nM vs. **B1** = 117 nM) did not only reduce inhibitory potency but increased the agonistic effect. The 4-hydroxy derivative (**B3** = 2,710 nM) led to reduction in potency but did not show any agonistic effects. However, other 4-hydroxy derivatives (e.g., **B15**) regained an agonistic effect, when regaining the inhibitory potency. Introduction of a 4-methoxy (**B4** = 493 nM) led to a more potent compound than a 4-hydroxy group but did not improve potency over the 4-iodo substituted lead
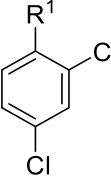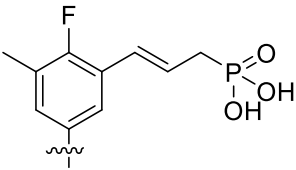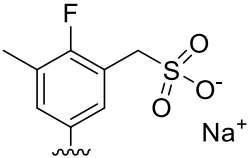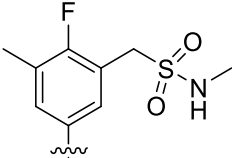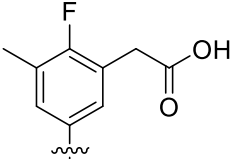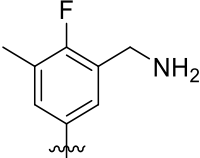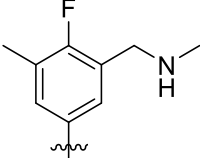
structure. The electron rich iodine in position 4 at was superior to the tested alternatives. Iodine is favorable for forming halide-hydrogen bonds, which could be formed in the binding pocket. As the 4-hydroxy derivative was inferior to iodine and methoxy, a hydrogen bond donor is not suitable at this position.
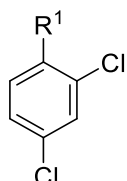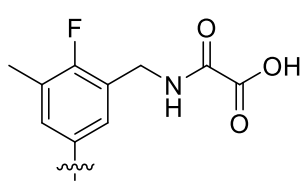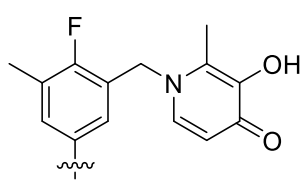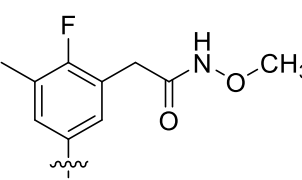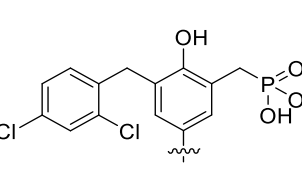
Exchanging the phosphonomethylene by a phosphonoethyele residue (**B1** = 117 nM vs. **B5** = 30.0 nM) did increase the inhibitory potency. The ethylene linker was superior compared to a propylene linker (**B5** = 859 nM[83L] vs. **B6** = 10,500 nM[, 83L]). Exchanging the phosphonic acid by a sulfonic acid (**B7** > 10,000 nM[83L]), a 3*N*-methylmethanesulfonamide (**B8** = 3,460 nM[83L]), or a carboxylic acid (**B9** = 21,600 nM[83L]) diminished the potency. Exchanging of the negatively charged acids to an amine (**B10** = 7,240 nM) resulted in a barely active compound. Methylation of the **B10** yielding a methylamine (**B11** = 492 nM) resulted in a relatively potent inhibitor (determined in calcium assays), while no inhibition could be detected in the β-arrestin assay. A (methylamino)-2-oxoacetic acid (**B12** > 10,000 nM) or methyl-3-hydroxy-2-methylpyridin-4(1*H*)-one (**B13** > 10,000 nM) resulted in a loss of inhibitory potency, while an *N*-methoxyacetamide (**B14** = 5,800 nM) was barely active. The phosphonate group of the lead **B2** and its derivatives is a communality with the above discussed xanthine derivatives. However, for xanthine derivatives a replacement was not possible without a major loss in potency. For biphenyl antagonists, on the other hand, the replacement to a methylamine was possible with only a minor reduction in inhibitory potency. The phosphonate is negatively charged at physiological pH and therefore prohibits a meaningful resorption. The possibility for replacement is an advantage which could be further exploited for more drug-like MRGPRX4 antagonists.

The introduction of an additional aromatic ring, where the methyl in position 5 was replaced by a 2,4-dichlorophenyl (**B15** = 0.790 nM), increased potency greatly over its orthologue (**B3** = 2,710 nM) and over the lead structure (**B2**= 1.77 nM) as determined in calcium assays. This implies, that plenty of room in the binding pocket is left, which can be exploited for improved inhibitory potency. A replacement of the 4-hydroxy residue of **B15** to the superior iodine, fluorine, or methoxy could prove beneficial.

Table 9: Biphenyl derivatives with modifications on Ring A.

Cmpd.# Internal Id	R[1]	Calcium assay[a]	β-Arrestin assay[b]
		IC$_{50}$ ± SEM (nM) (% change to control)	**IC$_{50}$ ± SEM (nM)** (% change to control)
		EC$_{50}$ ± SEM (nM); efficacy (%) (% change to control)	**EC$_{50}$ ± SEM (nM)**; efficacy (%) (% change to control)
B1 DM299A Yazh9992		**117** ± 32 [83S] 14,200 ± 2,100 [83L]* nd [83S] nd [83L]	> 100,000 (+98%) [83S] nd[83L] nd [83S] nd[83L]
B2 DM473A		**1.77** ± 0.5 [83S] 60.2 ± 14.2 [83L]* >10,000 (+2%) [83S] nd [83L] **Radioligand binding[c]** **K$_i$ ± SEM (nM):** **1.02** ± 0.34 [83S]	**68.8** ± 36.3 [§][83S] 552 ± 160 [83L]* >100,000 (+68%) [83S] nd [83L]
B3 Yazh956		**2,710** ± 500 [83S]* 1,440 ± 500[83L]* >10,000 (-3%) [83S]* >100,000 (-1%) [83L]*	**6,600** ± 1,340 [83S]* 5,660 ± 1,630 [83L]* >100,000 (-4%) [83S]* >100,000 (-11%) [83L]*
B4 SC217		**493** ± 169 [83S] nd [83L] > 10,000 (4%) [83S] nd [83L]	**1,280** ± 320 [§][83S] nd [83L] nd [83S] nd [83L]
B5 DM433A		**30.0** ± 13.0 [83S] 859 ± 181[83L]* nd [83S] nd [83L]	nd [83S] nd [83L] nd [83S] nd[83L]
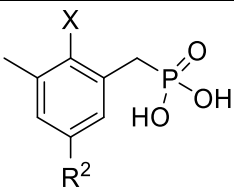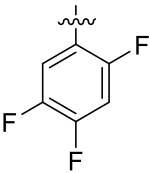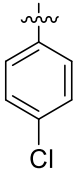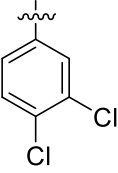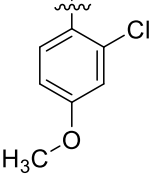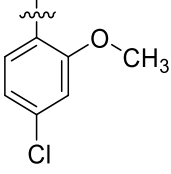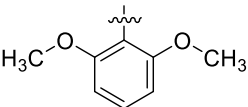
Cmpd.# Internal Id	R[1]	Calcium assay[a]	β-Arrestin assay[b]
		IC$_{50}$ ± SEM **(nM)** (% change to control)	IC$_{50}$ ± SEM **(nM)** (% change to control)
		EC$_{50}$ ± SEM **(nM)**; efficacy (%) (% change to control)	EC$_{50}$ ± SEM **(nM)**; efficacy (%) (% change to control)
B6 SC112		nd [83S] **10,500** ± 9,200 [83L] nd [83S] nd [83L]	nd [83S] **15,800** ± 3,900 [83L] nd [83S] nd [83L]
B7 SC001		nd [83S] **> 10,000 (-29%)** [83L] nd [83S] nd [83L]	nd [83S] **49,700** ± 6300 [83L] nd [83S] nd [83L]
B8 SC034.1		nd [83S] **3,460** ± 220 [83L] nd [83S] nd [83L]	nd [83S] **64,800** ± 32,800[83L] nd [83S] nd [83L]
B9 SC010		nd [83S] **21,600** ± 4,600 [83L] nd [83S] nd [83L]	nd [83S] **54,400** ± 7,000 [83L] nd [83S] nd [83L]
B10 SC143		**7,240** ± 1,200 [83S] nd [83L] nd [83S] nd [83L]	**40,500** ± 7,800 [83S] nd [83L] nd [83S] nd [83L]
B11 SC034		**492** ± 139 [83S] **17,600** ± 9,100 **> 10,000 (+12%)** [83S] nd [83L]	**> 100,000 (+34%)** [83S] **18,200** ± 2,640 [83L] **> 100,000 (+49%)** [83S] nd [83L]
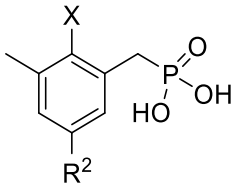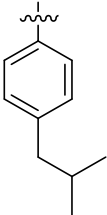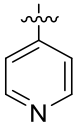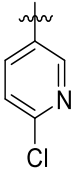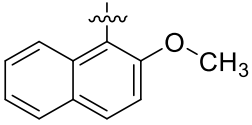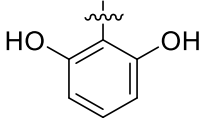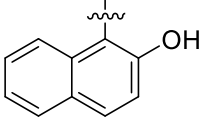
Cmpd.# Internal Id	R[1]	Calcium assay[a]	β-Arrestin assay[b]
		IC$_{50}$ ± SEM (nM) (% change to control)	**IC$_{50}$ ± SEM (nM)** (% change to control)
		EC$_{50}$ ± SEM (nM); efficacy (%) (% change to control)	**EC$_{50}$ ± SEM (nM)**; efficacy (%) (% change to control)
B12 SC145		>10,000 (-28%) [83S] nd [83L]	**47,500 ± 7,400** [§][83S] nd [83L]
		nd [83S] nd [83L]	nd [83S] nd [83L]
B13 SC199		>10,000 (-34%) nd [83L]	>100,000 (+2%) [83S] nd [83L]
		nd [83S] nd [83L]	>100,000 (+66%) [83S] nd [83L]
B14 SC207		**5,800 ± 1,680**[83S] nd [83L]	> 100,000 (+97%) [83S] nd [83L]
		> 10,000 (12%) [83S] nd [83L]	nd [83S] nd [83L]
B15 SC190		**0.790 ± 0.265** [83S] nd [83L]	**238 ± 180** [§][83S] nd [83L]
		> 10,000 (2%) [83S] nd [83L]	**47,200 ± 35,400; 108%**[83S] nd [83L]

[a]Calcium mobilization assays were performed either using LN229 natively expressing MRGPRX4-83S or 1321N1 astrocytoma cells recombinantly expressing MRGPRX4-83L. Efficacies are normalized to the maximal effect of PSB-18061 (see Figure 20). [b]β-Arrestin recruitment assays were performed using CHO-β-Arrestin cell lines either expressing MRGPRX4-83S or MRGPRX4-83L. Efficacies are normalized to the maximal effect of PSB-18061 (see Figure 20). [c]Radioligand binding assays performed with 1 nM [³H]PSB-18061 using HEK-MRGPRX4-83S membrane preperation. [83X]= results for the respective MRGPRX4 variant (83S or 83L). [§]= The inhibition was incomplete [*]= Data obtained by Yvonne Riedel; [$]= Data obtained by Josua Krebber. All compounds were tested at multiple concentrations.

Modifications of ring B are presented in Table 10. Replacing the 2',4'-dichlorophenyl by a 3',4'-dichlorophenyl (**B1** = 117 nM vs. **B18** = 285 nM) or a 2',4',5'-trifluorophenyl residue (**B16** = 243 nM) slightly reduced potency. A 4'-chlorophenyl substituent (**B17** = 2,000 nM) greatly reduced potency. Exchanging the 2',4'-dichlorophenyl residue for a 2'-chloro-4'-methoxyphenyl residue (**B19** = 125 nM) did not alter the inhibitory potency. Swapping of the substituents yielding a 2'-methoxy-4'-chlorophenyl derivative reduced potency (**B20** = 986 nM). A 2',6'-dimethoxyphenyl residue (**B21** = 1,940 nM) diminished the inhibitory potency, while the 2',6'-dihydroxyphenyl substitution increased it (**B26** = 1,280 nM vs. **B3** = 2,710 nM); however, different substitutions on ring A prevent a direct comparison. The lipophilic 4'-isobutylphenyl (**B22** = 1,310 nM) lead to decrease in inhibitory potency. Exchanging the phenyl by 4'-pyridyl, or a 4'-chloro-3'-pyridyl residue led to a loss in potency (**B23** > 10,000 nM[83L] and **B24** > 10,000 nM[83L]). Replacing ring B with a bulky 2-methoxynaphth-1-yl residue led to a compound with similar potency (**B25** = 125 nM), while a 2-hydroxynaphth-1-yl residue led to reduced inhibitory potency (**B27** = 4,950 nM). Compounds lacking a *o*- or *m*-substitution of ring B were consistently low potent, while the bulky 2-methoxynaphth-1-yl proved equally potent to its orthologue. The more hydrophilic 2-hydroxynaphth-1-yl reduced potency, inferring a lipophilic binding pocket around ring B.

Table 10: Modifications of Ring B

Cmpd.# Internal Id	X	R²	Calcium assay[a]	β-Arrestin assay[b]
			$IC_{50} \pm$ SEM **(nM)** (% change to control)	$IC_{50} \pm$ SEM **(nM)** (% change to control)
			$EC_{50} \pm$ SEM **(nM)**; efficacy (%) (% change to control)	$EC_{50} \pm$ SEM **(nM)**; efficacy (%) (% change to control)
B16 SC134	F		**243** ± 17 [83S] **2,350** ± 1,020 [83L] nd [83S] nd [83L]	> 100,000 (+48%) [83S] > 100,000 (+7%) [83S] nd [83S] nd [83L]
B17 SC119	F		**2,000** ± 450 [83S] **15,100** ± 6,200 [83L] * nd [83S] nd [83L]	> 100,000 (+257%) [83S] >100,000 [83L] * nd [83S] nd [83L]
B18 SC123	F		**285** ± 92 [83S] **1,820** ± 532 [83L] nd [83S] nd [83L]	nd [83S] >100,000 (+25%) [83L] **1,020** ± 80; 73% [83S] nd [83L]
B19 SC-RA002	F		**125** ± 62 [83S] nd [83L] >10,000 (+27%) [83S] nd [83L]	>100,000 (+118%) [83S] nd [83L] >100,000 (+50%) [83S] nd [83L]
B20 SC169	F		**986** ± 318 [83S] nd [83L] nd [83S] nd [83L]	>100,000 (+55%)[83S] nd [83L] nd [83S] nd [83L]
B21 SC192	F		**1,940** ± 730 [83S] nd [83L] nd [83S] nd [83L]	> 100,000 (+24%) [83S] nd [83L] nd [83S] nd [83L]

Cmpd.# Internal Id	X	R²	Calcium assay[a]	β-Arrestin assay[b]
			IC$_{50}$ ± SEM (nM) (% change to control)	**IC$_{50}$ ± SEM (nM)** (% change to control)
			EC$_{50}$ ± SEM (nM); efficacy (%) (% change to control)	**EC$_{50}$ ± SEM (nM)**; efficacy (%) (% change to control)
B22 SC131	F		**1,310** ± 350 [83S] **14,600** ± 9,300 [83L] nd [83S] nd [83L]	> 10,000 (+22%) [83S] **46,930** ± 2,540 [83L] > 10,000 (+41%) [83S] nd [83L]
B23 SC120	F		nd [83S] >10,000 (-24%) [83L] nd [83S] nd [83L]	nd [83S] >100,000 (-49%) [83L] nd [83S] nd [83L]
B24 SC121	F		nd [83S] >10,000 (-15%) [83L] nd [83S] nd [83L]	nd [83S] >100,000 (-40%) [83L] nd [83S] nd [83L]
B25 SC132	F		**125** ± 14 [83S] **1,740** ± 455 [83L] nd [83S] nd [83L]	> 100,000 (+65%) [83S] > 100,000 (+15%) [83L] nd [83S] nd [83L]
B26 SC202	OH		**1,280** ± 440 [83S] nd [83L] nd [83S] nd [83L]	>100,000 (-22%) [83S] nd [83L] nd [83S] nd [83L]
B27 SC201	OH		**4,950** ± 2,340 nd [83L] nd [83S] nd [83L]	>100,000 (+63%) [83S] nd [83L] >100,000 (+71%) [83S] nd [83L]

[a]Calcium mobilization assays were performed either using LN229 natively expressing MRGPRX4-83S

or 1321N1 astrocytoma cells recombinantly expressing MRGPRX4-83L. Efficacies are normalized to

the maximal effect of PSB-18061 (see Figure 20). [b]β-Arrestin recruitment assays were performed using CHO-β-Arrestin cell lines either expressing MRGPRX4-83S or MRGPRX4-83L. Efficacies are normalized to the maximal effect of PSB-18061 (see Figure 20). [83X]= results for the respective MRGPRX4 variant (83S or 83L). [$]= The inhibition was incomplete *= Data obtained by Yvonne Riedel; [$]= Data obtained by Josua Krebber. All compounds were tested at multiple concentrations.

B15 was identified as the most potent inhibitor of the biphenyl series, determined in the calcium assay. It was subsequently tested against carbachol, as a control to validate its inhibitory effect at MRGPRX4 (Figure 30). Reduction of the carbachol signal in calcium mobilization assays was visible, however only starting at a concentration around 1,000 nM. The most potent agonistic effect was determined for **B18** with an EC_{50} of 1,020 nM in the β-arrestin assay.
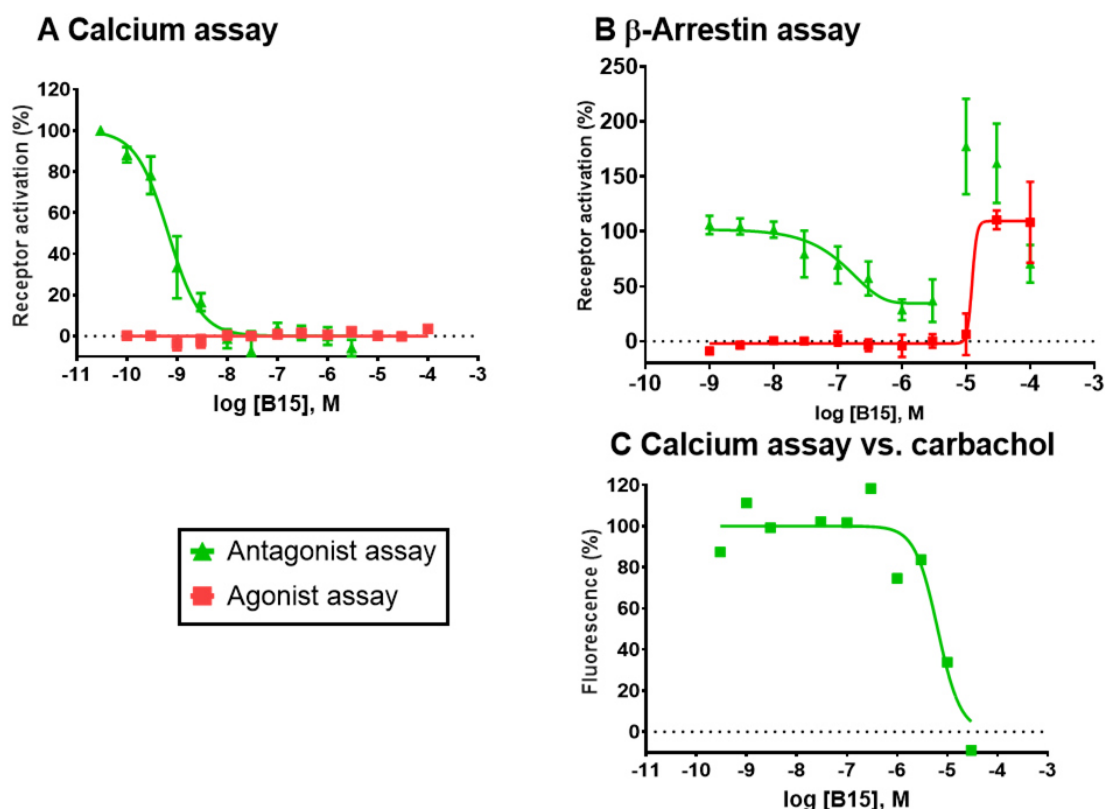
Figure 30: Assay results of **B15**. **A** Calcium assay results of antagonist and agonist assays. **B** β-Arrestin assay results of antagonist and agonist assay. **C.** Calcium assay results of antagonist assay versus carbachol.

The biphenyl derivatives are a challenging ligand class for MRGPRX4. The signal increase at higher concentrations impedes the determination of the inhibitory potency. As the signal increase is more pronounced in the β-arrestin assay, the curves

are shifted to the right, resulting in a generally increased IC_{50} value compared to the IC_{50} value determined in calcium mobilization assays. Nonetheless, the inhibitory potency of the lead **B2** could be improved. The functional antagonist **X60**, from the series of xanthine ligands, shares the biphenyl moiety with the here discussed antagonists. However, these biphenyl residues are likely binding to different parts of the binding pocket. This is as, the second commonality, the phosphonate residue, is expected to be anchored to the same position and consequently results in different orientations of the biphenyl moiety.

4.5.1 Mode of antagonism

The binding mode of the biphenyl antagonists was investigated in the calcium mobilization assay. Dilution series of the standard agonist, PSB-18061, were pre-incubated with different concentrations of the biphenyl antagonist **B2**, in order to determine whether **B2** behaves as competitive or allosteric antagonist (Experiments performed at 83L variant; see Figure 31A.). The maximum effect of the agonist was not decreased by the inhibitor, but the curve was shifted to the right. This is characteristic for a competitive inhibitor. The Schild regression (see Figure 31B.) is a linearized visualization of the same data. The calculated slope, the so-called Schild slope, is expected to be 1 for competitive antagonist. A slope of 1.28 was calculated for **B2**. In summary this data indicates a competitive antagonism of **B2**. This is in line with the results from the radioligand binding experiments presented in Figure 29. A K_B value of 31.9 nM was calculated, which is in good agreement with the EC_{50} determined in the calcium assay of 60.2 nM[83L] using a signle agonist concentraion (see Figure 29).
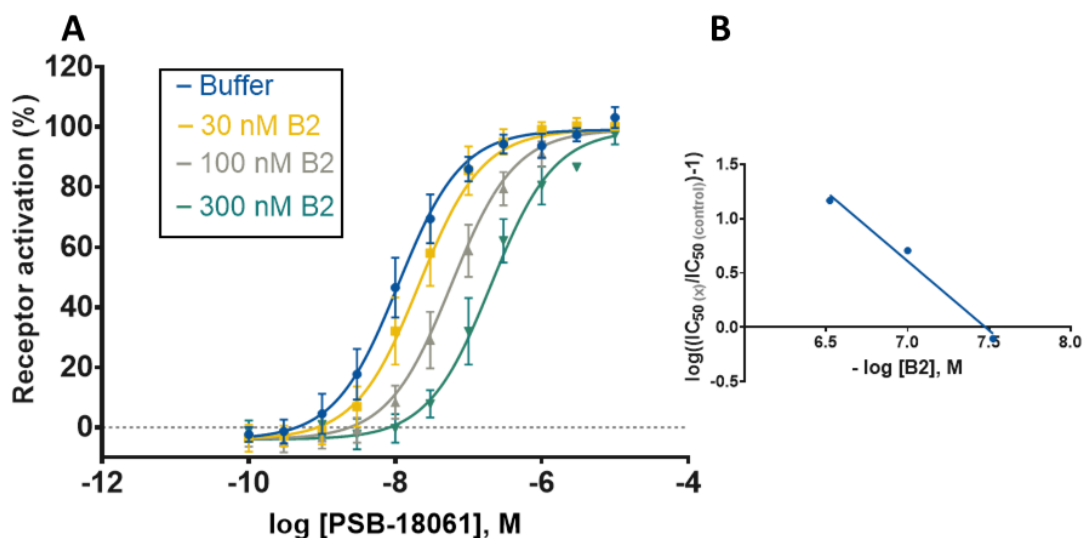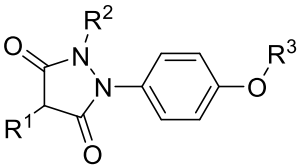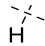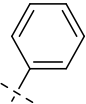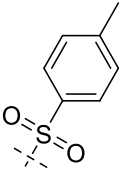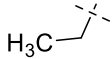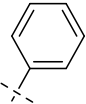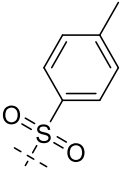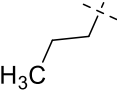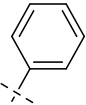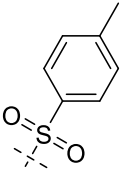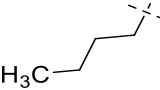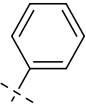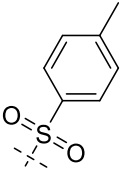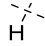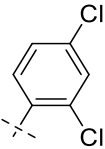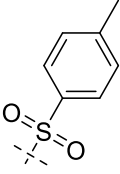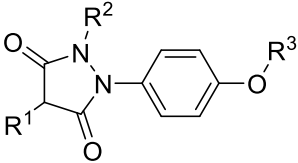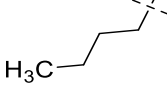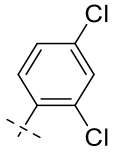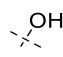
Figure 31: Gaddium / Schild EC_{50} shift, using the calcium assay on the 83L variant. **A** Curves of the standard agonist PSB-18061 with different concentrations of the biphenyl antagonist **B2**. Data points represent three independent experiments each performed in duplicates. A K_B of 31.9 nM is calculated. **B** Schild regression calculated from data obtained in Figure 31A. Y axis is drug ratio calculated as the "log of IC_{50} at specified antagonist concentration divided by IC_{50} in the absence of antagonist – 1". X axis is the negative log of the antagonist concentration in mol/l. A slope of -1.28 is calculated.

4.6 OXYPHENBUTAZONE DERIVATIVES

Several oxyphenbutazones were previously identified as MRGPRX4 antagonists, however, they had only been characterized on the minor variant 83L. Therefore, this thesis aimed to reevaluate their potential as MRGPRX4 antagonists at the main MRGPRX4 variant S83. **O5** (for structure and biological data see Table 11, as the most potent oxyphenbutazone derivative, was retested in the available assay systems on the variant 83S, and its inhibition in the calcium assay was validated by testing it against carbachol as a control (Figure 32). In the β-arrestin assay, an inhibition was measured, however, at higher concentrations a signal increase was observed. This signal increase was similar to the results of other antagonists at MRGPRX4 and is further discussed in chapter 4.7. In the calcium assay a clear inhibition was measured without any activation, however, the compound reduced the signal of carbachol, at concentrations of ~1,000 nM or higher. As this is well above the IC_{50} value of 228 nM at MRGPRX4, the effect did not interfere with the IC_{50} determination. However, the MRGPRX4 inhibition below 0% at concentrations above 1,000 nM by **O5** in the calcium assay cannot be understood as inverse agonism but is probably due to quenching of the background signal. The radioligand binding results show a displacement of the radioligand which is, however, incomplete. This is either due to precipitation of the compound, or to a binding to an allosteric site, which causes only a partial displacement of the radioligand. In Table 11 the structures and biological data of all evaluated oxyphenbutazone derivatives are displayed. Due to the similar structures, a quenching of the calcium signal by the other derivatives can be expected. Therefore, the IC_{50} in the calcium assay above 1,000 nM could be due to quenching instead of an actual MRGPRX4 inhibition. In conclusion, only for **O5** a valid inhibition could be determined.

Table 11: Structures and biological data of oxyphenbutazone derivatives at MRGPRX4

Cmpd.# Internal Id	R¹	R²	R³	Calcium assay[a]	β-Arrestin assay[b]
				$IC_{50} \pm$ SEM **(nM)** (% change to control)	$IC_{50} \pm$ SEM **(nM)** (% change to control)
				$EC_{50} \pm$ SEM **(nM)**; efficacy (%) (% change to control)	$EC_{50} \pm$ SEM **(nM)**; efficacy (%) (% change to control)
O1 DM179	H	(phenyl)	(tosyl/sulfonyl)	**5,790** ± 2,060 [83S] / **15,700** ± 3,200 [83L*]	>50,000 (+85%)[83S] / >50,000 (-43%)[83L*]
				nd [83S] / >10,000 (0%) [83L*]	nd [83S] / >50,000(+18%)[83L*]
O2 DM314	H_3C (ethyl)	(phenyl)	(sulfonyl)	**10,800** ± 1,760 [83S] / **17,800** ± 1,200 [83L*]	>10,000 (-20%) [83S] / >50,000(-42%)[83L*]
				nd [83S] / >10,000 (0%) [83L*]	nd [83S] / >50,000(+8%)[83L*]
O3 DM382	H_3C (propyl)	(phenyl)	(sulfonyl)	>10,000 (+5%) [83S] / **4,810** ± 490 [83L]	**22,700** ± 7,000[§][83S] / >50,000(-35%)[83L*]
				nd[83S] / >10,000 (-1%) [83L*]	nd [83S] / >50,000(+40%)[83L*]
O4 DM380	H_3C (butyl)	(phenyl)	(sulfonyl)	**6,090** ± 1,760 [83S] / **17,000** ± 5,000[83L*]	nd [83S] / >50,000(-4%)[83L*]
				nd [83S] / >10,000(+18%)[83L*]	nd [83S] / >10,000(+4%)[83L*]
O5 DM219	H	(dichlorophenyl)	(sulfonyl)	**228** ± 37 [83S] / **2,930** ± 750 [83L*]	**6,780** ± 1,530 [§][83S] / **6,090** ± 320[83L*]
				> 10,000 (-2%) [83S] / >10,000(+1%)[83L*]	~**11,500** (N=1) [83S] / >10,000(+15%)[83L*]

Cmpd.# Internal Id	R^1	R^2	R^3	Calcium assay[a]	β-Arrestin assay[b]
				IC$_{50}$ ± SEM **(nM)** (% change to control)	IC$_{50}$ ± SEM **(nM)** (% change to control)
				EC$_{50}$ ± SEM **(nM)**; efficacy (%) (% change to control)	EC$_{50}$ ± SEM **(nM)**; efficacy (%) (% change to control)
O6 DM399				>10,000(-6%) [83S] >10,000(-33%)[83L*]	**52,300** ± 12,800[83S] **50,400** ± 7,300 [83L*]
				nd [83S] >10,000(-1%)[83L*]	nd [83S] >50,000(+13%)[83L*]

[a]Calcium mobilization assays were performed either using LN229 natively expressing MRGPRX4-83S or 1321N1 astrocytoma cells recombinantly expressing MRGPRX4-83L. Efficacies are normalized to the maximal effect of PSB-18061 (see Figure 20). [b]β-Arrestin recruitment assays were performed using CHO-β-Arrestin cell lines either expressing MRGPRX4-83S or MRGPRX4-83L. Efficacies are normalized to the maximal effect of PSB-18061 (see Figure 20. [83X]= results for the respective MRGPRX4 variant (83S or 83L). $= The inhibition was incomplete *= Data obtained by Yvonne Riedel. All compounds were tested at multiple concentrations.
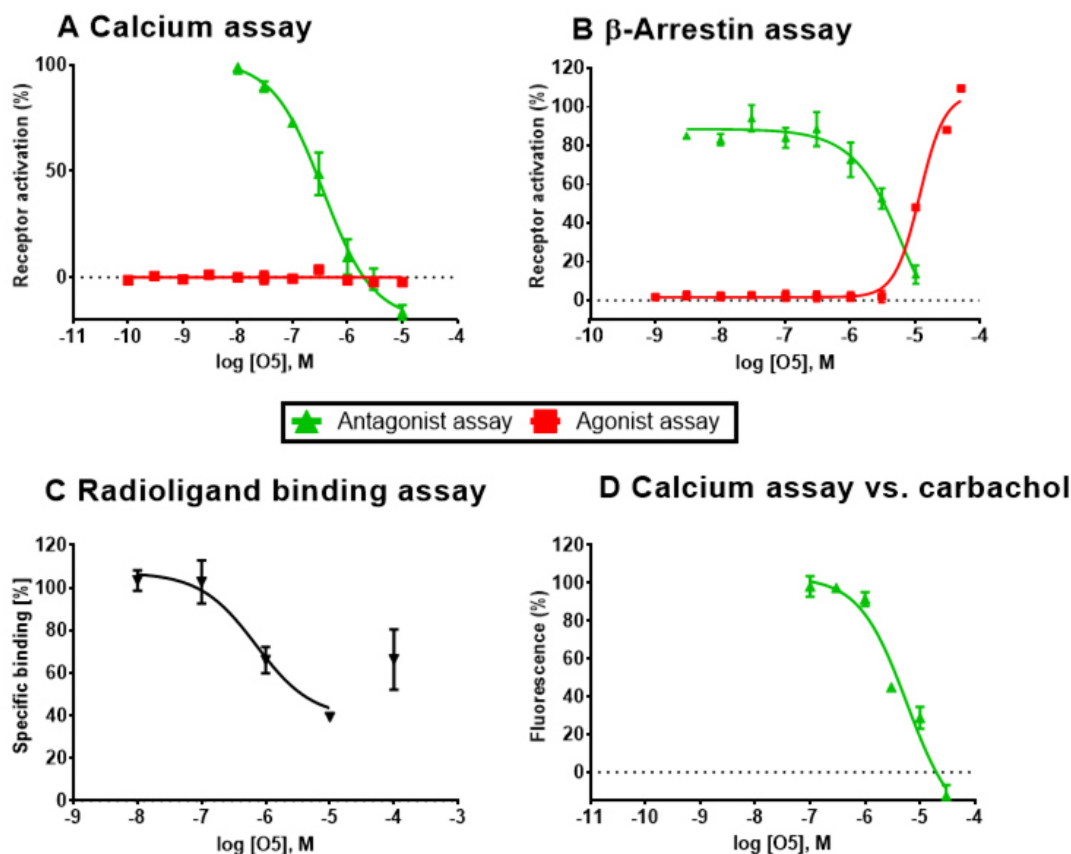
Figure 32: Assay results of **O5**. **A** Calcium assay results of antagonist and agonist assays. **B** β-Arrestin assay results of antagonist and agonist assay. **C.** Calcium assay results of antagonist assay versus carbachol. **C O5** tested in radioligand binding assay against 1 nM [^{3}H]PSB-18061. **D** Calcium assay results of antagonist assay versus carbachol.

O5 was tested in the calcium assay with and without washing steps after the 30 min of pre-incubation. The results imply a covalent binding mode, as the potency of **O5** was not reduced. As control, the biphenyl derivative **B2** was tested in the same setup and was found to be non-covalent (Figure 33).
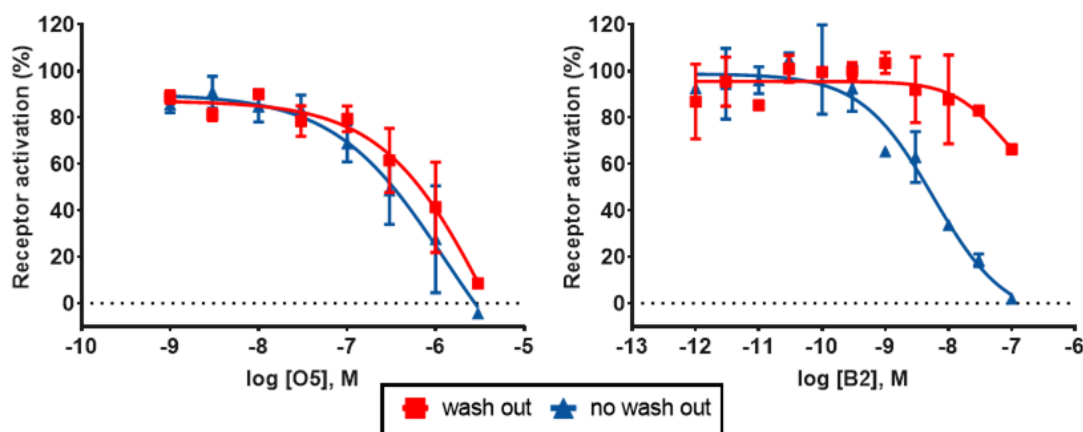
Figure 33: Wash-out experiments of **O5** and **B2**. In an antagonist calcium assay, the wells were washed three times after a 30 min pre-incubation with the respective antagonists and were afterwards activated with an EC_{80} concentration of PSB-18061.

O5 is the only oxyphenbutazone that could be verified as MRGPRX4-83S antagonist. However, assay interferences in the used systems were discovered. The incomplete displacement in the radioligand assay might indicate an allosteric binding mode or be due to precipitation of the compound in the radioligand binding assay. Moreover, binding was found to be irreversible. The compound was much more potent in blocking the calcium signal compared to β-arrestin recruitment. As for a competitive antagonist no bias can be expected, this indicates an allosteric binding mode.

4.7   COMPLEX BEHAVIOR OF THE MRGPRX4 ANTAGONISTS

Most MRGPRX4 inhibitors seemed to elicit a signal themselves at high concentrations, in addition to their inhibitory effects. This is true for antagonistic xanthine derivatives, biphenyl derivatives, and oxyphenbutazones. Exemplary curves obtained in β-arrestin assays are shown in Figure 34. This effect is more pronounced in the β-arrestin assay compared to the calcium assay, but often occurs at high concentrations in both assays. It has two major implications. Firstly, the data quality, especially for β-arrestin assays is reduced, as can be seen in Figure 34. The SEM values are exceptionally high, and the inhibition curves often do not reach 0%, and thus the

evaluation is inaccurate. Secondly, and more importantly, the origin of this effect must be scrutinized.
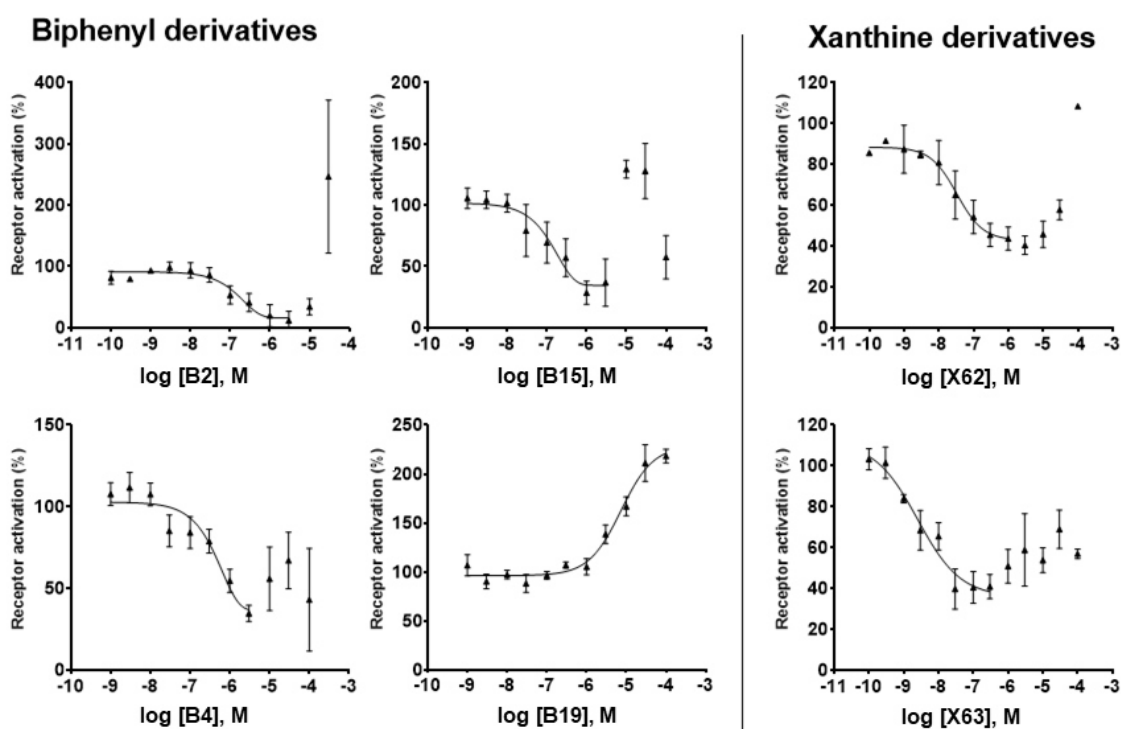
Figure 34: Exemplary β-arrestin assay results of antagonists on MRGPRX4-83S expressed in CHO-β-arrestin cells. The cells are preincubated for 30 min with respective inhibitors and activated with an EC_{80} concentration of the standard agonist (1 nM PSB-18061). Data points represent means ± SEM of at least three individual experiments performed in duplicates.

The following points have to be considered and taken into account. In the calcium assay, a full agonist can appear as an antagonist when tested as such. This is due to continuous activation of the receptor during the 30 min preincubation period which leads to receptor desensitization. However, it can be excluded that this is the reason for the here observed phenomenon. The "agonistic effect" appears at considerably higher concentrations, as can be seen in Figure 35. Moreover, this problem does not apply for the β-arrestin assay, were a preincubation with an agonist would just increase the signal. In conclusion, the observed inhibitory effects are independent of the signal increase at higher concentrations.
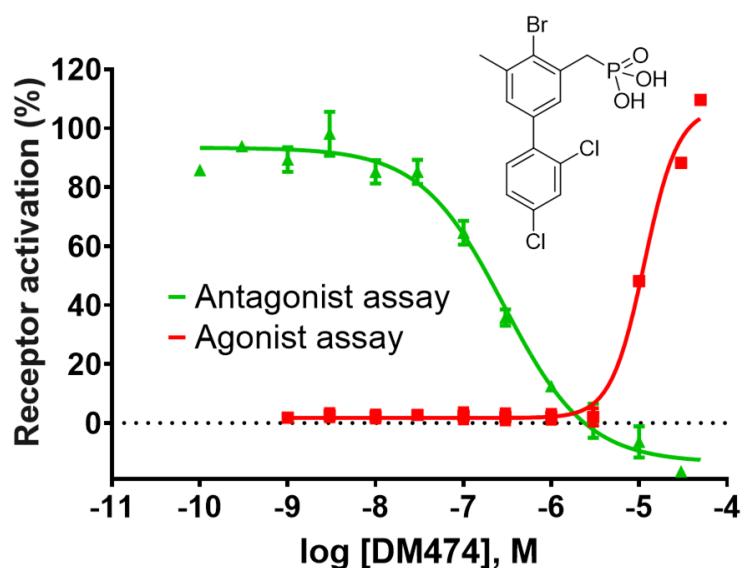
Figure 35: DM474 was tested in the calcium assay on the MRGPRX4-83L variant as an antagonist (green; 30 min preincubation with DM474 and stimulation with EC_{80} of standard agonist, PSB-18061) and tested as agonist (red; stimulation with DM474). $IC_{50} = 0.294 \pm 0.082$; $EC_{50} = 13.2 \pm 0.3$.

Due to the unexpected nature of these results, different experiments were conducted to investigate whether the agonistic effect is attributable to an actual MRGPRX4 activation or to assay interference. The performed experiments include:

(i)   Testing of cell viability with the MTT assay.

Results in Figure 36A show that, after 3 d of incubation, only biphenyl derivatives showed reduced cell viability, and only at high concentrations of 100 μM. Therefore, the signal increase is not due to cell death.

(ii)   Stimulation of wild type astrocytes in calcium assays.

Results in Figure 36B show that no agonism was recorded at concentrations of up to 50 μM. Therefore, no other receptor that is present in astrocytes provoked the calcium signal.

(iii) Blocking the signal with the $G\alpha_{q/11}$ protein inhibitor FR900359.

Results in Figure 36C show that the calcium signal of the biphenyl derivative was blocked by FR900359, similar to that of the xanthine agonist PSB-18061. Therefore, the signal is due to an activation of $G\alpha_{q/11}$ proteins.

(iv)   Testing of $G\alpha_{q/11}$ protein activation with the TruPath assay.

Results showed activation of all three $G\alpha_q$ proteins after stimulation by **B2**, and no activation without MRGPRX4 transfection. Explanatory results for G_{15} activation are provided in Figure 36D. This is an additional proof that biphenyl derivatives can in fact induce $G\alpha$ protein activation through MRGPRX4.
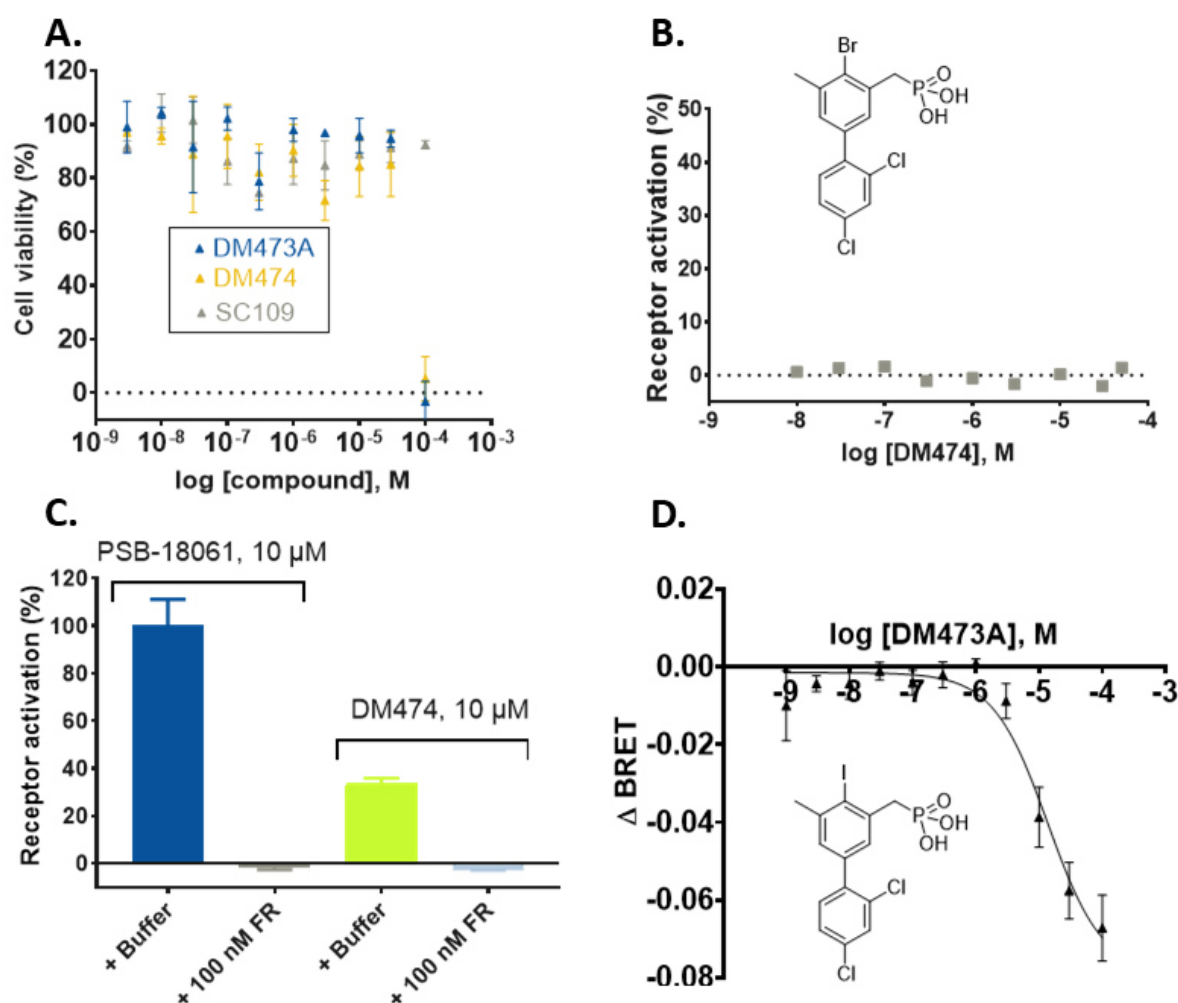
Figure 36: **A** MTT assay with three different antagonists. LN229 were incubated for 3d with the respective compounds. **B** Structure of DM474 and agonist test in calcium assays on wild-type astrocytes. **C** Calcium assay results of PSB-18061and DM474 in the presence and absence of the G_q protein blocker FR900359 (30 min of preincubation with 100 nM of FR900359). **D** Structure of **B2** and TruPath assay results on $G\alpha_{15}$ proteins. Results are means of four independent experiments performed in duplicates.

In view of these results, it can be concluded, that the agonistic behavior is actually due to an activation of MRGPRX4 at high concentrations. The previous notion, that biphenyl derivatives are not antagonists, but partial agonists, must be discarded since the activation is significantly less potent than the inhibition. Moreover, the agonistic effects often show "full" efficacy. An alternative explanation is the presence of a second binding site. It can be hypothesized, that these derivatives bind to the orthosteric, and additionally to an allosteric binding pocket. However, it is unclear, which does elicit which effect. One binding site is bound by the compounds with a high potency and results in an inhibition of the receptor, and the second binding site is bound at a lower potency and can elicit an activation that is independent from any binding to the other binding pocket. Notwithstanding, this would be very remarkable, and even more so due to the structural differences between biphenyl and xanthine antagonists.

The observation that most biphenyl derivatives showed an increased signal over 100% when tested as antagonist in β-arrestin assays, superseding the signal of the standard agonist alone, led to the question if at high concentrations the compounds act as positive allosteric modulators. Accordingly, as presented in Figure 37, **B19** was simultaneous incubated within the presence of the standard agonist PSB-18061 and without. The signal was not increased above that of the standard agonist alone. Hence, the 30-minute pre-incubation, applied in the antagonist assays (Figure 34), amplifies the signal. During the additional incubation time, β-arrestin can accumulate, and therefore a higher signal is observed. This, however, is not due to a synergistic effect of standard agonist and the test compound.
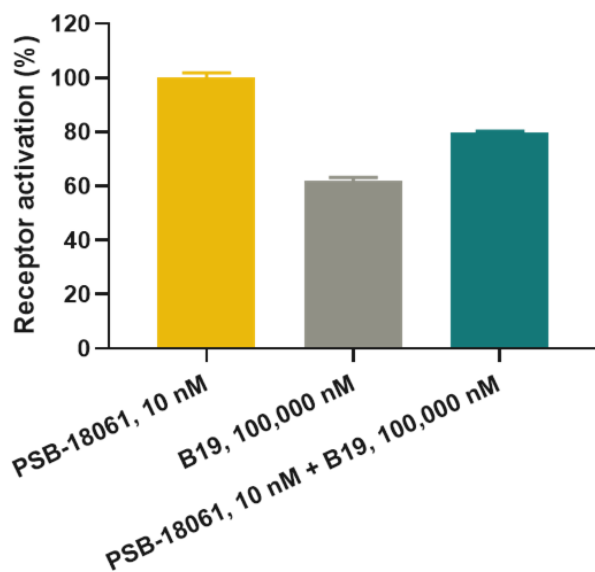
Figure 37: Agonist β-arrestin assay of the standard agonist and **B19** each alone and in combination. One experiment was performed in quadruplets.

In conclusion, biphenyl derived antagonists activate a $G\alpha_q$ protein-coupled pathway in high concentrations. Since their inhibition occurs already at considerably lower concentrations, a second binding pocket is assumed. One binding pocket does activate the receptor, and the other one inhibits it. The β-arrestin assay was found to be not the optimal assay to investigate the inhibition. As the IC_{50} value obtained in calcium assays and the K_i value of the radioligand binding assays provided similar results, these assays should be preferred as measurement for inhibitory potency. Nonetheless, the activation has to be monitored, at least for lead compounds, using β-arrestin and calcium assays. Only when a sufficient discrepancy between the measured IC_{50} and EC_{50} is present, the IC_{50} values are reliable.

4.8 COUPLING OF **MRGPRX4**

Gα protein coupling of MRGPRX4 was studied after activation with two different MRGPRX4 ligands, namely PSB-18061 and **X60**, using the TruPath assay system.[26] The measured pEC_{50} values, presented in Figure 38A, show that MRGPRX4, activated by the full agonist PSB-18061, couples a wide range of Gα proteins. However, due to the overexpression of the receptor and the respective Gα proteins in the assay, this may not reflect the physiological coupling.[19; 26] The efficacy, presented in Figure 38B and C, must also be considered. Here, the maximal activation is normalized to the maximal activation by a control receptor and compound (B) or to literature values (C). The controls were selected as the respective receptors are known to couple the respective Gα protein and produce a stable signal in the assay. Even though PSB-18061 showed a high potency at the $G\alpha_{Gust}$ protein, the low efficacy implies that coupling under physiological conditions would be neglectable. Normalization to maximal effects published by Olsen et al. (2020) results in largely comparable results as the ones produced by the control receptors (Figure 38C).[26] The efficacy at the $G\alpha_{15}$ protein was even higher, and for $G\alpha_{Gust}$ and $G\alpha_{12}$ considerably lower. The $G\alpha_{q/11}$ protein family showed a consistent high potency and relatively high efficacy, in special at $G\alpha_{15}$. Since $G\alpha_{15}$ proteins are highly expressed in immune cells, the predominant activation of $G\alpha_{15}$ could indicate a relevance of MRGPRX4 in immunological processes. But still, MRGPRX4 couples to at least one member of every Gα protein subfamily except $G\alpha_{s}$ proteins. This promiscuous coupling implies, that the downstream signaling events, elicited by MRGPRX4 activation, are dependent on the Gα protein expression of a respective cell.

X60 is a potent functional antagonist that showed only marginal activation in calcium assays (discussed in chapter 4.4.2). Hence it was analyzed, how the partial agonism is reflected by the activation of single Gα protein subtypes. The results in Figure 38 show that after activation with **X60**, MRGPRX4 only couples the $G\alpha_{15}$ protein, however, with low efficacy.
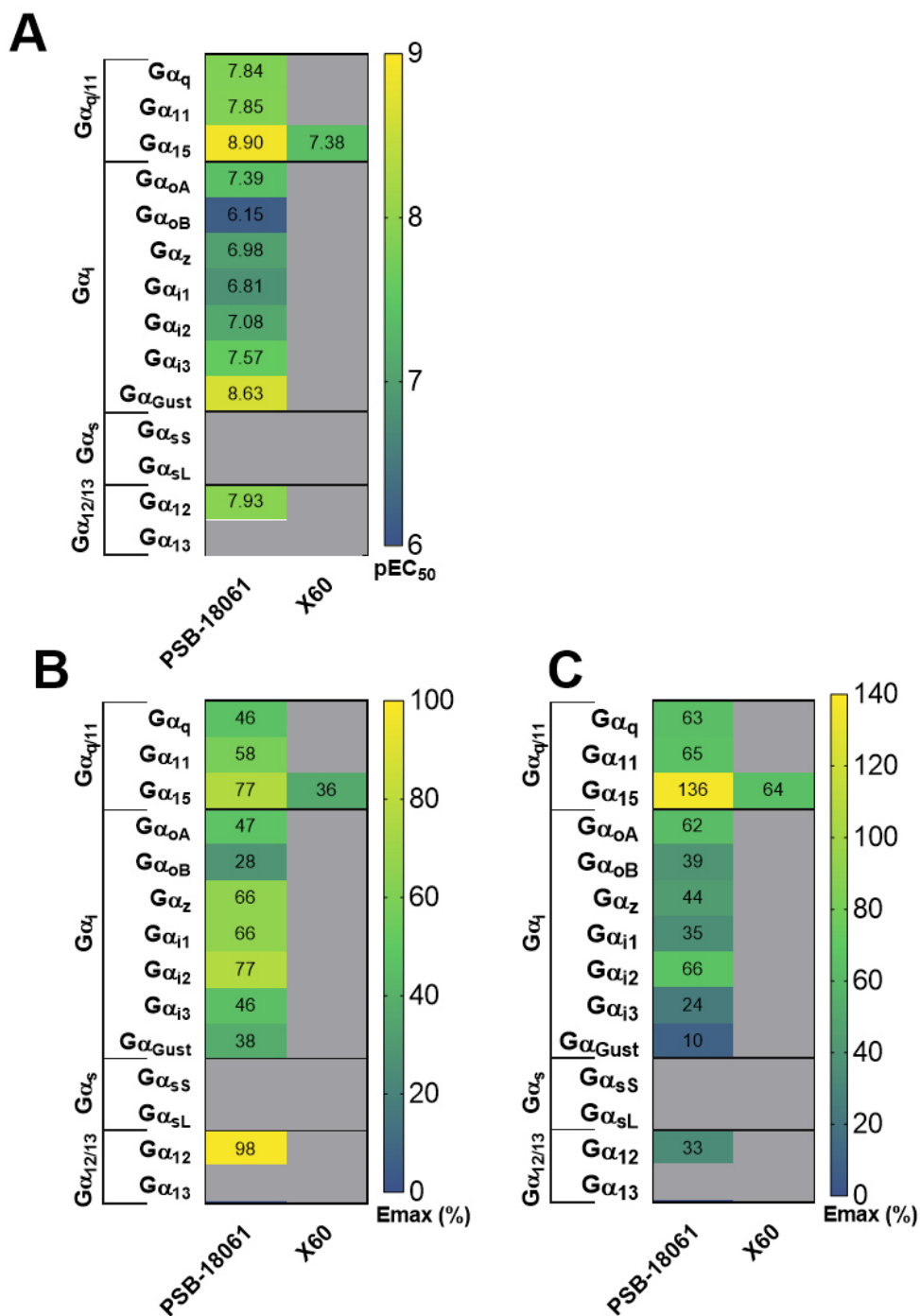
Figure 38: Gα protein coupling of MRGPRX4 after activation with the full agonist PSB-18061 and the functional antagonist **X60**. Data obtained by Josua Krebber. **A.** pEC_{50} of the compounds in activating the respective Gα protein subtype. **B.** Efficacy (%) of the compounds on the respective Gα protein subtype normalized to corresponding control receptor activated by the respective control compound ($Gα_{q/11}$ and $Gα_{12/13}$ – Neurotensin receptor 1, Neurotensin; $Gα_i$ - µ opioid receptor, DAMGO; $Gα_s$ – β2 adrenergic receptor, Isoproterenol; $Gα_{Gustducin}$ – κ opioid receptor, Salvinorin). **C.** Efficacy (%) of the compounds on the respective Gα protein subtype normalized to results from Olsen et al. (2020).[26] Grey = EC_{50} >100 µM.

4.9 DEORPHANIZATION APPROACHES

4.9.1 Manuscript in preparation: Thyroid hormone derivatives

The following manuscript was prepared in the scope of this thesis. The author performed the experiments (excluding selectivity assays) and has written the manuscript in close cooperation with Prof. Dr. Christa E. Müller.

Thyroxine (T4) and its metabolites are endogenous activators of the orphan mas-related G protein coupled receptor X4 (MRGPRX4)

Robin Gedschold, Ghazl Al-Hamwi, Christa E. Müller

Introduction

The MAS-related G protein-coupled receptor X4 (MRGPRX4) is a primate-specific orphan receptor.[45; 47; 52] The receptor is primarily coupled to Gαq proteins leading to calcium mobilization. Moreover it induces β-arrestin recruitment.[60; 67; 75] Several natural variants of the receptor have been reported, all of which occur with low frequency. The amino acid change S83L was found to have a substantial impact on the potency of several agonists; it had wrongly been assumed to be the major variant however its abundance is only 3.4%, while the main variant 83S is much more frequent (96.5%).[45; 74; 75] [REF pending] MRGPRX4 was found to be expressed in sensory neurons of dorsal root ganglia (DRG) and trigeminal ganglia. Moreover, expression was detected in CD[8+] cytotoxic T cells, skin cells, and several tumors.[45; 50; 60; 65; 69] The proposed therapeutic potential of MRGPRX4 ligands, range from wound healing, pain and itch, to cancer therapy.[45; 64; 65; 73; 77]

Several ligands have been discovered, e.g., the synthetic heterocyclic compound MS47134 (**I**, structure see Figure 39) and a recently published agonist series of potent agonists based on a xanthine scaffold, with the most potent compound being PSB-18061 (**II**, structure see Figure 39).[75] [REFs pending] Endogenous bile acids and bilirubin have also been found to activate MRGPRX4 at high micromolar concentrations. The most potent ones are deoxycholic acid (**III**, structure see Figure 39) and

ursodeoxycholic acid (**IV**, structure see Figure 39).[76; 77; 79] Their EC_{50} values at the main variant 83S of MRGPRX4 of 17 μM (**III**) and 48 μM (**IV**).[REF pending] At TRG5, the proposed bile acid receptor, **III** showing a EC_{50} value of 1 μM, in a cAMP assay.[81] (-)-Menthol (**V**, structure see Figure 39) was reported to act as a modulator of MRGPRX4, reducing agonists efficacy in β-arrestin recruitment assays, and to displace an MRGPRX4-specific radioligand. Both effects were observed at extraordinarily high concentrations of above 100 μM.[86] [RL REF] Another target for **V** is the transient receptor potential channel TRPM8, which is suspected to be responsible for its cooling effect.[87; 88] TRPM8 was shown to be activated by much lower concentrations of 0.1 μM.[89] MRGPRX4 is still considered an orphan receptor because the physiological metabolites reported so far all are only weakly potent.

I, MS47134
EC_{50} 13.3 μM

II, PSB-18061
EC_{50} 0.00154 μM

III, Deoxycholic acid
EC_{50} 16.9 μM

IV, Ursodeoxycholic acid
EC_{50} 47.5 μM

V, (-)-Menthol
K_i 186 μM
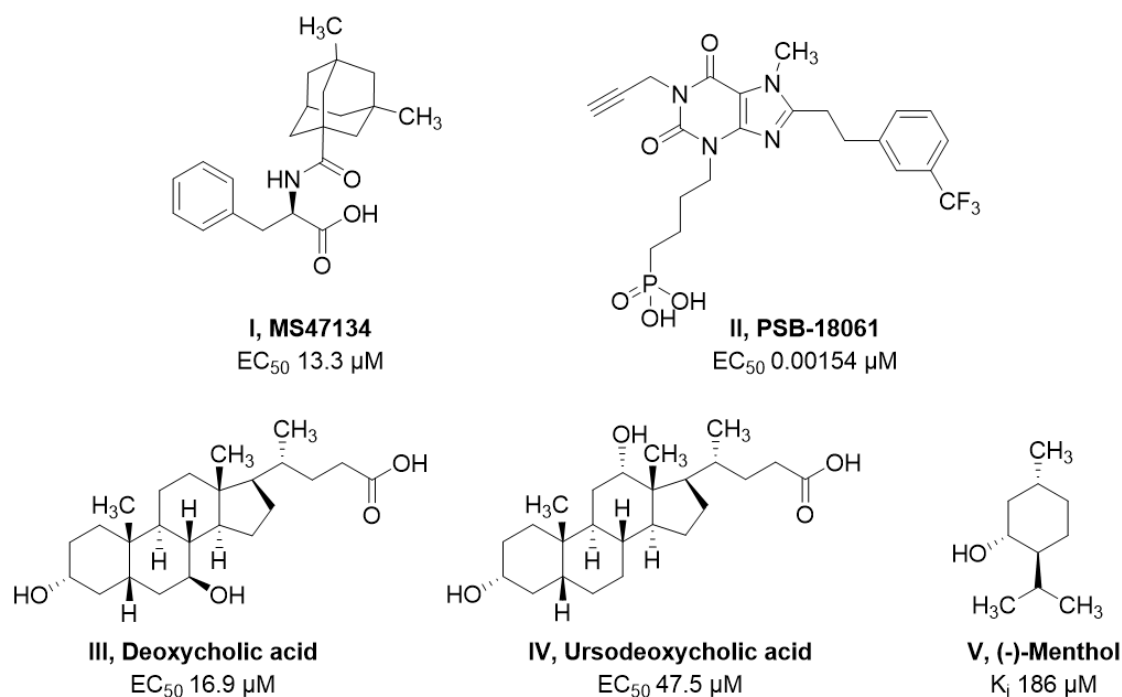
Figure 39: Structures of literature-known MRGPRX4 agonists. EC_{50} values as obtained in calcium mobilization assays, and K_i in radioligand binding assays.[REFs pending]

Here we identified the endogenous thyroid hormone L-thyroxine (T_4) and some of its metabolites to activate MRGPRX4. T_4 is a (pro)hormone, and a precursor of triiodothyronine (T_3), both of which activate nuclear thyroid hormone receptors. This nuclear receptor transmits effects such as cell growth, development, and regulation of metabolism, through direct genomic effects. The ligand receptor complex binds specific response elements on the DNA at the promoter region of target genes and

subsequently enhance their transcription.[113] Additionally, nongenomic effects have been reported, e.g. the induction of angiogenesis and proliferation. These latter effects were proposed to be transduced by membrane receptors; as one candidate the integrin $\alpha v\beta 3$ receptor has been identified.[113–115]

The hormones T_3 and T_4 are subject to different degradational pathways, which lead to a variety of metabolites (Figure 40).[116–119] Many metabolites were reported to possess physiological effects, similar as different from those of the parent hormones. 3,5,3'-Triiodothyroacetic acid for example is a T_3 mimetic, proposedly acting through thyroid receptors.[118] 3-Iodothyronamine on the other hand was shown to be a multi-target ligand, modulating 'trace amine-associated receptors' (TAARs, promiscuous GPCRs activated by aminergic metabolites), β-adrenergic receptors, and TRP channels, inducing hypothermia and bradycardia in mice.[118; 120]
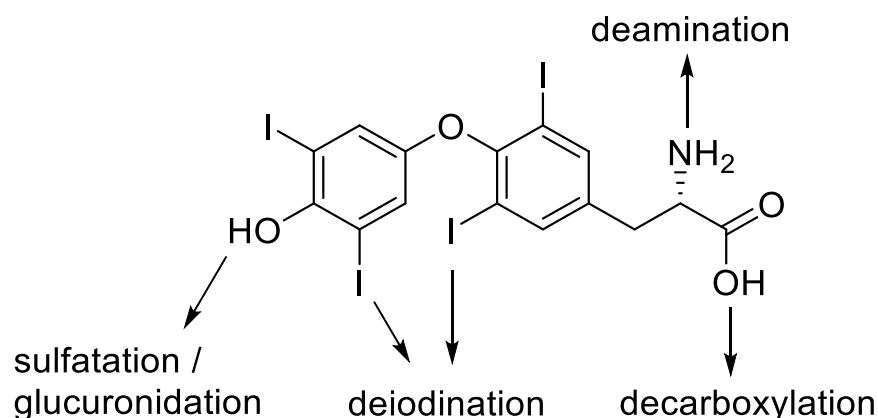
Figure 40: Metabolism of L-thyroxine (T_4); adapted from van der Spek et al. (2017).[116]

Results and discussion
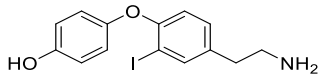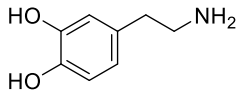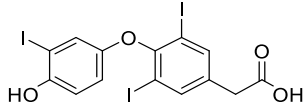
We utilized a calcium mobilization assay, employing LN229 glioblastoma cells, and as orthologue assay system a β-arrestin recruitment assay, based on enzyme complementation, as previously published. [REF pending] The thyroid hormone T_4 (**H1**) and selected metabolites with small molecular variations were investigated as ligands for MRGPRX4 (see Figure 41 & Table 12). **H1** was identified as a moderately potent agonist with EC_{50} values of 12.0 µM and 13.2 µM for calcium mobilization and β-arrestin recruitment. The efficacy compared to PSB-18061, the most potent MRGPRX4 agonist published so far, showed that **H1** acted as a partial MRGPRX4

agonist in both investigated assays. [REF pending] Besides **H1**, we evaluated the deiodinated metabolites, T_3 (**H2**) and 3,5-diiodthyronine (**H3**), the decarboxylated 3-iodothyronamine (**H6**), and the deaminated 3,5,3'-triiodothyroacetic acid (**H8**). All investigated compounds were still active, indicating that the amino acid function was not required. The metabolites were found to exhibit higher efficacies than **H1**, acting as highly efficacious or even full agonists. The common tyrosine motif prompted us to investigate tyrosine (**H4**) and its endogenous derivatives L-DOPA (**H5**) and dopamine (**H7**) as well. However, no activity at MRGPRX4 was detected, indicating that the second phenyl ring was required for receptor activation.

Assay interactions were ruled out and selectivity was ensured by testing the compounds at MRGPRX2 in the same β-arrestin recruitment assay system. The cells were treated with 100 μM of **H1**, **H3**, **H6** and **H8**. **H6** activated MRGPRX2 to 49%, while **H8** showed a small activation of 17%. Other derivatives did not show any activation over 5% at MRGPRX2 (normalized to 5 μM selective MRGPRX2 agonist CST-14, data not shown).

Table 12: Potency of thyroid hormones, their metabolites and related compounds as MRGPRX4 agonists.

Cmpd. number; name	Structure	Calcium assay[a] EC_{50} ± SEM (µM) [maximal activation[c]]	β-Arrestin assay[b] EC_{50} ± SEM (µM) [maximal activation[c]]	MRGPRX2 β-Arrestin assay[d] Activation at 100 µM
II PSB-18061 [REF pending]		**0.00154** ± 0.00015 **[100%]**	**0.00228** ± 0.00016 **[100%]**	**[0%]**
III Deoxycholic acid [REF pending]		**16.9** ± 0.9 **[80%]**	**1.68** ± 0.55 **[49%]**	nd
Amino acids				
H1 L-thyroxine (T$_4$)		**12.0** ± 5.0 **[11%]**	**13.2** ± 6.7 **[33%]**	**[-2%]**
H2 triiodothyronine (T$_3$)		**pending**	**pending**	nd
H3 3,5 Diiodthyronine		>10 **[11%]**	**11.6** ± 4.5 **[76%]**	**[0%]**
H4 Tyrosine		>10 **[-6%]**	>10 **[0%]**	nd
H5 L-DOPA		>10 **[-4%]**	>10 **[5%]**	nd

Cmpd. number; name	Structure	Calcium assay[a] EC_{50} ± SEM (μM) [maximal activation[c]]	β-Arrestin assay[b] EC_{50} ± SEM (μM) [maximal activation[c]]	MRGPRX2 β-Arrestin assay[d] Activation at 100 μM
Amines				
H6 3-Iodothyronamine		**21.1 ± 1.6** **[75%]**	**3.16 ± 0.79** **[96%]**	**[49%]**
H7 Dopamine		>10; **[0%]**	>10; **[2%]**	nd
Deaminated acid				
H8 3,5,3'-Triiodothyroacetic acid		**30.0** ± 5.7 **[63%]**	**25.9** ± 8.3 **[113%]**	**[17%]**

[a]Calcium mobilization assays were performed using LN229 natively expressing MRGPRX4-83S. [b]β-Arrestin recruitment assays were performed using CHO-β-Arrestin cell line expressing MRGPRX4-83S [c]Maximal effects are normalized to PSB-18061.
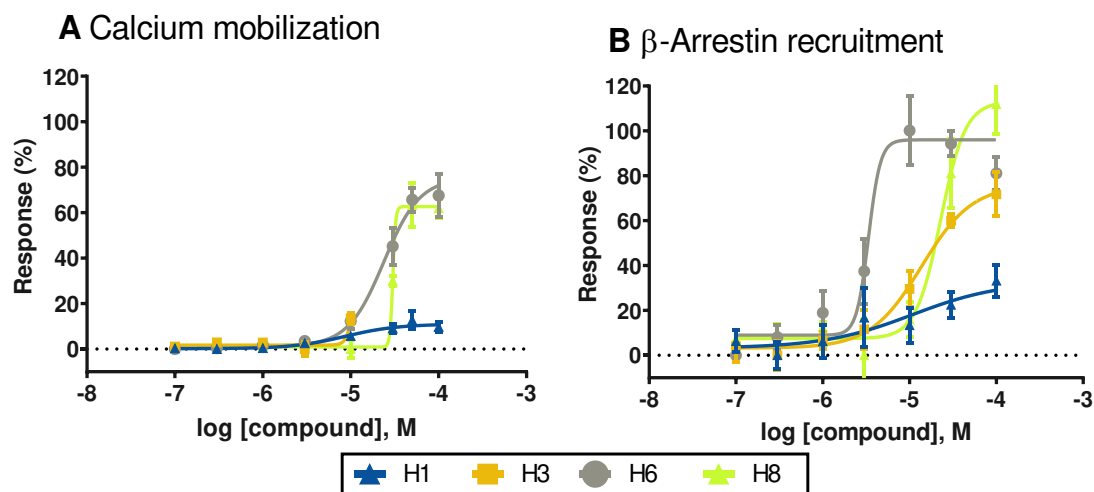
Figure 41: Functional assay results of the tested thyroid hormone **H1** and derivatives. Data points are means of at least three independent experiments performed in duplicates. Results are normalized to PSB-18061.

Next, competition binding experiments were performed employing [³H]PSB-18061.[REF pending] The radioligand binding was analyzed in presence of 100 and 30 µM of the functionally active thyroid hormone derivatives. Only **H8** was able to displace the radioligand at 30 µM (Figure 42A.). Partial displacement was observed for **H2**, **H3,** and **H6** at 100 µM, but not for the partial agonist **H1**. Subsequently, **H8** was closer investigated with a heterologous competition experiment, which produced a K_i of 1.60 ± 0.31 µM.
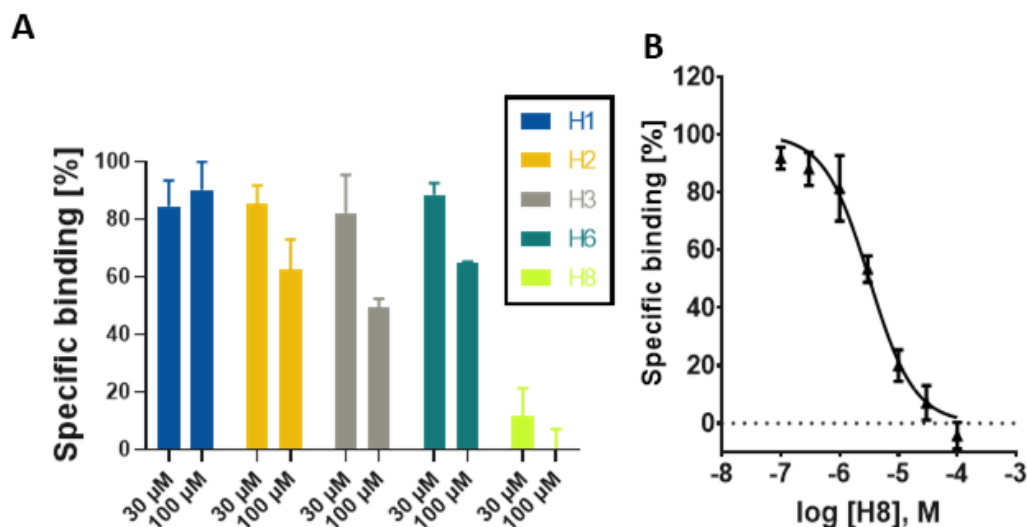
Figure 42: Competition binding of the MRGPRX4 radioligand [^{3}H]PSB-18061. **A** Radioligand (1 nM), HEK-MRGPRX4 membrane preparation (50 µg of protein) and 10 mM MgCl$_2$ were incubated for 1 h, at room-temperature before filtering through GF/A glass fiver filters with TRIS pH 7.4 supplemented with 0.1% BSA and 0.1% Tween20. **B** Competition curve of **H8**. A K$_i$ value of 1.60 ± 0.31 µM was calculated.

Discussion

Here we present, that the thyroid hormone **H1** and its metabolites active the orphan receptor MRGPRX4. The proposed physiological function of MRGPRX4 and the nongenomic thyroid functions show some commonalities. MRGPRX4 was reported to be pro-proliferative, to enhance cell migration and tumor progression, and to potentially improve wound healing.[64; 65; 73] Nongenomic thyroid functions are proposed to be pro-proliferative, and to elicit angiogenesis and tumor progression, and to enhance wound healing.[114] However, the determined potency of **H1** at MRGPRX4 is only in the low micromolar range, and moreover, it was found to be a partial agonist only. The thyroid hormones are strictly regulated hormones with low serum concentrations under healthy conditions, in the low picomolar range. Nongenomic effects of **H1** and **H2** are proposed to be mediated, at least partially, by the integrin αvβ3 receptor, requiring concentrations of 0.1 or 0.001 µM of **H1** or **H2** to induce their full effects.[115; 121] These concentrations are above the serum level, but considerably lower than the concentration required for MRGPRX4 activation.

The here presented thyroid hormone derivatives were tested for selectivity at MRGPRX2, where all derivatives showed EC$_{50}$ above 100 µM. Only the amine **H6** showed about 50% activation. However, this may not be due to the thyroid hormone scaffold, as other were completely inactive. Moreover, many amines were found to activate MRGPRX2 at high concentrations.[45]

The alkaline **H6** presents a novel type of MRGPRX4 ligand because it breaks the pattern of exclusively acidic MRGPRX4 ligands that are published to date. Concentrations of around 50 nM of **H6** were reported in blood plasma.[120] The metabolite was proposed to be a multi-target ligand, activating several GPCRs and ion channels with moderate potencies. A concentration of 0.1 µM is needed at the proposed main target, the TAAR1, and 1 µM was shown to modulate adrenergic receptors and to activate TRPM8.[120] The low-µM activity of **H6** on MRGPRX4 is thus in a similar range as that of other reported targets.

Part of the binding pocket of MRGPRX4 is thought to be positively charged, based on a published protein structure, which revealed two arginine residues in close proximity.[75] The phosphate of the series of xanthine agonists was found to occupy this positively charged binding pocket in a docking study.[xanthine ref] In contrast, this part of the binding pocket seems not to be occupied by the here discussed metabolites, but **H8**. This is as (i) the radioligand was not displaced by the metabolites, but by **H8**, and (ii) the alkaline **H6** does not have a residue which is negatively charged at physiological pH. **H8**, containing a carboxylic acid, therefore likely binds in an alternative binding mode. The displacement of the radioligand, which is part of this xanthine series, only by **H8** might indicate that the carboxylic acid coordinates around the same arginine side chains.

The thyroid hormone metabolites are a large class of endogenous compounds, of which only a fraction was investigated in the scope of this work. Serum concentrations of sulfatated metabolites are expected to be very low, as they are rapidly degraded and excreted because of their improved water solubility.[119] However, whether the negatively charged sulfate might improve MRGPRX4 agonistic behavior needs to be investigated in future. Moreover, the thyroid hormone metabolites could be utilized as scaffold for future drug development for MRGPRX4. The partial agonistic activity

of **H1** could be improved in order to develop MRGPRX4 antagonists, as no antagonist for MRGPRX4 is published to date.

4.9.2 Endogenous compounds investigated as potential MRGPRX4 agonists
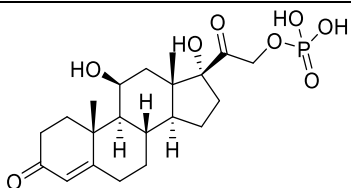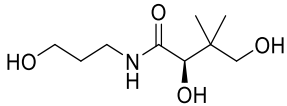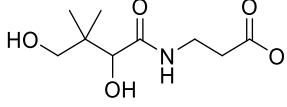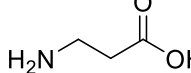
Based on literature research and on structural similarities, different endogenous compounds were selected and tested for activity at MRGPRX4. The nucleotide derivatives were selected for their similarity to the purine-based xanthine derivatives (see Table 13).

Table 13: Biological evaluation of different endogenous nucleotide derivatives at MRGPRX4

Name	Calcium assay[a] (activation %)	β-arrestin assay[b] (activation %)	Radioligand binding assay[c], (Inhibition %)
IMP	>100 µM (-4.7%)	nd	nd
NADH	>100 µM (1%)	nd	nd
Acteyl-CoA	nd	>100 µM (10%)	> 100 µM (12 ± 7 %)
AMP	>100 µM (3%)	nd	nd

In Table 14 other compounds are listed, as hydrocortisone phosphate, which combines the lipophilic core of bile acids and the phosphonate of the xanthine and biphenyl ligands discussed in this thesis. None of the tested compounds shows activation of MRGPRX4, as determined in the respective assay systems.

Table 14: Biological evaluation of different endogenous compounds at MRGPRX4

Name	Structure	Calcium assay[a] (activation %)	β-arrestin assay[b] (activation %)	Radioligand binding assay[c], (Inhibition %)
Hydrocortisone phosphate		>50 µM (3%) **(83L)**	>100 µM (-5%) **(83L)**	nd
Dexpanthenol		nd	>100 µM (9%)	> 100 µM (-6 ± 5%)
Pantothenic acid		nd	>100 µM (-7%)	nd
Beta-alanin		>10 µM (0%)	nd	nd

[a]Calcium mobilization assays were performed either using LN229 natively expressing MRGPRX4-83S or 1321N1 astrocytoma cells recombinantly expressing MRGPRX4-83L. Efficacies are normalized to the maximal effect of PSB-18061 (see Figure 20). [b]β-Arrestin recruitment assays were performed using CHO-β-arrestin cell lines either expressing MRGPRX4-83S or MRGPRX4-83L. Efficacies are normalized to the maximal effect of PSB-18061 (see Figure 20). [c]Radioligand binding assays performed with 1 nM [^{3}H]PSB-18061 using HEK-MRGPRX4-83S membrane preparations. nd = not determined

5 RESULTS AND DISCUSSION: SCRATCH ASSAY

5.1 STUDYING CELL MIGRATION IN WOUND HEALING ASSAYS

Cell migration is essential for the organization of multicellular organisms as it is, for example necessary for embryonic development, immune defense, and wound healing.[122; 123] Additionally, it plays a role in pathological processes, such as the angiogenesis of solid tumors.[124] Migration is a complex process influenced by a multitude of signals, where chemokines and growth factors are found to play a major role.[125–127] Migration can be divided into single-cell migration, such as the migration of leukocytes during an immune response, and collective migration, which is prevalent in cancer metastasis, embryonic development, and wound healing.[122] The latter is a relatively well understood physiological process of cell migration, where, after rupture of a cellular layer, cells migrate in order to close the wound.[122; 123] Therefore, so called wound healing assays are often used assay systems to monitor cellular migration. These assays are either two-dimensional (2D), or more sophisticated three-dimensional (3D) setups. As epithelial cells undergo a collective 2D migration while closing a wound, 2D wound healing assays are expected to emulate the physiological process well.[123] Therefore, the most used wound healing assays are 2D set ups.[128–130] Here, a monolayer of cells is generated and their migration into an artificially created cell-free zone - the wound - is measured. The wound can be generated either by cell depletion or by physical exclusion. The latter is achieved by placing a barrier into a cell culture dish. Cell depletion is achieved by mechanical, electrical, chemical, or thermal means.[131] A simple scratch assay is the most common technique: a pipette tip, or any other sharp tool, is used to create the cell free zone in form of a scratch. The main disadvantage is that every scratch is performed manually, one at a time. Thus, it is difficult to reproducibly create linear scratches.
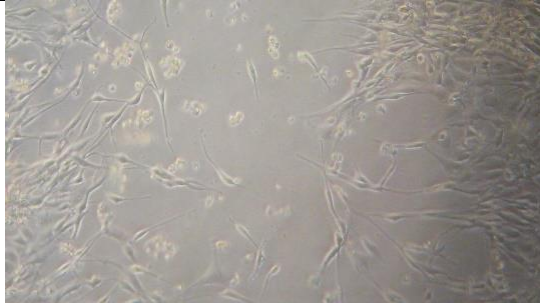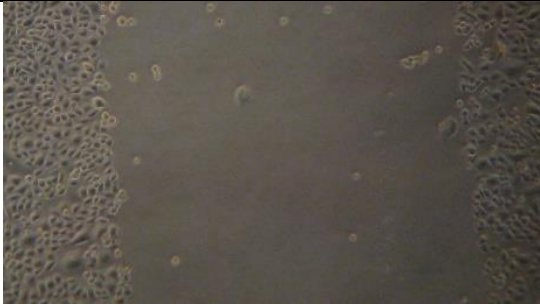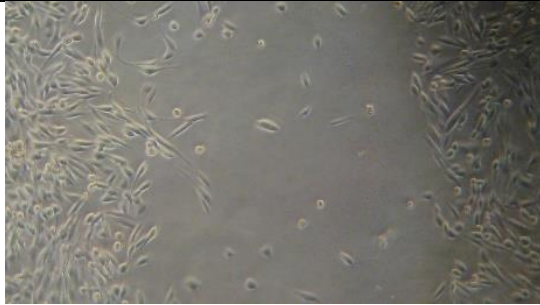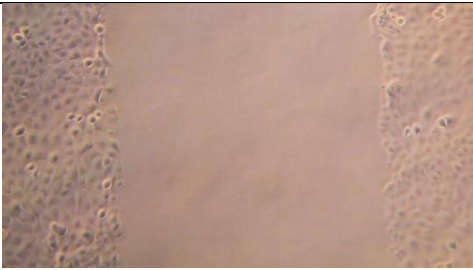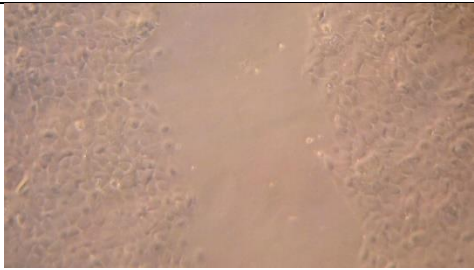
Cell proliferation is an unwanted confounder in such assays, as it would close the wound independent of migration. Therefore, serum starvation combined with preincubation with a proliferation inhibitor like mitomycin C is often used.[129] Ideally, the cells migrate in a coordinated movement called sheet migration. This is characterized by collective cell migration while maintaining intercellular junctions.[129]
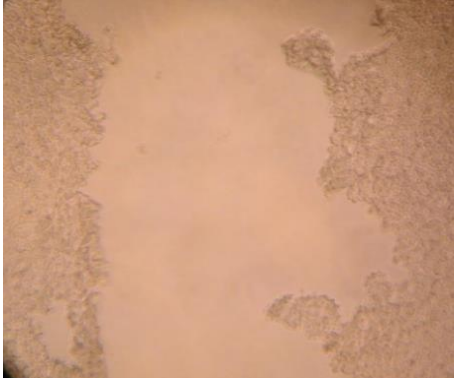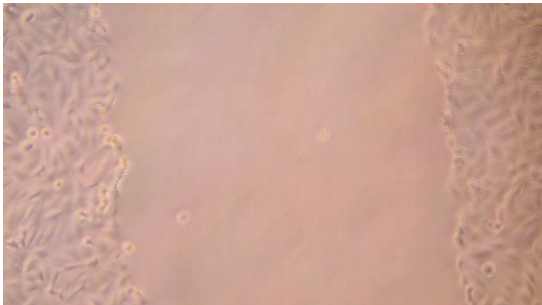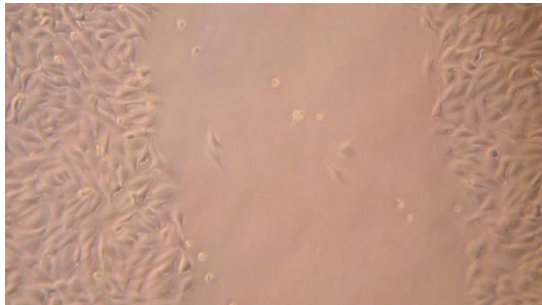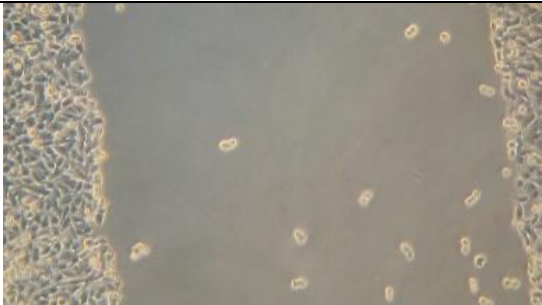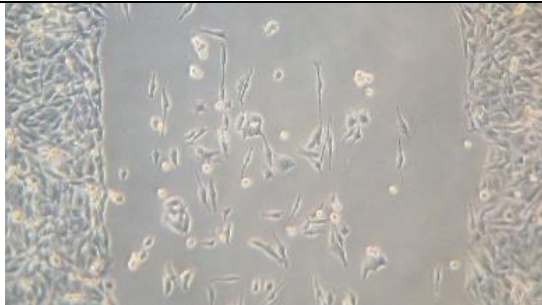
Therefore, it facilitates a reproducible and straightforward evaluation. Single cell migration can be analyzed by quantifying the distance a single cell travels.[128] Sheet migration, on the other hand, is most often quantified by the area the cells migrate as a function of time. This is done either by estimation, measurement of the width of the cell-free gap, or measurement of the cell-free area.[128–130] Doing this evaluation by hand is time-intensive and needs to be blinded in order to prevent unintentional bias during evaluation. Therefore, a partially automated approach should be used, where the cell-free area is automatically recognized and measured.[128; 130] One challenge for this, however, and for the non-automated approaches too, is recapturing the same part of the wound. In conclusion, a simple scratch assay is a cost-effective and simple method, but precise work and an objective evaluation are essential to obtain reproducible results.

5.2 ESTABLISHMENT OF THE METHOD

We aimed to establish a scratch assay, in order to evaluate the effects of GPCR activation on cell migration. For this objective, firstly, an appropriate cell line was searched for. Astrocytoma 1321N1, CHO, HaCaT, HEK-293, LN229, and Sk-Mel 28 (a melanoma cell line) cells were evaluated, as these cell lines were for scratch assays before.[132–137] Cells were seeded at an appropriate density into a 12-well plate and incubated for one day, until a consecutive monolayer was formed. The cells were treated with 5 µg/ml mitomycin C for 2h and subsequently scratched with a sterile 200 µl pipette tip. Afterwards, a serum-free medium was added. Pictures were taken directly after the scratch and after 24h. The pictures are presented in Table 15. Of the evaluated cells HaCaT cells showed the best properties for our objective. They exhibit sheet migration (a coordinated and collective migration) with clearly bordered scratches and are easy to evaluate. Astrocytoma and HEK cells proved disadvantageous, due to bad adherence to the plate that impeded the creation of clear and homogenous scratches. CHO cells showed single cell migration, what was to be avoided for a more straight-forward evaluation. While LN229 and Sk-Mel did show homogeneous scratches and sheet migration, the migration itself, however, was too slow to be analyzed after one day. Longer time periods were not applicable, as after more than one day of serum starvation the cells started to detach.

Table 15: Cell lines that were evaluated for their suitability in a scratch assay. nd = not determined, big layers of cells detached
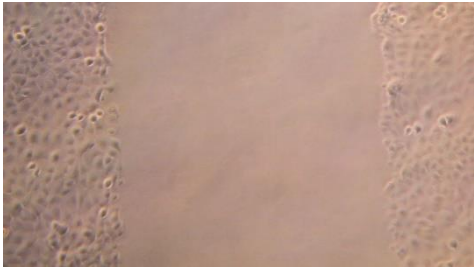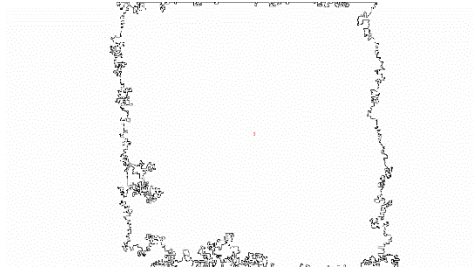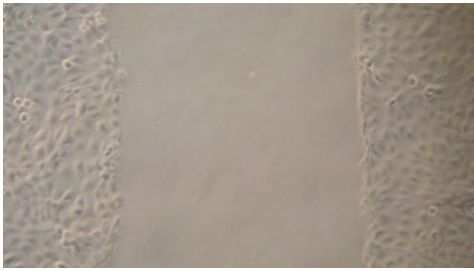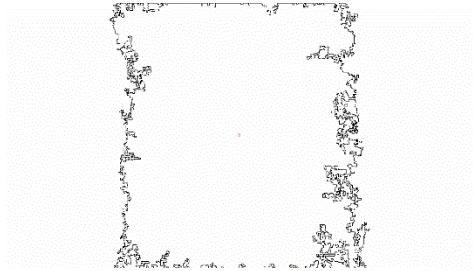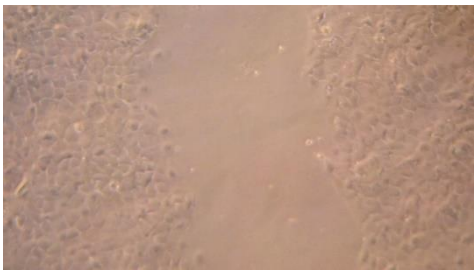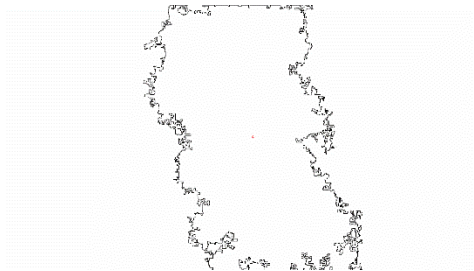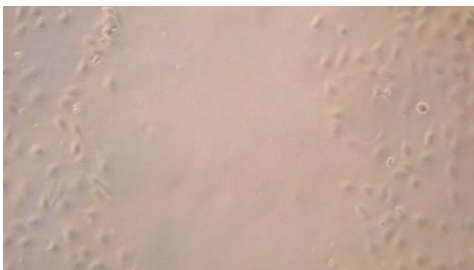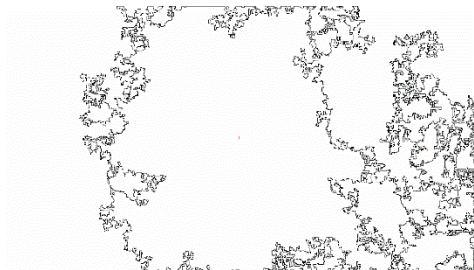
Astrocytoma 1321N1	
0h	**24h**
CHO	
0h	**24h**
HaCaT	
0h	**24h**

HEK-293	
0h	**24h**
	nd
LN229	
0h	**24h**
SK-Mel 28	
0h	**24h**

To allow an objective evaluation, a partially automated approach was used as described by Iesco and Pei (2018).[130] Accordingly, ImageJ (NIH; Bethesda, Maryland, U.S.) was employed to automatically recognize the scratch outlines and to measure the resulting area.[138] The generated outlines were visually controlled afterwards for plausibility. In Table 16 examples of scratches and automatically generated outlines

are presented. The reduced cell density after 48 h did not allow any meaningful evaluation.

Table 16: Scratches with automatically generated outlines by Image J, following the protocol from Iesco and Pei (2018).[130; 138]

0 h
1 h
24 h
48 h

5.3 INVESTIGATION OF MRGPRX EXPRESSION IN HaCaT CELLS AND RECOMBINANT EXPRESSION OF THE 83S AND 83L VARIANT

Initially, the response of HaCaT cells to different MRGPRX agonists was tested in a calcium assay, in order to detect possible effects. The cells were stimulated with of 10 µM either ATP (control, likely activating purinergic G protein-coupled receptors P2Y, which are reported to be expressed by native HaCaT cells[139]), CST-14 (MRGPRX2 agonist), Dipyridamol (MRGPRX3 agonist), or PSB-18061 (MRGPRX4 agonist). Initially, native HaCaT cells, and HaCaT cells treated for 5 d with 5 µg/ml of lipopolysaccharide (LPS) were studied. LPS was applied because it had been shown that MRGPRX expression can be induced in an inflammatory state.[65] No signal was measured for any MRGPRX agonist in both approaches (Figure 43A.). Hence, it is assumed that there are not sufficient functional MRGPRX receptors located on native HaCaT cells, and expression cannot be induced by LPS treatment.

As next step, only MRGPRX4 was studied, and HaCaT cells were lentivirally transfected with MRGPRX4-83L-mCherry, and the obtained polyclonal cells, as well as monoclones picked via fluorescence-activated cell sorting (FACS), were investigated. The poly- and monoclonal cells showed calcium signals after activation with PSB-18061, with a greatly increased signal for the monoclone (Figure 43B.). Four of the picked monoclones, namely clone (C) 3, 4, 6, and 8, were further investigated in calcium assays to compare expression levels. In calcium assays, a higher expression leads to a higher agonist potency and an increased signal, thus the results can be used as rough comparison of expression levels.[37] C3 was identified to be the optimal of the tested monoclones, while C8 had no visible MRGPRX4 signal (Figure 44). In addition to HaCaT-MRGPRX-83L cell line, a stable cell line of HaCaT-MRGPRX4-83S was generated. A vector without mCherry, but a G418 resistance was chosen, thus the cells were selected by treatment with the antibiotic, and no picking of monoclones was performed.
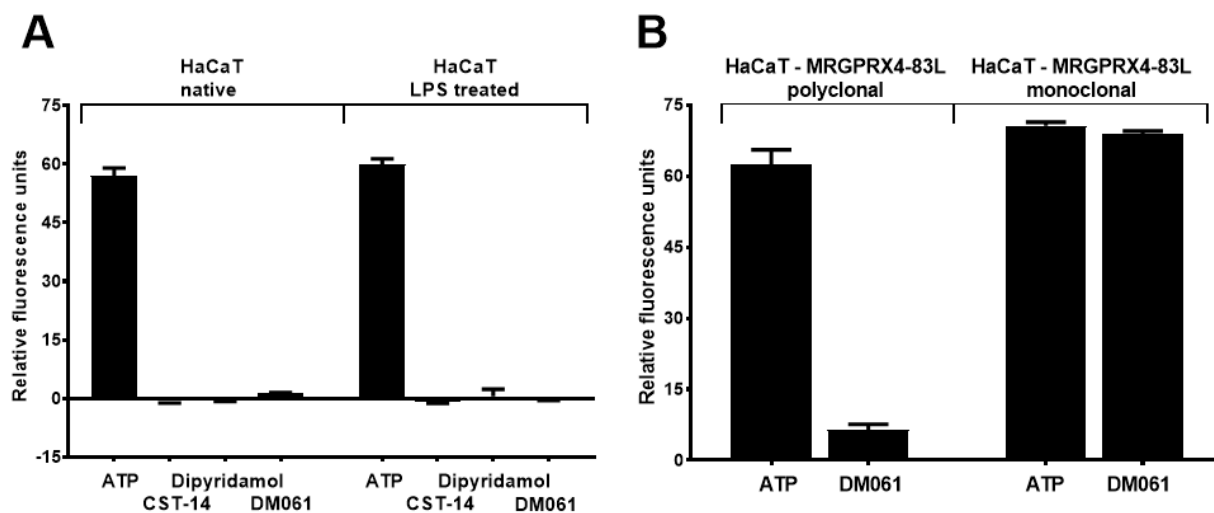
Figure 43: Calcium mobilization assays on HaCaT cell lines. **A.** Native HaCaT, and HaCaT treated with LPS (5 µg/ml) for 5 d were stimulated with 10 µM of the respective MRGPRX agonist (DM061 = PSB-18061). **B.** HaCaT cells transfected with MRGPRX4-83L, polyclonal and monoclonal (C3), were stimulated with 10 µM of the MRGPRX4 agonist PSB-18061 or ATP.
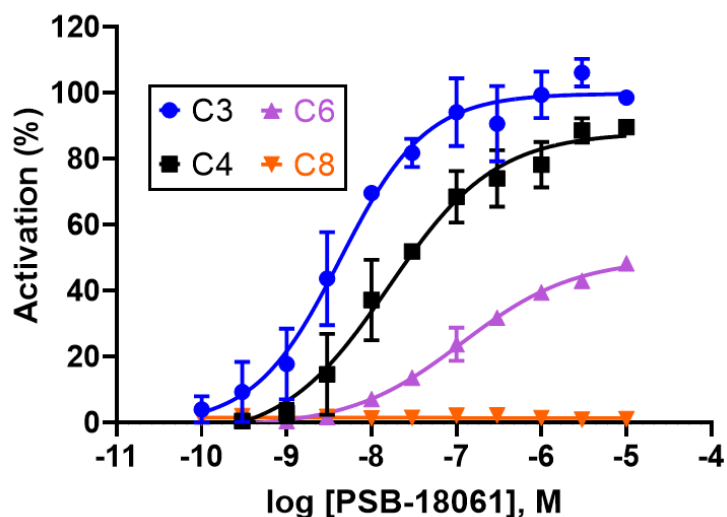
Figure 44: Preliminary calcium mobilization assay using different monoclones of HaCaT-MRGPRX4-83L. Experiments were performed in duplicates. Results are normalized to 10 µM ATP.

5.4 SCRATCH ASSAY RESULTS

The performed scratch assays did prove to be hardly reproducible overall. The migrated areas varied from experiment to experiment. In some, the migration of

controls was unsatisfactory and the assays could not be evaluated. In this chapter mostly representative single experiments are shown that are thought to represent results of multiple replicates. However, the extend of the observed effects did vary between two experiments.

Native HaCaT cells were investigated in the scratch assay with the MRGPRX4 agonist PSB-18061 and the antagonist **B2**. Moreover, we used dexpanthenol as a control, as it was observed to increase migration of HaCaT cells before.[140] None of the compounds altered migration compared to control in native HaCaT cells(Figure 45).
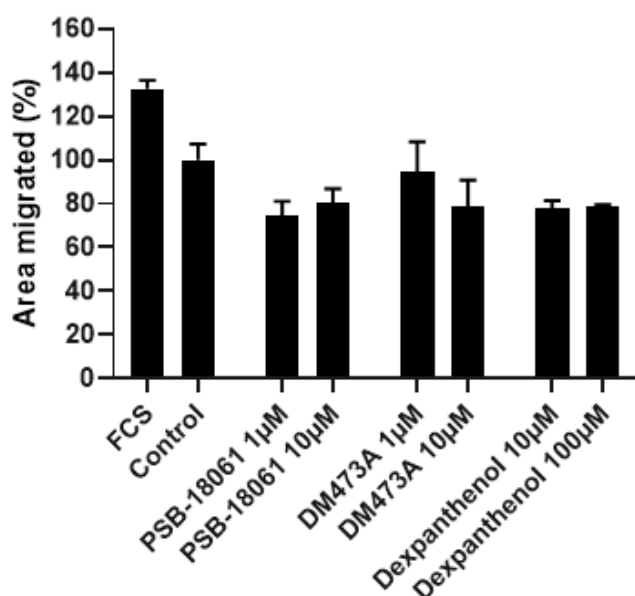
Figure 45: Preliminary control experiment using native HaCaT. The cells were treated with MRGPRX4 agonist, antagonist DM473A (**B2**) and dexpanthenol and evaluated in the scratch assay. Results are normalized to control. Data points are means ± SEM of one single experiment performed in quadruplicates.

Next, we compared the migration of untreated native HaCaTs and untreated C6, -3, and -4 of the MRGPRX4-83L monoclones. C6 (low MRGPRX4 expression) was shown to migrate comparable to native HaCaTs (Figure 46A.). The highly expressing C3 and -4, however, showed reduced migration. This suggests that a high MRGPRX4-83L expression does inhibit cell migration. In order to validate these result, C3 and native cells were treated with **B2**, a MRGPRX4 antagonist. Though the migration increased, the effect was small (Figure 46B.).
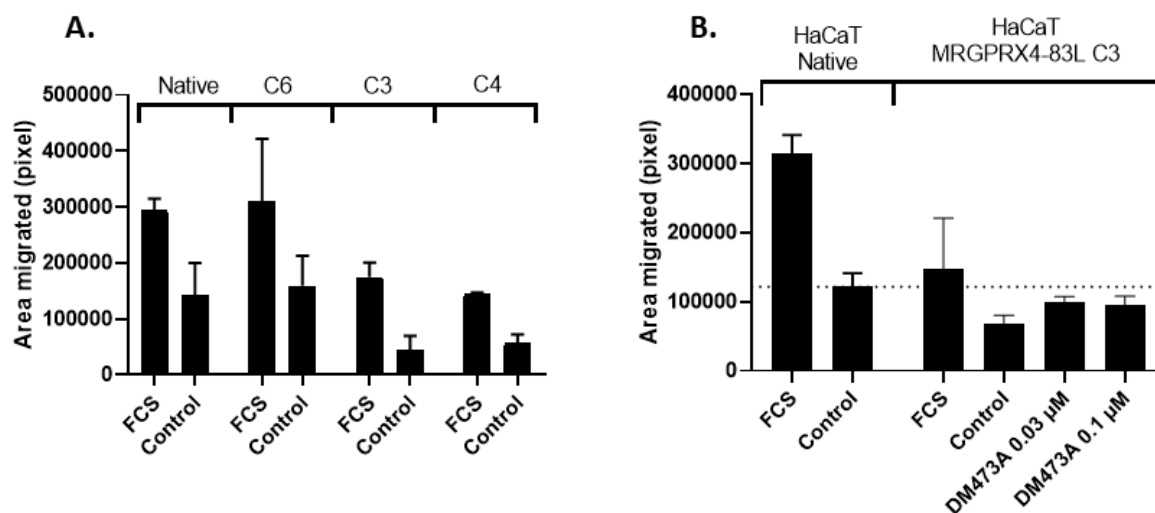
Figure 46: Effects of MRGPRX4-83L expression on migration. **A.** Migration of native HaCaT cells and clone 6 and 3 of MRGPRX4-83L-transfected cells were compared. Two experiments were performed in triplicates or quadruplicates. **B.** Effect of DM473A (**B2**), an MRGPRX4 antagonist, on migration of clone 3 of MRGPRX4-83L-transfected HaCaT cells. Dotted line represents migrated area of untreated native HaCaT cells.

Subsequently, we evaluated the effects of different concentrations of the MRGPRX4 agonist PSB-18061 on the migration of either C3 of the HaCaT-MRGPRX4-83L cell line and of HaCaT-MRGPRX4-83S cells. For the 83L variant no concentration-dependent inhibition was observed (Figure 47). At the 83S variant, all agonist concentrations resulted in lower migration compared to control but show no concertation dependence.
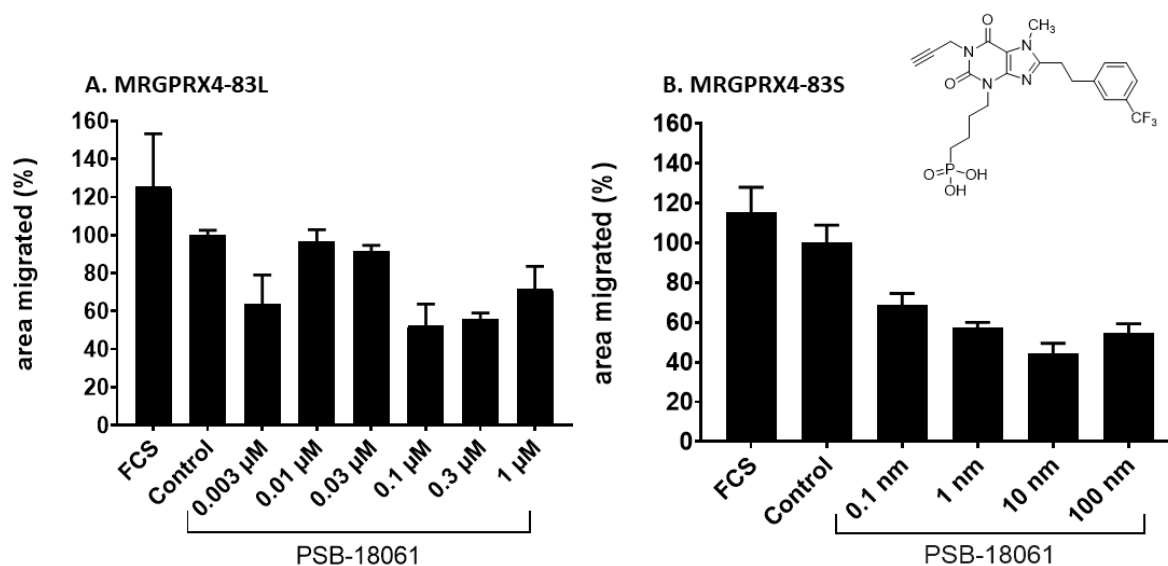
Figure 47: Effects of different concentrations of PSB-18061 on the migration of HaCaT-MRGPRX4-83L C3 and HaCat-MRGPRX4-83S cells. Data points are means of one single representative experiment performed in duplicates. Results are normalized to control (DMSO).

Next, we evaluated a second agonist with a higher potency on MRGPRX4-83L. SC095 (**X20**) showed opposing results as high concentrations activate migration contrary to expectations (Figure 48). However, as this effect was equally visible on native HaCaT, this is likely due to an unspecific effect of the compound.
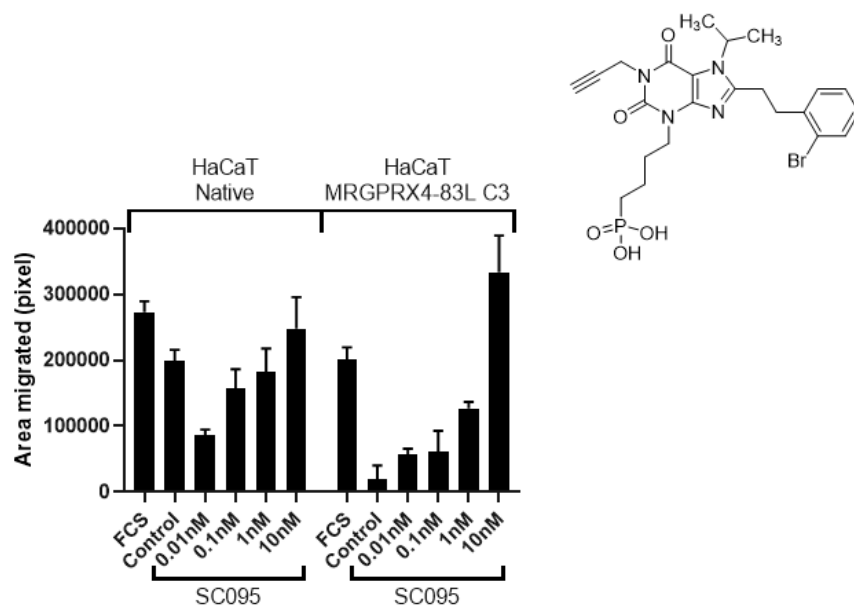
Figure 48: Effect of different concentrations of the MRGPRX4 agonist SC095 (**X20**) on the migration of HaCaT-MRGPRX4-83L-C3 cells. Data points are means of one single experiment performed in duplicates. Results are normalized to control (DMSO).

The scratch assay for MRGPRX4 did not show consistent results. The scratch areas proved to be hard to analyze and the deviations between different assays were often high. The most consistent results were achieved by comparison of different monoclones with presumably different MRGPRX4 expression levels. The transfected cells did show an overall reduced migration of the controls. However, comparison of transfected monoclones can be misleading as the overexpression of proteins can manipulate a cell in a multitude of ways. Agonists and antagonists did not show concentration-dependent effects.

The FCS controls did show a consistent decelerated wound closure as well for MMRGPRX4 transfected cells. Hence an effect on cell proliferation instead of migration could be hypothesized. However, in course of this thesis multiple MTT assays were performed (see chapter 4.4.5 and 4.7), which measure the count of viable cells after 3 days of incubation with test compounds. Neither with different MRGPRX4 antagonists, nor agonists were increased cell counts measured. Decreased cell counts were observed occasionally, likely due to unspecific cell death.

6 RESULTS AND DISCUSSION: GPR18 AND METHUOSIS

Excursus: Methuosis

Regulated cell death is an essential mechanism in multicellular organisms, allowing complex processes, as for example embryogenesis and immunity..[141; 142] Apoptosis is the best understood form of "deliberate" cell death. However, interest on the other forms of programmed cell death is rising, with methuosis being one example of these.[141–144] The name methuosis is derived from the Greek 'methuo' translating to 'drink to intoxication', which describes well the phenotype of this process.[144] The cell undergoes excessive accumulation of single membrane macropinosome-derived vacuoles, resulting in blatant morphological changes (see Figure 49A).[144; 145] The cytoplasm is replaced by these vacuoles, leading to diminished cell metabolism and plasma membrane integrity, ultimately leading to loss of viability and cell death.[144] In physiological settings macropinosomes are either recycled to the cell membrane or fused with lysosomes. These mechanisms were reported to be dysfunctional in methuosis, leading to an accumulation of vacuoles. The hallmarks of apoptosis, cell shrinkage or nuclear fragmentation, are not visible.[144]

Methuosis was shown to be provoked by over-activated Ras, as shown in U251 glioblastoma cells.[145; 146] Ras is a family of proto-oncogenes which regulate stimulate cell-growth and differentiation. Moreover, small molecules like the indole-based chalcone 3-(2-methyl-1*H* indol-3-yl)-1-(4-pyridinyl)-2-propen-1-one (MIPP) and the enhanced   3-(5-methoxy,2-methyl-1*H*-indol-3-yl)-1-(4-pyridinyl)-2-propen-1-one (MOMIPP) were found to induce methuosis within a few hours after application, which was found to be reversable by removing the compounds (see Figure 49A).[147; 148]

Vacuolization is not unique for methuosis, as for example autophagic cell death can show a similar phenotype.[144] However there are approaches to clearly identify methuosis: (i) Macropinocytosis is clathrin-independent, however needs cholesterol-rich membrane microdomains. Therefore, methuosis can be selectively blocked by a cholesterol-binding agent, e.g., filipin.[144; 149] (ii) In methuosis the macropinosomes mature to late endosomes, as they are not recycled. The lysosomal-associated

membrane protein 1 (LAMP1) and Rab7 are markers that selectively occur in late endosomes, and can be stained for fluorescence microscopy (see Figure 49B).[145; 150]
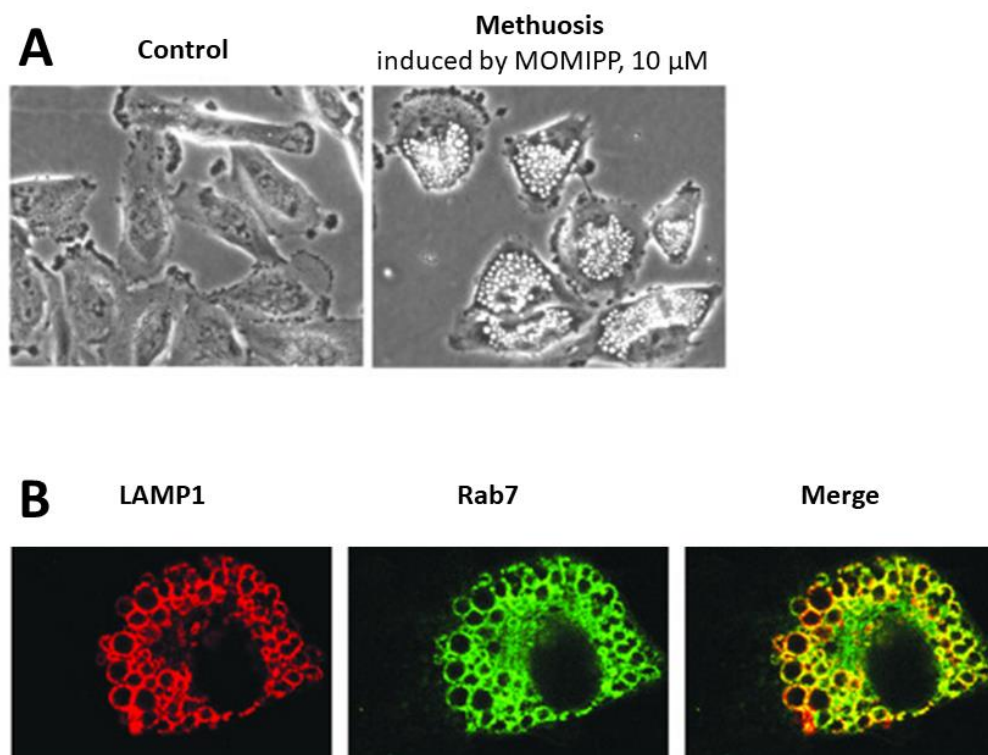
Figure 49: Morphological characteristic of methuosis. **A** U251 human glioblastoma cells treated for 4 h with or without methuosis inducing MOMIPP. Adapted from Li et al. (2019)[151]. **B** Fluorescence microscopy of U251 human glioblastoma cells undergoing methuosis. The late endosomal markers LAMP1 (red) and Rab7 (green) are stained. Adapted from Overmeyer et al. (2011).[147]

The (patho)physiological relevance of methuosis remains elusive. It is unclear whether this phenomenon occurs in vivo in response to intrinsic signaling. To date, it was only detected in the context of genetically engineered abnormal Ras activity, or as response to exogeneous small molecules. However, methuosis was shown to occur in a tumor cell culture that did not respond to induction of apoptosis. Methuosis-inducing drugs could therefore be a new approach to treat tumors. [143; 144]

6.1 ELICITING METHUOSIS IN CELL LINES WITH GPR18 AGONISTS

Trabbic et al. (2015) published compounds derived from MOMIPP that induced a distinct form of cell death, namely methuosis (structure of MOMIPP see Figure 50).[152]
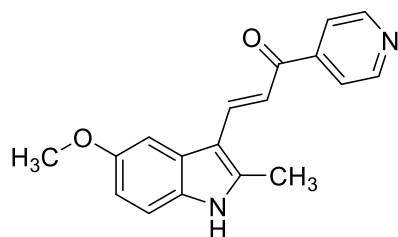
Figure 50: Structure of MOMIPP

As we found these compounds to act as agonists of the orphan GPCR GPR18, we set out to investigate whether GPR18 activation is triggering methuosis. As a first objective we aimed to reproduce methuosis in different cell lines with known GPR18 expression. The cell lines THP1 (leukemia cells), HaCaT and LN229 were shown to express GPR18 mRNA by PCR of extracted cDNA (results not shown). Additionally, CHO-β-arrestin-GPR18 cells, and HaCaT-GPR18, the latter retrovirally transfected with GPR18, were investigated. CHO-β-arrestin-GPR18 cells did not show any cytotoxicity in the MTT assay nor morphological changes after 3 d of incubation with various GPR18 ligands (Figure 51, microscopy pictures not shown).
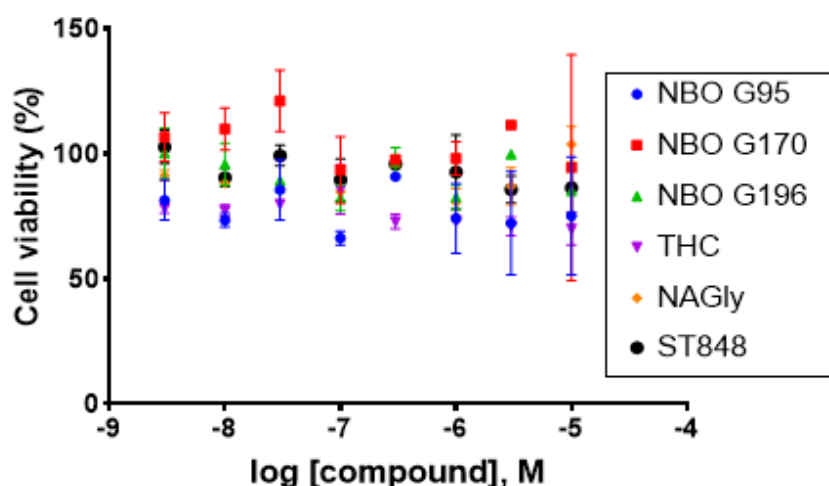
Figure 51: MTT assay results of CHO-β-arrestin GPR18 cells incubated for 3 d with respective GPR18 agonists and antagonist. On experiment was performed in duplicates.

THP1 cells are leukemia cells extracted from blood and therefore suspension cells. Hence, the morphological examination is not as straightforward as with adherent cells. A technique to fix suspension cells described by Mihara et al. (2015) was used.[153] Accordingly, after 3 d of incubation with GPR18 agonists, the THP1 cells were precipitated and fixed. Microscopic evaluation did not show any morphological changes between GPR18 agonist-treated cells and DMSO controls, however, a reduction in cell number was visible. It is likely, that only viable cells were fixed and therefore, the morphological changes cannot be observed. Without a microscopic evaluation, methuosis cannot be proven by our experiments. Therefore, THP1 cells were discarded as a model system to study methuosis.

Subsequently, native and GPR18-transfected HaCaT cells were investigated. In both cell lines, MOMIPP, NBO G196, and NBO G95 showed the morphological changes expected for methuosis (Figure 52). However, 10 µM of either THC or NAGly did not induce any change in morphology. Cytotoxicity experiments showed that all five compounds caused a reduction in cell viability, without any visible differences between native and transfected cells (see Figure 53)
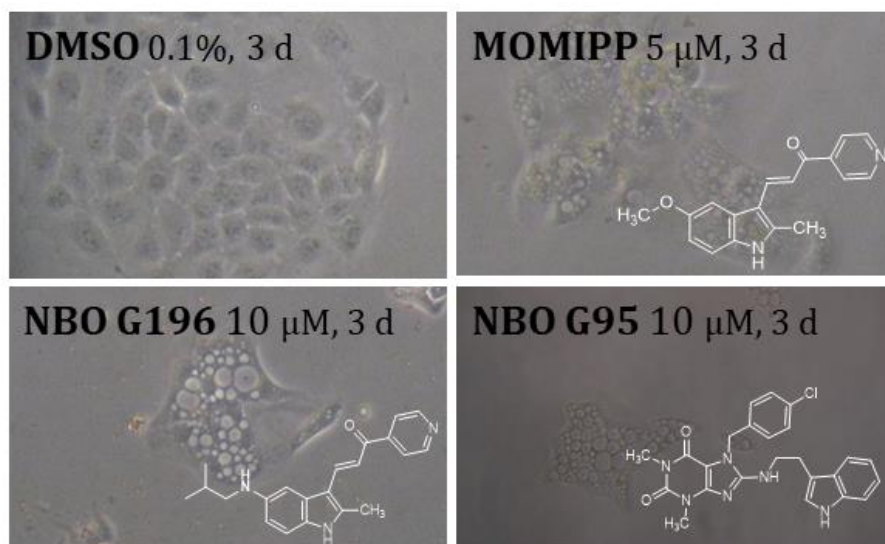
Figure 52: Light microscopy pictures of HaCaT after incubation with respective GPR18 agonists or control (0.1% DMSO). Native HaCaT and HaCaT transfected with GPR18 yield indistinguishable results. Cells were captured using a "Canon PowerShot G9" camera with a "SOLIGOR Adaptor Tube". Pictures are not to scale.
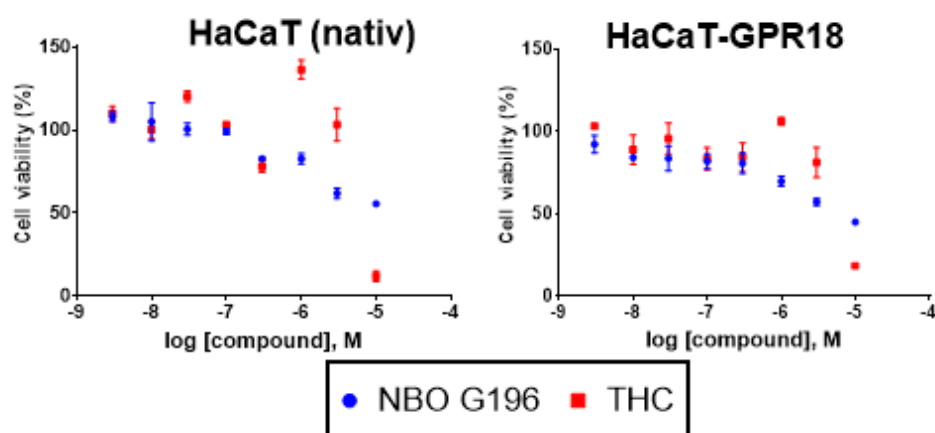
Figure 53: MTT-assay results after 3 d of incubation with either NBO G196 or THC using transfected or native HaCaT cells. Single experiment was performed in duplicates.

The GPR18 agonist CB173 was able to block the GPR18-dependent THC signal in β-arrestin assays. Therefore, the combination of THC with 10 μM CB173 was incubated for 3 d on native and GPR18-transfected HaCaT cells. However, no change in the viability compared to THC alone was recorded in either cell line (results Figure 54). This indicates that the THC cytotoxicity is probably not due to GPR18 activation.
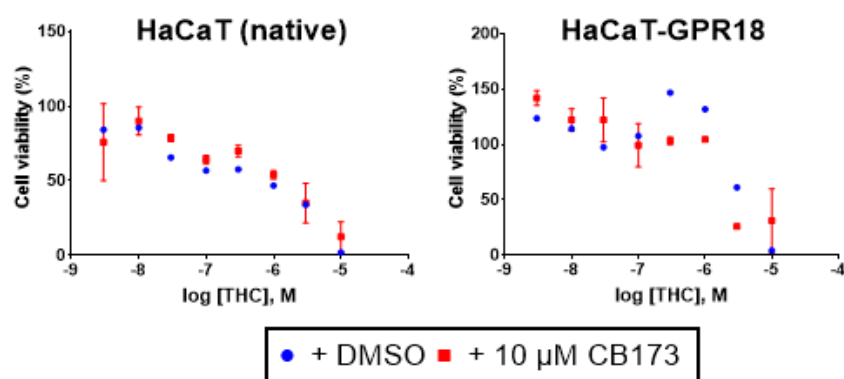
Figure 54: MTT-assay results after 3 d of incubation with THC with or without the GPR18 antagonist CB173 on transfected and native HaCaT cells. A single experiment was performed in duplicates.

Another antagonist, ST848, was cytotoxic on its own at high concentrations of 10 μM, as shown in Figure 55.
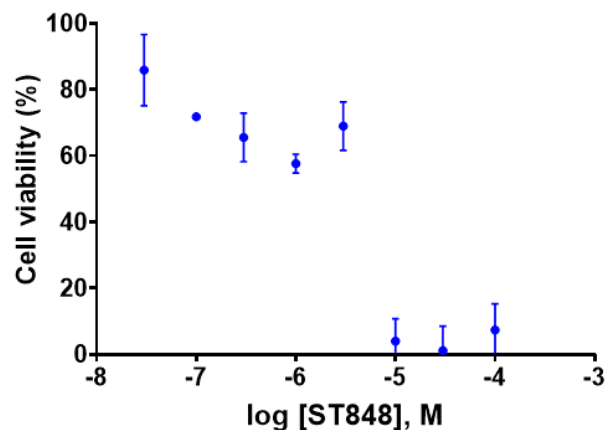
Figure 55: MTT-assay results of ST848 on GPR18 transfected HaCaT. One experiment was performed in duplicates.

LN229 glioblastoma cells were morphologically investigated for their response to GPR18 ligands. Like HaCaT cells, they showed signs of methuosis after treatment with MOMIPP and NBO G95, but no morphological change in response to THC (Figure 56). Notably, ST848, the GPR18 antagonist, shows some vacuolization too, even though to a much lower extent.
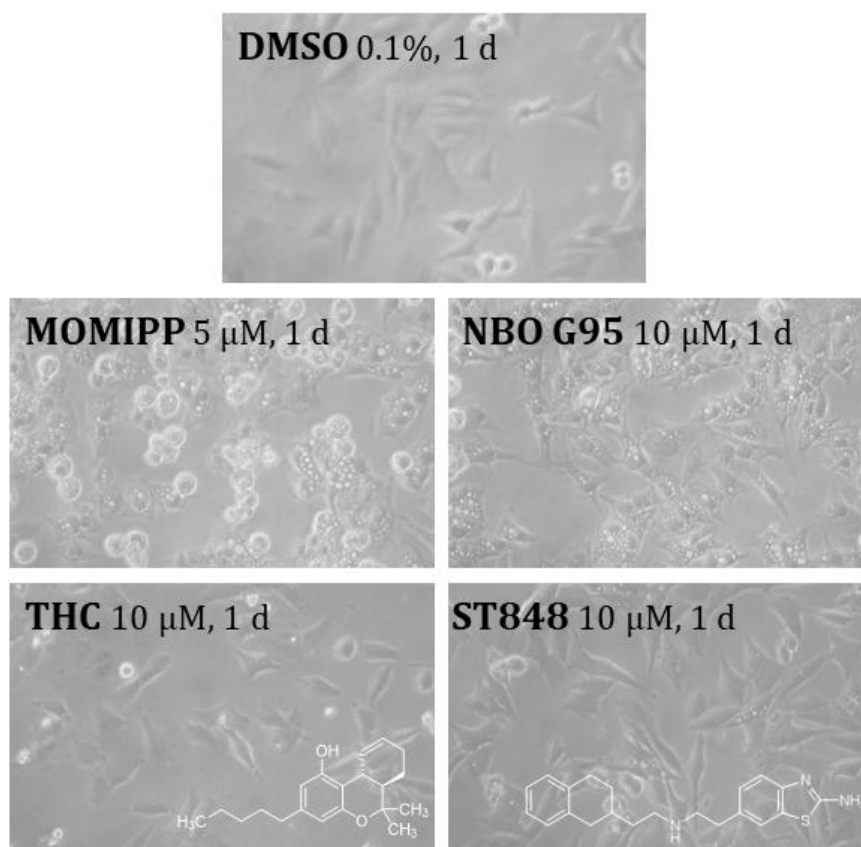
Figure 56: Light microscopy pictures of LN229 glioblastoma cells after incubation with respective GPR18 ligands or control (0.1% DMSO) (structures of MOMIPP and NBO G95 see Figure 52). Cells were captured using a "Canon PowerShot G9" camera with a "SOLIGOR Adaptor Tube".

In summary we were able to reproduce the morphological signs of methuosis in HaCaTs and LN229 glioblastoma cells with MOMIPP and structurally related, GPR18 agonists (NBO G95 and NBO G196). It was not possible to block this effect by antagonists, albeit only two antagonists with limitations were available. One antagonist, ST848, showed cytotoxicity at high concentrations and some vacuolization on its own. In CHO cells transfected with GPR18, no effect, neither morphological alterations nor on cell viability was observed with any of the investigated GPR18 ligands. With these contradictory results there is no proof that GPR18 activation triggers methuosis.

6.2 ATTEMPTS TO CREATE GPR18 KNOCK OUT CELLS

A direct control experiment with cells expressing GPR18 and showing methuosis and the same cells without GPR18 expression was set up. For this, we used the CRISPR-CAS9 technique to knock-out GPR18 from HaCaT and LN229 cells. The gene editing core facility of the University of Bonn supplied us with two lentiviral constructs. LentiCRISPR v2 plasmids were cloned, each containing one distinct guide RNA sequence specific for GPR18. When both constructs are active, a sequence of 200 base pairs of the GPR18 genome are expected to be cut out and deleted from the genome.

GPR18 knock-outs were generated by simultaneous lentiviral transfection of both constructs into HaCaT and LN229 glioblastoma cells. Transfected cells were selected by antibiotic treatment, and monoclones were picked. mRNA was extracted from polyclonal and monoclonal cells, translated to cDNA, and propagated by PCR. Subsequent analysis of the products by gel electrophoresis revealed that no genome contained the shortened GPR18 sequence. Additional sequencing of the products showed that all cell populations still expressed native GPR18 mRNA without any induced mutations at the locations of the guide RNA. Therefore, the lentiviral approach has not resulted in a functional knockout of GPR18 in HaCaT or LN229. Further experiments, e.g. using alternative transfection techniques, are planned.

7   PUBLICATION ON CONNEXIN

A CELLULAR ASSAY FOR THE IDENTIFICATION AND CHARACTERIZATION OF CONNEXIN GAP JUNCTION MODULATORS

Azeem Danish, **Robin Gedschold***, Sonja Hinz, Anke C. Schiedel, Dominik Thimm, Peter Bedner, Christian Steinhäuser, and Christa E. Müller*

*These authors contributed equally to this paper

Introduction

Gap junctions (GJs) are channels that allow the transfer of ions and small molecules between adjacent cells. Thereby they enable many processes, including muscle contraction, tissue homeostasis, metabolic transport, cell growth, and cell differentiation.[154; 155] One GJ between two cells is formed when two connexons, one from each cell, attach to each other. The respective connexons are oligomers of six connexins (Cx). In humans, 21 different Cx subtypes are known, which are named based on their molecular weight.[156–158] Therefore, the formed connexon can be homotypic or heterotypic. Of all Cx subtypes, Cx43 is the most frequently expressed one across many cell types and tissues.[159] Mutations in Cx26, Cx32 and Cx43 are linked to genetic diseases, namely keratitis-ichthyosis-deafness, X-linked Charcot–Marie–Tooth disease, and oculodentodigital dysplasia.[154; 160–165] Additionally, alterations in expression levels of Cx43 were detected in different neurological disorders, e.g. epilepsy, depression, and brain tumors.[162–164] Therefore, Cx43 is thought to play a role in the genesis of these diseases. Moreover, Cx43 knockout mice die soon after birth.[166] Hence, small molecules acting as modulators of connexins, or rather their GJs, are expected to have potential as future drugs.

Assays to identify such drug candidates were published before, but all of them have major drawbacks: Dye transfer assays, in which a dye is loaded into donor cells and transferred to acceptor cells, rely on a tedious evaluation that allows only small throughput, which is prohibitive for screening campaigns.[167; 168] Picoli et al. (2019)

developed an improved, high-throughput dye transfer assay, however, it requires costly imaging instruments, and was not able to produce stable, concentration-dependent effects of known GJ inhibitors, such as carbenoxolone and mefloquine. [169; 170] Further assays, for screening larger quantities of compounds, are based on a mediator molecule that is selectively generated in donor cells, and migrates through GJs to acceptor cells, where it activates or quenches a luminescence signal. Lee et al. (2015) used iodine as a mediator molecule, which is accumulated in donor cells via a transfected iodine transporter. After reaching the acceptor cells, iodine quenches the luminescence of yellow fluorescent protein.[171] This, however, only led to a signal decrease of around 50%, resulting in a small assay window. Haq et al. (2013) utilized Ca^{2+} as a mediator molecule, which activates aequorin in the acceptor cell.[172] However, Ca^{2+} was shown to activate protein kinase C-mediated phosphorylation of Cxs decreasing the permeability of the GJs.[173; 174] In conclusion, although several assays have been developed to identify GJ modulators, these methods are not satisfactory for application in a screening campaign. In order to identify novel GJ modulators, we set out to establish a new assay system and utilize it to screen compound libraries to identify a lead compound for Cx-targeted drug development.

Summary and outlook

HeLa cells were selected because they lack endogenous Cx expression. This allowed us to recombinantly express the desired Cx subunit without any background expression.[171] We selected cAMP as a mediator molecule, as it does not passively penetrate cell membranes, but was shown to migrate through GJs.[175] In order to selectively produce cAMP and express homotypic GJs, the donor cells were genetically engineered to express the $G\alpha_s$ protein-coupled adenosine A_{2A} receptor ($A_{2A}AR$) and Cx43. After addition of the A_{2A}-selective agonist CGS-21680, the transfected receptor activates adenylate cyclase, resulting in intracellular cAMP production. cAMP can then migrate through the GJs into acceptor cells, recombinantly expressing Cx43 as well as the cAMP GloSensor-20F (GloSensor luciferase, Promega), a firefly luciferase that oxidizes its substrate, luciferin, only in the presents of cAMP. As a product of this reaction oxyluciferin and a luminescence signal are produced.[176] The latter is easily quantifiable by a standard plate reader. In order to validate this approach, several experiments were performed: (i) immunofluorescence analysis of transfected cells to

prove Cx43 expression; (ii) stimulation of cells expressing either exclusively the GloSensor luciferase (GSL), or GSL in combination to the $A_{2A}AR$, with the $A_{2A}AR$ agonist CGS-21680. Upon stimulation, the cells only produced a luminescence signal when transfected with $A_{2A}AR$. Additionally, no signal was detected by activation of acceptor cells expressing GSL and Cx43 with the $A_{2A}AR$ agonist CGS-21680; (iii) co-cultivation of donor and acceptor cells without Cx43 transfection did not show any signal after activation with CGS-21680.

Subsequently, we produced a co-culture of "full" acceptor and donor cells, expressing Cx43, and it produced a stable signal after activation with CGS-21680. Additional blocking of cAMP degradation by addition of the phosphodiesterase inhibitor 3-isobutyl-1-methylxanthine (IBMX) drastically increased the signal. The thereby optimized assay setup led to a luminescence signal of about 40% of the signal obtained upon directly activating adenylate cyclase with forskolin, which served as a positive control. As a further validation step, the assay was tested against different concentrations of carbenoxolone, a commonly used GJ inhibitor. The compound showed a concentration-dependent inhibition with an IC_{50} of 44.4 ± 4.8 µM, being well in accordance with literature values that range from 17 to 210 µM.[170; 172] Finally, the assay was employed to screen a small compound library of 143 molecules at a concentration of 20 µM. After discarding false positives (cytotoxic molecules or modulators of either the $A_{2A}AR$ or GSL) one hit compound was detected. In summary, we established a novel assay system to measure Cx activity, and employed it to screen a small compound library, proving its utility for screening purposes. Moreover, the assay is not limited to Cx43, but should be easily adaptable to different Cx subtypes and combinations. Additionally, the easy assay setup and read-out can be performed without the need for sophisticated and costly equipment.

Author's contribution

The author performed the following experiments: fluorescence staining and microscopy, investigation of the known inhibitor carbenoxolone, most of the screening, and the hit validation experiments. Finally, the preparation of the manuscript, involving analysis of data, preparation of figures, and writing was conducted in assistance to the corresponding author Christa E. Müller.

8 SUMMARY

In this study the three poorly investigated membrane proteins MRGPRX4, GPR18, and connexin-43 were investigated. Assays and potent and selective tool-compounds were introduced, which will help to validate these proteins as future drug targets.

MRGPRX4 is an orphan receptor proposed to participate in wound healing, cancer growth, pain transmission and itch. However, no potent agonists nor antagonists have been available as tool compounds to validate the receptor as a possible drug target.

In this work, a radioligand binding assay for MRGPRX4 was developed and validated using the tritium-labeled agonist [^{3}H]PSB-18061. The radioligand displayed an K_D value of 0.761 nM, an association half-life of 4.34 min, and a dissociation half-life of 11.5 min at room temperature. The established binding assay was utilized to determine affinity and kinetic parameters at room temperature of unlabeled MRGPRX4 ligands. The affinities (K_i) determined in the radioligand binding assay correlated well with the potencies (EC_{50}) determined in calcium mobilization assays.

Different ligand classes, especially agonists and antagonists of the xanthine series were developed and optimized. We introduced agonists with picomolar affinities, being more than 10^5 times more potent than the MRGPRX4 agonists published so far. Moreover, we were able to identify potent antagonists, based in the same xanthine scaffold. These are the first MRGPRX4 antagonists described so far. The fact, that closely related structures with only minor differences can change the functional effect drastically shows that very steep structure-efficacy relationships exist, separating agonists from antagonists. Representative compounds were shown to be metabolically stable, although not able to permeate cell membranes, presumably due to their negatively charged phosphonate group.

The identification of thyroid hormones as MRGPRX4 agonists, presents a novel group of endogenous MRGPRX4 ligands. Despite their moderate potency, they are still nearly equipotent to other literature-known endogenous MRGPRX4 agonists, namely the bile acids deoxycholic acid and ursodeoxycholic acid.

GPR18 is a GPCR with much debated pharmacology. The receptor was found by our group to be activated by a series of chalcone-based compounds. In addition, these

compounds are described to elicit methuosis, a form of programmed, non-apoptotic cell death, through an unknown molecular mechanism. Consequently, it was investigated whether GPR18 is participating, or even responsible for this effect. Firstly, methuosis was reproduced with one chalcone-based compound, namely 3-(5-methoxy,2-methyl-1*H*-indol-3-yl)-1-(4-pyridinyl)-2-propen-1-one (MOMIPP) in a human keratinocyte cell line (HaCaT) and in human LN229 glioblastoma cells. Other, structurally unrelated, GPR18 agonists showed the same morphological signs of methuosis. With these preliminary results, however, it was not possible to unambiguously prove GPR18-dependence of this effect. Not all GPR18-expressing cell lines underwent methuosis after application of the compounds, as GPR18 transfected CHO cells neither showed signs of cell death nor morphological changes. Moreover, it has not been possible to block the effect by antagonists, but in contrast, one antagonist elicited the same morphological changes, although to a lower degree.

Connexin-43 is one subtype of connexins, which form gap junctions between two adjacent cells, and thereby allow the free diffusion of small molecules. As several diseases are linked to the dysfunction of these gap junctions, connexin-43 is a promising drug target which, however, needs to be validated. A screening assay to identify connexin43 modulators was established and validated. Using the literature-known antagonist carbenoxolone, concentration-dependent inhibition could be measured. The assay was subsequently applied to a small screening campaign, by which a new potential connexin-43 inhibitor was identified.

In conclusion this thesis resulted in the successful implementation of new assay systems. The identification, optimization, and characterization of novel ligands has paved the way to further study the so far poorly explored membrane proteins MRGPRX4, GPR18, and connexin-43.

9 MATERIAL AND METHODS

9.1 MATERIALS

9.1.1 Cell lines and culture medium

Dulbecco's Modified Eagle's Medium (DMEM), fetal calf serum (FCS), and penicillin/streptomycin (P/S) were purchased from GibcoBRL, Gaithersburg, MD, USA. G418 and Hygromycin were obtained from PAN Biotech (Aidenbach, Germany).

Table 17: Used cell lines with source and respective culture media. Concentration of medium additives are: FCS: 10%; P/S: 100 U ml^{-1} penicillin G, and 100 µg ml^{-1} streptomycin; G418: 800 µg ml^{-1}; hygromycin: 300 µg ml^{-1}

Cell line	*Source* (Plasmid/Transfection method)	Culture Medium
LN229 glioblastoma cells	ATCC®: CRL-2611 Provided by AK Prof. Dr. Bjorn Scheffler	DMEM + FCS + P/S
Astrocytoma 1321N1 -MRGPRX4-83L	(pLVX-MRGPRX4wt-IRES-mCherry/Lentiviral) generated by Yvonne Riedel	DMEM + FCS + P/S + G418
CHO-β-Arrestin MRGPRX4-83S	*DiscoverX, Fremont, CA*	F12 + FCS + P/S + G418 + Hygromycin
CHO-β-Arrestin MRGPRX4-83L	*DiscoverX, Fremont, CA* (ARMS1-ProLink™2/Lipofectamin) generated by Yvonne Riedel	F12 + FCS + P/S + G418 + Hygromycin
HEK-MRGPRX4-83S	(pQCXIP-MRGPRX4-83S/retroviral)	DMEM + FCS + P/S + G418
HaCaT-MRGPRX4-83S	(pQCXIP-MRGPRX4-83S/retroviral)	DMEM + FCS + P/S + G418
HaCaT-MRGPRX4-83L	(pLVX-MRGPRX4wt-IRES-mCherry/Lentiviral)	DMEM + FCS + P/S

9.1 MOLECULAR BIOLOGY

9.1.1 *Transformation of competent bacteria, propagation, and isolation of plasmids*

Competent bacteria were taken from the -80°C freezer and thawed on ice for 30 min. Approximately 10 – 50 ng of the plasmid were added to the bacteria and incubated for further 30 min on ice. Afterwards the bacteria were 'heat-shocked' in a water bath at 42°C for 45 sec, and subsequently cooled on ice for 2 minutes. 200 µl LB medium (Carl Roth GmbH & Co. KG, Karlsruhe) were added, and the cells were incubated at 37°C, 300 rpm for 1 h. LB medium containing the respective antibiotic (ampicillin, Cayman Chemical, Michigan, USA) was prepared and the bacteria were added to 200 ml and incubated in an incubator over-night. The plasmids were isolated by the use of the DNA midi-preparation kit (PureLink™ HiPure Plasmid-Filter-Midiprep-Kit, ThermoFisher) according to the manufacturers protocol.

9.1.2 *Sequencing*

Sequencing was performed by the company GATC Biotech AG, Germany.

9.2 CELL CULTURE

9.2.1 *Phosphate-buffered saline (PBS) Buffer preparation*

Deionized water was supplemented with NaCl (137 mM), KCl (2.5 mM), Na2HPO4 (7.5 mM), and KH2PO4 (1.5 mM) and the pH was adjusted to 7.4. The buffer was autoclaved and stored at room temperature.

9.2.2 *Cultivation of cells*

Cells were cultured in the respective culture medium (See section 9.1.1). The cells were incubated in humidified atmosphere at 37 °C with 5% CO_2 (10% for astrocytoma and HaCaT) in an incubator. After reaching ~80-90% confluency the cells were passaged. Old medium was disposed, cells were washed with PBS and subsequently detached by the use of trypsin 0.01% (Lonza Group Ltd, Basel, Switzerland) solution containing 0.6 mM EDTA (Carl Roth GmbH + Co. KG, Karlsruhe, Germany) with incubation at 37 °C for 5-10 min. Part of the cell suspension was transferred to an appropriate flask for further cultivation. All steps were performed under sterile

conditions (laminar air flow hood). Cells were routinely checked for mycoplasma contamination (detection by polymerase chain reaction (PCR)) and, when positive, disposed and replaced by a negative stock.

9.2.3 Cell counting

Detached cells were counted using a Neubauer cell chamber (hemocytometer). 10 µl cell suspension were pipetted under the coverslip. The viable cells in at least 2 of the 4 4x4-squares were counted. The mean multiplied by 10,000 corresponds to the cell number in one ml. Subsequently the cells were diluted to obtain the needed cell density.

9.2.4 Transient transfection (Lipofection)

For transient transfection via lipofection, cells were grown to ~80-90% confluence. The medium was disposed, cells were washed with PBS and Opti-MEM (GibcoBRL, Gaithersburg, MD, USA) was added to the cells. For one $25 cm^2$ flask 475 µl Opti-MEM were incubated with 25 µl lipofectamine™ 2000 (ThermoFisher) for 5 min at room-temperature (RT). Subsequently, 500 µl Opti-MEM containing 10 µg of the respective plasmid were added and incubated for further 20 min at RT. The lipofectamine - plasmid mixture was slowly pipetted on the cells. On the next day the transfection medium was replaced by standard medium. For longer usage of the transfected cell line the medium was changed into culture medium containing the respective antibiotic and renewed every second day until the non-transfected cell death process ended.

9.2.5 Retroviral transfection

1.5×10^6 Packaging cells (GP+envAM12, LGC Standards GmbH, Wesel, Germany) were seeded in a $25 cm^2$ flask, supplemented with 5 ml of culture medium, and incubated (37 °C, 5% CO_2, 24 h). Afterwards, the cells were transfected using Lipofectamine 2000 (Thermo Fisher Scientific) with 10 µg of DNA containing the retroviral plasmid (6.25 µg) and VSV-G plasmid (3.75 µg). After ~16 h, the medium was replaced with 3 mL of fresh culture medium containing 5 mM sodium butyrate (Sigma-Aldrich) followed by incubation at reduced temperature (32 °C, 5% CO_2, 48 h). The supernatant containing the virus particles was removed and the virus was harvested using a 2 µm sterile filter. The virus containing filtrate was mixed with 6 µL of

polybrene solution (4 mg/mL in H_2O, sterile filtered). The target cell line was seeded one day before transfection, and the with the virus particles in a 25 cm^2 flask. The medium was replaced by the virus containing mixture and the cells were incubated (32 °C, 5% CO_2, 2.5 h). After the incubation, the supernatant was replaced by 5 mL of fresh culture medium followed by incubation (37 °C, 5% CO_2, 48–72 h). Afterwards, the medium was changed into culture medium containing the respective antibiotic and renewed every second day until the non-transfected cell death process ended.

9.2.6 Lentiviral transfection

For lentiviral transfection the Lenti-X™ Packaging System from Clontech was used. HEK293T-packaging cells were harvested, and $1.5*10^6$ cells were seeded per 25 cm^2 flask. Two sterile tubes were prepared as followed:

Tube 1	Tube 2
185.5 µl Xfect Reaction Buffer	197.5 µl Xfect Reaction Buffer
12 µl Lenti-X HTX Packaging-Mix	2.5 µl Xfect Polymer
2.5 µl Lenti-X Vektor-DNA (1 µg/µl)	

The solution of tube 2 is transferred into tube 1, mixed and incubated for 10 min at RT. Afterwards the mixture was slowly pipetted on the packaging cells and they were incubated for 4 - 12 h at 37°C before the medium was replaced by culture medium. 30 µl sodiumbutyrat (500 mM) was added and the cells were incubated at 32°C for 48h. Whilst incubating, the target cell line was seeded in a 25 cm^2 flask ($5*10^5$ cells per flask). The medium of the packaging cells is filtered (45 µm filter) and the medium of the target cell line was replaced by the flow through. 6 µl polybrene (4 mg/ml) was added. After 2.5 h the medium is replaced by culture medium and the cells were incubated for 48 – 72 h.

9.2.7 Fluorescence-activated cell sorting

Fluorescence-activated cell sorting (FACS) was performed at the Flow Cytometry Core Facility of the medical faculty of the university Bonn. The transfected mCherry was detected at 610/20 nm. Single cells were picked into a 96-well plate. Single clones were incubated, trypsinized when appropriate, and further cultivated.

9.2.8 Picking monoclones

Monoclones were either picked by FACS if applicable, or manually. In the case of the latter, the cells were seeded in a density of 1 cell per well. The wells were controlled visually for the growth of one single colony. These monoclones were detached after a few days and step per step transferred to larger compartments (12-well plate, 6-well plate, cultivation flasks) until sufficient cells for further use were generated.

9.2.9 Membrane preparation

The respective cells were seeded in dishes and incubated until ~90% confluency was reached. The medium was decanted, and the cells were frozen for at least 30 minutes at -20°C. Afterwards around 2 mL of 5 mM TRIS supplemented with 2 mM EDTA (pH = 7.4) were added to each dish and the cells were mechanically detached with a rubber scraper. The collected cell suspension was pooled on ice. Using an UltraTurrax® (T25 basic, IKA Labortechnik, Staufen, Germany) the cells are lysed for 45 seconds at level 4 and subsequently centrifuged at 1,000 g for 10 minutes at 4°C. The supernatant is afterwards centrifuged at 48,000 g for 1 h at 4°C. Now the supernatant is discarded, and the pellet resuspended in 50 mM TRIS (pH = 7.4) and again centrifuged at 48,000 g for 1 h at 4°C. The pellet is resuspended in 50 mM TRIS (pH = 7.4), homogenized using a UltraTurrax® for 30 seconds, aliquoted and stored at -80°C for further use. The protein concentration is determined according to 9.5.1.

9.3 RADIOLIGAND BINDING ASSAYS

9.3.1 Filtration assay

The total and unspecific binding of the radioligand to protein was determined using a filtration assay. The radioligand (approximately 1 nM, [^{3}H]PSB-18061) was incubated with supplements (10 mM $MgCl_2$ in optimized condition), and excess cold ligand (1 µM, PSB-18061) or DMSO, and the protein source (100 µg protein of HEK-MRGPRX4-83S membrane preparation in optimized condition) in a total volume of 500 µl in TRIS-HCl (pH = 7.4). The protein was added last, and the incubation time was started. After 1.5 h at RT equilibrium is reached and the mixture was filtered through a glass fiber filter (GF/A in optimized condition) using TRIS-HCl supplemented with 0.1% TRIS and 0.1% BSA, with three quick washing steps using approximately 3 ml buffer.

The filters were subsequently incubated in scintillation cocktail (LumaSafe®) for 9 h before they were counted in a liquid scintillation counter. The binding was evaluated in counts per minute (CPM) and unspecific binding was subtracted from total binding in order to obtain the specific binding of the radioligand to MRGPRX4-83S.

Competitive binding experiments

The binding affinity of MRGPRX4 ligands was determined in competition binding experiments. Various concentrations of the competitor were mixed with radioligand, supplements, and protein source, filtered, and measured as described above. If applicable the results were normalized to control (DMSO, 100%) and unspecific binding (0%). K_i values were determined by the use of PRISM 8.0 (GraphPad Software Inc., San Diego, CA, USA) using the equation: "Binding – competitive: One site – Fit K_i".

Kinetic binding experiments

For association experiments, 50 µg protein of HEK-MRGPRX4-83S membrane preparation was added at several time points to premixed radioligand (approximately 1 nM, [3H]PSB-18061), with DMSO or cold ligand (1 µM, DM061) in TRIS-HCl buffer (pH = 7.4) supplemented with 10 mM $MgCl_2$. After the respective incubation time (between 30 seconds and one hour) the mixture was harvested and measured as described above. For dissociation experiments the radioligand was pre-incubated with the protein source in TRIS-HCl buffer (pH = 7.4) supplemented with 10 mM $MgCl_2$ for 30 minutes. At several time points 1 µM of the cold ligand (PSB-18061) or DMSO was added, and after the respective incubation time (between 30 seconds and two hours) harvested and measured as described above.

For heterologous kinetic studies, instead of the cold ligand the competitor was added in a concentration of approximately 3-fold of its K_i value. Incubation times were set between 30 seconds and three hours. The PRISM 8.0 function for "Kinetics of competitive binding"-fit was used for evaluation.

Saturation experiments

In saturation experiments different concentrations of the radioligand ([3H]PSB-18061) were incubated with 50 µg protein of HEK-MRGPRX4-83S membrane preparation, either with cold ligand (1 µM PSB-18061) or DMSO. After one-hour

incubation the samples were harvested and measured as described above. The PRISM 8.0 function for "Saturation binding: One site" was used for evaluation.

9.3.2 Autoradiography studies

Cryo-sectioning

The frozen samples were fixed, using Tissue-Tek® O.C.T.™ compound (Sakura Finetek, Alphen an de Rijn, NL), onto the mounting panel of the cryostat (Microm HM560, Thermo Scientific, Waltham, MA, USA). The tissues were trimmed until a cross-section of the whole sample was obtained. Subsequently 8 µM thick slices were cut and placed on a room-tempered microscopy slide. At least duplicates of all tissues were prepared for two independent cases. The slides containing the tissue sections were dried at RT for 60 minutes and subsequently stored at -20° enclosed in aluminum foil.

Autoradiography

The radioligand solution of [^{3}H]PSB-18061 was prepared in a sodium free and magnesium enriched autoradiography buffer (25 mM Tris, 5 mM KCl, 2 mM $CaCl_2$, 10 mM $MgCl_2$; pH_{RT} 7.4) at a concentration of approximal 2 nM. Non-specific binding was recorded in the presence of 10 µM cold ligand (DM061), and DMSO concentration of the total binding was adjusted (1% DMSO final concentration). The cryosections of tissues were equilibrated at RT with the modified autoradiography buffer (w/o radioligand) for 15 minutes. The excess buffer was removed, and the slides were dried at RT. Subsequently, the slides were incubated with the radioligand solution, with or without cold ligand, for 60min. After decanting the radioligand the slides were washed twice with ice-cold 50 mM Tris, pH 7.4 for 2 min and directly washed with ice-cold deionized water for 5 sec. The samples were dried at RT and placed on a photoplate (BAS TR2025, FUJIFILM, Minato, Japan) and incubated for 4 weeks. Afterwards the plates were scanned, and the obtained images were analyzed with AIDA (v 4.27). In order to quantify the radioactivity, calibrated standards (ART0123B/C; American Radiolabeled Chemicals, St. Louis, USA) were used. For each, total and for non-specific binding, at least duplicated from at least two different cases were prepared.

Staining of samples

All used tissues were stained by either Nissl-staining for brain tissues or Hematoxylin-Eosin(HE)-staining for the remaining. For Nissl-staining, slices were treated with Nissl staining solution (1.5% cresyl violet in aqueous ammonium acetate buffer, pH 4.6) for 5 min. Subsequently the slides were washed with first 70% and afterwards 100% ethanol and dried. For HE-staining a HE-staining kit (BIOZOL, Eching, Germany) was used. The slices were treated with Hematoxylin staining solution for 5 min, washed with deionized water, and treated in warm water for 3-5 min. Afterwards the slides were placed in 100% ethanol for 10 seconds and subsequently incubated with Eosin Y solution for 3 min. Afterwards the samples were first washed with 100% ethanol and then placed in 100% ethanol for 3 min and dried afterwards.

9.4 FUNCTIONAL ASSAY

9.4.1 β-Arrestin assay

The CHO-β-arrestin cells expressing the respective receptor were harvested with trypsin, centrifuged, and resuspended in culture medium. The cells were diluted to a concentration of $2.5*10^5$ cells/mL and 90 µL were seeded per well into a white 96-well plate. On the next day, the medium was replaced by 90 µL FCS free medium. After 2 h, 1 µl antagonists DMSO solution were added for antagonist assays and incubated for 30 minutes, 10 µL agonist containing 10% DMSO was added and incubated for further 90 minutes. Subsequently, 50 µL reagent mixture was added. It consists of 40 parts lysis buffer, 10.5 parts emerald II enhancer (Thermo Fisher Scientific, Waltham, MA, USA), and 1.1 parts galacton star (Thermo Fisher Scientific, Waltham, MA, USA). The plate was incubated for 60 min at RT in the dark. Afterwards the luminescence is measured. (Mithras LB 940, Berthold Technologies, Bad Wildbad, Germany). The data was analyzed using Prism 8.0 (GraphPad Software Inc., San Diego, CA, USA).

Lysis buffer preparation

Deionized water was supplemented with NaCl (150 mM), KH_2PO_4 (5 mM), K_2HPO_4 (5 mM), MgAcetat (10 mM), and 2% Chaps and the pH was adjusted to 7.4. The buffer was stored at -4°C.

9.4.2 Calcium assay

One day before the assay, the respective cells were harvested with trypsin, centrifuged, and resuspended in culture medium. 50,000 cells were seeded per well in 200 µl culture medium in a black clear bottom 96-well plate. On the next day, the medium was replaced with 40 µL dye solution (15 µL of 1 mM Fluo-4-AM (Thermo Fisher Scientific, Waltham, MA, USA); 15 µL of 20% Pluronic (Sigma Aldrich) in 4970 µL HBSS (Thermo Fisher Scientific, Waltham, MA, USA)). After 1-hour incubation at rt under shaking the dye was disposed. Subsequently HBSS was added in each well - for agonist assays 190 µl, for antagonist 189 µl. In antagonist assays, 1 µl antagonist dissolved in 100% DMSO was added and incubated for 30 minutes. Next, the plates are measured in a plate reader with pipetting function (FlexStation® 3 Multi-Mode Microplate Reader, Molecular Devices, LLC). 10 µL agonist were added from a prepared reagent plate with the agonists and controls in 10% DMSO, HBSS. The data was analyzed using Prism 8.0 (GraphPad Software Inc., San Diego, CA, USA). For antagonist assays the EC_{80} of the respective agonist (if not stated otherwise SC053) were used.

Preparation of 1 mM Fluo-4-AM stock

50 µg of Fluo-4-AM (Thermo Fisher Scientific, Waltham, MA, USA) were dissolved in 45.9 µl DMSO. Alequotes of 15 µl were prepared in the absence of light and stored at -20°C.

Preparation of 20% Pluronic stock

200 mg of Pluronic F-127 (Sigma-Aldrich, P2443) was dissolved in 800 µl DMSO. The solution was heated to 80°C and shaken until a clear solution without precipitant was achieved. The stock was stored at rt.

9.4.3 TruPath assay

Native HEK cells were harvested, trypsin was removed by centrifugation, and 10^6 cells were seeded per well in a six-well plate. After approximately 3h, when the cells attached, the medium was replaced by OPTI-MEM (Thermo Fisher Scientific, Waltham, MA, USA) and the cells are transfected with 100 ng of the receptor, Gα, Gβ, and Gγ subunit (The respective G protein subunits are combined as described by Olsen et al. (2020)[26]). For this, 2 µl lipofectamine is diluted in 248 µl OPTI-MEM,

incubated for 5 minutes (rt), and the plasmids are diluted in a total volume of 250 µl OPTI-MEM. The plasmids and the lipofectamine solution are mixed, incubated for further 20 minutes (rt) and subsequently slowly pipetted to the cells. After approximately 24 h incubation (37°C, 5% CO_2) the cells are detached, and 50,000 cells were seed per well into a white 96-well plate. On the next day, the medium is replaced by 60 µl HBSS containing 20 mM HEPES. 10 µl of a 500 nM Coelenterazine 400A (Cayman Chemical) solution is added, incubated for 5 min afterwards 30 µl agonists or control are added. After 5 min incubation the fluorescence was measured in a plate reader (LB940 Mithras) at 400 nm and 510 nm. The data is analyzed with GraphPad Prism 8.0.1.

9.4.4 MTT assay

Cell viability was tested with the MTT-assay. 1,000 cells were seeded in a 96-well plate. After one day incubation (37°C, 5% CO_2) the test compounds were added and incubated for 72h. Subsequently, 40µL MTT (5mg/mL) was added and incubated for one hour (37°C, 5% CO_2). Afterwards, the medium was disposed and replaced with 100µL DMSO. The plates were placed on a shaker for about 5 minutes, until formed precipitate was dissolved. The plates were placed in the Mithras LB 940 (BertholdTech) and the absorption at 600nm was measured. The results were normalized to controls with vehicle (1% DMSO = 100% survival) and high DMSO concentration (20% DMSO = 0% survival).

9.4.5 Scratch assay

On the backside of a 12-well plate a horizontal line was drawn on each well. 200,000 to 350,000 cells were seeded, depending on the cell type. After over-night incubation a confluent mono layer was formed. Mitomycin (5µg/mL) was added and incubated for 2h. Subsequently the medium was disposed, and the scratch was performed. A sterile 200µL pipette tip was used to scratch the cells straight from top to bottom. The cells were washed twice with PBS and supplemented with new medium without FCS or antibiotics. FCS controls were supplemented with Medium with FCS. The test compounds were added and the DMSO concentration was equalized (0,1%). The scratches were photographed with a "Canon PowerShot G9" camera with a "SOLIGOR Adaptor Tube" connected to a microscope with 10x magnification. To obtain pictures of the same spot, the line on the backside was used as placemark. Pictures were taken

right after the scratch and at specified time points ± 1 h. If dead cells / debris obstructed the picture, the medium was disposed, the cells were washed twice with PBS and supplemented with new medium (without FCS or antibiotics), and compounds respectively DMSO.

9.5 OTHER ASSAYS

9.5.1 Protein concentration determination, Bradford

The protein concentration was determined according to the Bradford protocol. For the calibration curve at least five dilutions between 400 and 50 µg/ml of BSA were prepared. The protein samples were diluted by 1/10, 1/20, and 1/40, to achieve at least two within the calibration line. Of every dilution 50 µl were mixed with 1 ml Bradford reagent and incubated for 5 min at room temperature. The absorbance was measured at λ=595 nm. An exemplary calibration curve is shown in Figure 57.
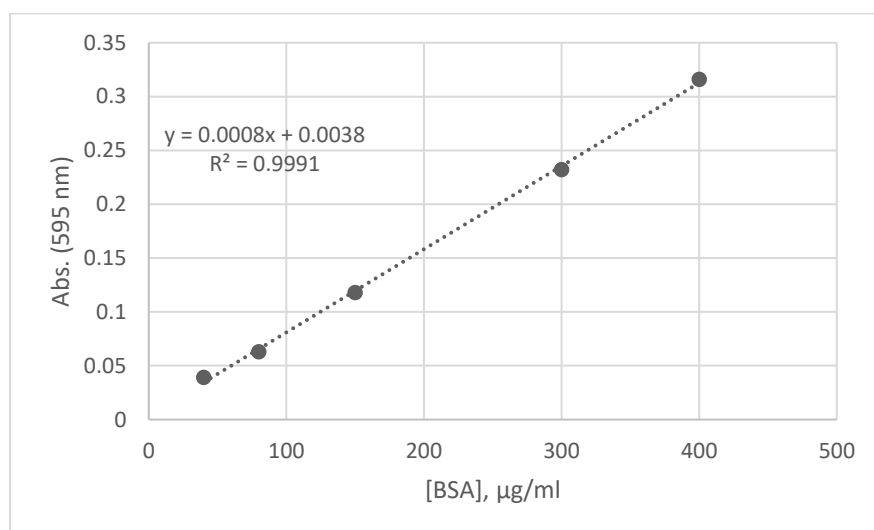
Figure 57: Example of a calibration curve for the Bradford assay; Abs., absorbance; BSA, bovine serum albumin

9.5.2 Determination of water solubility

The respective compounds were suspended in water and heated to 70°C under gentle shaking. After 1 h the suspensions were further incubated at rt for 3 or 7 days. Subsequently, the samples were centrifuged (10 min, 16,000 g) and filtrated (micropore filter, 0.2 µm). The resulting solution was analyzed by HPLC (HP1100, Agilent Technologies, Waldbronn, Germany) using an EC 50/2 Nucleodur C18 Gravity 3 µm column (Macherey-Nagel GmbH & Co. KG, Düren, Germany) with a column

temperature of 25 °C. The UV absorption was detected from 190 – 900 nm using a diode array detector (DAD). A standard curve of the respective compound was used to determine the concentration of the samples.

9.5.3 Sample preparation for fluorescence microscopy

A 6 well plate was prepared with one sterile microscopy cover slip per well. The respective cells were seeded into these wells, on top of the cover slips. The cells were incubated for one day until the cells reached the necessary confluency (37°C, 5% CO_2) and the coverslips were subsequently washed with PBS. The coverslips were treated with 4% paraformaldehyde in PBS for 20 min, which was replaced afterwards by a solution of 1% BSA in PBS for further 15 min. Subsequently the cells were incubated with the primary antibody (in 1% BSA/PBS) for 60 min, washed with 1% BSA/PBS, replaced by the secondary antibody (in 1% BSA/PBS) for 30 min, washed again and replaced by DAPI for 5 min. All incubation steps were performed at RT in the dark. Using fluoromount the stained coverslips were fixated on a microscopy slide and dried overnight in the dark at 4°C.

9.5.4 Metabolic stability

This experiment was performed by Pharmacelsus (contract research organization), Saarbrücken, Germany. For determination of metabolic stability human liver microsomes (0.5 mg/mL, mixed gender, pooled) were incubated with 1 µM of the respective compounds. Concentration of remaining compound was determined by HPLC-MS/MS.

9.6 DATA EVALUATION

Data was analyzed using PRISM 8.0 (GraphPad Software Inc., San Diego, CA, USA).

10 ABBREVIATIONS

Abbreviation	Name
2D	Two-dimensional
3D	Three-dimensional
3T1AM	3-Iodothyronamine
$A_{2A}AR$	Adenosine A_{2A} receptor
AMP	Adenosine monophosphate
AMP-IBP5	Antimicrobial peptide derived from insulin-like growth factor-binding protein 5
ASA-S	N-arachidonoyl-L-serine
BAM8-22	Bovine adrenal medulla peptide 8-22
BRET	Bioluminescence Resonance Energy Transfer
cAMP	Cyclic adenosine monophosphate
CHO	Chinese hamster ovary
CPM	Counts per minute
Cx	Connexin
DAD	Diode array detector
DCA	Deoxycholic acid
DMEM	Dulbecco's modified eagle's medium
DMSO	Dimethyl sulfoxide
DRG	Dorsal root ganglia
DTP	Guanosine trisphosphate
EDTA	Ethylenediaminetetraacetic acid
FACS	Fluorescence activated cell sorting
FCS	Fetal calf serum
FRET	Fluorescence resonance energy transfer
G protein	Guanosine triphosphate binding protein
GDP	Guanosine diphosphate
GJ	Gap junctions
GPCR	G protein-coupled receptor
GRK	G protein-coupled receptor kinase
GSL	GloSensor luciferase
HBSS	Hanks' balanced salt solution
HDP	Host defense peptide
HE	Eosin
HEK	Human embryonic kidney
HEPES	N-(2-hydroxyethyl)piperazine-N'-(2-ethanesulfonic acid)
HPLC	High performance liquid chromatography
HTS	High throughput screening

IBMX	Phosphodiesterase inhibitor 3-isobutyl-1-methylxanthine
IMP	Inosine monophosphate
LCA	Litocholic acid
LPS	Lipopolysaccharide
min	Minute(s)
Mrg	MAS related genes
MRGPR	MAS-related G protein-coupled receptor
MTT	3-(4,5-Dimethylthiazol-2-yl)-2,5-diphenyltetrazolium bromide
NADH	Nicotinamide adenine dinucleotide
NAGly	N-arachidoylglycine
P/S	Penicillin/streptomycin
PBS	Phosphate-buffered saline
PCR	Polymerase chain reaction
RT	Room-temperature
rpm	Rounds per minute
SAR	Structure-activity relationships
SEM	Standard error of the mean
SNSR	Sensory neuron–specific G protein–coupled receptor
T_3	Triiodothyronine
T3AM	3,3',5-Triiodothyronamine
T_4	L-Thyroxine
TB	Total binding
TCA	Taurocholic acid
TG	Trigeminal ganglia
THC	Tetrahydrocannabinol
Triac	3,5,3'-triiodothyroacetic acid
TRIS	Tris(hydroxymethyl)aminomethane
NB	Nonspecific binding
UDCA	Ursodeoxycholic acid
wt	Wild-type

11REFERENCES

(1) Alexander, S. P.; Christopoulos, A.; Davenport, A. P.; Kelly, E.; Mathie, A.; Peters, J. A.; Veale, E. L.; Armstrong, J. F.; Faccenda, E.; Harding, S. D.; Pawson, A. J.; Southan, C.; Davies, J. A.; Abbracchio, M. P.; Alexander, W.; Al-Hosaini, K.; Bäck, M.; Barnes, N. M.; Bathgate, R.; Beaulieu, J.-M.; Bernstein, K. E.; Bettler, B.; Birdsall, N. J. M.; Blaho, V.; Boulay, F.; Bousquet, C.; Bräuner-Osborne, H.; Burnstock, G.; Caló, G.; Castaño, J. P.; Catt, K. J.; Ceruti, S.; Chazot, P.; Chiang, N.; Chini, B.; Chun, J.; Cianciulli, A.; Civelli, O.; Clapp, L. H.; Couture, R.; Csaba, Z.; Dahlgren, C.; Dent, G.; Singh, K. D.; Douglas, S. D.; Dournaud, P.; Eguchi, S.; Escher, E.; Filardo, E. J.; Fong, T.; Fumagalli, M.; Gainetdinov, R. R.; Gasparo, M. de; Gerard, C.; Gershengorn, M.; Gobeil, F.; Goodfriend, T. L.; Goudet, C.; Gregory, K. J.; Gundlach, A. L.; Hamann, J.; Hanson, J.; Hauger, R. L.; Hay, D. L.; Heinemann, A.; Hollenberg, M. D.; Holliday, N. D.; Horiuchi, M.; Hoyer, D.; Hunyady, L.; Husain, A.; IJzerman, A. P.; Inagami, T.; Jacobson, K. A.; Jensen, R. T.; Jockers, R.; Jonnalagadda, D.; Karnik, S.; Kaupmann, K.; Kemp, J.; Kennedy, C.; Kihara, Y.; Kitazawa, T.; Kozielewicz, P.; Kreienkamp, H.-J.; Kukkonen, J. P.; Langenhan, T.; Leach, K.; Lecca, D.; Lee, J. D.; Leeman, S. E.; Leprince, J.; Li, X. X.; Williams, T. L.; Lolait, S. J.; Lupp, A.; Macrae, R.; Maguire, J.; Mazella, J.; McArdle, C. A.; Melmed, S.; Michel, M. C.; Miller, L. J.; Mitolo, V.; Mouillac, B.; Müller, C. E.; Murphy, P.; Nahon, J.-L.; Ngo, T.; Norel, X.; Nyimanu, D.; O'Carroll, A.-M.; Offermanns, S.; Panaro, M. A.; Parmentier, M.; Pertwee, R. G.; Pin, J.-P.; Prossnitz, E. R.; Quinn, M.; Ramachandran, R.; Ray, M.; Reinscheid, R. K.; Rondard, P.; Rovati, G. E.; Ruzza, C.; Sanger, G. J.; Schöneberg, T.; Schulte, G.; Schulz, S.; Segaloff, D. L.; Serhan, C. N.; Stoddart, L. A.; Sugimoto, Y.; Summers, R.; Tan, V. P.; Thal, D.; Thomas, W. W.; Timmermans, P. B. M. W. M.; Tirupula, K.; Tulipano, G.; Unal, H.; Unger, T.; Valant, C.; Vanderheyden, P.; Vaudry, D.; Vaudry, H.; Vilardaga, J.-P.; Walker, C. S.; Wang, J. M.; Ward, D. T.; Wester, H.-J.; Willars, G. B.; Woodruff, T. M.; Yao, C.; Ye, R. D. THE CONCISE GUIDE TO PHARMACOLOGY 2021/22: G protein-coupled receptors. *Br. J. Pharmacol.* **2021**, *178 Suppl 1*, S27-S156.

(2) Fredriksson, R.; Lagerström, M. C.; Lundin, L.-G.; Schiöth, H. B. The G-protein-coupled receptors in the human genome form five main families. Phylogenetic analysis, paralogon groups, and fingerprints. *Mol. Pharmacol.* **2003**, *63*, 1256–1272.

(3) Latorraca, N. R.; Venkatakrishnan, A. J.; Dror, R. O. GPCR Dynamics: Structures in Motion. *Chem. Rev.* **2017**, *117*, 139–155.

(4) Pavlos, N. J.; Friedman, P. A. GPCR Signaling and Trafficking: The Long and Short of It. *Trends Endocrinol. Metab.* **2017**, *28*, 213–226.

(5) Santos, R.; Ursu, O.; Gaulton, A.; Bento, A. P.; Donadi, R. S.; Bologa, C. G.; Karlsson, A.; Al-Lazikani, B.; Hersey, A.; Oprea, T. I.; Overington, J. P. A comprehensive map of molecular drug targets. *Nat. Rev. Drug Discov.* **2017**, *16*, 19–34.

(6) Sriram, K.; Insel, P. A. G Protein-Coupled Receptors as Targets for Approved Drugs: How Many Targets and How Many Drugs? *Mol. Pharmacol.* **2018**, *93*, 251–258.

(7) Kolakowski, L. F. GCRDb: a G-protein-coupled receptor database. *Recept. Channels* **1994**, *2*, 1–7.

(8) Stevens, R. C.; Cherezov, V.; Katritch, V.; Abagyan, R.; Kuhn, P.; Rosen, H.; Wüthrich, K. The GPCR Network: a large-scale collaboration to determine human GPCR structure and function. *Nat. Rev. Drug Discov.* **2013**, *12*, 25–34.

(9) Rosenbaum, D. M.; Rasmussen, S. G. F.; Kobilka, B. K. The structure and function of G-protein-coupled receptors. *Nature* **2009**, *459*, 356–363.

(10) Bond, R. A.; Ijzerman, A. P. Recent developments in constitutive receptor activity and inverse agonism, and their potential for GPCR drug discovery. *Trends Pharmacol. Sci.* **2006**, *27*, 92–96.

(11) Caron, M. G.; Barak, L. S. A Brief History of the β-Arrestins. *Methods Mol. Biol.* **2019**, *1957*, 3–8.

(12) Jeffrey S Smith; Robert J Lefkowitz; Sudarshan Rajagopal. Biased Signalling: From Simple Switches to Allosteric Microprocessors. *Nat. Rev. Drug Discov.* **2018**, *17*, 243.

(13) Eichel, K.; Zastrow, M. von. Subcellular Organization of GPCR Signaling. *Trends Pharmacol. Sci.* **2018**, *39*, 200–208.

(14) Caniceiro, A. B.; Bueschbell, B.; Schiedel, A. C.; Moreira, I. S. Class A and C GPCR dimers in neurodegenerative diseases. *Curr. Neuropharmacol.* **2022**.

(15) Wang, W.; Qiao, Y.; Li, Z. New Insights into Modes of GPCR Activation. *Trends Pharmacol. Sci.* **2018**, *39*, 367–386.

(16) Taylor, S. J.; Chae, H. Z.; Rhee, S. G.; Exton, J. H. Activation of the β1 isozyme of phospholipase C by α subunits of the Gq class of G proteins. *Nature* **1991**, *350*, 516–518.

(17) Voss, J. H.; Müller, C. E. Heterotrimeric G Protein A-Subunits - Structures, Peptide-Derived Inhibitors, and Mechanisms. *Curr. Med. Chem.* **2022**.

(18) Barnett, M. E.; Knapp, B. I.; Bidlack, J. M. Unique Pharmacological Properties of the Kappa Opioid Receptor Signaling Through Gαz as Shown with Bioluminescence Resonance Energy Tranfer. *Mol. Pharmacol.* **2020**, *98*, 462–474.

(19) Voss, J. H.; Mahardhika, A. B.; Inoue, A.; Müller, C. E. Agonist-Dependent Coupling of the Promiscuous Adenosine A 2B Receptor to Gα Protein Subunits. *ACS pharmacology & translational science* **2022**, *5*.

(20) Milligan, G.; Kostenis, E. Heterotrimeric G-proteins: a short history. *Br. J. Pharmacol.* **2006**, *147 Suppl 1*, S46-55.

(21) Sprang, S. R. Invited review: Activation of G proteins by GTP and the mechanism of Gα-catalyzed GTP hydrolysis. *Biopolymers* **2016**, *105*, 449–462.

(22) Simon, M. I.; Strathmann, M. P.; Gautam, N. Diversity of G proteins in signal transduction. *Science* **1991**, *252*, 802–808.

(23) Chen, Z.; Singer, W. D.; Sternweis, P. C.; Sprang, S. R. Structure of the p115RhoGEF rgRGS domain–Gα13/i1 chimera complex suggests convergent evolution of a GTPase activator. *Nat. Struct. Mol. Biol.* **2005**, *12*, 191–197.

(24) Offermanns, S.; Simon, M. I. G alpha 15 and G alpha 16 couple a wide variety of receptors to phospholipase C. *J. Biol. Chem.* **1995**, *270*, 15175–15180.

(25) Suzuki, N.; Hajicek, N.; Kozasa, T. Regulation and physiological functions of G12/13-mediated signaling pathways. *Neurosignals* **2009**, *17*, 55–70.

(26) Olsen, R. H.; DiBerto, J. F.; English, J. G.; Glaudin, A. M.; Krumm, B. E.; Slocum, S. T.; Che, T.; Gavin, A. C.; McCorvy, J. D.; Roth, B. L.; Strachan, R. T. "TRUPATH, an Open-Source Biosensor Platform for Interrogating the GPCR Transducerome". *Nat. Chem. Biol.* **2020**, *16*, 841–849.

(27) Gurevich, V. V.; Gurevich, E. V. GPCR Signaling Regulation: The Role of GRKs and Arrestins. *Front. Pharmacol.* **2019**, *10*, 125.

(28) Gutkind, J. S.; Kostenis, E. Arrestins as rheostats of GPCR signalling. *Nat. Rev. Mol. Cell. Biol.* **2018**, *19*, 615–616.

(29) Gurevich, V. V.; Gurevich, E. V. Arrestin-mediated signaling: Is there a controversy? *World J. Biol. Chem.* **2018**, *9*, 25–35.

(30) Grundmann, M.; Merten, N.; Malfacini, D.; Inoue, A.; Preis, P.; Simon, K.; Rüttiger, N.; Ziegler, N.; Benkel, T.; Schmitt, N. K.; Ishida, S.; Müller, I.; Reher, R.; Kawakami, K.; Inoue, A.; Rick, U.; Kühl, T.; Imhof, D.; Aoki, J.; König, G. M.; Hoffmann, C.; Gomeza, J.; Wess, J.; Kostenis, E. Lack of beta-arrestin signaling in the absence of active G proteins. *Nat. Commun.* **2018**, *9*, 341.

(31) Jean-Charles, P.-Y.; Kaur, S.; Shenoy, S. K. G Protein-Coupled Receptor Signaling Through β-Arrestin-Dependent Mechanisms. *J. cardiovasc. Pharmacol.* **2017**, *70*, 142–158.

(32) Pandey, S.; Kumari, P.; Baidya, M.; Kise, R.; Cao, Y.; Dwivedi-Agnihotri, H.; Banerjee, R.; Li, X. X.; Cui, C. S.; Lee, J. D.; Kawakami, K.; Maharana, J.; Ranjan, A.; Chaturvedi, M.; Jhingan, G. D.; Laporte, S. A.; Woodruff, T. M.; Inoue, A.; Shukla, A. K. Intrinsic bias at non-canonical, β-arrestin-coupled seven transmembrane receptors. *Mol. Cell.* **2021**, *81*, 4605-4621.e11.

(33) Rajagopal, S.; Kim, J.; Ahn, S.; Craig, S.; Lam, C. M.; Gerard, N. P.; Gerard, C.; Lefkowitz, R. J. Beta-arrestin- but not G protein-mediated signaling by the "decoy" receptor CXCR7. *Proc. Natl. Acad. Sci. U. S. A.* **2010**, *107*, 628–632.

(34) Kowalski, P. C.; Dowben, J. S.; Keltner, N. L. My Dad Can Beat Your Dad: Agonists, Antagonists, Partial Agonists, and Inverse Agonists. *Perspect. Psychiatr. Care* **2017**, *53*, 76–79.

(35) Schwartz, T. W.; Holst, B. Allosteric enhancers, allosteric agonists and ago-allosteric modulators: where do they bind and how do they act? *Trends Pharmacol. Sci.* **2007**, *28*, 366–373.

(36) Bassoni, D. L.; Raab, W. J.; Achacoso, P. L.; Loh, C. Y.; Wehrman, T. S. Measurements of β-arrestin recruitment to activated seven transmembrane receptors using enzyme complementation. *Methods Mol. Biol.* **2012**, *897*, 181–203.

(37) Ma, Q.; Ye, L.; Liu, H.; Shi, Y.; Zhou, N. An overview of Ca2+ mobilization assays in GPCR drug discovery. *Expert Opin Drug Discov* **2017**, *12*, 511–523.

(38) Cisewski, D. H.; Santos, C.; Koyfman, A.; Long, B. Approach to buprenorphine use for opioid withdrawal treatment in the emergency setting. *Am. J. Emerg. Med.* **2019**, *37*, 143–150.

(39) Winpenny, D.; Clark, M.; Cawkill, D. Biased ligand quantification in drug discovery: from theory to high throughput screening to identify new biased μ opioid receptor agonists. *Br. J. Pharmacol.* **2016**, *173*, 1393–1403.

(40) Miyano, K.; Manabe, S.; Komatsu, A.; Fujii, Y.; Mizobuchi, Y.; Uezono, E.; Ohshima, K.; Nonaka, M.; Kuroda, Y.; Narita, M.; Uezono, Y. The G Protein Signal-Biased Compound TRV130; Structures, Its Site of Action and Clinical Studies. *Curr. Top Med. Chem.* **2020**, *20*, 2822–2829.

(41) Pedersen, M. F.; Wróbel, T. M.; Märcher-Rørsted, E.; Pedersen, D. S.; Møller, T. C.; Gabriele, F.; Pedersen, H.; Matosiuk, D.; Foster, S. R.; Bouvier, M.; Bräuner-Osborne, H. Biased agonism of clinically approved μ-opioid receptor agonists and TRV130 is not controlled by binding and signaling kinetics. *Neuropharmacology* **2020**, *166*, 107718.

(42) Tsai, H.-C.; Han, M. H. Sphingosine-1-Phosphate (S1P) and S1P Signaling Pathway: Therapeutic Targets in Autoimmunity and Inflammation. *Drugs* **2016**, *76*, 1067–1079.

(43) Singer, I. I.; Tian, M.; Wickham, L. A.; Lin, J.; Matheravidathu, S. S.; Forrest, M. J.; Mandala, S.; Quackenbush, E. J. Sphingosine-1-phosphate agonists increase macrophage homing, lymphocyte contacts, and endothelial junctional complex formation in murine lymph nodes. *J. Immunol.* **2005**, *175*, 7151–7161.

(44) Bader, M.; Alenina, N.; Andrade-Navarro, M. A.; Santos, R. A. MAS and its related G protein-coupled receptors, Mrgprs. *Pharmacol. Rev.* **2014**, *66*, 1080–1105.

(45) Al Hamwi, G.; Riedel, Y. K.; Clemens, S.; Namasivayam, V.; Thimm, D. T.; Müller, C. E. Mas-related G protein-coupled receptors X (MRGPRX): Orphan GPCRs with potential as targets for future drugs. *Pharmacol. Ther.* **2022**.

(46) Young, D.; Waitches, G.; Birchmeier, C.; Fasano, O.; Wigler, M. Isolation and characterization of a new cellular oncogene encoding a protein with multiple potential transmembrane domains. *Cell* **1986**, *45*, 711–719.

(47) Bader, M.; Alenina, N.; Young, D.; Santos, R. A.; Touyz, R. M. The Meaning of Mas. *Hypertension* **2018**, *72*, 1072–1075.

(48) Jackson, T. R.; Blair, L. A.; Marshall, J.; Goedert, M.; Hanley, M. R. The mas oncogene encodes an angiotensin receptor. *Nature* **1988**, *335*, 437–440.

(49) Ambroz, C.; Clark, A. J.; Catt, K. J. The mas oncogene enhances angiotensin-induced Ca2+i responses in cells with pre-existing angiotensin II receptors. *Biochim. Biophys. Acta.* **1991**, *1133*, 107–111.

(50) Dong, X.; Han, S.; Zylka, M. J.; Simon, M. I.; Anderson, D. J. A diverse family of GPCRs expressed in specific subsets of nociceptive sensory neurons. *Cell* **2001**, *106*, 619–632.

(51) Paola M.C. Lembo; Eric Grazzini; Thierry Groblewski; Dajan O'Donnell; Marie-Odile Roy; Ji Zhang; Cyrla Hoffert; Jack Cao; Ralf Schmidt; Manon Pelletier; Maryse Labarre; Mylene Gosselin; Yves Fortin; Denis Banville; S.H. Shen; Peter Ström; Kemal Payza; Andy Dray; Philippe Walker; Sultan Ahmad. Proenkephalin A gene products activate a new family of sensory neuron–specific GPCRs. *Nat. Neurosci.* **2002**, *5*, 201–209.

(52) Solinski, H. J.; Gudermann, T.; Breit, A. Pharmacology and signaling of MAS-related G protein-coupled receptors. *Pharmacol. Rev.* **2014**, *66*, 570–597.

(53) Anthony P. Davenport; Stephen P. H. Alexander; Joanna L. Sharman; Adam J. Pawson; Helen E. Benson; Amy E. Monaghan; Wen Chiy Liew; Chidochangu P. Mpamhanga; Tom I. Bonner; Richard R. Neubig; Jean Philippe Pin; Michael Spedding; Anthony J. Harmar. International Union of Basic and Clinical Pharmacology. LXXXVIII. G Protein-Coupled Receptor List: Recommendations for New Pairings with Cognate Ligands. *Pharmacol. Rev.* **2013**, *65*, 967–986.

(54) Zylka, M. J.; Dong, X.; Southwell, A. L.; Anderson, D. J. Atypical expansion in mice of the sensory neuron-specific Mrg G protein-coupled receptor family. *Proc. Natl. Acad. Sci. U. S. A.* **2003**, *100*, 10043–10048.

(55) Le Pichon, C. E.; Chesler, A. T. The functional and anatomical dissection of somatosensory subpopulations using mouse genetics. *Front. Neuroanat.* **2014**, *8*, 21.

(56) Tatemoto, K.; Nozaki, Y.; Tsuda, R.; Konno, S.; Tomura, K.; Furuno, M.; Ogasawara, H.; Edamura, K.; Takagi, H.; Iwamura, H.; Noguchi, M.; Naito, T. Immunoglobulin E-independent activation of mast cell is mediated by Mrg receptors. *Biochem. Biophys. Res. Commun.* **2006**, *349*, 1322–1328.

(57) Rau, K. K.; McIlwrath, S. L.; Wang, H.; Lawson, J. J.; Jankowski, M. P.; Zylka, M. J.; Anderson, D. J.; Koerber, H. R. Mrgprd enhances excitability in specific populations of cutaneous murine polymodal nociceptors. *J. Neurosci.* **2009**, *29*, 8612–8619.

(58) Santos, R. A. S.; Simoes e Silva, A. C.; Maric, C.; Silva, D. M. R.; Machado, R. P.; Buhr, I. de; Heringer-Walther, S.; Pinheiro, S. V. B.; Lopes, M. T.; Bader, M.; Mendes, E. P.; Lemos, V. S.; Campagnole-Santos, M. J.; Schultheiss, H.-P.; Speth, R.; Walther, T. Angiotensin-(1-7) is an endogenous ligand for the G protein-coupled receptor Mas. *Proc. Natl. Acad. Sci. U. S. A.* **2003**, *100*, 8258–8263.

(59) Guan, Y.; Liu, Q.; Tang, Z.; Raja, S. N.; Anderson, D. J.; Dong, X. Mas-related G-protein-coupled receptors inhibit pathological pain in mice. *Proc. Natl. Acad. Sci. U. S. A.* **2010**, *107*, 15933–15938.

(60) Burstein, E. S.; Ott, T. R.; Feddock, M.; Ma, J.-N.; Fuhs, S.; Wong, S.; Schiffer, H. H.; Brann, M. R.; Nash, N. R. Characterization of the Mas-related gene family: structural and functional conservation of human and rhesus MrgX receptors. *Br. J. Pharmacol.* **2006**, *147*, 73–82.

(61) Uno, M.; Nishimura, S.; Fukuchi, K.; Kaneta, Y.; Oda, Y.; Komori, H.; Takeda, S.; Haga, T.; Agatsuma, T.; Nara, F. Identification of physiologically active substances as novel ligands for MRGPRD. *J. Biomed. Biotechnol.* **2012**, *2012*, 816159.

(62) Chen, H.; Ikeda, S. R. Modulation of ion channels and synaptic transmission by a human sensory neuron-specific G-protein-coupled receptor, SNSR4/mrgX1, heterologously expressed in cultured rat neurons. *J. Neurosci.* **2004**, *24*, 5044–5053.

(63) Jacques T Weissman; Jian-Nong Ma; Anthony Essex; Yan Gao; Ethan S Burstein. G-protein-coupled receptor-mediated activation of rap GTPases: characterization of a novel G α i regulated pathway. *Oncogene* **2004**, *23*, 241–249.

(64) Chieosilapatham, P.; Niyonsaba, F.; Kiatsurayanon, C.; Okumura, K.; Ikeda, S.; Ogawa, H. The antimicrobial peptide derived from insulin-like growth factor-binding protein 5, AMP-IBP5, regulates keratinocyte functions through Mas-related gene X receptors. *J. Dermatol. Sci.* **2017**, *88*.

(65) Kiatsurayanon, C.; Niyonsaba, F.; Chieosilapatham, P.; Okumura, K.; Ikeda, S.; Ogawa, H. Angiogenic peptide (AG)-30/5C activates human keratinocytes to produce cytokines/chemokines and to migrate and proliferate via MrgX receptors. *J. Dermatol. Sci.* **2016**, *83*, 190–199.

(66) UniProt: the universal protein knowledgebase in 2021. *Nucleic Acids Res.* **2021**, *49*, D480-D489.

(67) Kroeze, W. K.; Sassano, M. F.; Huang, X.-P.; Lansu, K.; McCorvy, J. D.; Giguère, P. M.; Sciaky, N.; Roth, B. L. PRESTO-Tango as an open-source resource for interrogation of the druggable human GPCRome. *Nat. Struct. Mol. Biol.* **2015**, *22*, 362–369.

(68) Roy, S.; Ganguly, A.; Haque, M.; Ali, H. Angiogenic host defense peptide AG-30/5C and bradykinin B2 receptor antagonist icatibant are G protein biased agonists for MRGPRX2 in mast cells. *J. Immunol.* **2019**, *202*, 1229–1238.

(69) MRGPRX4 protein expression summary - The Human Protein Atlas. https://www.proteinatlas.org/ENSG00000179817-MRGPRX4. Published Online: August 08, **2022**.

(70) Uhlén, M.; Fagerberg, L.; Hallström, B. M.; Lindskog, C.; Oksvold, P.; Mardinoglu, A.; Sivertsson, Å.; Kampf, C.; Sjöstedt, E.; Asplund, A.; Olsson, I.; Edlund, K.; Lundberg, E.; Navani, S.; Szigyarto, C. A.-K.; Odeberg, J.; Djureinovic, D.; Takanen, J. O.; Hober, S.; Alm, T.; Edqvist, P.-H.; Berling, H.; Tegel, H.; Mulder, J.; Rockberg, J.; Nilsson, P.; Schwenk, J. M.; Hamsten, M.; Feilitzen, K. von; Forsberg, M.; Persson, L.; Johansson, F.; Zwahlen, M.; Heijne, G. von; Nielsen, J.; Pontén, F. Proteomics. Tissue-based map of the human proteome. *Science* **2015**, *347*, 1260419.

(71) Kim, M.-S.; Pinto, S. M.; Getnet, D.; Nirujogi, R. S.; Manda, S. S.; Chaerkady, R.; Madugundu, A. K.; Kelkar, D. S.; Isserlin, R.; Jain, S.; Thomas, J. K.; Muthusamy, B.; Leal-Rojas, P.; Kumar, P.; Sahasrabuddhe, N. A.; Balakrishnan, L.; Advani, J.; George, B.; Renuse, S.; Selvan, L. D. N.; Patil, A. H.; Nanjappa, V.; Radhakrishnan, A.; Prasad, S.; Subbannayya, T.; Raju, R.; Kumar, M.; Sreenivasamurthy, S. K.; Marimuthu, A.; Sathe, G. J.; Chavan, S.; Datta, K. K.; Subbannayya, Y.; Sahu, A.; Yelamanchi, S. D.; Jayaram, S.; Rajagopalan, P.; Sharma, J.; Murthy, K. R.; Syed, N.; Goel, R.; Khan, A. A.; Ahmad, S.; Dey, G.; Mudgal, K.; Chatterjee, A.; Huang, T.-C.; Zhong, J.; Wu, X.; Shaw, P. G.; Freed, D.; Zahari, M. S.; Mukherjee, K. K.; Shankar, S.; Mahadevan, A.; Lam, H.; Mitchell, C. J.; Shankar, S. K.; Satishchandra, P.; Schroeder, J. T.; Sirdeshmukh, R.; Maitra, A.; Leach, S. D.; Drake, C. G.; Halushka, M. K.; Prasad, T. S. K.; Hruban, R. H.; Kerr, C. L.; Bader, G. D.; Iacobuzio-Donahue, C. A.; Gowda, H.; Pandey, A. A draft map of the human proteome. *Nature* **2014**, *509*, 575–581.

(72) Sjöstedt, E.; Zhong, W.; Fagerberg, L.; Karlsson, M.; Mitsios, N.; Adori, C.; Oksvold, P.; Edfors, F.; Limiszewska, A.; Hikmet, F.; Huang, J.; Du, Y.; Lin, L.; Dong, Z.; Yang, L.; Liu, X.; Jiang, H.; Xu, X.; Wang, J.; Yang, H.; Bolund, L.; Mardinoglu, A.; Zhang, C.; Feilitzen, K. von; Lindskog, C.; Pontén, F.; Luo, Y.; Hökfelt, T.; Uhlén, M.; Mulder, J. An atlas of the protein-coding genes in the human, pig, and mouse brain. *Science* **2020**, *367*.

(73) Gylfe, A. E.; Kondelin, J.; Turunen, M.; Ristolainen, H.; Katainen, R.; Pitkänen, E.; Kaasinen, E.; Rantanen, V.; Tanskanen, T.; Varjosalo, M.; Lehtonen, H.; Palin, K.; Taipale, M.; Taipale, J.; Renkonen-Sinisalo, L.; Järvinen, H.; Böhm, J.; Mecklin, J. P.; Ristimäki, A.; Kilpivaara, O.; Tuupanen, S.; Karhu, A.; Vahteristo, P.; La Aaltonen. Identification of candidate oncogenes in human colorectal cancers with microsatellite instability. *Gastroenterology* **2013**, *145*.

(74) Sherry, S. T.; Ward, M. H.; Kholodov, M.; Baker, J.; Phan, L.; Smigielski, E. M.; Sirotkin, K. dbSNP: the NCBI database of genetic variation. *Nucleic Acids Res.* **2001**, *29*, 308–311.

(75) Cao, C.; Kang, H. J.; Singh, I.; Chen, H.; Zhang, C.; Ye, W.; Hayes, B. W.; Liu, J.; Gumpper, R. H.; Bender, B. J.; Slocum, S. T.; Krumm, B. E.; Lansu, K.; McCorvy, J. D.; Kroeze, W. K.; English, J. G.; DiBerto, J. F.; Olsen, R. H. J.; Huang, X.-P.; Zhang, S.; Liu, Y.; Kim, K.; Karpiak, J.; Jan, L. Y.; Abraham, S. N.; Jin, J.; Shoichet, B. K.; Fay, J. F.; Roth, B. L. Structure, function and pharmacology of human itch GPCRs. *Nature* **2021**, 1–6.

(76) Meixiong, J.; Vasavda, C.; Snyder, S. H.; Dong, X. MRGPRX4 is a G protein-coupled receptor activated by bile acids that may contribute to cholestatic pruritus. *Proc. Natl. Acad. Sci. U. S. A.* **2019**, *116*, 10525–10530.

(77) Yu, H.; Zhao, T.; Liu, S.; Wu, Q.; Johnson, O.; Wu, Z.; Zhuang, Z.; Shi, Y.; Peng, L.; He, R.; Yang, Y.; Sun, J.; Wang, X.; Xu, H.; Zeng, Z.; Zou, P.; Lei, X.; Luo, W.; Li, Y. MRGPRX4 is a bile acid receptor for human cholestatic itch. *Elife* **2019**, *8*.

(78) Song, M.-H.; Shim, W.-S. Lithocholic Acid Activates Mas-Related G Protein-Coupled Receptors, Contributing to Itch in Mice. *Biomol. Ther. (Seoul)* **2021**.

(79) Meixiong, J.; Vasavda, C.; Green, D.; Zheng, Q.; Qi, L.; Kwatra, S. G.; Hamilton, J. P.; Snyder, S. H.; Dong, X. Identification of a bilirubin receptor that may mediate a component of cholestatic itch. *Elife* **2019**, *8*.

(80) Beuers, U.; Kremer, A. E.; Bolier, R.; Elferink, R. P. J. O. Pruritus in cholestasis: facts and fiction. *Hepatology* **2014**, *60*, 399–407.

(81) Kawamata, Y.; Fujii, R.; Hosoya, M.; Harada, M.; Yoshida, H.; Miwa, M.; Fukusumi, S.; Habata, Y.; Itoh, T.; Shintani, Y.; Hinuma, S.; Fujisawa, Y.; Fujino, M. A G Protein-coupled Receptor Responsive to Bile Acids. *J. Biol. Chem.* **2003**, *278*, 9435–9440.

(82) Maruyama, T.; Miyamoto, Y.; Nakamura, T.; Tamai, Y.; Okada, H.; Sugiyama, E.; Nakamura, T.; Itadani, H.; Tanaka, K. Identification of membrane-type receptor for bile acids (M-BAR). *Biochem. Biophys. Res. Commun.* **2002**, *298*, 714–719.

(83) Thomas, C.; Pellicciari, R.; Pruzanski, M.; Auwerx, J.; Schoonjans, K. Targeting bile-acid signalling for metabolic diseases. *Nat. Rev. Drug Discov.* **2008**, *7*, 678–693.

(84) Bartholomew, T. C.; Summerfield, J. A.; Billing, B. H.; Lawson, A. M.; Setchell, K. D. Bile acid profiles of human serum and skin interstitial fluid and their relationship to pruritus studied by gas chromatography-mass spectrometry. *Clin. Sci. (Lond)* **1982**, *63*, 65–73.

(85) Neale, G.; Lewis, B.; Weaver, V.; Panveliwalla, D. Serum bile acids in liver disease. *Gut* **1971**, *12*, 145–152.

(86) Kozlitina, J.; Risso, D.; Lansu, K.; Olsen, R. H. J.; Sainz, E.; Luiselli, D.; Barik, A.; Frigerio-Domingues, C.; Pagani, L.; Wooding, S.; Kirchner, T.; Niaura, R.; Roth, B.; Drayna, D. An African-specific haplotype in MRGPRX4 is associated with menthol cigarette smoking. *PLoS Genet.* **2019**, *15*.

(87) McKemy, D. D.; Neuhausser, W. M.; Julius, D. Identification of a cold receptor reveals a general role for TRP channels in thermosensation. *Nature* **2002**, *416*, 52–58.

(88) Peier, A. M.; Moqrich, A.; Hergarden, A. C.; Reeve, A. J.; Andersson, D. A.; Story, G. M.; Earley, T. J.; Dragoni, I.; McIntyre, P.; Bevan, S.; Patapoutian, A. A TRP Channel that Senses Cold Stimuli and Menthol. *Cell* **2002**, *108*, 705–715.

(89) Paschke, M.; Tkachenko, A.; Ackermann, K.; Hutzler, C.; Henkler, F.; Luch, A. Activation of the cold-receptor TRPM8 by low levels of menthol in tobacco products. *Toxicol. Lett.* **2017**, *271*, 50–57.

(90) Gantz, I.; Muraoka, A.; Yang, Y. K.; Samuelson, L. C.; Zimmerman, E. M.; Cook, H.; Yamada, T. Cloning and chromosomal localization of a gene (GPR18) encoding a

novel seven transmembrane receptor highly expressed in spleen and testis. *Genomics* **1997**, *42*, 462–466.

(91) Morales, P.; Lago-Fernandez, A.; Hurst, D. P.; Sotudeh, N.; Brailoiu, E.; Reggio, P. H.; Abood, M. E.; Jagerovic, N. Therapeutic Exploitation of GPR18: Beyond the Cannabinoids? *J. Med. Chem.* **2020**, *63*, 14216–14227.

(92) Tissue expression of GPR18 - Summary - The Human Protein Atlas. https://www.proteinatlas.org/ENSG00000125245-GPR18/tissue. Published Online: April 26, **2021**.

(93) Vassilatis, D. K.; Hohmann, J. G.; Zeng, H.; Li, F.; Ranchalis, J. E.; Mortrud, M. T.; Brown, A.; Rodriguez, S. S.; Weller, J. R.; Wright, A. C.; Bergmann, J. E.; Gaitanaris, G. A. The G protein-coupled receptor repertoires of human and mouse. *Proc. Natl. Acad. Sci. U. S. A.* **2003**, *100*, 4903–4908.

(94) Irving, A.; Abdulrazzaq, G.; Chan, S. L. F.; Penman, J.; Harvey, J.; Alexander, S. P. H. Cannabinoid Receptor-Related Orphan G Protein-Coupled Receptors. *Adv. Pharmacol.* **2017**, *80*, 223–247.

(95) Console-Bram, L.; Brailoiu, E.; Brailoiu, G. C.; Sharir, H.; Abood, M. E. Activation of GPR18 by cannabinoid compounds: a tale of biased agonism. *Br. J. Pharmacol.* **2014**, *171*, 3908–3917.

(96) McHugh, D.; Page, J.; Dunn, E.; Bradshaw, H. B. Δ(9) -Tetrahydrocannabinol and N-arachidonyl glycine are full agonists at GPR18 receptors and induce migration in human endometrial HEC-1B cells. *Br. J. Pharmacol.* **2012**, *165*.

(97) Qin, Y.; Verdegaal, E. M. E.; Siderius, M.; Bebelman, J. P.; Smit, M. J.; Leurs, R.; Willemze, R.; Tensen, C. P.; Osanto, S. Quantitative expression profiling of G-protein-coupled receptors (GPCRs) in metastatic melanoma: the constitutively active orphan GPCR GPR18 as novel drug target. *Pigment Cell Melanoma Res.* **2011**, *24*, 207–218.

(98) Milman, G.; Maor, Y.; Abu-Lafi, S.; Horowitz, M.; Gallily, R.; Batkai, S.; Mo, F.-M.; Offertaler, L.; Pacher, P.; Kunos, G.; Mechoulam, R. N-arachidonoyl L-serine, an endocannabinoid-like brain constituent with vasodilatory properties. *Proc. Natl. Acad. Sci. U. S. A.* **2006**, *103*, 2428–2433.

(99) Zhang, X.; Maor, Y.; Wang, J. F.; Kunos, G.; Groopman, J. E. Endocannabinoid-like N-arachidonoyl serine is a novel pro-angiogenic mediator. *Br. J. Pharmacol.* **2010**, *160*, 1583–1594.

(100) Kohno, M.; Hasegawa, H.; Inoue, A.; Muraoka, M.; Miyazaki, T.; Oka, K.; Yasukawa, M. Identification of N-arachidonylglycine as the endogenous ligand for orphan G-protein-coupled receptor GPR18. *Biochem. Biophys. Res. Commun.* **2006**, *347*, 827–832.

(101) McHugh, D.; Hu, S. S. J.; Rimmerman, N.; Juknat, A.; Vogel, Z.; Walker, J. M.; Bradshaw, H. B. N-arachidonoyl glycine, an abundant endogenous lipid, potently drives directed cellular migration through GPR18, the putative abnormal cannabidiol receptor. *BMC Neurosci.* **2010**, *11*, 44.

(102) van Lu, B.; Puhl, H. L.; Ikeda, S. R. N-Arachidonyl glycine does not activate G protein-coupled receptor 18 signaling via canonical pathways. *Mol. Pharmacol.* **2013**, *83*, 267–282.

(103) Finlay, D. B.; Joseph, W. R.; Grimsey, N. L.; Glass, M. GPR18 undergoes a high degree of constitutive trafficking but is unresponsive to N-Arachidonoyl Glycine. *PeerJ.* **2016**, *4*, e1835.

(104) Bondarenko, A. I.; Drachuk, K.; Panasiuk, O.; Sagach, V.; Deak, A. T.; Malli, R.; Graier, W. F. N-Arachidonoyl glycine suppresses Na^+/Ca^{2+} exchanger-mediated Ca^{2+} entry into endothelial cells and activates BK(Ca) channels independently of GPCRs. *Br. J. Pharmacol.* **2013**, *169*, 933–948.

(105) Console-Bram, L.; Ciuciu, S. M.; Zhao, P.; Zipkin, R. E.; Brailoiu, E.; Abood, M. E. N-arachidonoyl glycine, another endogenous agonist of GPR55. *Biochem. Biophys. Res. Commun.* **2017**, *490*, 1389–1393.

(106) Deak, A. T.; Groschner, L. N.; Alam, M. R.; Seles, E.; Bondarenko, A. I.; Graier, W. F.; Malli, R. The endocannabinoid N-arachidonoyl glycine (NAGly) inhibits store-operated Ca2+ entry by abrogating STIM1/Orai1 interaction. *J. Cell. Sci.* **2012**, *126*, 879–888.

(107) Alexander, S. P.; Battey, J.; Benson, H. E.; Benya, R. V.; Bonner, T. I.; Davenport, A. P.; Eguchi, S.; Harmar, A.; Holliday, N.; Jensen, R. T.; Karnik, S.; Kostenis, E.; Liew, W. C.; Monaghan, A. E.; Mpamhanga, C.; Neubig, R.; Pawson, A. J.; Pin, J.-P.; Sharman, J. L.; Spedding, M.; Spindel, E.; Stoddart, L.; Storjohann, L.; Thomas, W. G.; Tirupula, K.; Vanderheyden, P. Class A Orphans (version 2019.5) in the IUPHAR/BPS Guide to Pharmacology Database. *1* **2019**, *2019*.

(108) McHugh, D.; Roskowski, D.; Xie, S.; Bradshaw, H. B. Δ(9)-THC and N-arachidonoyl glycine regulate BV-2 microglial morphology and cytokine release plasticity: implications for signaling at GPR18. *Front. Pharmacol.* **2014**, *4*, 162.

(109) Pertwee, R. G.; Howlett, A. C.; Abood, M. E.; Alexander, S. P. H.; Di Marzo, V.; Elphick, M. R.; Greasley, P. J.; Hansen, H. S.; Kunos, G.; Mackie, K.; Mechoulam, R.; Ross, R. A. International Union of Basic and Clinical Pharmacology. LXXIX. Cannabinoid receptors and their ligands: beyond CB_1 and CB_2. *Pharmacol. Rev.* **2010**, *62*, 588–631.

(110) Bernetti, M.; Masetti, M.; Rocchia, W.; Cavalli, A. Kinetics of Drug Binding and Residence Time. *Annu. Rev. Phys. Chem.* **2019**, *70*, 143–171.

(111) Katritch, V.; Fenalti, G.; Abola, E. E.; Roth, B. L.; Cherezov, V.; Stevens, R. C. Allosteric sodium in class A GPCR signaling. *Trends. Biochem. Sci.* **2014**, *39*, 233–244.

(112) Pasternak, G. W.; Snowman, A. M.; Snyder, S. H. Selective enhancement of 3Hopiate agonist binding by divalent cations. *Mol. Pharmacol.* **1975**, *11*, 735–744.

(113) Cayrol, F.; Sterle, H. A.; Díaz Flaqué, M. C.; Barreiro Arcos, M. L.; Cremaschi, G. A. Non-genomic Actions of Thyroid Hormones Regulate the Growth and Angiogenesis of T Cell Lymphomas. *Front. Endocrinol.* **2019**, *10*, 63.

(114) Davis, P. J.; Goglia, F.; Leonard, J. L. Nongenomic actions of thyroid hormone. *Nat. Rev. Endocrinol.* **2016**, *12*, 111–121.

(115) Barreiro Arcos, M. L.; Sterle, H. A.; Paulazo, M. A.; Valli, E.; Klecha, A. J.; Isse, B.; Pellizas, C. G.; Farias, R. N.; Cremaschi, G. A. Cooperative nongenomic and genomic actions on thyroid hormone mediated-modulation of T cell proliferation involve up-regulation of thyroid hormone receptor and inducible nitric oxide synthase expression. *J. Cell. Physiol.* **2011**, *226*, 3208–3218.

(116) van der Spek, A. H.; Fliers, E.; Boelen, A. The classic pathways of thyroid hormone metabolism. *Mol. Cell. Endocrinol.* **2017**, *458*, 29–38.

(117) Fröhlich, E.; Wahl, R. Physiological Role and Use of Thyroid Hormone Metabolites - Potential Utility in COVID-19 Patients. *Front. Endocrinol.* **2021**, *12*, 587518.

(118) Köhrle, J. The Colorful Diversity of Thyroid Hormone Metabolites. *Eur. Thyroid. J.* **2019**, *8*, 115–129.

(119) Robin P Peeters; Theo J Visser. Metabolism of Thyroid Hormone. In *Endotext [Internet].* Peeters, R. P.; Visser, T. J., Eds.; MDText.com, Inc.

(120) Hoefig, C. S.; Zucchi, R.; Köhrle, J. Thyronamines and Derivatives: Physiological Relevance, Pharmacological Actions, and Future Research Directions. *Thyroid* **2016**, *26*, 1656–1673.

(121) Barreiro Arcos, M. L.; Gorelik, G.; Klecha, A.; Genaro, A. M.; Cremaschi, G. A. Thyroid hormones increase inducible nitric oxide synthase gene expression downstream from PKC-zeta in murine tumor T lymphocytes. *Am. J. Physiol. Cell Physiol.* **2006**, *291*, C327-36.

(122) Trepat, X.; Chen, Z.; Jacobson, K. Cell migration. *Compr. Physiol.* **2012**, *2*, 2369–2392.

(123) Yamada, K. M.; Sixt, M. Mechanisms of 3D cell migration. *Nat. Rev. Mol. Cell Biol.* **2019**, *20*, 738–752.

(124) Lamalice, L.; Le Boeuf, F.; Huot, J. Endothelial cell migration during angiogenesis. *Circ. Res.* **2007**, *100*, 782–794.

(125) Mayor, R.; Etienne-Manneville, S. The front and rear of collective cell migration. *Nat. Rev. Mol. Cell Biol.* **2016**, *17*, 97–109.

(126) Sun, Y.; Liu, W.-Z.; Liu, T.; Feng, X.; Yang, N.; Zhou, H.-F. Signaling pathway of MAPK/ERK in cell proliferation, differentiation, migration, senescence and apoptosis. *J. Recept. Signal Transduct. Res.* **2015**, *35*, 600–604.

(127) Holroyd, A. K.; Michie, A. M. The role of mTOR-mediated signaling in the regulation of cellular migration. *Immunology Letters* **2018**, *196*, 74–79.

(128) Chun-Chi Liang; Ann Y Park; Jun-Lin Guan. In vitro scratch assay: a convenient and inexpensive method for analysis of cell migration in vitro. *Nat. Protoc.* **2007**, *2*, 329–333.

(129) Jonkman, J. E. N.; Cathcart, J. A.; Xu, F.; Bartolini, M. E.; Amon, J. E.; Stevens, K. M.; Colarusso, P. An introduction to the wound healing assay using live-cell microscopy. *Cell Adh. Migr.* **2014**, *8*, 440–451.

(130) Ieso, M. L. de; Pei, J. V. An accurate and cost-effective alternative method for measuring cell migration with the circular wound closure assay. *Biosci. Rep.* **2018**, *38*.

(131) Ashby, W. J.; Zijlstra, A. Established and Novel Methods of Interrogating Two-Dimensional Cell Migration. *Integr. Biol. (Camb)* **2012**, *4*, 1338–1350.

(132) Khan, Z. S.; Vanapalli, S. A. Probing the mechanical properties of brain cancer cells using a microfluidic cell squeezer device. *Biomicrofluidics* **2013**, *7*.

(133) Chen, J.; Liu, T.; Wang, H.; Wang, Z.; Lv, Y.; Zhao, Y.; Yang, N.; Yuan, X. Elevation in the Expression of circ_0079586 Predicts Poor Prognosis and Accelerates Progression in Glioma via Interactions with the miR-183-5p/MDM4 Signaling Pathway. *Onco. Targets Ther.* **2020**, *13*, 5135–5143.

(134) Asmus, S. E.; Batey, K. G.; Gale-Butto, S. N.; Schmitt, B. L. Using the scratch assay to study cell migration in an inquiry-based cell biology lab. *J. Biol. Ed.* **2019**, *53*, 157–164.

(135) Xiao, Q.; Ying, J.; Qiao, Z.; Yang, Y.; Dai, X.; Xu, Z.; Zhang, C.; Xiang, L. Exogenous hydrogen sulfide inhibits human melanoma cell development via suppression of the PI3K/AKT/ mTOR pathway. *J. Dermatol. Sci.* **2020**, *98*, 26–34.

(136) Lin, Y.; Shao, Q.; Zhang, M.; Lu, C.; Fleming, J.; Su, S. Royal jelly-derived proteins enhance proliferation and migration of human epidermal keratinocytes in an in vitro scratch wound model. *BMC Complement Altern. Med.* **2019**, *19*, 175.

(137) Dhillon, P. K.; Li, X.; Sanes, J. T.; Akintola, O. S.; Sun, B. Method comparison for analyzing wound healing rates. *Biochem. Cell Biol.* **2017**, *95*, 450–454.

(138) Schneider, C. A.; Rasband, W. S.; Eliceiri, K. W. NIH Image to ImageJ: 25 years of image analysis. *Nat. Methods* **2012**, *9*, 671–675.

(139) Lee, W. K.; Choi, S. W.; Lee, H. R.; Lee, E. J.; Lee, K. H.; Kim, H. O. Purinoceptor-mediated calcium mobilization and proliferation in HaCaT keratinocytes. *J. Dermatol. Sci.* **2001**, *25*, 97–105.

(140) Fonseca, D. F. S.; Carvalho, J. P. F.; Bastos, V.; Oliveira, H.; Moreirinha, C.; Almeida, A.; Silvestre, A. J. D.; Vilela, C.; Freire, C. S. R. Antibacterial Multi-Layered Nanocellulose-Based Patches Loaded with Dexpanthenol for Wound Healing Applications. *Nanomaterials (Basel)* **2020**, *10*.

(141) Tait, S. W. G.; Ichim, G.; Green, D. R. Die another way--non-apoptotic mechanisms of cell death. *J. Cell. Sci.* **2014**, *127*, 2135–2144.

(142) Tsujimoto, Y. Multiple ways to die: non-apoptotic forms of cell death. *Acta. Oncol.* **2012**, *51*, 293–300.

(143) Kornienko, A.; Mathieu, V.; Rastogi, S. K.; Lefranc, F.; Kiss, R. Therapeutic agents triggering nonapoptotic cancer cell death. *J. Med. Chem.* **2013**, *56*, 4823–4839.

(144) Maltese, W. A.; Overmeyer, J. H. Methuosis: nonapoptotic cell death associated with vacuolization of macropinosome and endosome compartments. *Am. J. Pathol.* **2014**, *184*, 1630–1642.

(145) Yan, G.; Elbadawi, M.; Efferth, T. Multiple cell death modalities and their key features (Review). *World Acad. Sci. J.* **2020**.

(146) Overmeyer, J. H.; Kaul, A.; Johnson, E. E.; Maltese, W. A. Active Ras Triggers Death in Glioblastoma Cells Through Hyperstimulation of Macropinocytosis. *Mol. Cancer Res.* **2008**, *6*, 965–977.

(147) Overmeyer, J. H.; Young, A. M.; Bhanot, H.; Maltese, W. A. A chalcone-related small molecule that induces methuosis, a novel form of non-apoptotic cell death, in glioblastoma cells. *Mol. Cancer* **2011**, *10*, 69.

(148) Robinson, M. W.; Overmeyer, J. H.; Young, A. M.; Erhardt, P. W.; Maltese, W. A. Synthesis and evaluation of indole-based chalcones as inducers of methuosis, a novel type of nonapoptotic cell death. *J. Med. Chem.* **2012**, *55*, 1940–1956.

(149) Grimmer, S.; van Deurs, B.; Sandvig, K. Membrane ruffling and macropinocytosis in A431 cells require cholesterol. *J. Cell Sci.* **2002**, *115*, 2953–2962.

(150) Racoosin, E. L.; Swanson, J. A. Macropinosome maturation and fusion with tubular lysosomes in macrophages. *J. Cell Biol.* **1993**, *121*, 1011–1020.

(151) Li, Z.; Mbah, N. E.; Overmeyer, J. H.; Sarver, J. G.; George, S.; Trabbic, C. J.; Erhardt, P. W.; Maltese, W. A. The JNK signaling pathway plays a key role in methuosis (non-apoptotic cell death) induced by MOMIPP in glioblastoma. *BMC Cancer* **2019**, *19*, 77.

(152) Trabbic, C. J.; Overmeyer, J. H.; Alexander, E. M.; Crissman, E. J.; Kvale, H. M.; Smith, M. A.; Erhardt, P. W.; Maltese, W. A. Synthesis and Biological Evaluation of Indolyl-Pyridinyl-Propenones Having Either Methuosis or Microtubule Disruption Activity. *J. Med. Chem.* **2015**, *58*, 2489–2512.

(153) Mihara, K.; Nakayama, T.; Saitoh, H. A Convenient Technique to Fix Suspension Cells on a Coverslip for Microscopy. *Curr. Protoc. Cell Biol.* **2015**, *68*.

(154) Giaume, C.; Naus, C. C.; Sáez, J. C.; Leybaert, L. Glial connexins and pannexins in the healthy and diseased brain. *Physiol. Rev.* **2021**, *101*, 93–145.

(155) Vinken, M.; Vanhaecke, T.; Papeleu, P.; Snykers, S.; Henkens, T.; Rogiers, V. Connexins and their channels in cell growth and cell death. *Cell. Signal.* **2006**, *18*, 592–600.

(156) Bedner, P.; Steinhäuser, C.; Theis, M. Functional redundancy and compensation among members of gap junction protein families? *Biochim. Biophys. Acta Biomembr.* **2012**, *1818*, 1971–1984.

(157) Salameh, A. Life cycle of connexins: regulation of connexin synthesis and degradation. *Adv. Cardiol.* **2006**, *42*, 57–70.

(158) Kar, R.; Batra, N.; Riquelme, M. A.; Jiang, J. X. Biological role of connexin intercellular channels and hemichannels. *Arch. Biochem. Biophys.* **2012**, *524*.

(159) Lampe, P. D.; TenBroek, E. M.; Burt, J. M.; Kurata, W. E.; Johnson, R. G.; Lau, A. F. Phosphorylation of connexin43 on serine368 by protein kinase C regulates gap junctional communication. *J. Cell. Biol.* **2000**, *149*, 1503–1512.

(160) Solan, J. L.; Lampe, P. D. Specific Cx43 phosphorylation events regulate gap junction turnover in vivo. *FEBS Lett.* **2014**, *588*, 1423–1429.

(161) Meggouh, F.; Benomar, A.; Rouger, H.; Tardieu, S.; Birouk, N.; Tassin, J.; Barhoumi, C.; Yahyaoui, M.; Chkili, T.; Brice, A.; LeGuern, E. The first de novo mutation of the connexin 32 gene associated with X linked Charcot-Marie-Tooth disease. *J. Med. Genet.* **1998**, *35*, 251–252.

(162) Koppelhus, U.; Tranebjaerg, L.; Esberg, G.; Ramsing, M.; Lodahl, M.; Rendtorff, N. D.; Olesen, H. V.; Sommerlund, M. A novel mutation in the connexin 26 gene (GJB2) in a child with clinical and histological features of keratitis-ichthyosis-deafness (KID) syndrome. *Clin. Exp. Dermatol.* **2011**, *36*, 142–148.

(163) Guerrero, P. A.; Schuessler, R. B.; Davis, L. M.; Beyer, E. C.; Johnson, C. M.; Yamada, K. A.; Saffitz, J. E. Slow ventricular conduction in mice heterozygous for a connexin43 null mutation. *J. Clin. Invest.* **1997**, *99*, 1991–1998.

(164) Gutstein, D. E.; Morley, G. E.; Tamaddon, H.; Vaidya, D.; Schneider, M. D.; Chen, J.; Chien, K. R.; Stuhlmann, H.; Fishman, G. I. Conduction slowing and sudden arrhythmic death in mice with cardiac-restricted inactivation of connexin43. *Circ. Res.* **2001**, *88*, 333–339.

(165) Vasconcellos, J. P. C.; Melo, M. B.; Schimiti, R. B.; Bressanim, N. C.; Costa, F. F.; Costa, V. P. A novel mutation in the GJA1 gene in a family with oculodentodigital dysplasia. *Arch. Ophthalmol.* **2005**, *123*, 1422–1426.

(166) Maass, K.; Ghanem, A.; Kim, J.-S.; Saathoff, M.; Urschel, S.; Kirfel, G.; Grümmer, R.; Kretz, M.; Lewalter, T.; Tiemann, K.; Winterhager, E.; Herzog, V.; Willecke, K. Defective epidermal barrier in neonatal mice lacking the C-terminal region of connexin43. *Mol. Biol. Cell* **2004**, *15*, 4597–4608.

(167) Babica, P.; Sovadinová, I.; Upham, B. L. Scrape loading/dye transfer assay. *Methods Mol. Biol.* **2016**, *1437*, 133–144.

(168) El-Fouly, M. H.; Trosko, J. E.; Chang, C.-C. Scrape-loading and dye transfer. *Exp. Cell Biol.* **1987**, *168*, 422–430.

(169) Picoli, C.; Soleilhac, E.; Journet, A.; Barette, C.; Comte, M.; Giaume, C.; Mouthon, F.; Fauvarque, M.-O.; Charvériat, M. High-Content Screening Identifies New Inhibitors of Connexin 43 Gap Junctions. *Assay Drug Dev. Technol.* **2019**, *17*, 240–248.

(170) Burnham, M. P.; Sharpe, P. M.; Garner, C.; Hughes, R.; Pollard, C. E.; Bowes, J. Investigation of connexin 43 uncoupling and prolongation of the cardiac QRS complex in preclinical and marketed drugs. *Br. J. Pharmacol.* **2014**, *171*, 4808–4819.

(171) Lee, J. Y.; Choi, E. J.; Lee, J. A new high-throughput screening-compatible gap junctional intercellular communication assay. *BMC Biotechnol.* **2015**, *15*.

(172) Haq, N.; Grose, D.; Ward, E.; Chiu, O.; Tigue, N.; Dowell, S. J.; Powell, A. J.; Chen, M. X. A high-throughput assay for connexin 43 (Cx43, GJA1) gap junctions using codon-optimized aequorin. *Assay Drug Dev. Technol.* **2013**, *11*, 93–100.

(173) Lurtz, M. M.; Louis, C. F. Intracellular calcium regulation of connexin43. *Am. J. Physiol. Cell Physiol.* **2007**, *293*, C1806-13.

(174) Imanaga, I.; Hai, L.; Ogawa, K.; Matsumura, K.; Mayama, T. Phosphorylation of connexin in functional regulation of the cardiac gap junction. *Exp. Clin. Cardiol.* **2004**, *9*, 161–164.

(175) Peter Bedner; Heiner Niessen; Benjamin Odermatt; Markus Kretz; Klaus Willecke; Hartmann Harz. Selective permeability of different connexin channels to the second messenger cyclic AMP. *J. Biol. Chem.* **2006**, *281*, 6673–6681.

(176) Fan, F.; Binkowski, B. F.; Butler, B. L.; Stecha, P. F.; Lewis, M. K.; Wood, K. V. Novel genetically encoded biosensors using firefly luciferase. *ACS Chem. Biol.* **2008**, *3*, 346–351.

12 ACKNOWLEDGEMENTS

The last four years were a challenging, but a fruitful and throughout nice time. This was supported by dear people close to me at work and in private.

Zuallererst möchte ich meiner Doktormutter und Betreuerin dieser Arbeit, Prof. Dr. Christa E. Müller, danken. Liebe Christa, Du hast mir die Promotion hier ermöglicht. Vielen Dank, dass Du mir die Promotionsstelle und die interessanten und herausfordernden Projekte zugeteilt hast. Du hast mir Freiheiten in den Projekten gelassen, aber auch mit zahlreichen Meetings (welche ich immer mit neuer Motivation verlassen habe) und hilfreichen Tipps für den positiven Ausklang meiner Promotion gesorgt. Ich habe die Promotion gestartet, um eigenständiges wissenschaftliches Arbeiten zu erlernen, und um an dieser Herausforderung zu wachsen. Dank Dir war das möglich, und ich kann nun behaupten meine Ansprüche, und mehr, erfüllt zu haben.

Ich danke den weiteren Mitgliedern meiner Prüfungskommission PD Dr. Anke Schiedel, Prof. Dr. Günther Weindl und Prof. Dr. Rainer Manthey für die Zeit, die Sie in das Lesen und Bewerten meiner Dissertation investiert haben und, dass sie meinen letzten Schritt zur Promotion unterstützen.

Vielen Dank an die Graduiertenschule BIGSDrugS, und deren Organisatorinnen Doro und Amelie. BIGSDrugS hat mir nicht nur die Teilnahme an einigen interessanten Workshops und Vorträgen ermöglicht, sondern auch die Teilnahme an einer Konferenz finanziert.

Dr. Winnie Deuther-Conrad vom Helmholtz Zentrum Dresden-Rossendorf möchte ich herzlich danken für das Ermöglichen der Autoradiographie Studien. Danke, dass Du Deine Zeit investiert hast uns alles zu zeigen und ausführlich zu erklären.

Sophie möchte ich für das Bereitstellen zahlreicher Substanzen und eine hervorragende Zusammenarbeit danken. Vielen Dank für die Auffrischungen in organischer Chemie, welche ich hin und wieder nötig hatte und die zahlreichen Diskussionen über unser Projekt die immer zielführend waren.

Thanks Andhika, for introducing me into your favorite research topic (GPR18), the ordering of the CO_2 bottles, and all the sweets.

Vielen Dank an unsere Technischen Assistentinnen Chrisi, Christin, Katharina, und Marion. Ihr haltet den Laden am Laufen! An Christin ein besonderer Dank für die Einarbeitung am Anfang meiner Zeit, und an Chrisi, dass Du dich am Ende von mir hast einarbeiten lassen. Ihr wart alle immer da, wenn ich Hilfe gebraucht habe.

Vielen Dank an Josua Krebber für die Unterstützung im Labor während deiner Bachelorarbeit.

Vielen Dank an das Team des 7. Semester. Dominik – vielen Dank für die ausgesprochen gute Planung der Abläufe des Praktikums. Vielen Dank an alle Kollegen mit denen einige der Aufsichtsschichten angenehmer wurden.

I want to thank the whole research group of Prof. Dr. Christa E. Müller for a consistently nice and productive work environment. For all the help in the beginning, and the advice and insights throughout the whole time. So many incubation times we spent chatting in the lab made me much smarter and helped my work to prosper.

An meine Bürokollegen Bea, Marion und Mariam (und manchmal Chrisi). Vielen Dank für ein angenehmes Büroklima mit motivierendem Kaffeegeruch in der Luft.

An meine Lieblingskollegen Jan und Laura. Ihr habt so ziemlich jeden Moment meiner Promotion mit mir geteilt - ob Auf oder Ab. Für zahlreiche Kaffee- und Mittagspausen bin ich euch sehr dankbar. Es freut mich, dass unsere Freundschaft weiter bestehen bleibt, auch wenn wir aufgrund einiger Kilometer Entfernung uns vorerst mit Buchclubtreffen über Zoom begnügen müssen.

Liebe Mama. Wer hätte vor einigen Jahren noch gedacht, dass ich mal eine Danksagung für meine Doktorarbeit schreibe. Du hast immer an mich geglaubt - und mir das auch gezeigt. Du hast die Grundsteine gelegt und mir ein Interesse an der Welt vermittelt mit dem ich Schule, Studium und nun auch die Promotion gemeistert habe. Nur dank Dir bin ich jetzt da, wo ich bin. Vielen Dank für Alles!

Liebe Kim. Du hast einen Großteil der Promotionszeit mit mir ausgestanden. Du hast mich immer bestärkt und motiviert, und auch mal für die nötige Ablenkung von der Arbeit gesorgt. Dich kennengelernt zu haben war das größte Glück und ich freue mich auf jeden weiteren Schritt in meinem Leben, da ich weiß, dass wir ihn zusammen gehen.

13 APPENDICES

13.1 MANUSCRIPT AND SUPPORTING INFORMATION: CONNEXIN

In this section the article 'A cellular assay for the identification and characterization of connexin gap junction modulators' is printed. The introduction is given in chapter 7. The article was published by the 'International Journal of Molecular Sciences' by MDPI. MDPI publishes open access, and copyright is retained by the authors.

Article

A Cellular Assay for the Identification and Characterization of Connexin Gap Junction Modulators

Azeem Danish [1,†], Robin Gedschold [1,†], Sonja Hinz [1], Anke C. Schiedel [1], Dominik Thimm [1], Peter Bedner [2], Christian Steinhäuser [2,*] and Christa E. Müller [1,*]

[1]   PharmaCenter Bonn, Pharmaceutical Institute, Pharmaceutical & Medicinal Chemistry, Rheinische Friedrich-Wilhelms-Universität Bonn, An der Immenburg 4, D-53121 Bonn, Germany; adanish32@googlemail.com (A.D.); rgedscho@uni-bonn.de (R.G.); shinz@uni-bonn.de (S.H.); schiedel@uni-bonn.de (A.C.S.); dthimm@uni-bonn.de (D.T.)

[2]   Institute of Cellular Neuroscience, Medical Faculty, Rheinische Friedrich-Wilhelms-Universität Bonn, Venusberg-Campus 1, D-53127 Bonn, Germany; Peter.Bedner@ukbonn.de

*   Correspondence: Christian.Steinhaeuser@ukbonn.de (C.S.); christa.mueller@uni-bonn.de (C.E.M.)

†   They contributed equally to this paper.

Abstract: Connexin gap junctions (Cx GJs) enable the passage of small molecules and ions between cells and are therefore important for cell-to-cell communication. Their dysfunction is associated with diseases, and small molecules acting as modulators of GJs may therefore be useful as therapeutic drugs. To identify GJ modulators, suitable assays are needed that allow compound screening. In the present study, we established a novel assay utilizing HeLa cells recombinantly expressing Cx43. Donor cells additionally expressing the Gs protein-coupled adenosine A_{2A} receptor, and biosensor cells expressing a cAMP-sensitive GloSensor luciferase were established. Adenosine A_{2A} receptor activation in the donor cells using a selective agonist results in intracellular cAMP production. The negatively charged cAMP migrates via the Cx43 gap junctions to the biosensor cells and can there be measured by the cAMP-dependent luminescence signal. Cx43 GJ modulators can be expected to impact the transfer of cAMP from the donor to the biosensor cells, since cAMP transit is only possible via GJs. The new assay was validated by testing the standard GJ inhibitor carbenoxolon, which showed a concentration-dependent inhibition of the signal and an IC_{50} value that was consistent with previously reported values. The assay was demonstrated to be suitable for high-throughput screening.

Keywords: compound library; connexin-43; gap junctions; GloSensor luciferase; HeLa cells; screening

1. Introduction

Gap junction (GJ) channels are important for cell-to-cell communication in most tissues. They enable the free diffusion of molecules up to a molecular weight of about 1000 Da including second messengers, amino acids, ions, glucose and other metabolites [1]. Gap junctional intercellular communication regulates embryonic development and coordinates many processes including smooth and cardiac muscle contraction, tissue homeostasis, apoptosis, metabolic transport, cell growth and cell differentiation [1,2].

Connexins constitute a multigene family whose members can be divided based on their molecular weight. In humans, 21 connexin subtypes have been identified, and more than one connexin subtype can typically be found on the same cell [3–5]. The oligomerization of six connexins leads to the formation of a connexon that can either be homomeric or heteromeric. The docking of two connexons of adjacent cells leads to the formation of intercellular channels that may constitute either homotypic or heterotypic, or combined heterotypic/heteromeric arrangements of GJs [2,5]. Among all connexins in humans, Cx43 is the most abundantly and widely expressed connexin type, being present in many cell types and tissues [6].

Several human diseases have been linked to germline mutations of connexin family members [1,7]. For instance mutations in Cx26 result in keratitis-ichthyosis-deafness and mutations in Cx32 cause the X-linked Charcot–Marie–Tooth disease [8,9]. Mutations in Cx43 are linked to oculodentodigital dysplasia characterized by developmental abnormalities, and total disruption of this gene causes cardiac arrhythmias [10–14]. Changes in the expression levels of Cx43 have been reported for some neurological disorders in humans such as epilepsy, depression, and brain metastasis, implying its crucial role in the etiology or progression of these diseases [9–11]. Cx43 knockout mice die shortly after birth. Moreover, mouse models with a Cx43 truncated at the *C*-terminus exhibited a defect in skin barrier function with mislocalized Cx43 GJs, which also resulted in the death of the animals soon after birth [15].

Assays for testing connexin activity have previously been developed. They are based on dye transfer or quantification of a transferred molecule using luminescence detection. In the dye transfer assays, donor cells are loaded with a membrane-impermeable dye. After incubation with acceptor cells the dye can diffuse though GJs to the acceptor cells, and the extent of this effect is a measure of GJ permeability. The assays are mostly evaluated visually, but automated approaches have also been established [16–18]. Picoli et al. (2019) published a dye transfer assay in a high-throughput screening (HTS) format [19]. However, sophisticated imaging instrumentation is required to automatize the evaluation. Moreover, GJ inhibitors neither displayed stable nor clear concentration-dependent effects in this assay. Other established assays, which are based on luminescence, utilize a mediator molecule selectively generated in the donor cells. This compound migrates through the GJs into the acceptor cells where it activates or quenches a luminescence-emitting protein. Because of their real-time read-out, luminescence assays are suitable for HTS approaches. Lee et al. (2015) published an HTS assay, utilizing donor cells transfected with an iodide transporter and acceptor cells transfected with the yellow fluorescent protein (YFP) [20]. After iodide is taken up by the donor cells, it migrates to the biosensor cells via the GJs. The YFP fluorescence is quenched by iodide, allowing direct measurement of GJ permeability. However, the measured fluorescence could only be reduced by up to 50%, resulting in only a small assay window, which appears unsatisfactory. Another HTS assay, introduced by Haq et al. (2013), utilizes Ca^{2+} diffusion through GJs [21]. Either a G_q protein-coupled adrenergic receptor or a TRPV1 ion channel was used to increase intracellular Ca^{2+} concentrations in the donor cells. The acceptor cells recombinantly expressed aequorin intracellularly, which produces luminescence in the presence of Ca^{2+}. However, Ca^{2+} can induce protein kinase C-mediated phosphorylation of Cxs and calmodulin resulting in an inhibition of GJs, which limits the significance of this assay [22,23].

Thus, despite the recent development of several assays for testing and identifying GJ modulators, all reported methods are far from ideal and each is associated with a number of drawbacks. Therefore, we set out to establish a novel assay to allow the screening of compound libraries as a basis for the development of GJ modulators.

2. Results

2.1. Assay Design

In the present study, we selected cAMP as a suitable analyte which cannot penetrate cell membranes passively due to its negative charge, but is able to migrate through GJs from a donor cell to a biosensor cell [24]. A genetically engineered firefly luciferase known as cAMP GloSensor-20F (GloSensor luciferase, Promega), which can detect cAMP with high sensitivity, was selected for detecting intracellular cAMP in real time (Figure 1a). Firefly luciferase catalyzes the oxidation of its substrate luciferin in the presence of Mg^{2+}, ATP and O_2 to produce oxyluciferin, AMP, CO_2 and a luminescence signal (Figure 1b). GloSensor luciferase is a genetically engineered form of firefly luciferase, which contains the conserved cAMP binding domain B from protein kinase A regulatory subunit IIβ (see Figure 1a). Binding of intracellular cAMP to the enzyme favors the functional luciferase

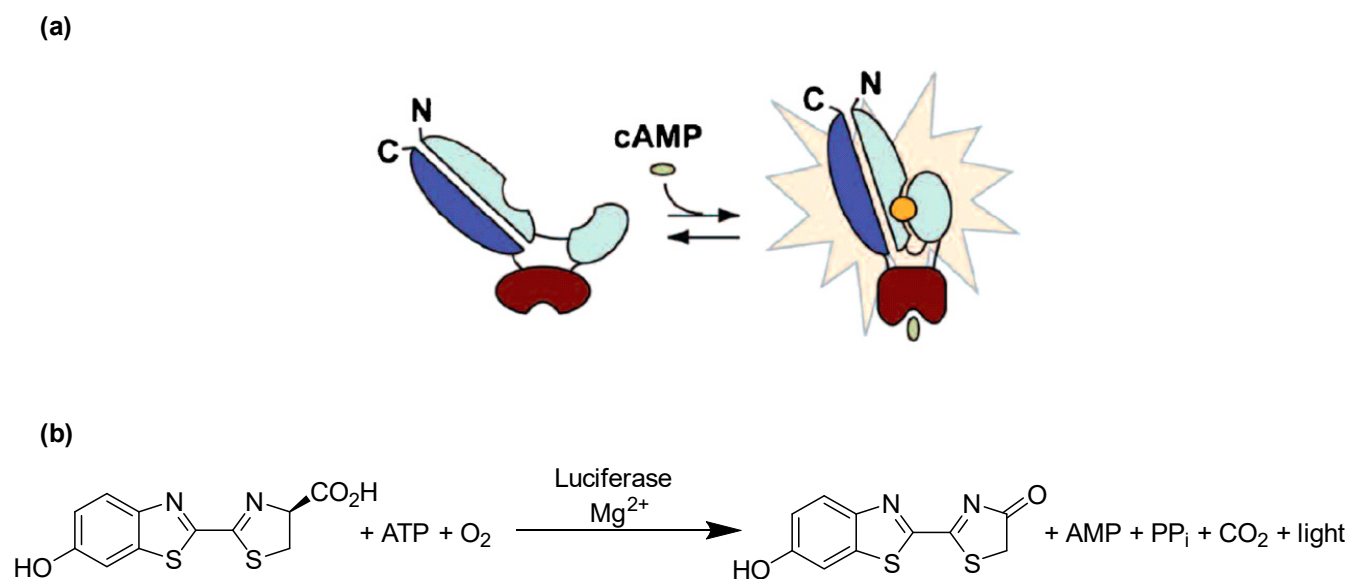conformation, which then metabolizes luciferin to oxyluciferin, thereby producing a yellow-green light [25].

(a)

(b)

Figure 1. Principle of cAMP detection using the engineered GloSensor luciferase. (**a**) GloSensor luciferase in the open conformation shows negligible activity resulting in a low luminescence background, whereas binding of cAMP to the cAMP binding site favors the closed conformation and hence activates the luciferase, which metabolizes luciferin to oxyluciferin, producing luminescence. (**b**) Luciferase catalyzes the oxidation of luciferin using molecular oxygen and ATP in the presence of Mg^{2+} to produce oxyluciferin, which is highly unstable in an electronically excited state and produces light upon returning to its electronical ground state. Modified based on published figure [25].

Our experimental strategy was to create donor cells which coexpress the human (h) G_s protein-coupled adenosine A_{2A} receptor ($A_{2A}AR$) as well as Cx43. In addition, biosensor cells expressing the cAMP-sensing GloSensor luciferase along with Cx43 were engineered. $A_{2A}AR$ activation by the A_{2A}-selective agonist CGS-21680 was expected to lead to adenylate cyclase activation resulting in an increase in intracellular cAMP concentrations in the donor cells. cAMP would then migrate into the biosensor cells via Cx43 GJs and could then activate the cAMP-dependent GloSensor luciferase. This was expected to result in a quantifiable luminescence signal. The principle of the designed assay is depicted in Figure 2. To initially evaluate and validate the feasibility of the new assay, preliminary experiments were performed (see below).

2.2. Preparation and Evaluation of Recombinant Cells

For the experiments, we aimed at utilizing a cell line that shows no or only low native Cx43 expression. HeLa cells, an immortal cervical cancer cell line, were selected because they are known to be communication-deficient due to low or lacking Cx expression [20]. First, we confirmed very low native Cx43 expression in this cell line (see Figure S1 of Supporting Information). The recombinant expression of Cx43 in HeLa cells led to significant Cx43 levels as confirmed by fluorescence microscopy using a Cx43-specific antibody (Figure 3).

The HeLa cells were transiently transfected either with $A_{2A}AR$ and GloSensor luciferase (HeLa-$A_{2A}AR$-GSL), or only with GloSensor luciferase (HeLa-GSL). These cell constructs were subsequently tested for their luminescence signals after activation using the selective $A_{2A}AR$ agonist CGS-21680, or the nonselective AR agonist NECA (Figure 4). Forskolin, which is a direct activator of adenylate cyclase, was employed as a positive control, while the solvent DMSO (1%) served as negative control. As expected, HeLa-$A_{2A}AR$-GSL as well as HeLa-GSL cells produced a luminescence signal upon stimulation

with forskolin (10 µM), which was completely independent of AR expression. The nonselective adenosine receptor (AR) agonist NECA showed a much weaker signal in HeLa-GSL as compared to HeLa-A_{2A}AR-GSL cells. The moderate signal observed for NECA is due to native expression of A_{2B}ARs [26,27], which are also Gs protein-coupled like the A_{2A}ARs. In contrast, the A_{2A}AR-selective agonist CGS-21680, employed at a high concentration of 100 µM, only produced a cAMP-dependent luminescence signal in HeLa-A_{2A}AR-GSL, but not in HeLa-GSL cells.
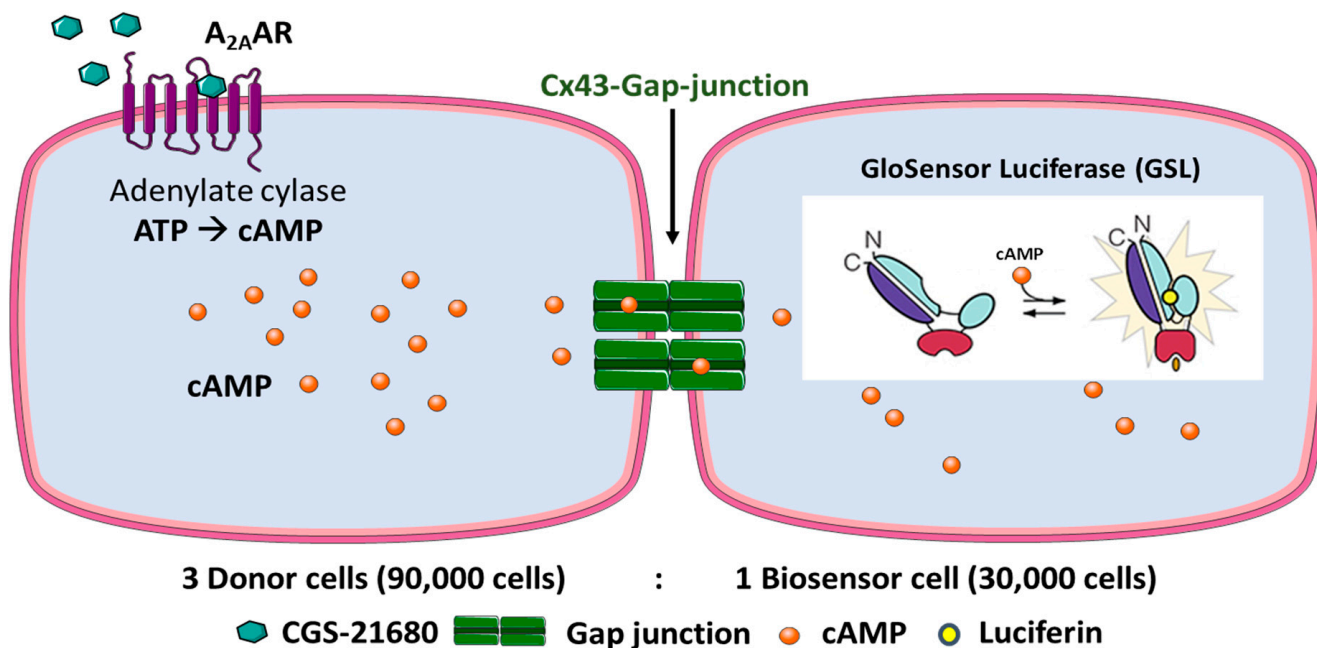

Figure 2. Design of the Cx43 GJ assay. HeLa cells expressing A_{2A}AR and Cx43 are denoted as donor cells and HeLa cells expressing GloSensor luciferase and Cx43 as biosensor cells. The cell lines were cocultured in a ratio of 3:1 (donor: biosensor cells) for 4 h to allow the formation of Cx43 GJs. The cells were then equilibrated with buffer containing the substrate (luciferin) of the engineered cAMP-dependent luciferase. Upon activation of the G_s protein-coupled A_{2A}ARs, cAMP levels in the donor cells are increased. cAMP can then migrate via the Cx43 GJs to the biosensor cells. There, cAMP binds to the GloSensor luciferase which results in a conformational change that leads to an activation of the GloSensor luciferase, creating a luminescence signal by oxidation of luciferin. Depiction of GloSensor luciferase is based on reference [25].

Based on these findings, we concluded that native HeLa cells do not express functional A_{2A}ARs. This makes the A_{2A}AR an excellent cAMP-generating tool by activating it with the A_{2A}AR-selective agonist CGS-21680 after recombinant expression in HeLa cells. Our results were in agreement with the previously reported expression profile of A_{2A}A- and A_{2B}ARs in native HeLa cells, where A_{2B}AR expression was found to be higher than that of A_{2A}AR, and in such cases, A_{2A} signaling is not observed since it is blocked by A_{2B}ARs [26,27].

As a next step, biosensor cells were created which coexpress GloSensor luciferase and Cx43. The heterologous expression of two or more proteins in the same cell may result in reduced expression levels of each protein due to high occupancy of the cellular translational machinery. Moreover, part of the cAMP produced in the donor cells might be released into the extracellular space through Cx43 hemichannels [28]. Therefore, experiments were performed to compare transiently transfected HeLa cells expressing only GloSensor luciferase with cells coexpressing GloSensor luciferase and Cx43 with regard to the luminescence signal induced by cAMP (Figure 5). Forskolin (10 µM)-mediated activation of adenylate cyclase in HeLa cells only transfected with GloSensor luciferase resulted in similar luminescence signals as compared to HeLa cells transfected with both GloSensor luciferase and Cx43 while the A_{2A}AR-selective agonist CGS-21680 (1 µM) was inactive as expected since the cells did not express functional A_{2A}ARs. These results clearly showed

that coexpression of Cx43 and GloSensor luciferase in HeLa cells yielded sufficiently high cAMP-dependent luminescence signals for the planned assay.
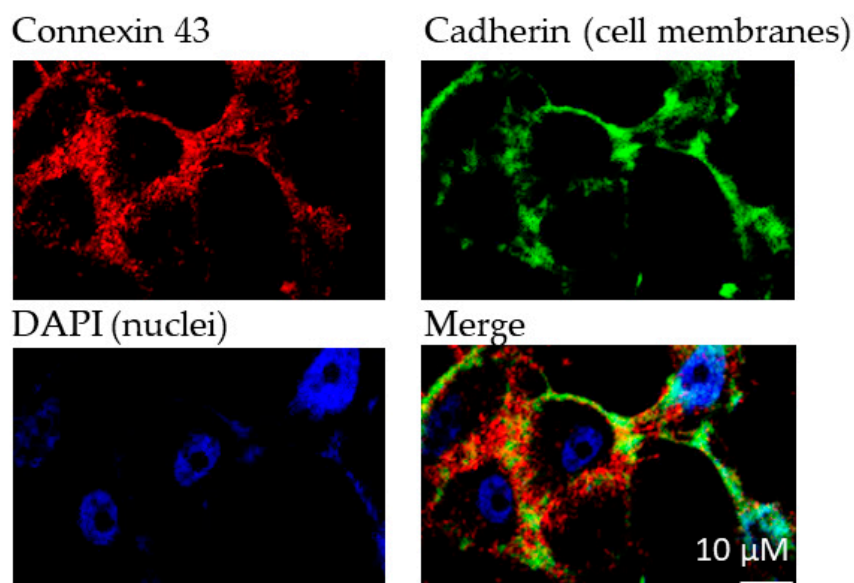
Figure 3. Immunofluorescence analyses of Cx43 expression in transfected HeLa cells. Cadherin was used to stain cell membranes. Primary antibodies (1:1000): antipan cadherin (mouse), anti Cx43 (rabbit); secondary antibodies (1:500): Alexa 488 (antimouse), Alexa 594 (antirabbit). DAPI (1:10,000) was used to stain cell nuclei.
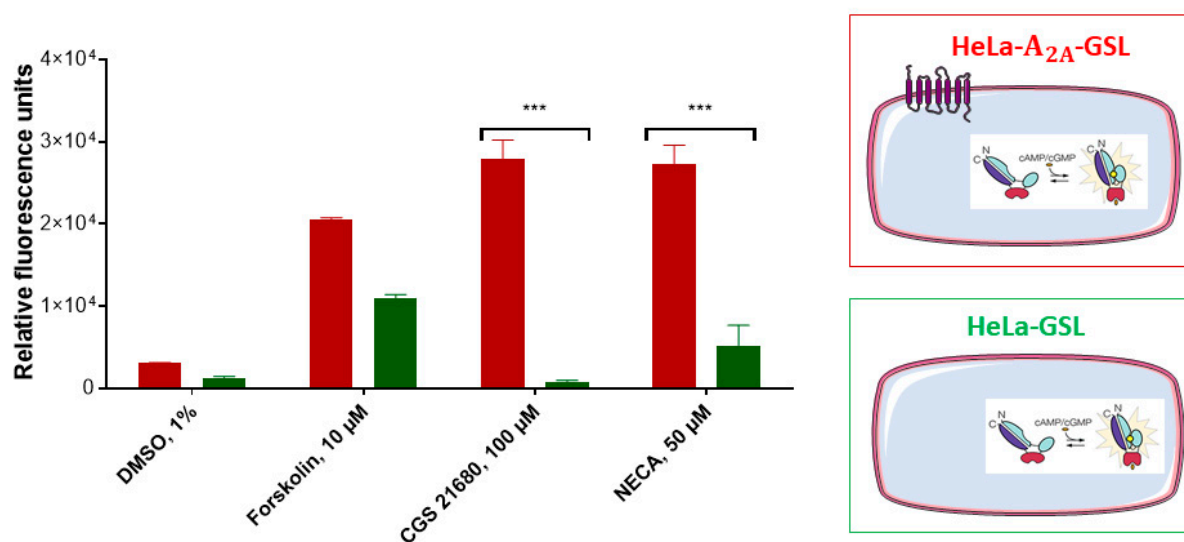
Figure 4. Assessment of adenosine receptor-mediated cAMP production in A_{2A} AR-transfected (red) and nontransfected (green) HeLa- cells. The cAMP-activated GloSensor luciferase was cotransfected resulting in cAMP-dependent luminescence signals. Cells (60,000/well) were incubated with medium supplemented with 2% GloSensor luciferase reagent for 2 h at 37 °C. After addition of DMSO or compound dissolved in DMSO (forskolin, 10 µM, CGS-21680, 100 µM, or NECA, 50 µM) the cells were incubated at 37 °C for 15 min. Signals induced by adenosine receptor agonists CGS-21680 or NECA were significantly different between both cell lines (*** $p < 0.001$, 2-way ANOVA). For details see Section 4.

2.3. Assay Optimization

To investigate GJ-mediated coupling between donor and biosensor cells, we cocultured the cells at a ratio of 3:1 (donor: biosensor cells) and incubated them at 37 °C for 4 h. This ratio of donor to biosensor cells was found to be optimal based on preliminary studies

181

using different cell numbers and ratios. The culture medium was then replaced by an assay buffer containing luciferin (the substrate of the GloSensor luciferase) in which the cells were incubated for 2 h at room temperature. Upon activation of the A_{2A} ARs, recombinantly expressed only in the donor cells by the selective agonist CGS-21680, a luminescence signal was detected. However, the assay window was very small, only slightly above the DMSO control and much smaller than that observed with forskolin (Figure 6a).
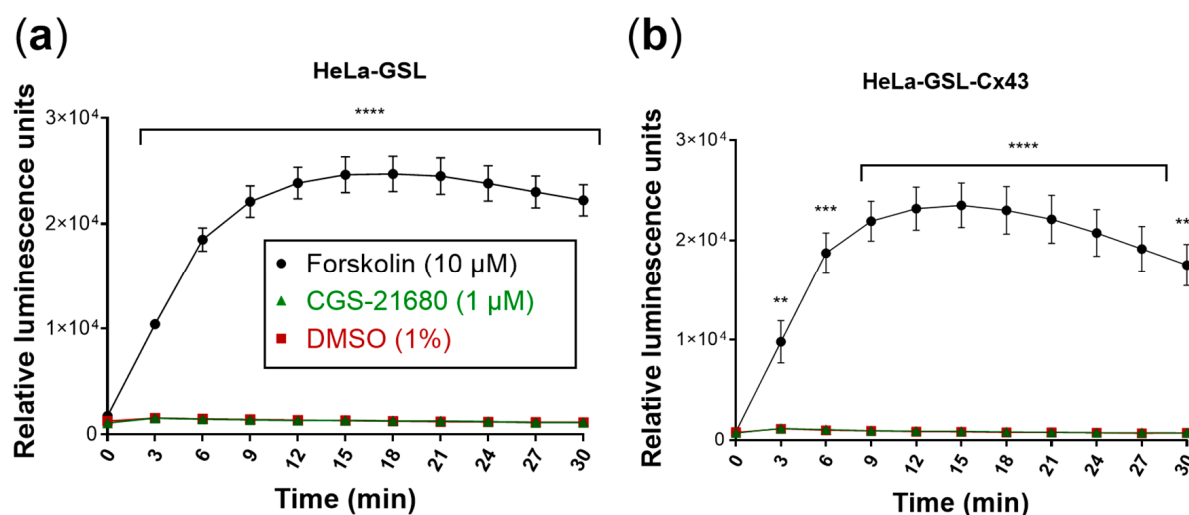

Figure 5. Evaluation of the biosensor cells. Forskolin (10 μM) was used as a positive control and DMSO (1%) as a negative control. Means ± SEM of three individual experiments performed in duplicates are given. (**a**) Biosensor cells produced luminescence only in response to forskolin (10 μM). Luminescence response to CGS-21680 (1 μM) was not different from control (DMSO). (**b**) Cx43 transfection of biosensor (HeLa-GSL) cells did not affect luminescence responses. Statistical significance calculated with repeated measures 2-way ANOVA and Dunnet's multiple comparisons test comparing treatments to control (DMSO, 1%). ** $p < 0.01$, *** $p < 0.001$, **** $p < 0.0001$.
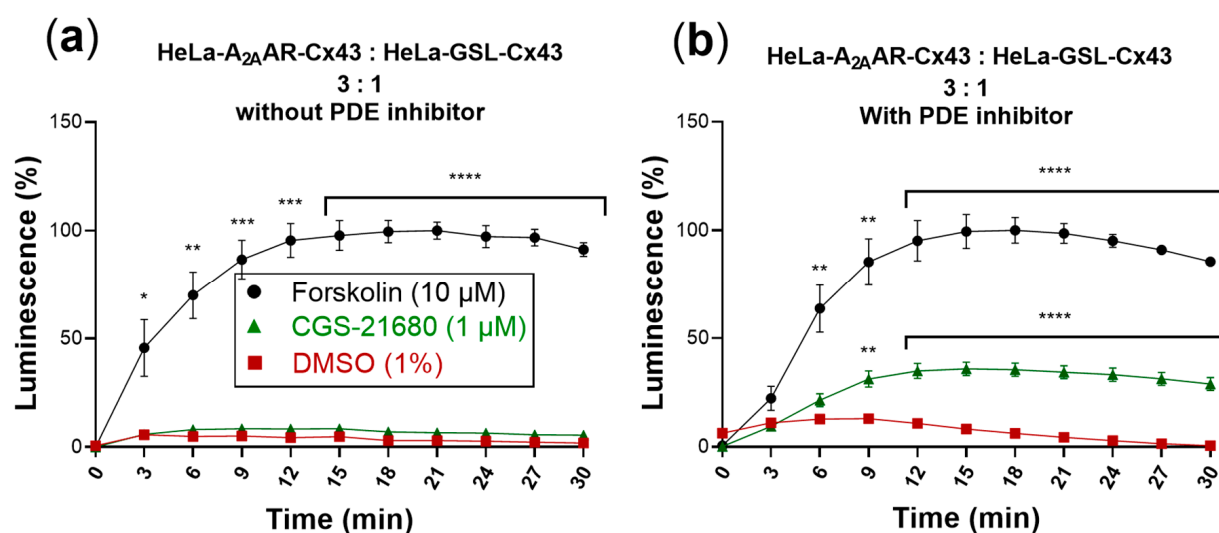
Figure 6. cAMP-dependent luminescence signal due to activation of cocultures of donor and biosensor cells (3:1) by the selective A_{2A} AR agonist CGS-21680 (1 μM). Forskolin (10 μM) was used as positive control and DMSO (1%) served as negative control. Data are normalized to the maximal effect of forskolin (100%). Data represent means ± SEM of three individual experiments performed in duplicates. (**a**) Activation without PDE inhibitor. Only forskolin displayed a significantly increased luminescence signal compared to control. (**b**) Activation in the presence of the PDE inhibitor IBMX (200 μM). Statistical significance calculated with repeated measures 2-way ANOVA and Dunnet's multiple comparisons test comparing treatments to control (DMSO, 1%). * $p < 0.05$, ** $p < 0.01$, *** $p < 0.001$, **** $p < 0.0001$.

cAMP produced in the cytosol is quickly hydrolyzed by phosphodiesterases (PDEs) yielding AMP. The addition of PDE inhibitors, such as 3-isobutyl-1-methylxanthine (IBMX), allows intracellular accumulation of cAMP. We therefore wondered whether the addition of an PDE inhibitor would lead to an increased luminescence signal. Thus, cocultures of donor and biosensor cells were additionally incubated with IBMX (200 µM) for 45 min at room temperature in assay buffer, after the 4 h incubation period in cell culture medium. The subsequent activation of A_{2A}ARs by CGS-21680 produced a significantly increased luminescence signal (Figure 6b).

The luminescence signal produced by the biosensor cells in response to activation of A_{2A}ARs expressed in the donor cells amounted to about 40% of the signal obtained in response to forskolin.

In order to verify that the activation of the GloSensor luciferase in the biosensor cells was entirely mediated by cAMP migrating from the donor cells via Cx43 GJs, both donor and biosensor cells that were not transfected with Cx43 were studied. In this crucial experiment, donor cells (HeLa-A_{2A}AR) and biosensor cells (HeLa-GSL) lacking Cx43 were cocultured in a ratio of 3:1. The same experimental procedure was performed as for the actual Cx43 GJs assay (see above). Stimulation of the cocultured, Cx43-lacking donor and biosensor cells with CGS-21680 (1 µM) did not result in any increase in the luminescence signal (Figure 7) indicating that the cAMP produced in the donor cells did not reach the biosensor cells due to the lack of Cx43 channels. Only when the cocultured cells were treated with forskolin (10 µM), a high luminescence signal was observed showing that the biosensor cells were functional. These results confirmed that native HeLa cells are devoid of efficient cell-to-cell communication, and that the cAMP generated in the donor cells could only be transported via heterologously transfected GJ proteins to the biosensor cells to yield a luminescence signal. This is in line with our findings from Western blot experiments performed to analyze endogenous Cx43 expression in HeLa cells (Figure S1). Although very low levels of endogenous Cx43 could be detected in the blots, they are apparently unable to form functional GJs in HeLa cells at levels detectable by our developed assay.
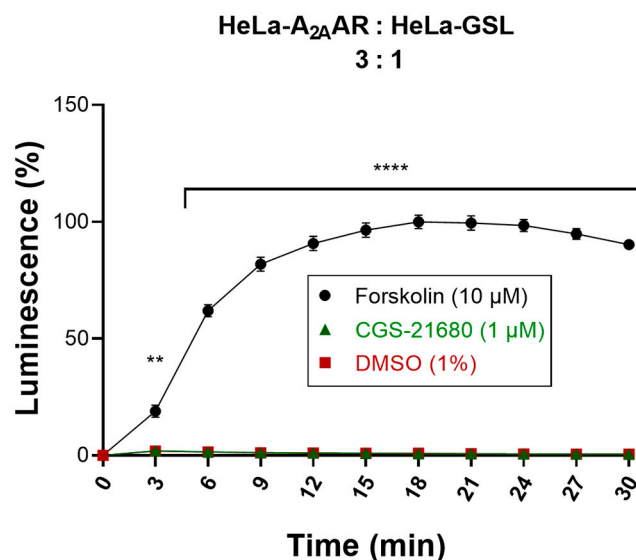
Figure 7. Evaluation of cocultured donor and biosensor cells lacking Cx43 GJs. Activation of cocultures of Cx43-deficient donor and biosensor cells by the selective A_{2A}AR agonist CGS-21680. Forskolin (10 µM) was used as a positive control and DMSO (1%) served as a negative control. Data are normalized to the maximal effect of forskolin (100%). Data represent means ± SEM of three individual experiments performed in duplicates. Statistical significance calculated with repeated measures 2-way ANOVA and Dunnet's multiple comparisons test comparing treatments to control (DMSO, 1%). ** $p < 0.01$, **** $p < 0.0001$.

2.4. Assay Validation I: Effect of the Gap Junction Blocker, Carbenoxolone

As a next step, the effect of the most commonly used Cx43 GJ blocker, carbenoxolone [29], a steroidlike derivative of the natural product glycyrrhetinic acid, was investigated. Carbenoxolone showed a concentration-dependent inhibition of the luminescence signal in the newly developed Cx GJ assay with an IC_{50} value of 44.5 ± 4.8 μM (Figure 8). This corresponds well with the literature IC_{50} values ranging from 17 to 210 μM [21,30]. No relevant cytotoxicity in the HeLa cells was observed at the employed concentrations as confirmed by the 3-(4,5-dimethylthiazol-2-yl)-2,5-diphenyltetrazoliumbromid (MTT) assay as a measure for cell viability (Figure S2).
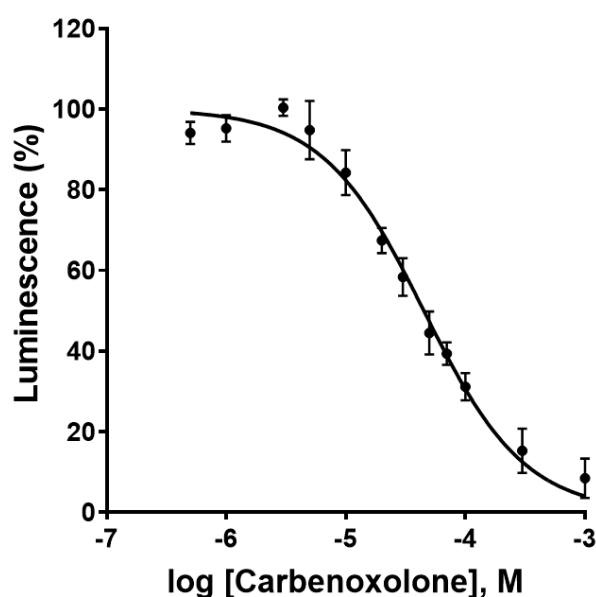

Figure 8. Concentration-dependent inhibition of Cx43 gap junctions by the blocker carbenoxolone as determined in the newly developed assay. Data points represent means $\pm$ SEM from 3 separate experiments. $IC_{50} = 44.5 \pm 4.8$ μM.

2.5. Assay Validation II: Suitability for High-Throughput Screening

Next, we evaluated the suitability of the optimized assay for high-throughput screening (HTS) by calculating the screening window coefficient known as Z'-factor. This dimensionless factor provides valuable information on the assay window, i.e., the separation between positive and negative controls. To this end, the luminescence pre-readout of the cocultures was compared with the luminescence signal obtained upon reaching a plateau after 19 min of stimulation with CGS-21680 (1 μM). Using the following Equation (1):

$$Z' = 1 - \frac{(3\sigma_{c^+} + 3\sigma_{c^-})}{|(\mu_{c^+} - \mu_{c^-})|} \tag{1}$$

(σ, standard deviation; μ, mean; c^+, positive control; c^-, negative control), the Z'-factor of the current assay was calculated to be 0.5. This corresponds to an HTS assay of sufficiently good quality [31]. The assay window was high with a signal to control ratio of about 3 (Figure 9). Thus, the newly developed functional Cx GJ assay can serve as an HTS platform to identify and characterize GJ modulators.

2.6. Screening of a Compound Library

Finally, we employed the developed assay to screen a small compound library containing 143 bioactive molecules (part of the Tocris compound library, https://www.tocris.com/products/tocriscreen-mini_2890). The compounds were tested at a concentration of 10 μM, and hits were defined as compounds showing a 25% decrease or increase in the

signal compared to control (Figure S3). Initially, eleven hits were obtained, of which ten had to be subsequently discarded. The reasons were high cytotoxicity or cAMP-inducing activity on HeLa-GSL cells. These effects resulted in false positive assay results. One Cx43 GJ-inhibiting hit remained, U-54494A hydrochloride, an experimental tool compound that is, however, no longer commercially available and could therefore not be further characterized up to now. Interestingly, the compound was described as possessing anticonvulsant properties [32].
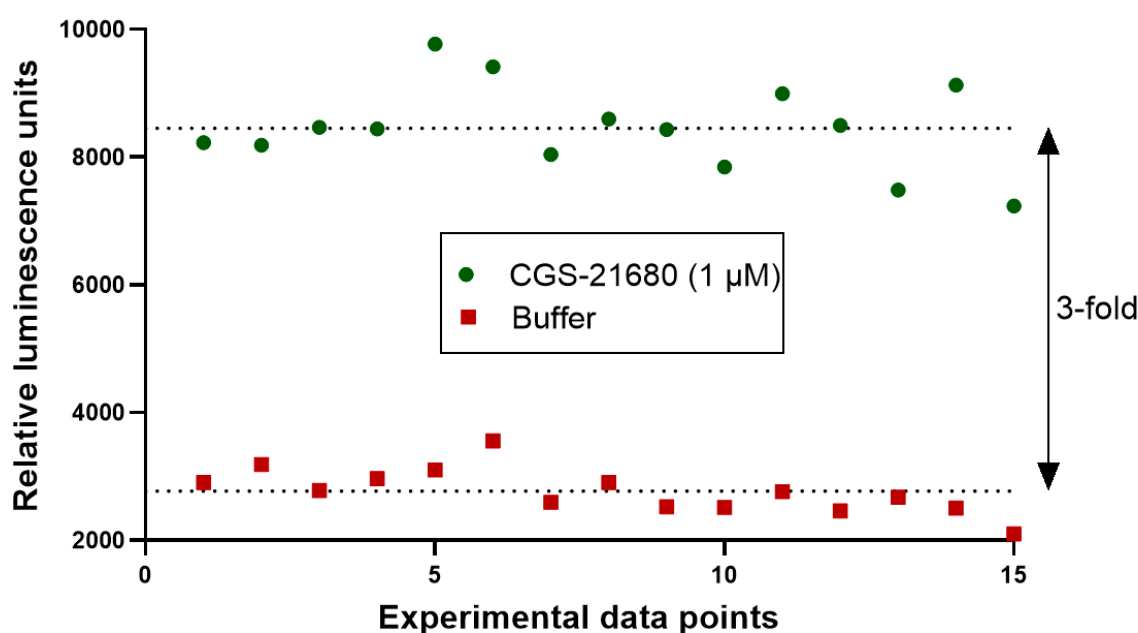

Figure 9. Evaluation of suitability of the newly developed Cx43 GJ assay for high-throughput screening (HTS). The quality of the assay was assessed by calculating the screening window coefficient (Z′-Factor) as previously described [31]. A coculture of donor cells (90,000 cells/well) and biosensor cells (30,000 cells/well) at a ratio of 3:1 was incubated in assay buffer for 45 min. Prior to the addition of the A_{2A} AR agonist CGS-21680 (1 μM) to the coculture, basal luminescence was measured (red data points, negative control). The coculture was then activated by the addition of CGS-21680 (1 μM). The luminescence signal had reached a stable plateau 19 min after stimulation, and data points were measured as positive controls (green data points). We measured 15 separate data points for positive and negative controls, indicating reproducibility and an assay window of about 3-fold.

3. Discussion

Connexins form GJs that allow the exchange of molecules between adjacent cells, thereby facilitating even long-distance cell communication. The functional modulation of GJs, inhibition as well as enhancement, has been proposed as a novel strategy for the treatment of various diseases. These include cardiac diseases, such as arrhythmias, remodeling after cardiac infarction, and atherosclerosis [33,34], brain diseases, e.g., epilepsy and neurodegenerative diseases [35,36], and even cancer [37]. Notably, a recent study suggested that loss of GJ coupling represents a cause of human temporal lobe epilepsy [38].To identify novel GJ modulators, a suitable assay for compound screening was required. However, the previously reported assays all appeared to be fraught with various drawbacks, such as low sensitivity, low signal-to-noise ratio, propensity to interfere with test compounds, or lacking suitability for HTS [16–21]. Therefore, we designed a completely new approach based on the sensitive measurement of luminescence by an engineered luciferase that is sensitive to the polar second messenger cAMP [25]. We selected communication-deficient HeLa cells, a permanent human cancer cell line that lacks the expression of functional GJs [39]. cAMP is produced intracellularly from ATP by the enzyme adenylate cyclase (AC). G protein-coupled receptors that activate Gs proteins lead to the stimulation of AC and thus to cAMP production [40]. This is a fast response occurring within a few seconds after

receptor activation. We had previously observed that HeLa cells do not express functional A_{2A}ARs, only A_{2B}ARs [27]. Therefore, we recombinantly expressed A_{2A}ARs along with Cx43 in HeLa cells to obtain donor cells, while biosensor cells were transfected with Cx43 and the cAMP-sensitive luciferase (GloSensor luciferase, GSL). In fact, a number of control experiments demonstrated that the cells behaved as expected. While HeLa-GSL cells did not respond to application of the A_{2A}-selective AR agonist CGS-21680, the same cell line cotransfected with the A_{2A}AR showed a large luminescence signal upon treatment with the A_{2A}AR agonist. As expected, forskolin, a direct activator of AC that was used as a positive control, always led to a luminescence signals. Since cAMP is rapidly degraded by PDEs, we had to add a nonspecific PDE inhibitor (IBMX) prior to the experiments. A mixture of donor cells expressing A_{2A}ARs plus Cx43, and biosensor cells expressing the cAMP-sensitive luciferase (GSL) plus Cx43 at a proportion of 3:1 resulted in a satisfactory signal of the A_{2A}AR agonist CGS-21680 (1 μM) in the presence of IBMX. The same cells, but lacking Cx43, gave no signal under the same conditions proving that the assay worked as intended. It should be noted that an increase in cAMP concentration might itself exert modulatory effects on the Cx GJs, such as changes in permeability or increased expression of Cx. However, at least the latter effect would take much longer than the duration of the assay. The assay could finally be validated by the known GJ inhibitor carbenoxolone, which is the most frequently used GJ inhibitor that has been explored and utilized in many studies [19,21,29,30,38]. We determined an IC_{50} value of 44.5 μM, which is good in agreement with the literature data [21,30] and which was demonstrated to be not due to cell toxicity as evidenced by its results in an MTT assay performed to assess cell viability (see Figure S2). Our new assay was also found to be very suitable for HTS, with a Z' value of 0.5 [31]. Finally, a first compound library was screened, leading to the discovery of the first hit compounds. In future studies, resynthesis and characterization of the most promising hit compound will have to be performed. The assay is also ready for the screening of further compound libraries to identify novel modulators of Cx43 GJs that can subsequently be optimized by medicinal chemistry approaches. The newly developed assay is not limited to Cx43, but can be expected to have the potential for broad application by adapting it to other members of the Cx family.

4. Materials and Methods

4.1. Cultivation of Cells

HeLa cells with a low endogenic connexin expression were a gift of K. Willecke. They were cultivated in an appropriate cell culture flask with culture medium consisting of Dulbecco's Modified Eagle Medium (DMEM, Thermo Fisher Scientific, Waltham, MA, USA) supplemented with 10% fetal calf serum (Sigma-Aldrich, Darmstadt, Germany), 100 U/mL penicillin G, and 100 μg/mL streptomycin (Thermo Fisher Scientific). Medium for transfected cells was additionally supplemented with 800 μg/mL G418 (Merck KGaA, Darmstadt, Germany). All steps were performed under sterile conditions (laminar air flow hood). The cultures were incubated at 37 °C in a humidified atmosphere with 5% CO_2 in an incubator. Cells were regularly passaged after they had reached a confluence of 80–90%. The old medium was taken off and the cells were washed twice with sterile PBS to remove residual medium. The cells were detached using a trypsin 0.01% (Lonza Group Ltd., Basel, Switzerland) solution containing 0.6 mM EDTA (Carl Roth GmbH + Co. KG, Karlsruhe, Germany) with incubation at 37 °C for 2–3 min.

4.2. Buffer Preparation for Cell Culture (PBS)

NaCl (137 mM), KCl (2.5 mM), Na_2HPO_4 (7.5 mM), and KH_2PO_4 (1.5 mM) were dissolved in deionized water and pH was adjusted to 7.4 with HCl (37%). The buffer was autoclaved and stored at room temperature.

4.3. Expression Vectors and Molecular Cloning

The coding region of the human $A_{2A}AR$ was subcloned into the retroviral vector pQCXIN into the NotI and BamHI restriction sites. The following primers were designed:

f-hA$_{2A}$-NotI: 5′-gtgacagcggccgcatgcccatcatgggctcctc-3′ and r-hA$_{2A}$-BamHI: 5′-cttac taggatcctcaggacactcctgctccatc-3′. The following PCR program using Pyrobest™ DNA polymerase (Takara Bio, Mountain View, CA, USA) was applied: 10 s at 98 °C and 30 cycles consisting of 10 s at 98 °C, 30 s at 62–66 °C, and 1 min at 72 °C followed by a final elongation step of 10 min at 72 °C. The PCR product was purified and digested with NotI and BamHI. The retroviral vector pQCXIN was cut with NotI and BamHI and after purification it was ligated with the cut PCR product. The correct assembly of the gene was verified by sequencing (Eurofins, Ebersberg, Germany).

The plasmid encoding for the modified firefly luciferase pGloSensor™-20F cAMP was purchased from Promega (Madison, WI, USA).

The plasmid encoding for the mouse Cx43 was kindly provided by Prof. Dr. Klaus Willecke, Life and Medical Sciences Institute (LIMES), University of Bonn. The coding region of the mouse Cx43 was subcloned with XhoI and XbaI into the pcDNA™4/myc-His A vector, which was cut with XhoI and XbaI. The following primers were designed:

f-mCx43-XhoI: 5′- GAGCTACTCGAGACCATGGGTGACTGGAGCGCC-3′,

r-mCx43-XbaI: 5′- CATCATTCTAGATTAAATCTCCAGGTCATCAGGCCGAGG-3′.

The PCR was conducted as described above. The PCR product was purified and digested with XhoI and XbaI and ligated with the prepared vector pcDNA™4/myc-His A. The correct assembly of the gene was verified by sequencing (Eurofins, Ebersberg, Germany).

4.4. Retroviral Transfection

Packaging cells GP+envAM12 (1.5×10^6 cells) (LGC Standards GmbH, Wesel, Germany) were seeded in a 25 cm^2 flask with 5 mL of culture medium followed by incubation (37 °C, 5% CO$_2$, 24 h) prior to transfection. Next day the cells were transfected using Lipofectamine 2000 (Thermo Fisher Scientific) with 10 μg of DNA comprising the retroviral plasmid (6.25 μg) and VSV-G plasmid (3.75 μg). After 15 h of transfection, the old culture medium was exchanged with 3 mL of fresh culture medium supplemented with 5 mM sodium butyrate (Sigma-Aldrich) followed by incubation (32 °C, 5% CO$_2$, 48 h). The supernatant (3 mL) containing the virus particles was removed and sterile filtered using a 2 μm filter to harvest the viruses. The filtrate containing the viruses was mixed with 6 μL of polybrene solution (4 mg/mL in H$_2$O, sterile filtered). Subsequently, the medium of the target cell line (HeLa) within a 25 cm^2 flask was replaced with the mixture and the cells were incubated (37 °C, 5% CO$_2$, 2.5 h). After the incubation, the mixture containing the viruses was discarded and 5 mL of fresh culture medium supplemented with G418 was added to the cells followed by incubation (37 °C, 5% CO$_2$, 48–72 h). After three days of incubation, the medium was changed until the nontransfected cell death process ended.

4.5. Lipofectamine Transfection (Lipofection)

For transfection, cells (2×10^6) were seeded in a 25 cm^2 culture flask containing culture medium followed by incubation (37 °C, 5% CO$_2$, 16 h). The old culture medium was exchanged against 6.25 mL of new full culture medium without antibiotics and the culture was incubated (37 °C, 5% CO$_2$, 3 h). Basal medium (600 μL) without any supplements was mixed with 25 μL of Lipofectamine 2000 (Thermo Fisher Scientific) and incubated for 5 min at RT. Plasmid-DNA (10 μg) was diluted in basal medium without any supplements to make a final volume of 625 μL. Both solutions were mixed giving a mixture of 1225 μL, which was incubated for 20 min at room temperature. The transfection mixture was then dropwise added to the cells followed by incubation (37 °C, 5% CO$_2$, 24–48 h).

4.6. Sample Preparation for Fluorescence Microscopy

Cells were seeded in 6 well plates. Prior to the cells, one sterile microscopy coverslip was added to each well. After one day of incubation (37 °C, 5% CO$_2$) the coverslips

were washed in PBS and incubated with 4% paraformaldehyde/PBS for 20 min at room temperature. Subsequently cells were incubated with PBS + 1% BSA for 15 min, with the primary antibody for 60 min, with the secondary antibody for 30 min and with DAPI for 5 min. Between every step, the coverslips were washed with PBS + 1% BSA. Incubation steps were performed at room temperature in the dark. One drop of mounting medium (Fluoromount) was placed on a slide and the coverslip containing the cells was placed onto the drop. The sample was left to dry overnight in the dark at 4 °C.

4.7. Characterization of Recombinant Cells

HeLa cells were transiently transfected with the $A_{2A}AR$ and GloSensor luciferase (HeLa-A_{2A}AR-GSL) or only with GlosSensor luciferase (HeLa-GSL). The cells were seeded into wells (60,000/well) and incubated overnight. The growth medium was replaced with medium supplemented with 2% GloSensor luciferase reagent and incubated for 2 h at 37 °C. After addition of the compounds dissolved in DMSO the cells were incubated at 37 °C for 15 min. The luminescence was subsequently measured in a plate reader (Mithras LB 940, Berthold Technologies, Bad Wildbad, Germany) without any filters.

4.8. Buffer Preparation for Cx43 GJ Assay (HBSS + BSA)

HEPES (20 mM), NaCl (137 mM), glucose (5.5 mM), KCl (5.4 mM), $NaHCO_3$ (4.2 mM), $CaCl_2$ (1.25 mM), $MgCl_2$ (1 mM), $MgSO_4$ (0.8 mM), KH_2PO_4 (0.44 mM) and Na_2HPO_4 (0.34 mM) were dissolved in autoclaved water and pH was adjusted to 7.4. The buffer was stored at 4 °C. BSA (0.1%, *w/v*) (AppliChem, Darmstadt, Germany) was dissolved in buffer prior to use.

4.9. Optimized Cx43 Gap Junction Assay

Donor cells were retrovirally transfected with A_{2A}ARs and biosensor cells with GloSensor-20F (Promega, Madison, WI, USA), respectively. Both cell lines were transfected with Cx43 via lipofection.

On the day of the experiment, donor and biosensor cells were harvested by trypsinization, centrifuged, and resuspended in culture medium. Cell aggregates were dislodged by slow pipetting and cells were counted. Initially, 30,000 biosensor cells per well were dispensed in a 96-well solid bottom white plate followed by 90,000 donor cells to maintain a 3:1 ratio of donor and biosensor cells. Both donor and biosensor cells were mixed by pipetting and the coculture was incubated for 4 h at 37 °C, 5% CO_2. After the incubation, the full DMEM medium was replaced by HBSS buffer supplemented with 0.1% BSA, 200 μM IBMX and 2% GloSensor cAMP reagent (Promega, Madison, WI, USA) ("assay buffer") followed by incubation for 1 h in the dark at room temperature. For the evaluation of GJ inhibitors, the compounds were added directly when DMEM full medium was replaced with the assay buffer. The plate was then placed in a plate reader (Mithras LB 940, Berthold Technologies, Bad Wildbad, Germany) without any filter for the basal luminescence readout. Subsequently, either CGS-21680 (10 μM) (Bio-Techne GmbH, Wiesbaden-Nordstadt, Germany), DMSO (1%) or forskolin (10 μM) (AppliChem, Darmstadt, Germany) was added, and luminescence from each well was measured, either in a kinetic mode for 1 s with an interval of 3 min over a total duration of 30 min, or as a single point after 15–20 min.

4.10. Data Evaluation and Statistical Analyis

The data were analyzed using Prism 8.0 (GraphPad Software Inc., San Diego, CA, USA). Differences between means were tested for significance by 2-way ANOVA or repeated measures 2-way ANOVA and Dunnet's multiple comparisons test. The NIS Element Advanced Research software 4.0 was used for microscopy image acquisition and analysis.

Supplementary Materials: Supplementary materials can be found at https://www.mdpi.com/1422-0067/22/3/1417/s1. Figure S1: Expression profile of connexin 43 in wild-type and transfected cell lines, Figure S2: Cytotoxicity assay of carbenoxolone, Figure S3: Screening results using the developed assay.

References

1. Giaume, C.; Naus, C.C.; Sáez, J.C.; Leybaert, L. Glial connexins and pannexins in the healthy and diseased brain. *Physiol. Rev.* **2021**, *101*, 93–145. [CrossRef] [PubMed]
2. Vinken, M.; Vanhaecke, T.; Papeleu, P.; Snykers, S.; Henkens, T.; Rogiers, V. Connexins and their channels in cell growth and cell death. *Cell. Signal.* **2006**, *18*, 592–600. [CrossRef] [PubMed]
3. Bedner, P.; Steinhäuser, C.; Theis, M. Functional redundancy and compensation among members of gap junction protein families? *Biochim. Biophys. Acta Biomembr.* **2012**, *1818*, 1971–1984. [CrossRef] [PubMed]
4. Salameh, A. Life cycle of connexins: Regulation of connexin synthesis and degradation. *Adv. Cardiol.* **2006**, *42*, 57–70. [CrossRef] [PubMed]
5. Kar, R.; Batra, N.; Riquelme, M.A.; Jiang, J.X. Biological role of connexin intercellular channels and hemichannels. *Arch. Biochem. Biophys.* **2012**, *524*, 2–15. [CrossRef]
6. Lampe, P.D.; TenBroek, E.M.; Burt, J.M.; Kurata, W.E.; Johnson, R.G.; Lau, A.F. Phosphorylation of connexin43 on serine368 by protein kinase C regulates gap junctional communication. *J. Cell Biol.* **2000**, *149*, 1503–1512. [CrossRef] [PubMed]
7. Solan, J.L.; Lampe, P.D. Specific Cx43 phosphorylation events regulate gap junction turnover In Vivo. *FEBS Lett.* **2014**, *588*, 1423–1429. [CrossRef]
8. Meggouh, F.; Benomar, A.; Rouger, H.; Tardieu, S.; Birouk, N.; Tassin, J.; Barhoumi, C.; Yahyaoui, M.; Chkili, T.; Brice, A.; et al. The first de novo mutation of the connexin 32 gene associated with X linked Charcot-Marie-tooth disease. *J. Med. Genet.* **1998**, *35*, 251–252. [CrossRef]
9. Koppelhus, U.; Tranebjaerg, L.; Esberg, G.; Ramsing, M.; Lodahl, M.; Rendtorff, N.D.; Olesen, H.V.; Sommerlund, M. A Novel mutation in the connexin 26 gene (GJB2) in a child with clinical and histological features of Keratitis-Ichthyosis-deafness (KID) syndrome. *Clin. Exp. Dermatol.* **2011**, *36*, 142–148. [CrossRef]
10. Guerrero, P.A.; Schuessler, R.B.; Davis, L.M.; Beyer, E.C.; Johnson, C.M.; Yamada, K.A.; Saffitz, J.E. Slow ventricular conduction in mice heterozygous for a connexin43 null mutation. *J. Clin. Investig.* **1997**, *99*, 1991–1998. [CrossRef]
11. Gutstein, D.E.; Morley, G.E.; Tamaddon, H.; Vaidya, D.; Schneider, M.D.; Chen, J.; Chien, K.R.; Stuhlmann, H.; Fishman, G.I. Conduction slowing and sudden arrhythmic death in mice with cardiac-restricted inactivation of connexin43. *Circ. Res.* **2001**, *88*, 333–339. [CrossRef] [PubMed]
12. Reaume, A.G.; de Sousa, P.A.; Kulkarni, S.; Langille, B.L.; Zhu, D.; Davies, T.C.; Juneja, S.C.; Kidder, G.M.; Rossant, J. Cardiac malformation in neonatal mice lacking connexin43. *Science* **1995**, *267*, 1831–1834. [CrossRef] [PubMed]
13. Vasconcellos, J.P.C.; Melo, M.B.; Schimiti, R.B.; Bressanim, N.C.; Costa, F.F.; Costa, V.P. A Novel Mutation in the GJA1 Gene in a family with Oculodentodigital dysplasia. *Arch. Ophthalmol.* **2005**, *123*, 1422–1426. [CrossRef] [PubMed]
14. Pace, N.P.; Benoit, V.; Agius, D.; Grima, M.A.; Parascandalo, R.; Hilbert, P.; Borg, I. Two novel GJA1 variants in Oculodentodigital dysplasia. *Mol. Genet. Genom. Med.* **2019**, *7*, e882. [CrossRef] [PubMed]
15. Maass, K.; Ghanem, A.; Kim, J.-S.; Saathoff, M.; Urschel, S.; Kirfel, G.; Grümmer, R.; Kretz, M.; Lewalter, T.; Tiemann, K.; et al. Defective epidermal barrier in neonatal mice lacking the C-terminal region of connexin43. *Mol. Biol. Cell* **2004**, *15*, 4597–4608. [CrossRef]
16. Babica, P.; Sovadinová, I.; Upham, B.L. Scrape loading/dye transfer assay. *Methods Mol. Biol.* **2016**, *1437*, 133–144. [CrossRef]
17. El-Fouly, M.H.; Trosko, J.E.; Chang, C.-C. Scrape-Loading and Dye Transfer. *Exp. Cell Biol.* **1987**, *168*, 422–430. [CrossRef]
18. Ziambaras, K.; Lecanda, F.; Steinberg, T.H.; Civitelli, R. Cyclic stretch enhances gap junctional communication between osteoblastic cells. *J. Bone Miner. Res.* **1998**, *13*, 218–228. [CrossRef]

19. Picoli, C.; Soleilhac, E.; Journet, A.; Barette, C.; Comte, M.; Giaume, C.; Mouthon, F.; Fauvarque, M.-O.; Charvériat, M. High-content screening identifies new inhibitors of connexin 43 gap junctions. *Assay Drug Dev. Technol.* **2019**, *17*, 240–248. [CrossRef]

20. Lee, J.Y.; Choi, E.J.; Lee, J. A new high-throughput screening-compatible gap junctional intercellular communication assay. *BMC Biotechnol.* **2015**, *15*, 1–9. [CrossRef]

21. Haq, N.; Grose, D.; Ward, E.; Chiu, O.; Tigue, N.; Dowell, S.J.; Powell, A.J.; Chen, M.X. A high-throughput assay for Connexin 43 (Cx43, GJA1) gap junctions using codon-optimized aequorin. *Assay Drug Dev. Technol.* **2013**, *11*, 93–100. [CrossRef] [PubMed]

22. Lurtz, M.M.; Louis, C.F. Intracellular calcium regulation of connexin43. *Am. J. Physiol. Cell. Physiol.* **2007**, *293*, 1806–1813. [CrossRef] [PubMed]

23. Imanaga, I.; Hai, L.; Ogawa, K.; Matsumura, K.; Mayama, T. Phosphorylation of connexin in functional regulation of the cardiac gap junction. *Exp. Clin. Cardiol.* **2004**, *9*, 161–164. [PubMed]

24. Bedner, P.; Niessen, H.; Odermatt, B.; Kretz, M.; Willecke, K.; Harz, H. Selective permeability of different connexin channels to the second messenger cyclic AMP. *J. Biol. Chem.* **2006**, *281*, 6673–6681. [CrossRef] [PubMed]

25. Fan, F.; Binkowski, B.F.; Butler, B.L.; Stecha, P.F.; Lewis, M.K.; Wood, K.V. Novel genetically encoded biosensors using firefly luciferase. *ACS Chem. Biol.* **2008**, *3*, 346–351. [CrossRef]

26. Pettengill, M.A.; Lam, V.W.; Ojcius, D.M. The danger signal adenosine induces persistence of chlamydial infection through stimulation of A2b receptors. *PLoS ONE* **2009**, *4*, e8299. [CrossRef]

27. Hinz, S.; Navarro, G.; Borroto-Escuela, D.; Seibt, B.F.; Ammon, Y.-C.; de Filippo, E.; Danish, A.; Lacher, S.K.; Červinková, B.; Rafehi, M.; et al. Adenosine A_{2A} receptor ligand recognition and signaling is blocked by A_{2B} receptors. *Oncotarget* **2018**, *9*, 13593–13611. [CrossRef]

28. Valiunas, V. Cyclic nucleotide permeability through unopposed connexin hemichannels. *Front. Pharmacol.* **2013**, *4*, 75. [CrossRef]

29. Davidson, J.S.; Baumgarten, I.M. Glycyrrhetinic acid derivatives: A novel class of inhibitors of gap-junctional intercellular communication. structure-activity relationships. *J. Pharmacol. Exp. Ther.* **1988**, *246*, 1104–1107.

30. Burnham, M.P.; Sharpe, P.M.; Garner, C.; Hughes, R.; Pollard, C.E.; Bowes, J. Investigation of connexin 43 uncoupling and prolongation of the cardiac QRS complex in preclinical and marketed drugs. *Br. J. Pharmacol.* **2014**, *171*, 4808–4819. [CrossRef]

31. Zhang, J.H.; Chung, T.D.Y.; Oldenburg, K.R. A simple statistical parameter for use in evaluation and validation of high throughput screening assays. *J. Biomol. Screen.* **1999**, *4*, 67–73. [CrossRef] [PubMed]

32. Von Voigtlander, P.F.; Hall, E.D.; Ochoa, M.C.; Lewis, R.A.; Triezenberg, H.J. U-54494A: A unique anticonvulsant related to kappa opioid agonists. *J. Pharmacol. Exp. Ther.* **1987**, *243*, 542–547.

33. Johnson, R.D.; Camelliti, P. Role of non-myocyte gap junctions and connexin hemichannels in cardiovascular health and disease: Novel therapeutic targets? *Int. J. Mol. Sci.* **2018**, *19*, 866. [CrossRef] [PubMed]

34. Leybaert, L.; Lampe, P.D.; Dhein, S.; Kwak, B.R.; Ferdinandy, P.; Beyer, E.C.; Laird, D.W.; Naus, C.C.; Green, C.R.; Schulz, R. Connexins in cardiovascular and neurovascular health and disease: Pharmacological implications. *Pharmacol. Rev.* **2017**, *69*, 396–478. [CrossRef] [PubMed]

35. Steinhäuser, C.; Grunnet, M.; Carmignoto, G. Crucial role of astrocytes in temporal lobe epilepsy. *Neuroscience* **2016**, *323*, 157–169. [CrossRef] [PubMed]

36. Takeuchi, H.; Suzumura, A. Gap junctions and hemichannels composed of connexins: Potential therapeutic targets for neurodegenerative diseases. *Front. Cell. Neurosci.* **2014**, *8*, 189. [CrossRef]

37. Nalewajska, M.; Marchelek-Myśliwiec, M.; Opara-Bajerowicz, M.; Dziedziejko, V.; Pawlik, A. connexins-therapeutic targets in cancers. *Int. J. Mol. Sci.* **2020**, *21*, 9119. [CrossRef]

38. Bedner, P.; Dupper, A.; Hüttmann, K.; Müller, J.; Herde, M.K.; Dublin, P.; Deshpande, T.; Schramm, J.; Häussler, U.; Haas, C.A.; et al. Astrocyte uncoupling as a cause of human temporal lobe epilepsy. *Brain* **2015**, *138*, 1208–1222. [CrossRef]

39. Manthey, D.; Willecke, K. Transfection and expression of exogenous connexins in mammalian cells. *Methods Mol. Biol.* **2001**, *154*, 187–199. [CrossRef]

40. Dessauer, C.W.; Watts, V.J.; Ostrom, R.S.; Conti, M.; Dove, S.; Seifert, R. International union of basic and clinical pharmacology. CI structures and small molecule modulators of mammalian adenylyl cyclases. *Pharmacol. Rev.* **2017**, *69*, 93–139. [CrossRef]

International Journal of
Molecular Sciences

MDPI

A Cellular Assay for the Identification and Characterization of Connexin Gap Junction Modulators

Azeem Danish[1#], Robin Gedschold[1#], Sonja Hinz[1], Anke C. Schiedel[1], Dominik Thimm[1], Peter Bedner[2], Christian Steinhäuser[2*] and Christa E. Müller[1] *

[1] PharmaCenter Bonn, Pharmaceutical Institute, Pharmaceutical & Medicinal Chemistry, Rheinische Friedrich-Wilhelms-Universität Bonn, An der Immenburg 4, D-53121 Bonn, Germany; christa.mueller@uni-bonn.de

[2] Institute of Cellular Neuroscience, Medical Faculty, Rheinische Friedrich-Wilhelms-Universität Bonn, Venusberg-Campus 1, D-53127 Bonn, Germany

* Correspondence: christa.mueller@uni-bonn.de; Christian.Steinhaeuser@ukbonn.de

#equal contribution
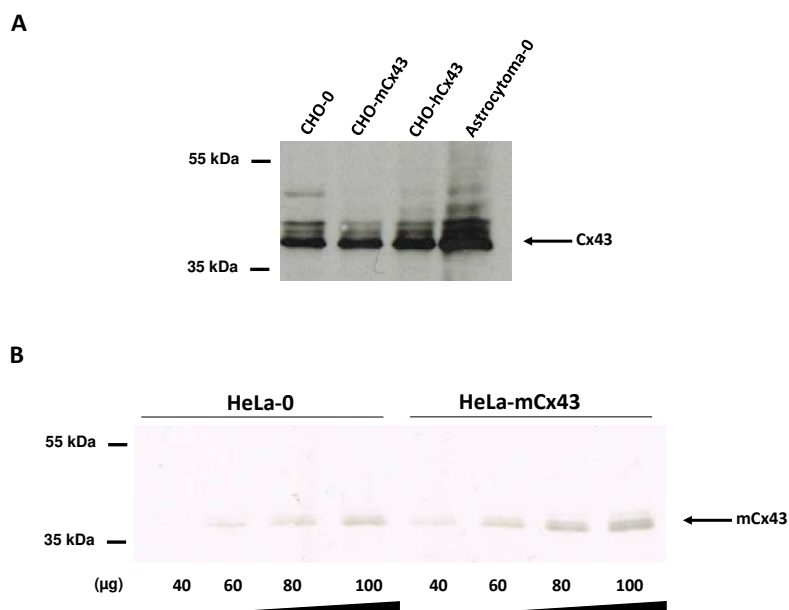
Table of Contents

Figure S1. Expression profile of Cx43 in wild-type and Cx43-transfected cell lines. (**A**) Western blot analysis of heterologous expression of human and mouse Cx43 in stable CHO cell lines and endogenous expression of Cx43 in native CHO and astrocytoma cell lines. For the analyses, 30 μg of each protein sample per well was loaded onto SDS-gel. (**B**) Western blot analysis of endogenous Cx43 expression in native HeLa cell lines and heterologous expression of mouse Cx43 in HeLa cells post 48 h transient transfection. Cells were lysed, cleared by centrifugation, and the supernatants were subsequently used for analysis. The Cx43 protein bands were detected using primary polyclonal rabbit anti-Cx43 antibodies (1:2500) and secondary horseradish peroxidase (HRP) conjugated anti-rabbit antibodies (1:4000). Chemoluminescence from nitrocellulose blots was captured on X-ray films which were developed in fixing solutions.
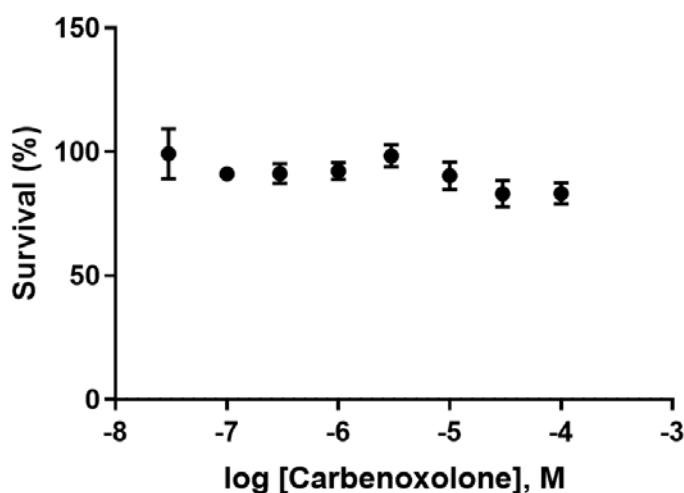

Figure S2. Cytotoxicity of carbenoxolone in HeLa cells measured by the MTT assay. Normalized results (Buffer = 100%; DMSO (20%) = 0%). Data points are means ± SEM of three independent experiments in duplicates.
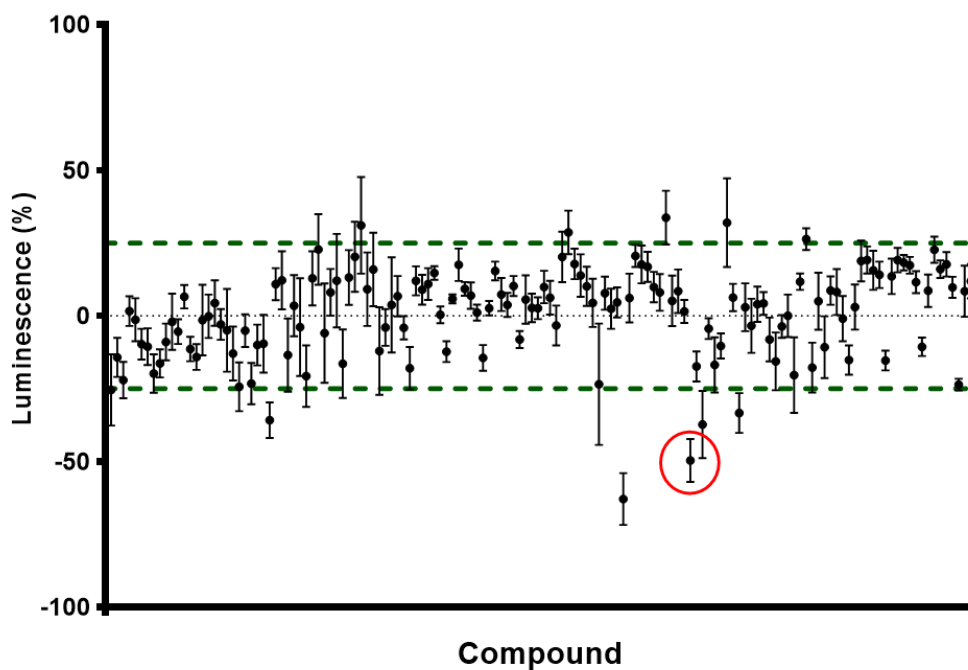
Figure S3. Screening results. A library comprising 143 small bioactive molecules was screened by the new GJ assay at a concentration of 10 μM. Data points represent means ± SEM of three independent experiments in duplicates. Compounds with >25% change in luminescence compared to the signal induced by CGS-21680 were classified as hits. CGS-21680 effect = 0%; Buffer = -100%. Circled in red is U-54494A hydrochloride which was identified as a confirmed hit compound.